BOND FORMATION IN MASS SPECTROMETRY: ELECTRON IMPACT INDUCED MIGRATION OF ARYLTHIO GROUPS AND CLUSTERING REACTIONS IN CHEMICAL IONISATION REAGENT GASES.

by

P. E. Glaspy

A thesis submitted in partial fulfilment of the requirements of the Degree of Doctor of Philosophy in the University of London.

The Bourne Laboratory
Royal Holloway College
Egham, Surrey.

March 1984

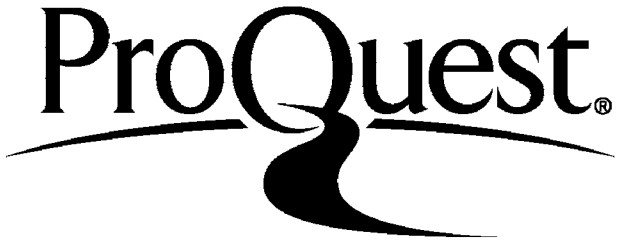

To my parents.

ACKNOWLEDGEMENTS

I am indebted to my supervisor, Dr R.A.Hancock, for his constant help and encouragement during the course of my research and also for his aid in obtaining an ORS Award, without which this research would not have been completed.

Thanks are also due to Professor B.S.Thyagarajan for his continued moral and intellectual support.

Grateful acknowledgement is given to Messrs. B. Smethurst, R.Lane, J.Turner, G.Waters and P.Willmore for their technical assistance, Mr D. Carter for providing B/E linked scans and exact mass analyses at the School of Pharmacy, and Messrs. T.Traugott, R.Martin and R.Martinez for technical assistance in syntheses in the early stages of this work.

I would also like to thank Schwester M.Sans for her constant interest in my work and for her many financial contributions.

Finally, many thanks are due to Mrs S.Partin for typing an apparently never-ending manuscript.

Bond Formation in Mass Spectrometry: Electron Impact Induced Migration of Arylthio Groups and Clustering Reactions in Chemical Ionisation Reagent Gases.

by P. E. Glaspy

ABSTRACT

Electron impact induced rearrangements have been observed in compounds containing either two arylthio groups or an arylthio group and an arylsulphonyl group. In addition to the loss of sulphur dioxide from the molecular ion and a sulphone-sulphinate rearrangement, 3-arylsulphonyl-2-arylthiopropenes exhibited the rearrangement to a bisarylsulphide ion (analogous to that reported for the isomeric 1-arylsulphonyl-2-arylthiopropenes). A series of 1-arylsulphonyl-4-arylthio-2-butynes also underwent sulphone-sulphinate rearrangement and rearranged to the bisarylsulphide ions, in the absence of sulphur dioxide or sulphur extrusion. The formation of the bisarylsulphide ion from the molecular ion of these compounds is postulated to occur after an initial {1,3} arylthio shift giving an ion analogous to the molecular ion of 3-arylsulphonyl-2-arylthiopropene.

A skeletal rearrangement of N-(4'-arylsulphonyl-2'-butynyl)-N-(4"-arylthio-2"-butynyl)anilines resulted in the elimination of $Ar^1SO_2SAr^2$ from the molecular ion, but not ions arising from a sulphone-sulphinate rearrangement or extrusion of sulphur or sulphur dioxide.

The rearrangement of N,N- bis(4'-arylthio-2'-butynyl)anilines via consecutive {1,3} arylthio shifts,

followed by elimination of a bisaryldisulphide moiety, was supported by the behaviour of N-(4'-arylthio-2'-butynyl)-N-(2"-arylthio-2"-propenyl)-p-toluidines and N,N-bis(2'arylthio-2'-propenyl)-p-toluidines. Their molecular ions are analogous to the rearranged molecular ions of the N,N-bis(4'-arylthio-2'-butynyl)anilines after one or two arylthio shifts, respectively. No extrusion of sulphur is observed, but rather the elimination of a bisaryldisulphide moiety occurs.

A series of 1,8-bis(arylthiomethyl)naphthalenes and 1,2-bis(arylthio)acenaphthenes were synthesised. Electron impact showed no loss of Ar^1SSAr^2 from the naphthalene derivatives, owing to the predominance of C-S bond cleavage. However, the acenaphthene derivatives readily eliminated a bisaryldisulphide moiety and a qualitative substituent effect was observed for the formation of $Ar^1SSAr^{2+\cdot}$ ions.

In a separate investigation, the kinetics of ion-molecule clustering reactions in a number of chemical ionisation reagent gases were studied. Rate coefficients were obtained at various ion-source field strengths for the formation of proton or deuteron bound dimers at pressures of ca.0.01-0.4 Torr ($450^{o}K$). Changes from overall third to second order kinetics were observed with increasing pressure, in accord with an energy transfer mechanism. Using the higher values of pressure, rate coefficients were obtained and corresponded to the formation of the excited collision complexes. Rate coefficients for the association reaction of the MH^+ (or MD^+) ions in methylamine, dimethylamine, trimethyl-

amine, ammonia-d_3, water and deuterium oxide, at an ion exit energy of 0.52 eV (450^{o}K), were respectively: 1.77 $\pm$ 0.04, 1.18 $\pm$ 0.02, 0.54 $\pm$ 0.01, 0.77 $\pm$ 0.02, 0.267 $\pm$ 0.006 and 1.09 $\pm$ 0.06 (x 10^{-11} cm^3 $molec^{-1}$ s^{-1}). Simple kinetic methods for estimating the ion-source pressures of these gases are described. The disappearance rate coefficients for the major primary ions of the above gases were also determined.

Preface

As the title implies, this thesis is divided into two parts, each of which contains a separate introduction.
Part One is concerned with the synthesis and electron impact induced rearrangement of a variety of organosulphur compounds.
Part Two describes the investigation of ion-molecule reactions in chemical ionisation reagent gases and the determination of the rate coefficients associated with these reactions.

CONTENTS

PART ONE

1. INTRODUCTION

1.1 General aspects of mass spectrometry

1.1.1 Sample ionisation

The ionisation of chemical compounds in the ion-source of a mass spectrometer can be achieved by imparting energy to the vaporised sample by a variety of means. Methods currently employed include subjecting the sample to beams of electrons, α-particles or photons. Ionisation can also be achieved by placing the sample in a high-strength electric field. Of these methods, electron impact (E.I.) is the most prevalent, due to its ease of implementation.

E.I. mass spectra are routinely obtained by bombarding a sample with electrons having energies of 70 eV, produced by a heated filament. An electron with sufficient energy striking a sample molecule (ABC) results in the ejection of an electron from the sample molecule.

$$ABC + e \xrightarrow[-2e]{} ABC^{+\cdot} \qquad (1.1.1\text{-}1)$$

The radical cation formed by this event has a mass to charge ratio (m/z) equal to the molecular mass of the sample and is termed the molecular ion. The molecular ion ($ABC^{+\cdot}$) is generally unstable and may simply fragment to give a radical and a cation,

$$ABC^{+\cdot} \longrightarrow AB^{+} + C\cdot \qquad (1.1.1\text{-}2)$$

or rearrange prior to fragmentation (e.g. as in 1.1.1 - 3) in which a neutral fragment is lost with concurrent formation of a new bond).

$$ABC^{+\cdot} \longrightarrow AC^{+\cdot} + B \qquad (1.1.1 - 3)$$

The molecular ion and the ions formed by its fragmentation are termed primary ions. When ions are formed at pressures higher than those employed for E.I. mass spectrometry (vide infra) the formation of secondary ions, resulting from ion-molecule reactions, becomes more prevalent.

$$A^{+} + ABC \longrightarrow \text{products} \qquad (1.1.1 - 4)$$

Whereas Part One of this thesis discusses the E.I. induced fragmentations and rearrangements of various organo-sulphur compounds, examples of ion-molecule reactions will be discussed in Part Two.

1.1.2 Instrumentation.

Numerous types of mass spectrometers have been developed and detailed descriptions of their construction and theory of operation can be found in texts such as those by McFadden[1], Kiser[2], Beynon[3] and Middleditch[4]. Mass spectrometers used for structure elucidation can be classified into three groups, according to the type of analyser by which separation of the ions is achieved, namely:

A. Magnetic field deflection

1) Single-focusing

2) Double-focusing

B. Quadrupole

C. Time of flight

A single focusing, single magnetic-sector instrument was used in this study. The other types of instruments given above will be discussed briefly, with an emphasis placed on single-focusing mass spectrometers.

1.1.2.1 Single-focusing mass spectrometers.

A single-focusing mass spectrometer is depicted in Figure 1.1.2.1 - 1 in block diagram form.

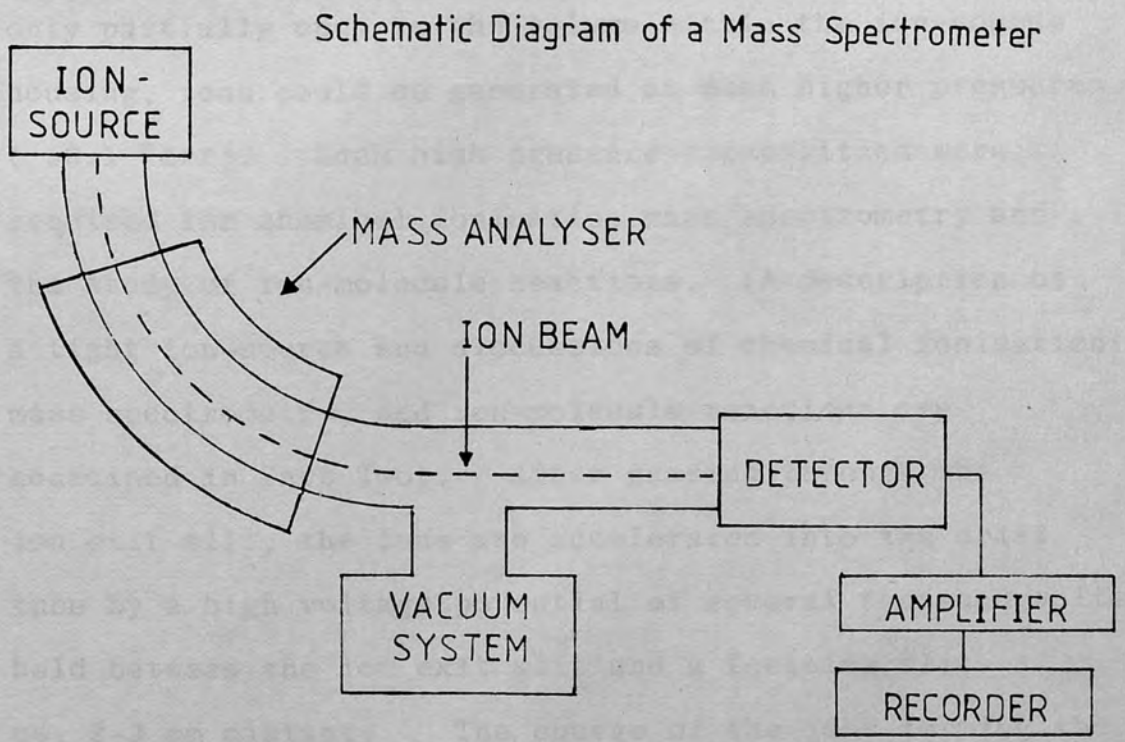

Figure (1.1.2.1-1)

An efficient vacuum system, composed of mechanical and diffusion vacuum pumps, is used to generate vacuums of ca.10^{-6} torr in the ion-source, flight tube and detector. Samples are introduced into the ion source via the inlet system. Gases may be introduced directly into the ion-source, but solids and liquids require prior vaporisation. Ions are formed in the ion-source by electron impact (discussed in 1.1.1) and are propelled through a slit (the ion-exit slit) by an electric field generated by a low potential (1-50V).

In early systems, the ion-source was open to the ion-source housing and only very low sample pressures were possible. With the advent of "tight" ion-sources, in which ionisation occurs within an enclosed chamber, only partially open to the volume within the ion-source housing, ions could be generated at much higher pressures (>0.1 Torr). Such high pressure capabilities were required for chemical ionisation mass spectrometry and the study of ion-molecule reactions. (A description of a tight ion-source and discussions of chemical ionisation mass spectrometry, and ion-molecule reactions are contained in Part Two). After passing through the ion exit slit, the ions are accelerated into the drift tube by a high voltage potential of several thousand volts, held between the ion exit slit and a focusing slit ca. 2-3 mm distant. The charge of the ions forming the ion-beam is determined by the sign of the accelerating

voltage. The ion-beam passes between the poles of an electromagnet where it is resolved into its components by an applied magnetic field. The resolved ion-beams, which are analysed according to the mass to charge ratios (m/z) of the ions of which they are composed, continue through another slit (the collector slit) and impinge upon a detector. The signal generated by the detector is amplified and sent either to a recorder, for a permanent record of the mass spectrum, to a computer interface or to an oscilloscope for continuous monitoring of ion intensities.

The detector must have a fast response time and a high gain in order for a suitable signal to be generated. The electron multiplier is almost ideal in both respects and is the most common detector currently used. The electron multiplier is composed of a series of plates held at voltages decreasing stepwise from a negative potential of several thousand volts to zero. Figure 1.1.2.1-2 is a schematic representation of a multistage electron multiplier.

Schematic Diagram of an Electron Multiplier

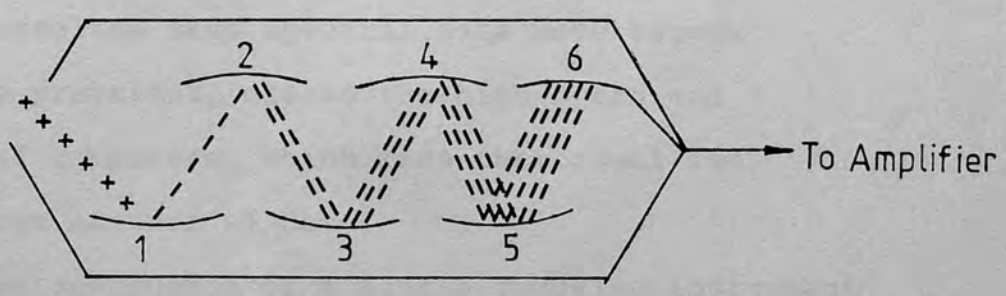

Figure 1.1.2.1 - 2

Collision of a positive ion with the first plate (the cathode, 1) causes the emission of several secondary electrons which are accelerated and strike the next electrode (dynode,2). The additional secondary electrons emitted at the first dynode are then accelerated towards the next dynode and the process is repeated several times until a current, which is capable of amplification and recording, is produced at the collector electrode (anode,6). Multiplier tubes in common usage contain 12-20 stages and have gains of ca. 10^5 to 10^7. Typically, 2%-beryllium-copper is used in the production of electrodes for electromultipliers.

Fast response time and high sensitivity are also pre-requisites for a suitable recorder in order for the permanent record to accurately reflect the abundances of ions in a mass spectrum. In common usage are oscillographic recorders which record the spectrum on ultraviolet light sensitive paper, by means of a galvanometer system comprised of several galvanometers with different sensitivities. (This type of recorder is discussed further in the experimental section of Part Two).

In recent years, the use of computers to collect, store and correlate mass spectral data have become increasingly prevalent, due to the high speed and efficiency of computers, which make them ideal for handling large amounts of data.

The resolution of a single focusing instrument (or any other type of mass spectrometer) is determined

by comparing two adjacent peaks of equal height, separated by a valley whose height is ca.10% that of the peaks. The resolution (R) is defined as

$$R = M/\Delta M \qquad (1.1.2.1 - 1)$$

where M is the higher mass number of the two peaks and ΔM is the difference between the mass numbers.

Low resolution instruments, such as single-focusing mass spectrometers, can be defined arbitrarily as those which separate unit masses up to m/z 2000 and thus have resolutions of 2000 or less.

The resolution of a single-focusing mass spectrometer is limited in part by the magnetic analyser, which is not a true mass separator, but rather separates ions according to their momenta. Since the ions accelerated into the magnetic analyser do not have exactly the same energies, due to differences in position before acceleration and variation in thermal energies, the resultant divergence of the ion beam broadens each individual peak and limits the optimum resolution of the instrument. The analysis by a magnetic sector of ions accelerated through an electric field can be understood as follows.

The work done on an ion passing through a potential field of V volts is expressed by zeV, with z equal to the number of charges on the ion and e equal to the electronic charge. Since work equals the kinetic energy gained by the ion:

$$mv^2/2 = zeV \qquad (1.1.2.1 - 2)$$

where m is the mass and v is the velocity of the ion. Application of a perpendicular magnetic field of strength, B, relative to the direction of motion of the ion-beam, exerts a force F_B on each ion. F_B is orthogonal to both the direction of motion of the ion and to the applied field. The magnitutude of F_B is given by

$$F_B = Bzev \qquad (1.1.2.1 - 3)$$

If the path of the ion-beam describes an arc of radius r, the centripetal force F_C can be expressed as

$$F_C = mv^2/r \qquad (1.1.2.1 - 4)$$

and a stable trajectory results when F_B equals F_C. Thus,

$$v = Bzer/m \qquad (1.1.2.1 - 5)$$

and substitution into (1.1.2.1 - 2) yields

$$m/z = eB^2r^2/2V \qquad (1.1.2.1 - 6)$$

Mass spectrometers of the type described above have a fixed radius of curvature. Since r is constant, scanning of the magnetic field (variation of B) or the accelerating voltage (variation of V) results in a scan of m/z for the ions passing through the collector slit and being detected.

If an ion leaves the source intact and fragments during acceleration, a broad peak, often corresponding to a non-integral mass is recorded. Such

ions are termed metastable.

The appearance of peaks corresponding to a metastable ion can be understood in terms of an ion of mass m_1 falling through a potential difference V_1 before decomposing to give an ion of mass m_2. The original ion is assumed to be formed with zero kinetic energy and fragmentation releases only a small amount of internal energy. If the ion and the neutral fragment formed in the dissociation traverse the remainder of the field together, then the ion of mass m_2 will enter the analyser region at velocity v, (cf. equation (1.1.2.1 - 2)).

$$m_2 v^2/2 = (m_2/m_1)\, z\, e\, V + z\, e\, (V - V_1) \qquad (1.1.2.1 - 7)$$

The ion traverses the magnetic field in an arc with a radius of curvature given by

$$r = \frac{m_2 v}{Bze} = \left(\frac{2V}{B^2 ze}\right)^{\frac{1}{2}} \left[\frac{m_2^2}{m_1}\left(1 + \frac{m_1 (V - V_1)}{m_2 V}\right)\right]^{\frac{1}{2}} \qquad (1.1.2.1 - 8)$$

The radius of curvature of an ion m^* (the metastable ion) is given by

$$r = \left(\frac{2V}{B^2 ze}\right)^{\frac{1}{2}} (m^*)^{\frac{1}{2}} \qquad (1.1.2.1 - 9)$$

Equating equations (1.1.2.1 - 8) and (1.1.2.1 - 9) and solving for m^* shows that a metastable transition gives rise to a peak in the spectrum at a position corresponding to m^* such that

$$m^* = \frac{m_2^2}{m_1}\left(1 + \frac{m_1 . (V - V_1)}{mV}\right) \qquad (1.1.2.1 - 10)$$

If dissociation of the parent ion occurs after full acceleration but immediately prior to entering the analyser, then $V_1 \approx V$ and equation (1.1.2.1 -10) reduces to

$$m^* = \frac{m_2^2}{m_1} \qquad (1.1.2.1 - 11)$$

The peaks corresponding to metastable ions are usually called metastable peaks, although the term is a misnomer.

1.1.2.2 Double-focusing mass spectrometers.

Double-focusing instruments incorporate an energy focusing sector in addition to the magnetic sector and the resolutions achieved with double-focusing instruments are much greater than those of single-focusing analysers due to the reduction of energy divergence of the ion beam. Energy focusing is achieved by passage of the ion-beam through a curved electostatic sector held at field strength E. The ion-beam describes a curved path, with the centripetal force on an ion (F_C) equal to Ee. Setting the centripetal force equal to the centrifugal force and solving for the radius of curvature (r) yields

$$r = mv^2/Ee \qquad (1.1.2.2 - 1)$$

Thus, the radius of trajectory of a given ion is dependent only on the energy of the ion. Ions of similar mass and

differing velocities will be separated by the electrostatic sector. Proper positioning of the collector slit results in the detection of ions which are focused in terms of both energy and momentum (i.e. double-focused) and resolutions of 10,000 to 75,000 are obtainable. At high resolutions, accuracy of a few parts per million enable ionic composition to be determined via exact mass analysis. Instruments in which the ion-beam passes through the electrostatic sector before being mass analysed are described as having conventional geometry. Although most double-focusing geometries provide double-focusing at a point, such as the Nier-Johnson configuration[5] (in which the ion-beam path is approximately semicircular), the Mattauch-Herzog[6] mass spectrometer (in which the direction of curvature is reversed through the magnetic sector) achieves double-focussing in a plane at the boundary of the magnetic sector and is thus ideal for detection by a photographic plate. The Nier-Johnson type of geometry is the more widely used of the two configurations. The analysis of metastable ions by linked scanning of the electrostatic and magnetic sectors will be discussed in section 1.2.

1.1.2.3 Quadrupole mass analysers

Quadrupole mass analysers, also known as quadrupole mass filters, are comprised of four parallel hyperbolic or circular rods held at a constant DC voltage (U) such that the sign of the potential is the same on

opposite rods. A radio frequency component (V_o cos wt, wt=2πf with f equal to the frequency) is superimposed on the DC voltage such that the potential difference (P.D.) between the two pairs of rods is

$$P.D. = U \pm V_o \cos wt \qquad (1.1.2.3 - 1)$$

An ion accelerated by a low potential (5 - 30 volts) into the volume between adjacent electrode of opposite polarity will oscillate as it passes through the mass filter. At a specific applied frequency, only ions of a given mass will undergo stable oscillation and reach the detectors. (Unless the ratio U/V_o is less than one, all ions will impinge on the negative electrodes). Since there is no further acceleration of the ions in the quadrupole field the ions pass through the field at their original velocity and with a low accelerating potential, a sufficient number of oscillations are undergone by the ions to produce low resolution mass separation. Mass scanning is usually obtained by varying U and V_o such that the ratio U/V_o is maintained at a constant value. A mass scan can also be obtained by varying the frequency with V and V_o kept constant, but mass calibration is more difficult. The resolution of a quadrupole mass analyser is limited by the precision with which the electrodes are aligned, the presence of contaminants on the electrode (pump oil, sample condensation, etc.) and errant motion due to thermal velocity components in the x or y directions, as well as the position of entry of the ions. Resolutions of 500-700

are typical, although resolutions greater than 1000 have been reported.

1.1.2.4 Time of flight mass spectrometers

In a time of flight mass spectrometer, ions are repelled out of the ion-source by a pulsed voltage of several nanoseconds duration and are accelerated into a field-free drift area by an accelerating voltage of several thousand volts. The constant velocities with which specific ions traverse the field-free drift area are determined by the accelerating voltage and will differ for ions of differing masses. Thus, by correlating arrival time at the detector with the time of initial voltage pulsation, the masses of the ions detected at any given moment can be determined. In practice, the repeller voltage is pulsed at a frequency of 10,000 to 50,000 hertz and for a 1-meter drift table, flight times of 1-30 x 10^{-6} seconds are typical. Although the ions are assumed to be formed in an infinitely narrow plane at zero thermal velocity, the resolution of a time-of-flight mass spectrometer (typically 500-600) is related to variations in the positions and velocities of the ions. Additional factors include the duration and sharpness of the pulsed repeller voltage as well as whether the ions are formed by continuous or pulsed electron impact.

If the velocity of the ions is assumed to originate primarily from the accelerating voltage, then the approximate time of flight of an ion can be

calculated as follows. Rearrangement of equation (1.1.2.1 - 2) gives

$$v = \sqrt{2 z e V/m} \qquad (1.1.2.4 - 1)$$

and, since the flight time t is equal to $v^{-1}\ell$, where ℓ equals the path length

$$t = \sqrt{m\ell^2/2 z e V} \qquad (1.1.2.4 - 2)$$

Thus, for ions of masses m_1 and m_2, the difference in time of flight (Δt) can be expressed as

$$\Delta t = (\sqrt{\ell^2/2 z e V}) (\sqrt{m_2} - \sqrt{m_1}) \qquad (1.1.2.4 - 3)$$

Since Δt is on the order of 10^{-7} to 10^{-8} seconds, the detection and amplification devices must have correspondingly fast response times and detection by an electron multiplier is required. The popularity of time of flight mass spectrometers ranks third behind magnetic sector and quadrupole instruments, respectively.

1.2 Methods for the elucidation of fragmentation pathways.

As discussed in section 1.1.2.1, the presence of metastable peaks in the mass spectrum of a compound can be helpful in assigning parent-daughter relationships between ions, but in the absence of abundant metastable peaks or in cases in which a metastable peak could conceivably be assigned to more than one transition, unambiguous determination of fragmentation pathways becomes more difficult. Several special scanning techniques used in conjunction with double-focusing instruments enable the ions formed by fragmentation of metastable ions to be detected directly. For example, if a metastable ion decomposes after acceleration and prior to entering the electrostatic sector of a conventional double-focusing mass spectrometer, the daughter ion alone will be transmitted when the accelerating voltage is increased (i.e. the ratio of V/E is increased).[7,8]

Since an ion produced by fragmentation after acceleration has only a fraction of the original kinetic energy of the metastable ion, an ion kinetic energy (I.K.E.) spectrum can be obtained by placing a detector between the sectors of a conventional double-focusing instrument and scanning the voltage across the electrostatic sector. The fraction of kinetic energy retained by the daughter ion is equal to m_2/m_1 (m_2 and m_1 defined as before) and thus the fractional mass loss for each

beam of ions detected is determined directly[9]. If a reversed geometry is employed, in which the magnetic sector precedes the electrostatic sector, the ions of interest can be mass analysed and daughter ions formed by fragmentation between the sectors analysed according to their kinetic energy as above.[10]

This technique produces mass analysed ion kinetic energy (M.I.K.E.) spectra, which enable specific parent-daughter relationships between ions to be determined unambiguously.

More recently, techniques have been developed in which two of the three parameters associated with double-focusing instruments (accelerating voltage V, electrostatic sector voltage E and magnetic field strength B) are scanned simultaneously. In one method, the daughter ions from a specific parent ion are detected by scanning E and V such that the ratio E^2/V is kept constant.[11a] Mass ranges are limited, however, by scans involving changes in accelerating voltage and variations in intensities can also occur. Such drawbacks are avoided by linked scanning of B and E.[11b]

A daughter ion of mass m_2 formed in the first field free region by fragmentation of an ion of mass m_1, will possess the same velocity as the parent ion (i.e. v_1), instead of the velocity it would normally possess if it were formed in the ion source. The field strengths B_1 and B_2, at which m_1 and m_2 are focused in a magnetic sector of radius r, can be expressed by:

$$B_1=m_1v_1/re \qquad (1.2 - 1)$$

and

$$B_2=m_2v_1/re \qquad (1.2 - 2)$$

respectively. For an electrostatic sector of radius r', the electric field strengths at which m_1 and m_2 are focused with the same velocity are:

$$E_1=m_1v_1^2/r'e \qquad (1.2 - 3)$$

and

$$E_2=m_2v_1^2/r'e \qquad (1.2 - 4)$$

Dividing equation (1.2 - 1) by (1.2 - 2) and (1.2 - 3) by (1.2 - 4) yields:

$$B_1/B_2 = m_1/m_2 \qquad (1.2 - 5)$$

and

$$E_1/E_2 = m_1/m_2 \qquad (1.2 - 6)$$

Thus, since then

$$B_1/B_2 = E_1/E_2 \qquad (1.2 - 7)$$

it becomes apparent that ions formed by fragmentation of a given parent ion in the first field free region of a double focusing mass spectrometer will be detected by a scan in which the ratio B/E remains constant:

$$B_1/E_1 = B_2/E_2 \qquad (1.2 - 8)$$

(and by extension)

$$B_1/E_1 = B_2/E_2 = B_3/E_3 = B_m/E_m \qquad (1.2 - 9)$$

The correct value of B/E for the detection of product ions corresponds to a particular energy and the resulting energy discrimination produces spectra of good resolution. This gain in resolution is at the expense of information about kinetic energy loss during fragmentation, which can be obtained from analysis of peak changes in a M.I.K.E. scan. The energy information is also retained by scans in which B^2/E is kept constant and metastable ions of constant mass are transmitted. A "precursor-ion" spectrum is thus obtained for a given ion formed in the first field free region. The ability to perform linked B and E scans on all types of double focusing instruments, independent of the order in which the ion-beam passes through the magnetic and electrostatic sectors is a great advantage.

In recent years, the technique of tandem mass spectrometry, in which two (or more) analysers are operated independently, has been developed by reseachers such as McLafferty, Jennings and Beynon, and has been reviewed.[12] The great advantage of tandem mass spectrometry, also known as multisector mass spectrometry, (m.s./m.s.), lies in the ability to select a specific ion and determine directly products arising from its reaction. In addition to studying unimolecular dissociation (metastable ion analysis), the ion-beam can be passed through a target gas in a cell between the analysers and products formed by collision induced dissociation or other ion-molecule reactions can be studied. Since

ions are selected specifically, m.s./m.s. can be used to determine unknowns in mixtures without the need for prior chemical separation and is thus an important analytical technique. Several combinations of various analyses are applicable, such as quadrupole/magnetic, magnetic/quadrupole or quadrupole/quadrupole, and the two sectors in a double focusing instrument can be employed in tandem as well. A preferable configuration has a quadrupole or magnetic analyser as the first sector. The data obtained from ms/ms is generally considered to be superior to that from linked scans, since the parent ion resolution is greater.[12]

1.3 Electron impact induced rearrangement of sulphides and sulphones.

1.3.1 Theoretical aspects.

As a physical description of the mass spectral behaviour of organic compounds, the quasi-equilibrium theory (Q.E.T.)[13] has gained general acceptance. The ionisation of a molecule occurs in ca. 10^{-15} seconds and yields the excited molecular ion via a Franck-Condon transition such that bond lengths are unchanged. A "quasi-equilibrium" is then established between all possible energy states by rapid transitions before fragmentation takes place. As a result, the probabilities for the various possible fragmentation of an ion are independent of the mode of ionisation, the structure of its precursors or the mechanistic route by which the decomposing ion was originally derived. Instead, the probability of an ion's decomposition by any given process is a function only of its internal energy and structure. Some of the possible energy states of an ion correspond to activated complexes which can undergo decomposition. The rate constant for a given reaction is a function of the energy state population of the activated complex relative to the population of all other energy states of the ion and can be described by the Rice-Rampsburger-Kassel-Marcus theory[14a]:

$$k = \frac{1}{h} \frac{Z^*}{Z} \frac{\Sigma P^*(E-E_a)}{\rho(E)} \qquad (1.3.1 - 1)$$

where E_a is the minimum energy at which an energy state can be populated for the reaction at minimum energy, h is Planck's constant, and Z and Z* are the partition functions for the adiabatic degrees of freedom of the ion and activated complex, respectively. $P^*(E-E_a)$ represents the number of energy states of the activated complex in the energy range $E-E_a$ and $\rho(E)$ is the state density of the ion. Only active degrees of freedom are able to contribute energy freely to bond dissociation, with the internal energy, E, distributed randomly over all degrees of freedom. One degree of freedom in the activated complex is transformed into the translational coordinate requiring E_a, allowing only $E-E_a$ to be available for distribution. The number of identical routes by which the reaction can occur is included in Z*/Z.

A simplified version of R.R.K.M. theory[14b] is often encountered in the literature and takes the form:

$$k=\nu(E-E_a/E)^{s-1} \qquad (1.3.1 - 2)$$

with ν equal to a frequency factor and s equal to the number of effective oscillators in the ion. Currently, theory is limited to the calculation of the spectra of only relatively simple molecules and a mechanistic approach has proved to be of far more practical use.

1.3.2. Sulphones

1.3.2.1. Dialkylsulphones

With the exception of dimethyl and methylethyl sulphones, the spectra of saturated dialkylsulphones are dominated by hydrocarbon fragments.[15-19] Dialkylsulphones, as a class, do not undergo skeletal rearrangement although hydrogen migration gives ions arising from loss of an alkene or alkenyl moiety from the molecular ion[15,16,17]. For example, ethene is lost from diethylsulphone to give $RSO_2H^{+\cdot}$[17] (Scheme 1.3.2.1 - 1) and $RSO_2H_2^{+}$ arises via double hydrogen rearrangement in the spectra of higher members, such as di-n-butylsulphone[17] (Scheme 1.3.2.1 -2).

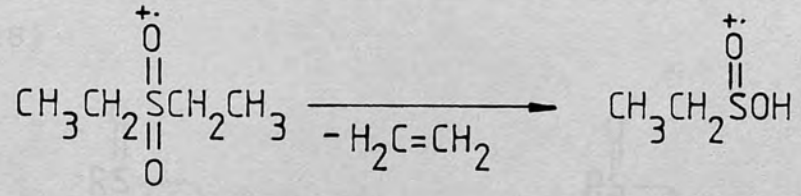

Scheme 1.3.2.1 -1

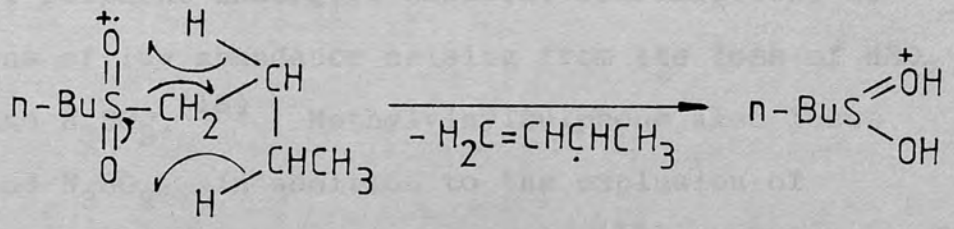

Scheme 1.3.2.1 -2

Deuterium labelling experiments have shown that hydrogen migrations to sulphonyl oxygens associated with the loss of an alkene or alkenyl moiety are not site-specific[16] (thus Scheme 1.3.2.1 -2 is a representation of only one possible mechanism). The prevalent hydrocarbon fragments arise from further decomposition of the $\{M\text{-alkene}\}^{+\cdot}$ and $\{M\text{-alkenyl}\}^{+}$ ions. Cleavage of the β C-C bond with hydrogen migration is also observed in the spectra of derivatives having alkyl chains larger than ethyl.[16] The loss of a hydroxyl radical from the molecular ion is a minor process in dialkylsulphones having γ-hydrogens on a secondary carbon. This site specificity has been proven by labelling experiments and the loss of hydroxyl can be envisaged to proceed via a McLafferty rearrangement:[16]

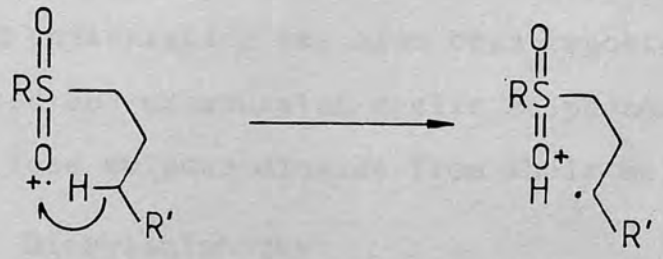

Scheme 1.3.2.1 - 3

Dimethyl sulphone undergoes skeletal rearrangement to give ions of low abundance arising from the loss of $HSO_2\cdot$, H_2SO_2 and $H_3SO_2\cdot$.[18] Methylvinylsulphone also loses $HSO_2\cdot$ and $H_3SO_2\cdot$ in addition to the explusion of sulphur dioxide from the molecular ion[18]. The second most abundant ion in the spectrum of methylvinylsulphone

corresponds to CH_3SO^+.[19] Analogous ions are generally of low abundance in the mass spectra of saturated dialkylsulphones and arise via loss of oxygen from the RSO_2^+ ion. The CH_3SO^+ ion in the spectrum of methylvinylsulphone can arise via prior sulphone-sulphinate rearrangement of the molecular ion (i.e. migration of the vinyl group from sulphur to oxygen, as shown in Scheme 1.3.2.1 - 4) analogous to the migration of vinyl groups observed in vinylarylsulphones (see section 1.3.2.3).

Scheme 1.3.2.1 -4

The sulphone-sulphinate rearrangement of cyclic sulphones containing β unsaturation has also been reported.[20] Some saturated and unsaturated cyclic sulphones have been reported to lose sulphur dioxide from their molecular ions.[20,21]

1.3.2.2 Diarylsulphones

Electron impact induced rearrangements reported for diarylsulphones include the loss of a hydroxy radical[22], sulphur dioxide[22,23], $HSO_2\cdot$ [22], H_2SO_2[22] and water[22] from the molecular ion. Sulphone -sulphinate rearrangements are also a common feature[22,24] and, as Scheme 1.3.2.2 - 1 shows, migration of either aryl group may occur in diarylsulphones having dissimilar aryl substituents.[22,24]

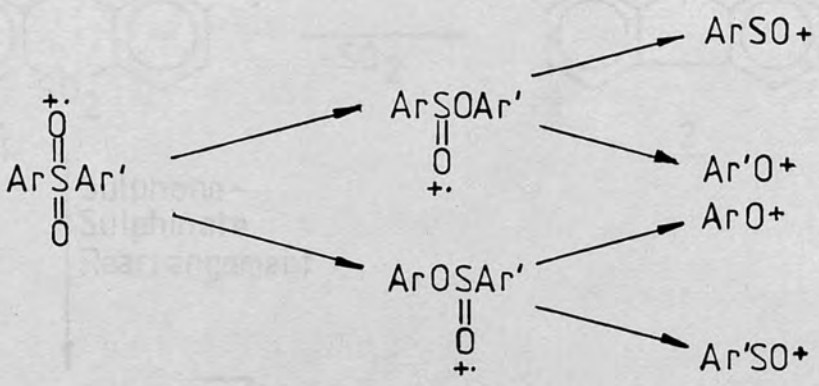

Scheme 1.3.2.2 - 1

Since the migration of an aryl group indicates that the electron deficiency is largely localised in a non-bonding oxygen orbital, aryl groups which are better able to donate electrons should migrate preferentially.[25a] In fact, the migratory aptitude of the phenyl group has been shown to increase with increasing substitution by methyl groups.[22]

Aromatic heterocyclic sulphones also undergo skeletal rearrangement and have been shown to lose sulphur dioxide (e.g. 1 → 2) [26,27] The presence of sulphone-sulphinate rearrangement is evidenced by the appearance of $\{M-SO\}^{+\cdot}$ ions in the mass spectra of 1.[27]

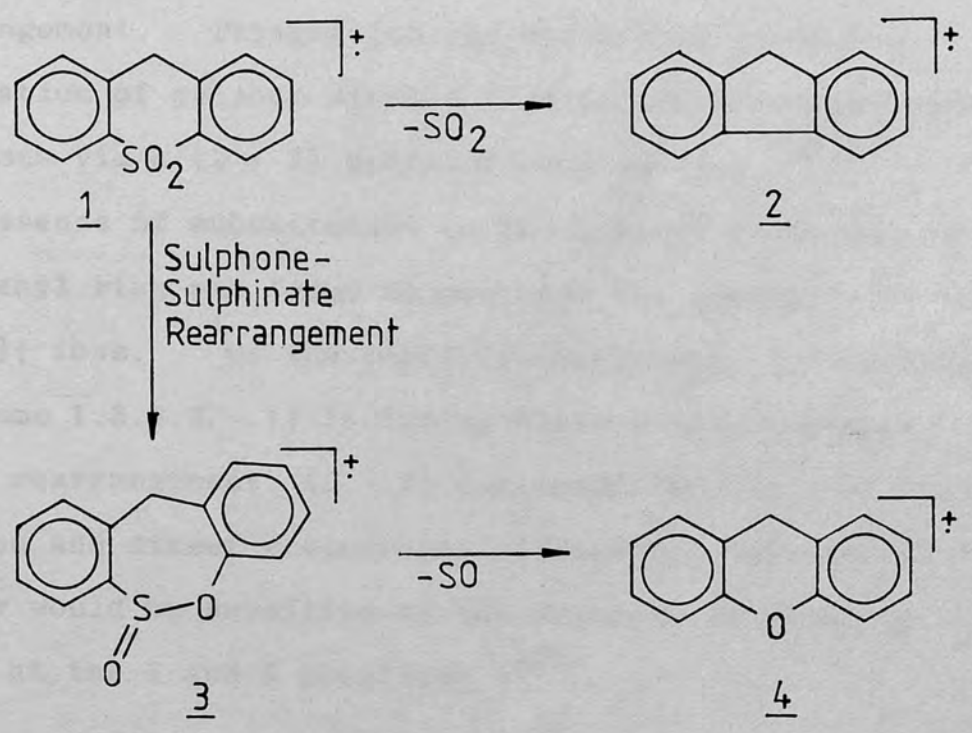

Scheme 1.3.2.2 - 2

1.3.2.3 Alkylarylsulphones

Alkylarylsulphones bearing saturated alkyl groups do not undergo skeletal rearrangement via extrusion of sulphur dioxide, $HSO_2\cdot$ or H_2SO_2[15,17,28]. The loss of sulphur dioxide has been noted, however, in the spectrum of 2-chloroethyl-p-nitrophenylsulphone[29]. Hydrogen migrations to sulphonyl oxygen occur in the molecular ion of n-hexylphenylsulphone[17] and in some 2-hydroxyethyl-sulphones[29], leading to the loss of a hydroxyl radical or $HSO_2\cdot$, respectively. The elimination of sulphur dioxide from vinylarylsulphones[30,31] allylarylsulphones[32]

and propynylarylsulphones[33] suggest that the presence of unsaturation in the alkyl group facilitates skeletal rearrangement. Thyagarajan and Bates have shown that elimination of sulphur dioxide from propynylphenylsulphone, 5, arises via a {2 + 2} cycloaddition pathway [33,34]. The presence of substituents on the 2 and 6 positions of the phenyl ring was found to decrease the abundance of the $\{M-SO_2\}^{+\cdot}$ ions. Of the possible mechanisms, (illustrated in Scheme 1.3.2.3 - 1) including Claisen rearrangement, Smiles rearrangement, {2 + 2} cycloaddition, {2 + 4} cycloaddition and direct chelotropic elimination, only the {2 + 2} pathway would be sensitive to the presence of blocking groups at the 2 and 6 positions.[33]

Possible Pathways for Elimination of SO_2 from Arylpropynylsulphones

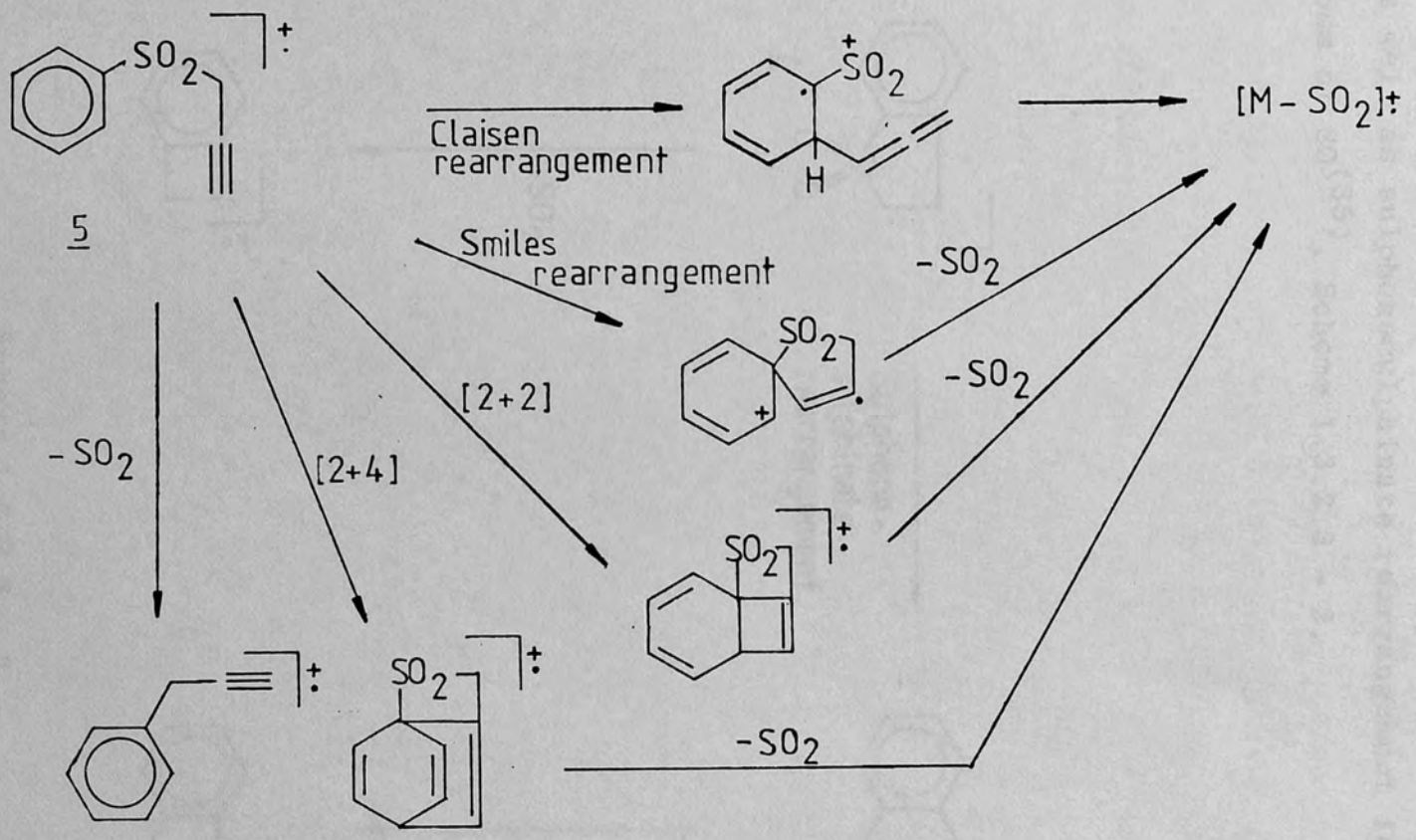

Scheme 1.3.2.3 - 1

The loss of SO_2 also occurs from the molecular ion of 2,3-dihydro-benzo{b}thiophene-1,1-dioxide, 6, as well as sulphone-sulphinate rearrangement followed by loss of SO[35], Scheme 1.3.2.3 - 2.

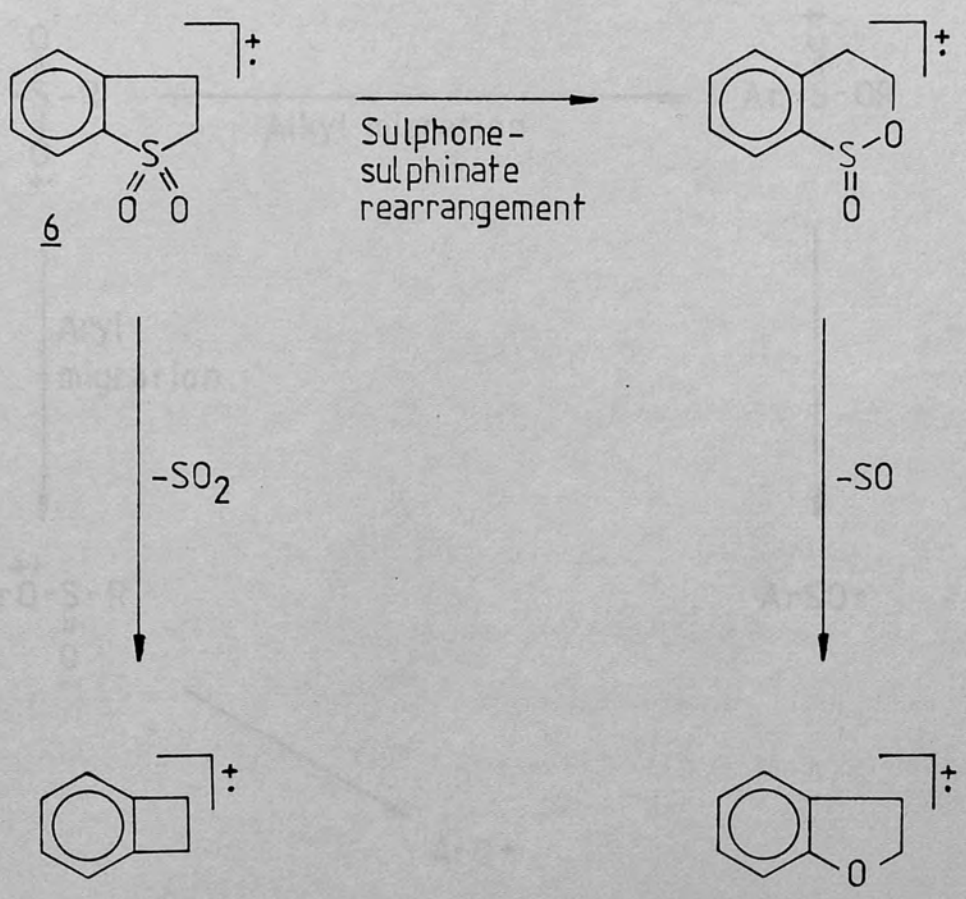

Scheme 1.3.2.3 - 2

Generally, in the mass spectra of alkylarylsulphones, sulphone-sulphinate rearrangements predominate over the elimination of sulphur dioxide.[15,24,28,29,30,36-38]

A further consideration in the sulphone-sulphinate rearrangements of alkylarylsulphones is the possibility of alkyl versus aryl migration to the sulphonyl oxygens (Scheme 1.3.2.3 - 3).

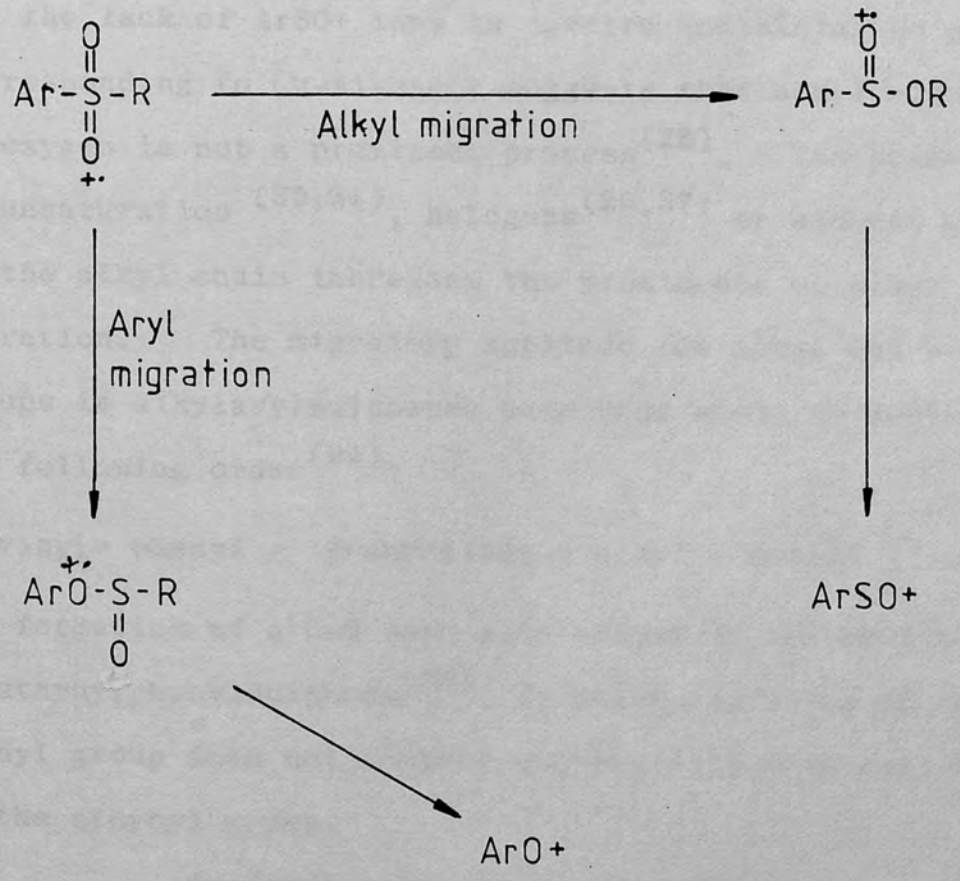

Scheme 1.3.2.3 - 3

In simple alkylarylsulphones, such as methylarylsulphones,[28,38] ethylarylsulphones,[28] i-propylarylsulphones[28] and t-butylarylsulphones[28], the ratio of relative abundances of ArO+ versus ArSO+ decreases with increased size and branching of the alkyl chain. However, the ArSO+ ions may be formed by the loss of a hydroxyl radical from the $\{M\text{-alkene}\}^{+\cdot}$ ions (analogous to those found in the spectra of dialkylsulphones) as well as *sulphone-sulphinate* rearrangement and the lack of ArSO+ ions in spectra containing no peaks corresponding to $\{M\text{-alkene}\}^{+}$ suggests that alkyl migration to oxygen is not a prominent process[28]. The presence of unsaturation[30,31], halogens[29,37] or hydoxyl groups[29] on the alkyl chain increases the prominence of alkyl migration. The migratory aptitude for alkyl and aryl groups in alkylarylsulphones have been shown to decrease in the following order[24]:

vinyl> phenyl > β-substituted ethyl > methyl

The formation of a C-O bond also occurs in the molecular ion of ethynylphenylsulphone[39], in which migration of the phenyl group does not compete successfully with migration of the ethynyl group.

Skeletal rearrangement involving the migration of chlorine or a hydroxyl group from the alkyl chain with concomitant elimination of an alkene has been observed in studies of β-substituted ethylarylsulphones.[40] This rearrangement, illustrated for 2-chloroethylphenylsulphone 7 in Scheme 1.3.2.3 - 4, is postulated to proceed through

a McLafferty-type rearrangement of the molecular ion.

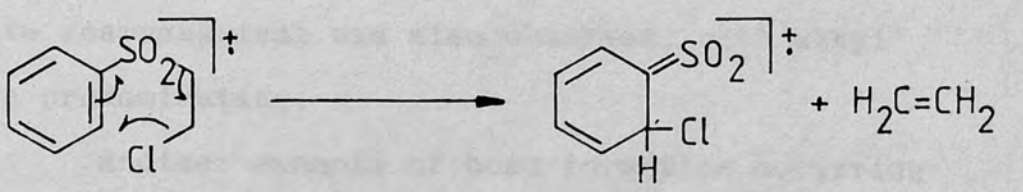

7

Scheme 1.3.2.3 - 4

An unusual rearrangement, resulting in the formation of a C-S bond between the sulphur of a β-arylthio group and a phenyl ring carbon was noted in the mass spectra of trans-1-arylsulphonyl-2-arylthiopropenes, 8 (41). The molecular ion is postulated to rearrange in a manner similar to the Smiles rearrangement (42) to yield a bisarylsulphide ion, 9.

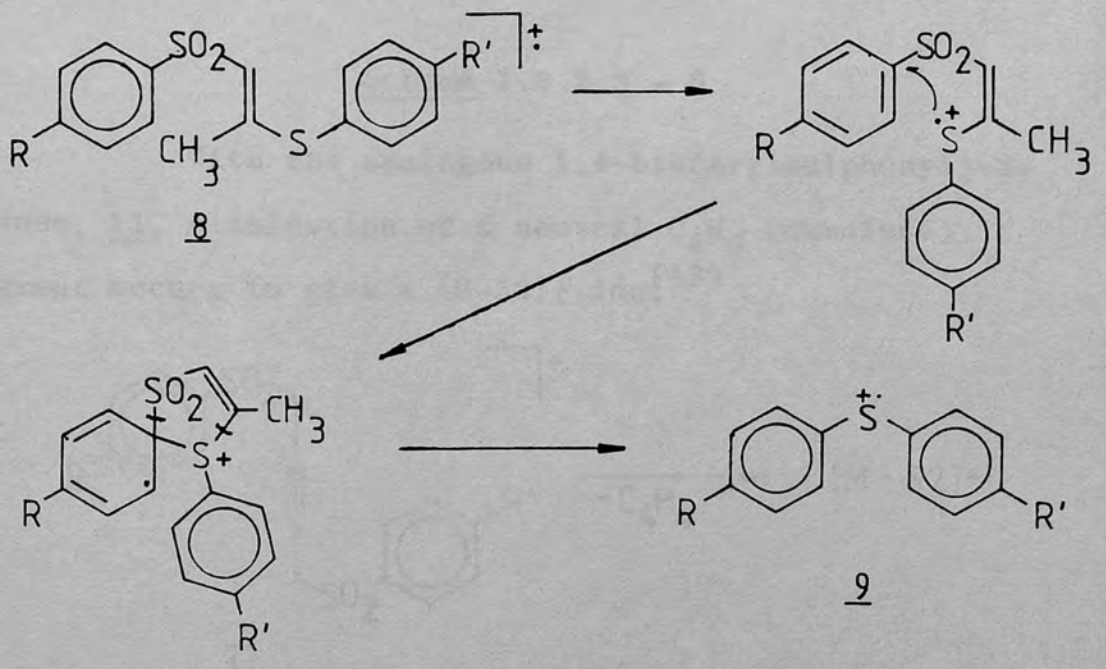

Scheme 1.3.2.3 - 5

The intensities of the bisarylsulphide ion were in the region of 4.34 to 10.33% Σ at 20 eV. Sulphone-sulphinate rearrangement was also observed, with alkyl migration predominating.

Another example of bond formation occurring under electron impact conditions is the elimination of a neutral C_4H_6 moiety (butadiene) from the molecular ions of 1,4-bis(arylsulphonyl)-2-butenes[32], 10.

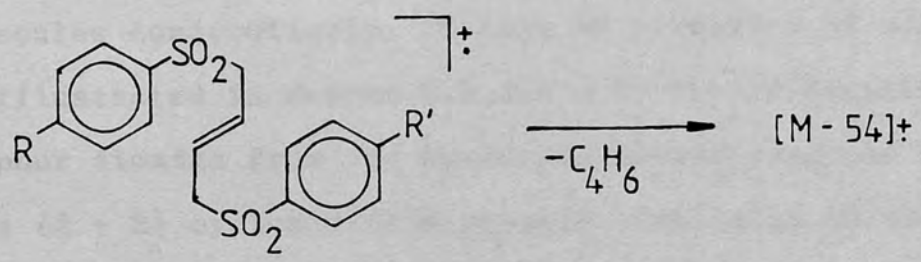

10

Scheme 1.3.2.3 - 6

With the analogous 1,4-bis(arylsulphonyl)-2-butynes, 11, elimination of a neutral C_4H_4 (cumulene) fragment occurs to give a {M-52}+ ion.[43]

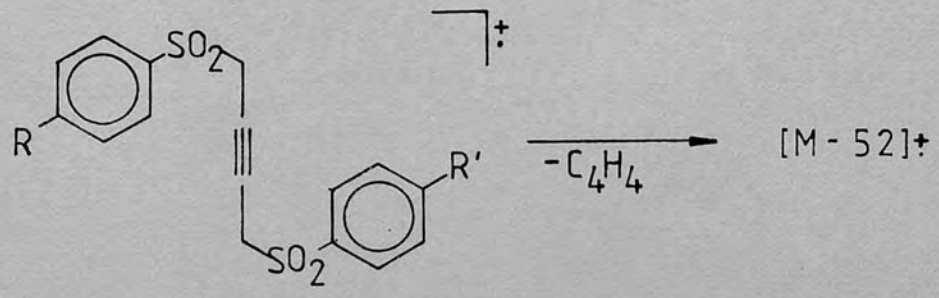

11

Scheme 1.3.2.3 - 7

Although the elimination of cumulene could arise from a Claisen rearrangement or a direct interaction pathway, thermal Claisen rearrangements of propynylarylsulphones are not known and the direct interaction pathway was preferred.[43] Interestingly, neither 10 nor 11 exhibited loss of sulphur dioxide.

Further support for the direct interaction mechanism was provided by a study of 1,6-bis(arylsulphonyl)-2,4-hexadiynes, 12 which extrude two sulphur dioxide molecules consecutively, in lieu of formation of $\{M-76\}^{+\cdot}$.[44] As illustrated in Scheme 1.3.2.3 - 8, the elimination of sulphur dioxide from the hexadiyne derivatives can occur by a {2 + 2} cycloaddition pathway, analogous to that postulated for propynylarylsulphone.

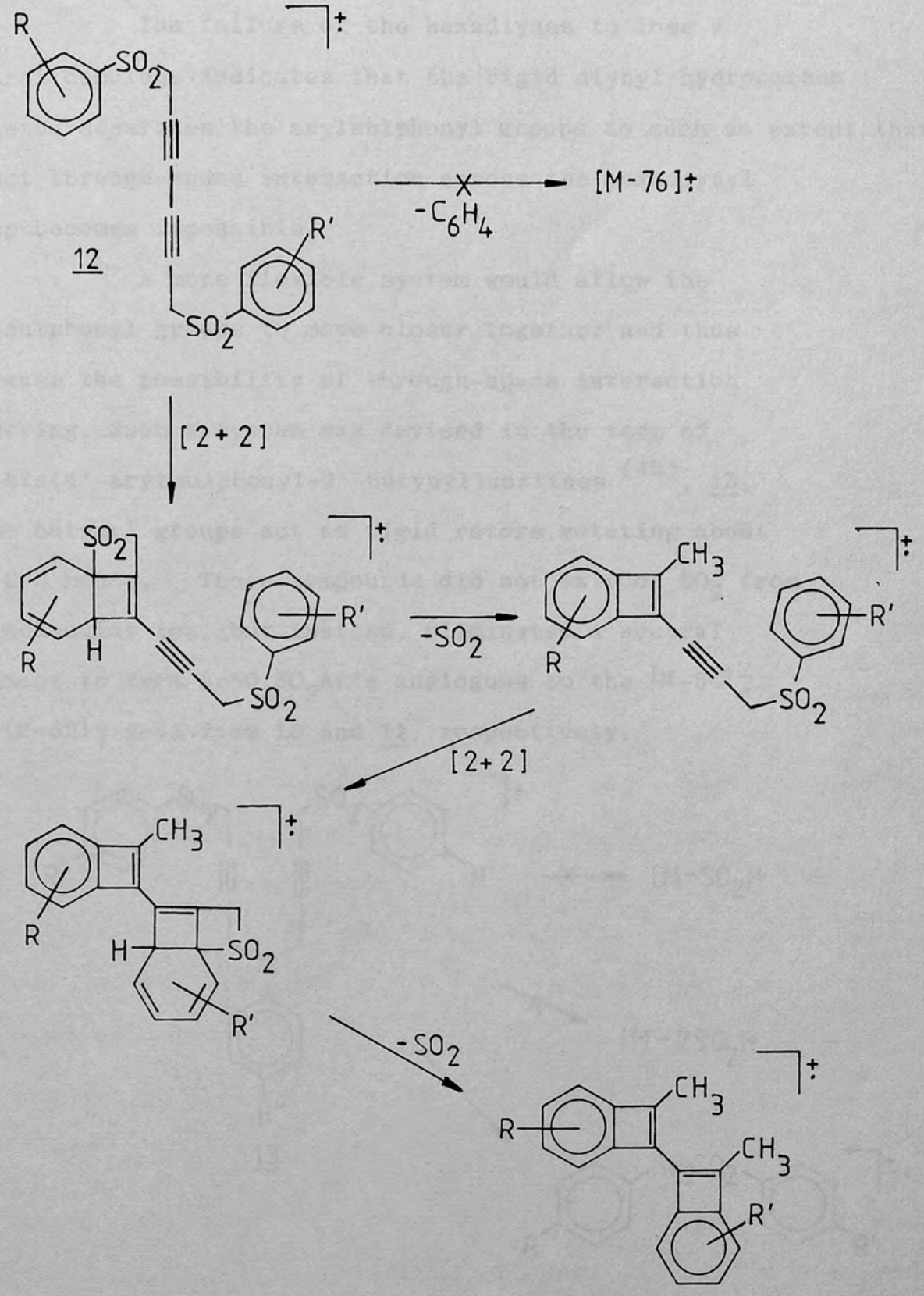

Scheme 1.3.2.3 - 8

The failure of the hexadiynes to lose a neutral cumulene indicates that the rigid diynyl hydrocarbon skeleton separates the arylsulphonyl groups to such an extent that direct through-space interaction across the hexadiynyl group becomes impossible.

A more flexible system would allow the arylsulphonyl groups to move closer together and thus increase the possibility of through-space interaction occurring. Such a system was devised in the form of N,N-bis(4'-arylsulphonyl-2'-butynyl)anilines [45], 13, whose butynyl groups act as rigid rotors rotating about the C-N bonds. These compounds did not extrude SO_2 from the molecular ion, but instead, eliminated a neutral fragment to form $ArSO_2SO_2Ar'^{\ddagger}$ analogous to the $\{M-54\}^{\ddagger}$ and $\{M-52\}^{\ddagger}$ ions from 10 and 11, respectively.

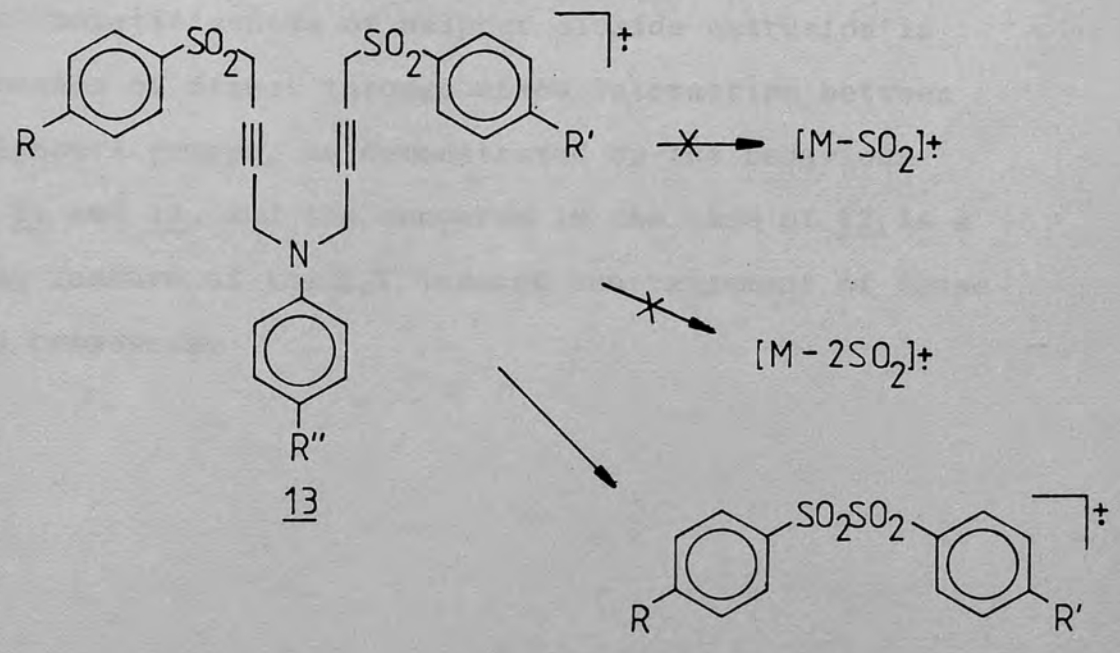

Scheme 1.3.2.3 - 9

As in the case of 10 and 11 the formation of $ArSO_2SO_2Ar'^{+\cdot}$ from the molecular ion was proposed to occur via the direct interaction pathway, shown in Scheme 1.3.2.3 - 10.

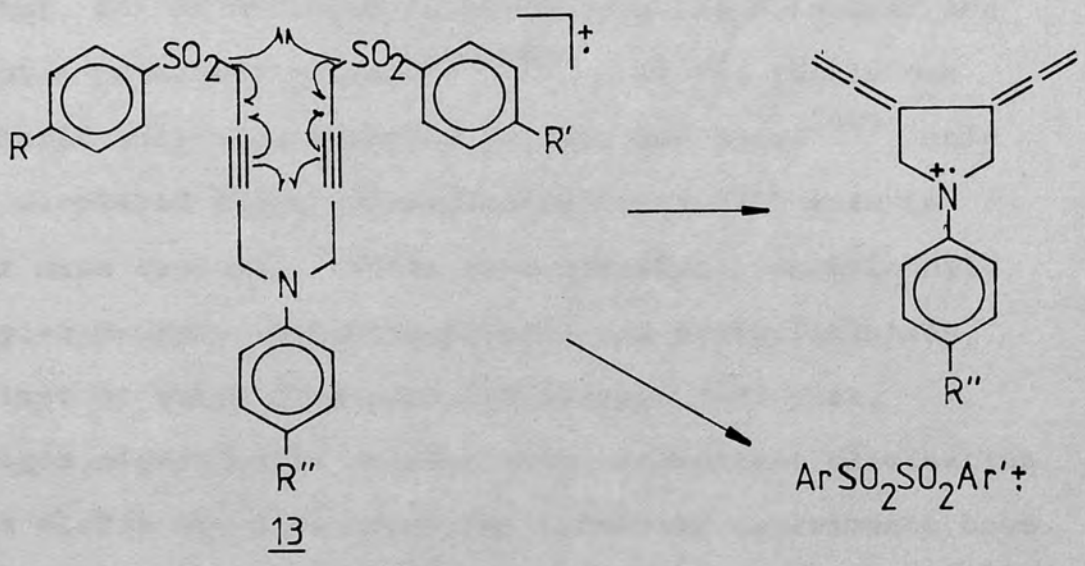

Scheme 1.3.2.3 -10

The non-competitiveness of sulphur dioxide extrusion in the presence of direct through-space interaction between the sulphonyl groups, as demonstrated by the behaviour of 10, 11 and 13, and the converse in the case of 12, is a striking feature of the E.I. induced rearrangement of these related compounds.

1.3.3 Sulphides

1.3.3.1 Dialkylsulphides

Mass spectral studies of saturated aliphatic dialkylsulphides have shown that the elimination of sulphur, HS· or hydrogen sulphide from the molecular ion is not a prominent process[46-49]. Of the thirty one aliphatic sulphides reported by Levy and Stahl[46], only five displayed peaks corresponding to $\{M-32\}^{+\cdot}$ ions in their mass spectra. These were dimethyl-, methylethyl-, methyl-n-propyl-, methylisopropyl- and diethylsulphide, the last of which displayed the largest M-32 peak. Hydrogen migration to sulphur with concomitant elimination of an olefin may also occur and labelling experiments have shown the migrating hydrogens to originate mainly from the β-position, although donation by other sites is also possible.[35]

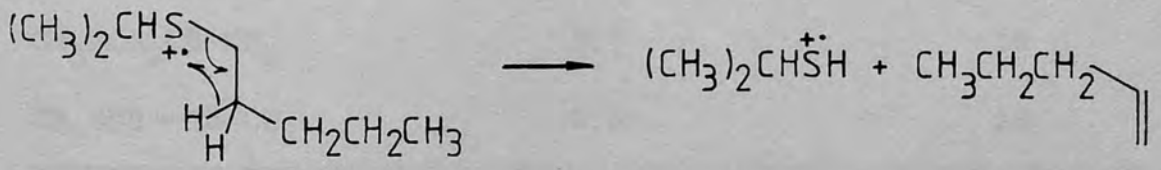

Scheme 1.3.3.1 - 1

The introduction of unsaturation into the alkyl chain significantly increases the relative abundance of ions arising from skeletal rearrangement. This is particularly evident with methylvinyl sulphide in

comparison with methylethylsulphide, when the relative abundances of the corresponding $\{M-SH\}^+$ ions are considered. Table 1.3.3.1 - 1 contains the relative abundances of the $\{M-SH\}^+$ ions for methylethylsulphide, methyl-n-propylsulphide and some of their unsaturated analogues.

TABLE 1.3.3.1 - 1

Relative abundances of $\{M-HS\}^+$ ions in the mass spectra of some saturated and unsaturated dialkylsulphides.

Compound	Relative Abundance of $\{M-HS\}^+$ Ion	Reference
$CH_3SCH_2CH_3$	0.5	46
$CH_3SCH=CH_2$	95.1	18
$CH_3SC\equiv CH$	10.0	18
$CH_3SCH_2CH_2CH_3$	0.8	46
$CH_3SCH_2CH=CH_2$	2.6	18
$CH_3SCH=CH-CH_3$	5.5	18

The skeletal rearrangements of alicyclic thioethers predominately involve the loss of hydrocarbon fragments, e.g. the losses of a methyl radical from ethylenesulphide[50] and thiacyclohexane[51] 14, ethylene from thiacyclopentane[52], and an ethyl radical from thiacycloheptane[51]. All such eliminations result in ring contraction, as in Scheme 1.3.3.1 - 2.

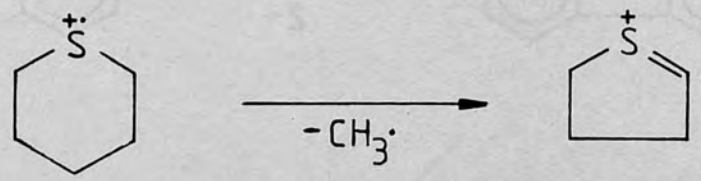

14

Scheme 1.3.3.1 - 2

The loss of HS· from the molecular ions of thiacyclopentane,[52] -hexane[51] and -heptane[57] has also been observed.

1.3.3.2 Diarylsulphides

The mass spectra of diarylsulphides have not received as much attention as dialkylsulphides, but skeletal rearrangements have been reported for some of those studied. Diphenylsulphide gives rise to $\{M-S\}^{+\cdot}$ $\{M-HS\}^{+}$, $\{M-H_2S\}^{+\cdot}$ and $\{M-H_3S\}+$ ions in its mass spectrum [23,53-55]. Peaks corresponding to $\{M-H_3S\}^{+}$ are also present in the mass spectrum of benzylphenylsulphide.[54] The presence of significant substitution scrambling in the molecular ion of diphenyl sulphide is indicated by the presence of $\{M-CH_3\}^{+}$ and $\{M-CS\}^{+\cdot}$ ions in its mass spectrum[55].

A noteworthy sequential loss of two sulphurs from 15 has also been reported.[56]:

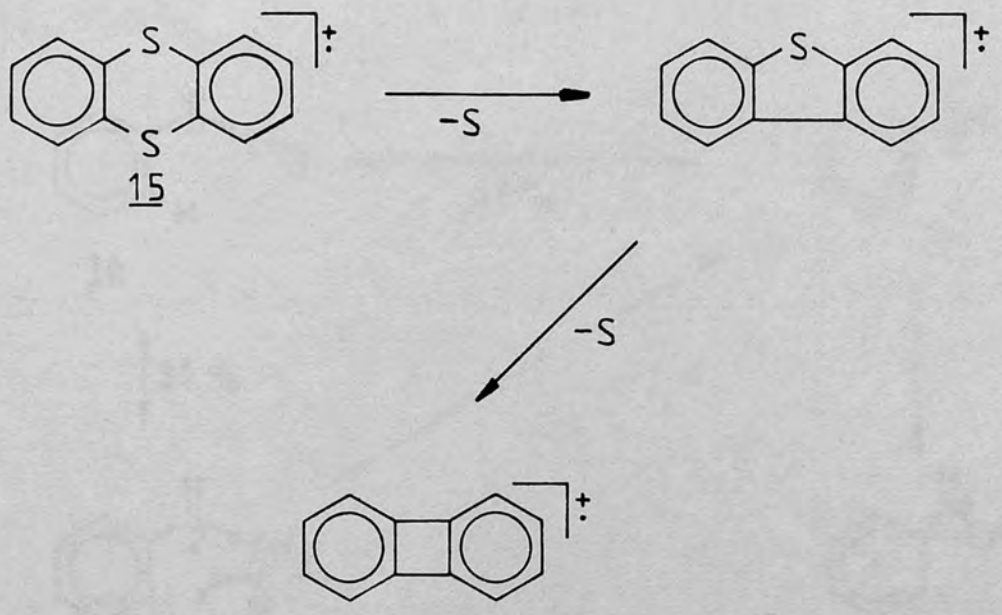

Scheme 1.3.3.2 - 1

1.3.3.3 Alkylarylsulphides

Hydrogen migration to sulphur accompanying the elimination of HS· occurs in the molecular ions of alkylarylsulphides bearing the shortest, nonbranched alkyl groups[23,28,57-59]. Deuterium labelling studies[57] of methylphenylsulphide, 16, established that 69% of the migrating hydrogens are derived from the methyl group. A rearrangement pathway for the formation of the tropylium ion, 17, via loss of HS· from 18 or 19, as shown in Scheme 1.3.3.3 - 1, was proposed for the skeletal rearrangement of 16.[57]

For comparison, the relative abundance of the $\{M-HS\}^+$ ion in the mass spectra of some alkylarylsulphides are collected in Table 1.3.3.3 -1.

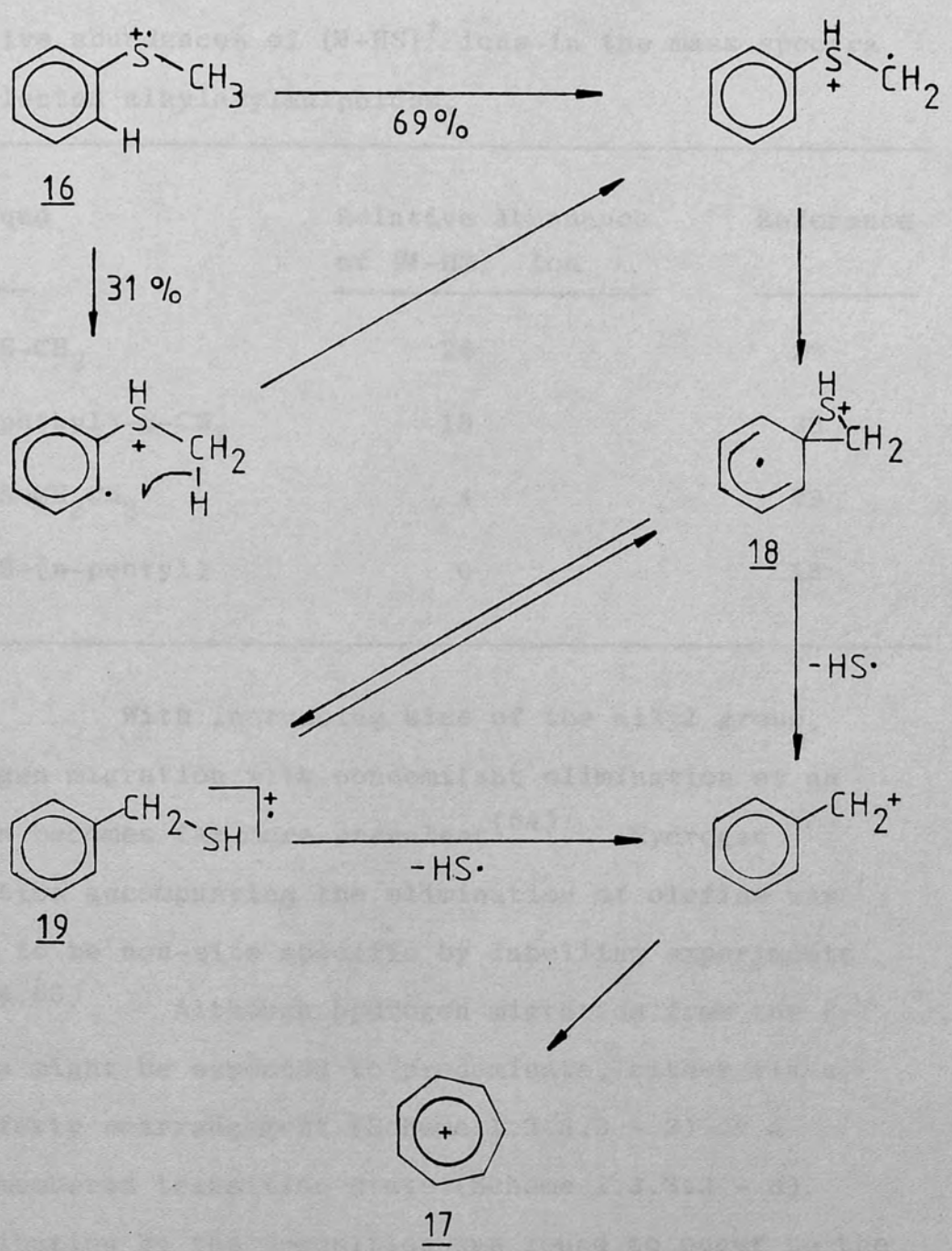

Scheme 1.3.3.3 - 1

TABLE 1.3.3.3 - 1

Relative abundances of $\{M-HS\}^+$ ions in the mass spectra of selected alkylarylsulphides.

Compound	Relative Abundance of $\{M-HS\}^+$ Ion	Reference
C_6H_5-S-CH_3	26	23
(2-naphthyl)-S-CH_3	13	23
C_6H_5-S-CH_2CH_3	4	23
C_6H_5-S-(n-pentyl)	0	18

With increasing size of the alkyl group, hydrogen migration with concomitant elimination of an olefin becomes far more prevalent[54]. Hydrogen migration accompanying the elimination of olefins was shown to be non-site specific by labelling experiments [48,54,60]. Although hydrogen migration from the β-carbon might be expected to predominate, either via a McLafferty rearrangement (Scheme 1.3.3.3 - 2) or a four membered transition state (Scheme 1.3.3.3 - 3), contribution by the β-position was found to occur to the extent of only 19%[60].

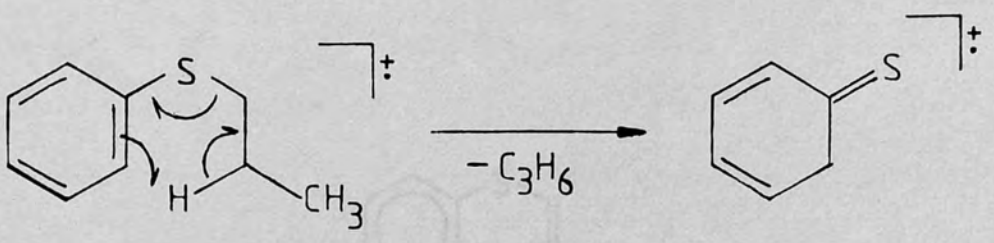

Scheme 1.3.3.3 -2

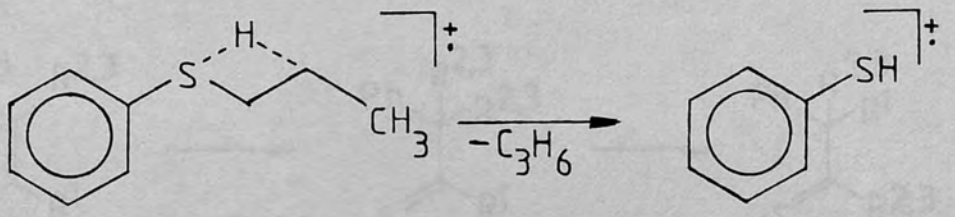

Scheme 1.3.3.3 - 3

As in the case of alkylarylsulphones (see section 1.3.2.3), the presence of unsaturation in the alkyl group is marked by an increase in skeletal rearrangements, e.g. the relative abundance of the $\{M\text{-}HS\}^+$ ion in the mass spectrum of 20 is 39%[54], which is higher than that observed in the spectrum of methylphenylsulphide (see Table 1.3.3.3 - 1).

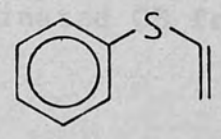

20

Weringa studied a number of phenylvinylsulphides, 21, and observed the formation of $\{R^{1,2,3}CS\}^+$ and $\{PhCS\}^+$(61) In addition, $\{M-HS\}^+$, $\{M-H_2S\}^{+\cdot}$ and $\{M-H_3S\}^+$ ions were also formed. Scheme 1.3.3.3 - 4 illustrates the mechanism proposed by Weringa.

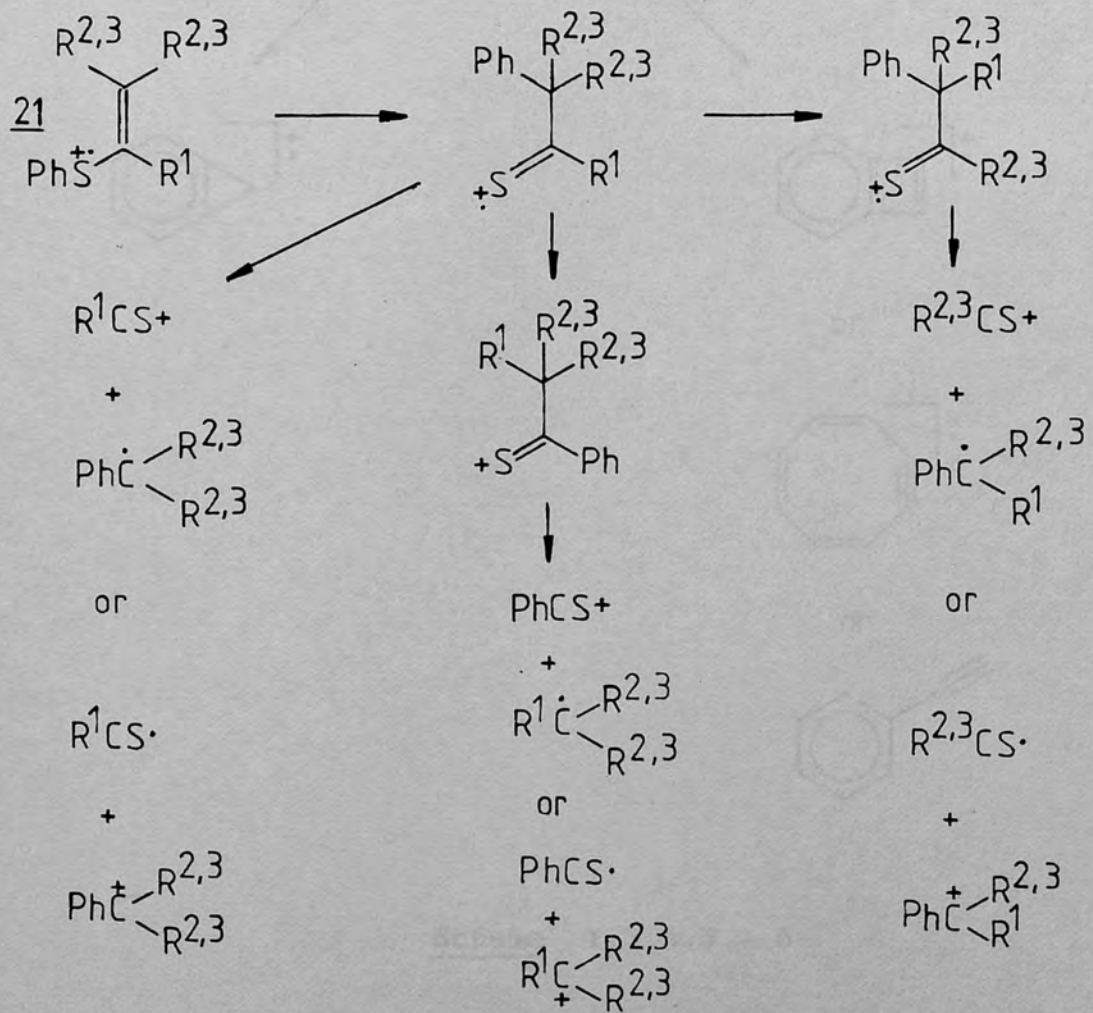

Scheme 1.3.3.3 - 4

The loss of sulphur from benzo{b}thiophen, 22, and 2-phenylthiephen was reported by Porter[55]. These cyclic systems also eliminated CS from the molecular ion.

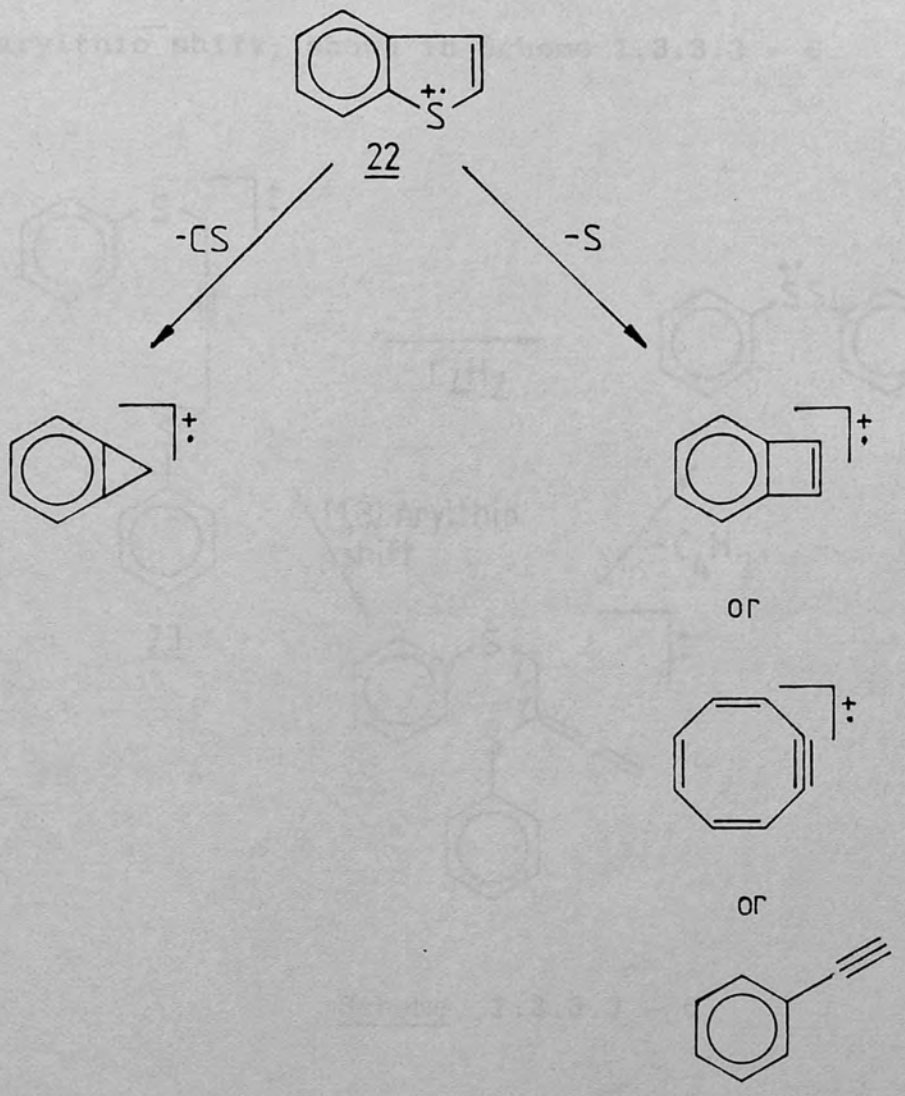

Scheme 1.3.3.3 - 5

The molecular ions of 1,4-bis(arylthio)-2-butynes[62], 23, and 1,6-bis(arylthio)-2,4-hexadiynes[44], 24, eliminate a neutral cumulene to give rise to bisaryldisulphide ions. The elimination of a cumulene from 23 can occur without the need for prior rearrangement and would be similar to the formation of the $\{M-52\}^+$ ion from 1,4-bis(arylsulphonyl)-2-butynes (see section 1.3.2.3). Alternatively, the elimination may occur after an initial {1,3} arylthio shift, shown in Scheme 1.3.3.3 - 6.

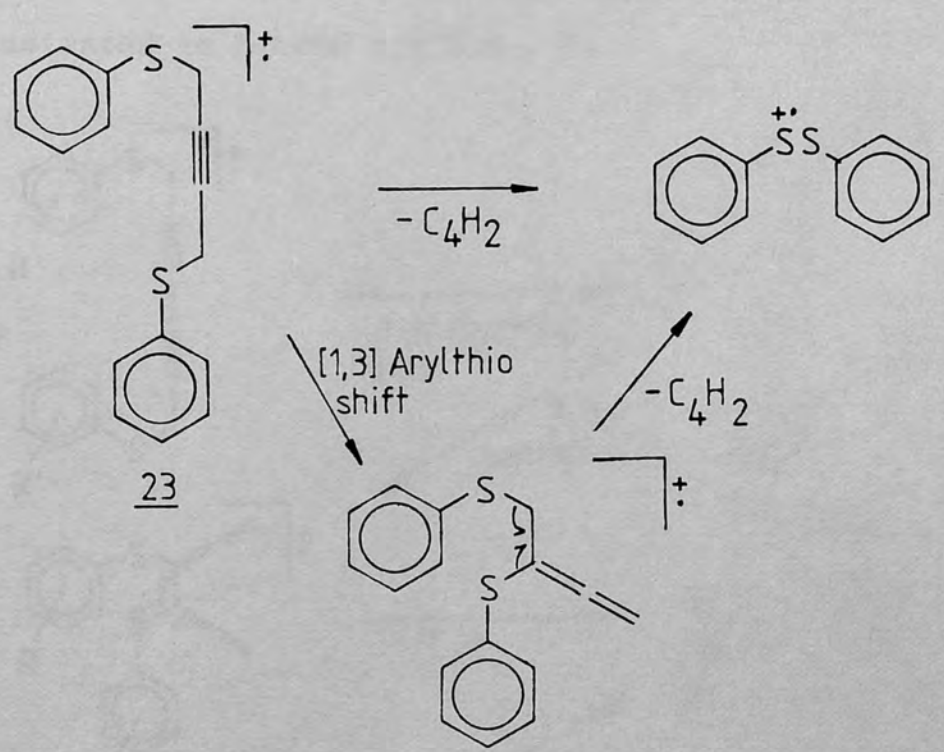

Scheme 1.3.3.3 - 6

However, in the case of 24, the intervening six-carbon chain prevents the occurrence of direct through space interaction between the sulphurs in the unrearranged molecular ion. Such interaction was not observed in the corresponding bissulphones (section 1.3.2.3) and should not be present in 24. At least one arylthio shift is required to bring the sulphurs within a distance approximate to that in 23, and a second arylthio shift of either arylthio group is then possible, bringing the two sulphurs into even greater proximity, as illustrated in Scheme 1.3.3.3 - 7.

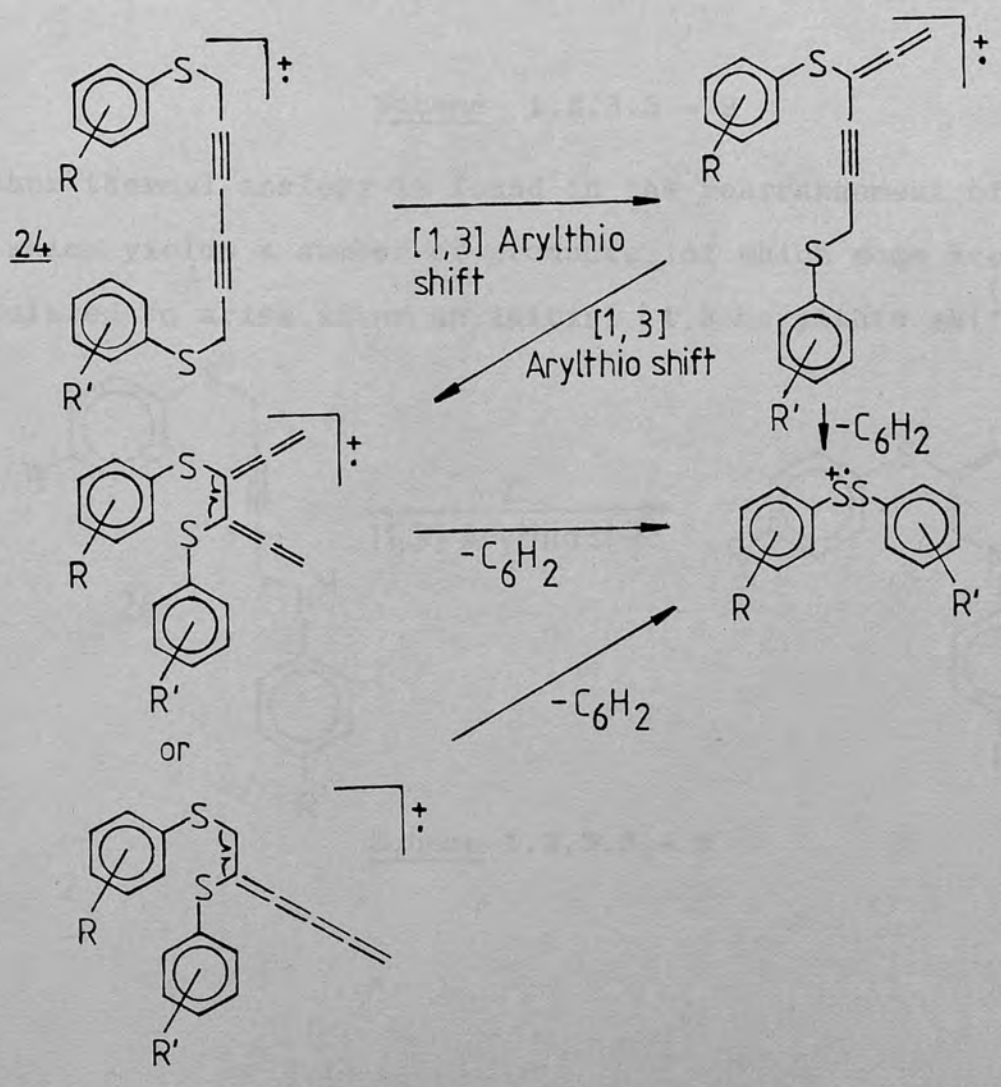

Scheme 1.3.3.3 - 7

Such arylthio migrations find ample thermal analogies in the rearrangements of propynylarylsulphides (25, R=H), and butynylarylsulphides (25, R=CH_3), as reported by Kwart and George.(63)

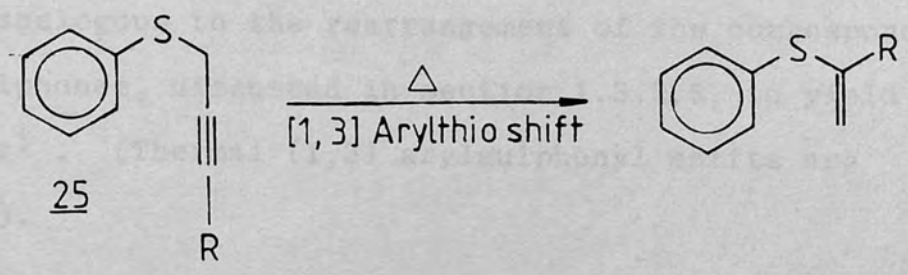

Scheme 1.3.3.3 - 8

Another thermal analogy is found in the rearrangement of 26, which yields a number of products, of which some are postulated to arise after an initial {1,3} arylthio shift.(64)

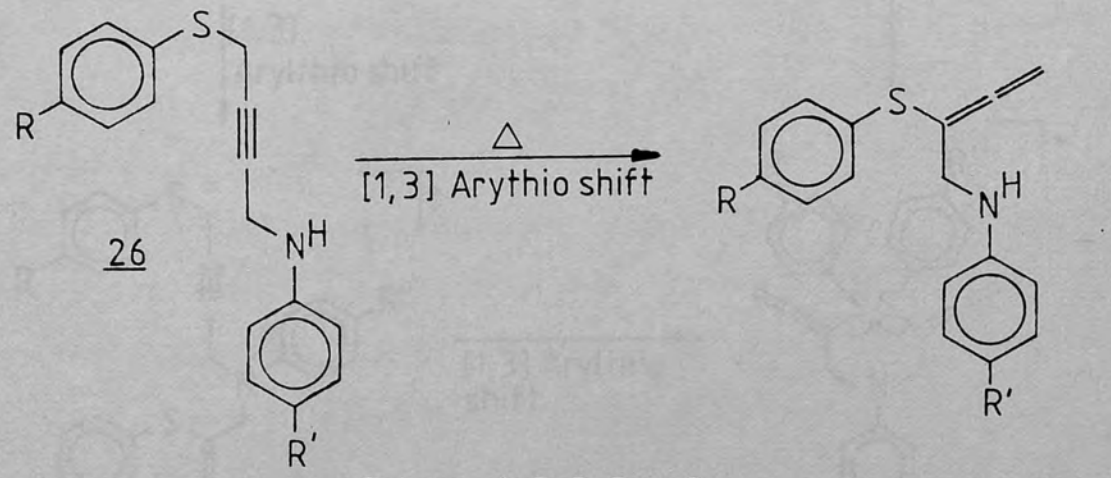

Scheme 1.3.3.3 - 9

Bisaryldisulphide ions were also formed from the E.I. induced rearrangement of N,N-bis(4'-arylthio-2'-butynyl) anilines, 27.[45] As depicted in Scheme 1,3.3.3 - 10, the bisaryldisulphide ions can be formed directly from 27, or via intermediate ions 28 and 29, by means of one and two arylthio shifts, respectively. The direct formation route is analogous to the rearrangement of the corresponding bissulphones, discussed in section 1.3.2.3, to yield $ArSO_2SO_2Ar^{+\cdot}$. (Thermal {1,3} arylsulphonyl shifts are not known).

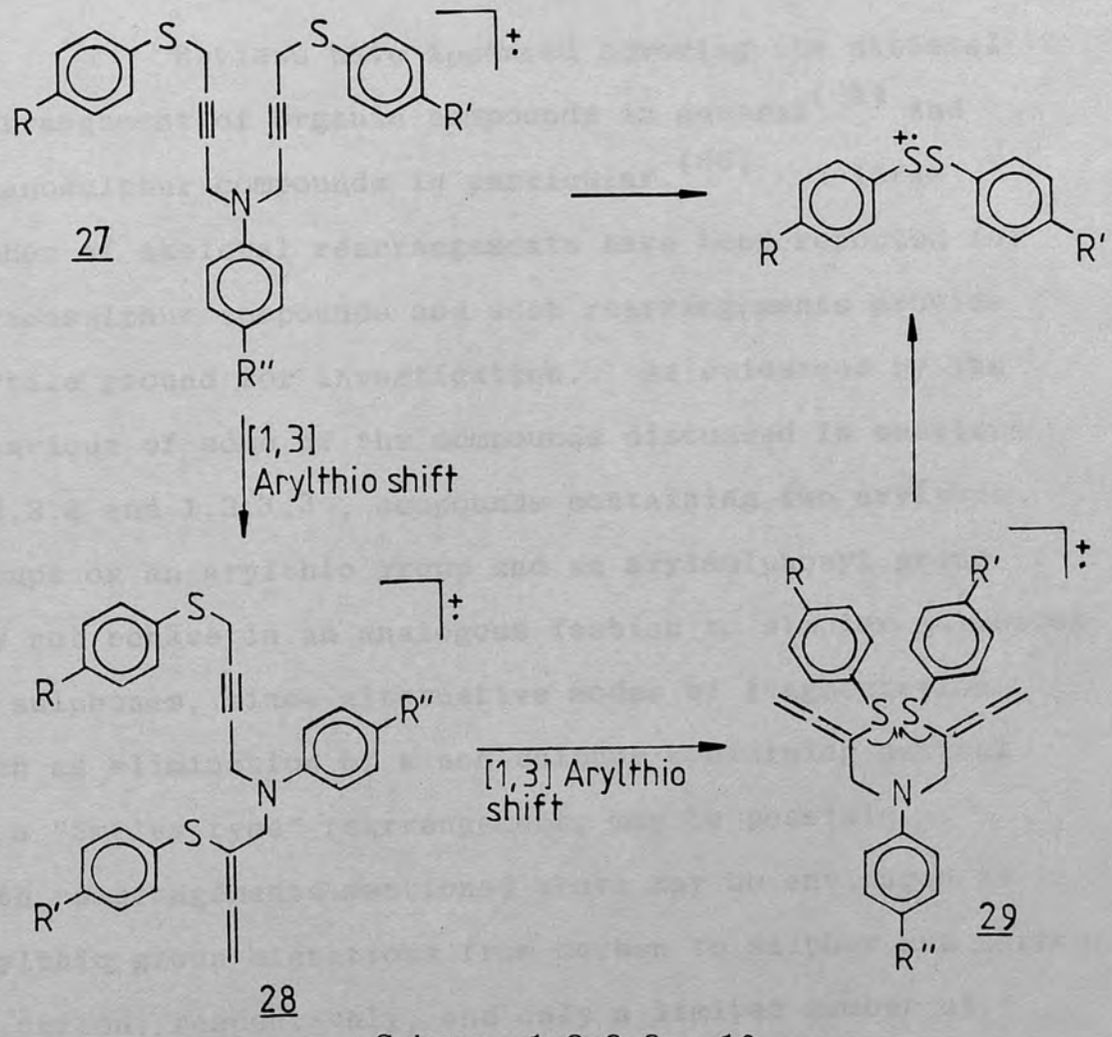

Scheme 1.3.3.3 - 10

The distance between the two sulphur atoms in 29 is comparable to that in 27 and formation of $ArSSAr'^{+\cdot}$ from 29 was thought to be just as probable. An E.I. induced elimination of sulphur was not observed to occur from 23, 24 or 27, lending support to the premise that the presence of through space interaction between the sulphur atoms provide additional modes of fragmentation which compete successfully with the extrusion of sulphur.

1.3.4 Objectives in the study of the E.I. induced fragmentation of organosulphur compounds.

Reviews have appeared covering the skeletal rearrangement of organic compounds in general[65] and organosulphur compounds in particular.[66] A large number of skeletal rearrangements have been reported for organosulphur compounds and such rearrangements provide fertile ground for investigation. As evidenced by the behaviour of some of the compounds discussed in sections 1.3.2.3 and 1.3.3.3 , compounds containing two arylthio groups or an arylthio group and an arylsulphonyl group may not behave in an analogous fashion to simpler sulphides or sulphones, since alternative modes of fragmentation, such as elimination of a non-sulphur containing neutral or a "Smiles type" rearrangement, may be possible. Both rearrangements mentioned above may be envisaged as arylthio group migrations from carbon to sulphur and carbon to carbon, respectively, and only a limited number of

examples have been reported. Further investigation into such rearrangements is desirable in order to determine the generality of such processes and to provide further elucidation of their reaction mechanisms.

2. 3-ARYLSULPHONYL-2-ARYLTHIOPROPENES

2.1 Synthetic methods

The synthesis of 3-phenylsulphonyl-2-phenylthiopropene 30a has been reported by Stirling[67] and his procedure for the base catalysed addition of thiophenol to 3-phenylsulphonylpropyne, 32, was followed throughout. Scheme 2.1.-1 illustrates the sequence of reactions in the preparation of 3-arylsulphonyl-2-arylthiopropenes, 30a-j.

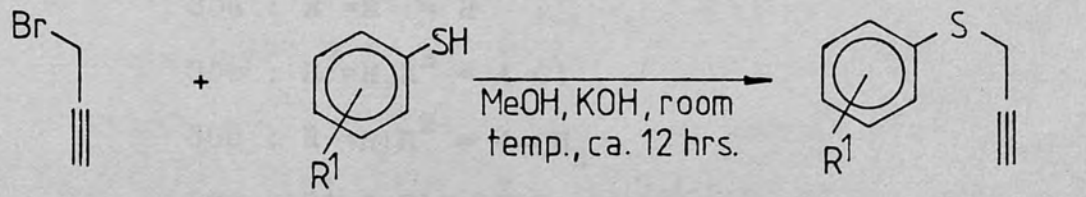

31, ca. 50%

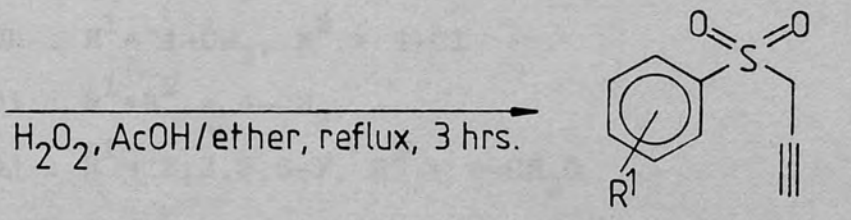

32, 65-99%

Scheme 2.1 -1

(cont'd next page)

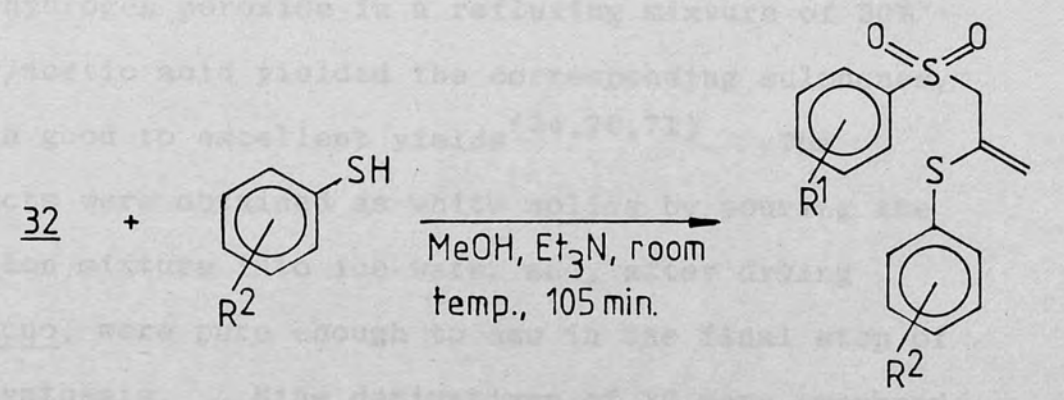

30, 13 - 100%

30a : $R^1=R^2$ = H

30b : R^1=H, R^2 = 4-Cl

30c : R^1=H, R^2 = 4-CH_3

30d : R^1=4-Cl, R^2=H

30e : $R^1=R^2$ = 4-Cl

30f : R^1= 4-Cl, R^2= 4-CH_3

30g : R^1= 4-CH_3, R^2 = H

30h : R^1= 4-CH_3, R^2 = 4-Cl

30i : $R^1=R^2$ = 4-CH_3

30j : R^1= 2,3,5,6-F, R^2 = 4-CH_3O

Scheme 2.1 -1

Three known derivatives of 31 (R^1 =H,4-Cl and 4-CH_3) were prepared by the reaction of the appropriate potassium thiophenolate salts, produced in situ, with propargyl bromide in methanol[68,69] and were purified by distillation at reduced pressure. A previously unknown 2,3,5,6-tetra-

fluoro derivative was prepared and purified in the same manner. Oxidation of the propynylarylsulphides with hydrogen peroxide in a refluxing mixture of 50% ether/acetic acid yielded the corresponding sulphones, 32, in good to excellent yields[34,70,71]. The products were obtained as white solids by pouring the reaction mixture into ice-water and, after drying *in vacuo*, were pure enough to use in the final step of the synthesis. Nine derivatives of 30 were prepared by the reaction of the appropriate arenethiol (R^2= H,4-Cl or 4-CH_3) with 32 (R^1=H,4-Cl or 4-CH_3) in methanol containing one equivalent of triethylamine, at ambient temperature. The reaction proceeds via base catalysed isomerisation of 32 to an allene and a subsequent nucleophilic attack at the central carbon by the thiophenolate ion.[67] The unsubstituted derivative, 30a thus prepared was identical in all respects to that reported by Stirling.

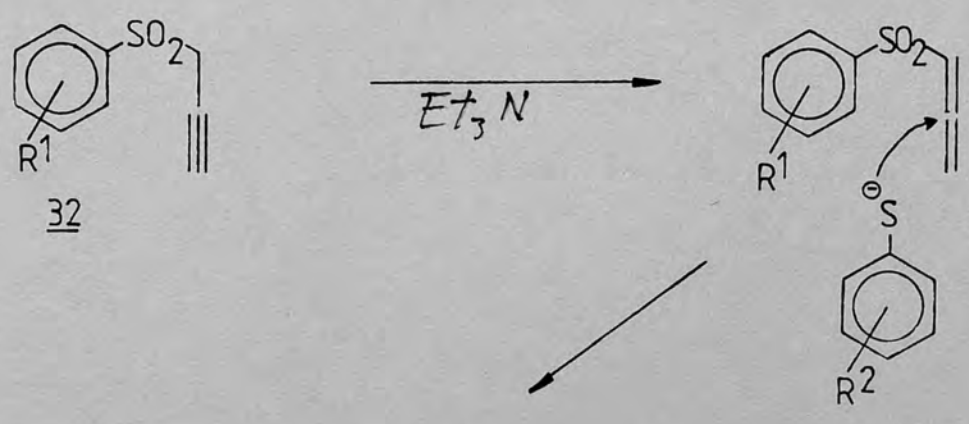

32 30

Scheme 2.1 -2

With the exception of 30a, all of the derivatives prepared, including the tetrafluoro derivative 30j, were previously unknown. All of the derivatives were obtained as white solids, which displayed a single spot in their thin layer chromatograms. They were characterised by their n.m.r. and mass spectra and no other isomers were detected. All the derivatives of 30 gave excellent results upon elemental analysis. With the exception of 30j, the yields for the last step in the synthesis were greater than 95%. The low yield of the tetrafluoro derivative (13%) was due to difficulties in recrystallising the crude product.

2.2 E.I. induced fragmentation results.

Abundant molecular ions were observed at 70 eV, in all cases. The elimination of an arylsulphonyl radical was a common and major process, with the base peak corresponding to the $\{M-Ar^1SO_2\}^+$ ion in five of the ten cases. (Note: $Ar^1 = R^1C_6H_4$, $Ar^2 = R^2C_6H_4$. This notation will be used throughout to distinguish between aryl groups). The 3-arylsulphonyl-2-arylthio-propenes, 30a-j, also underwent skeletal rearrangement upon electron impact. Both the facile loss of sulphur dioxide and formation of an ion corresponding to $\{M-104\}^{+\cdot}$ were observed in all cases. Scheme 2.2 - 1 summarises the principal fragmentation pathways of 30a-j and Table 2.2 - 1 indicates the relative abundances of significant ions in their mass spectra. Parent-daughter ion relationships were established by the presence of appropriate metastable ions in the normal single-focused spectra (see Table 2.2 - 2) and by B/E linked scanning, focusing on ions of interest in the spectra of 30a,i and j (see Tables 2.2. - 3 to 2.2. - 5).

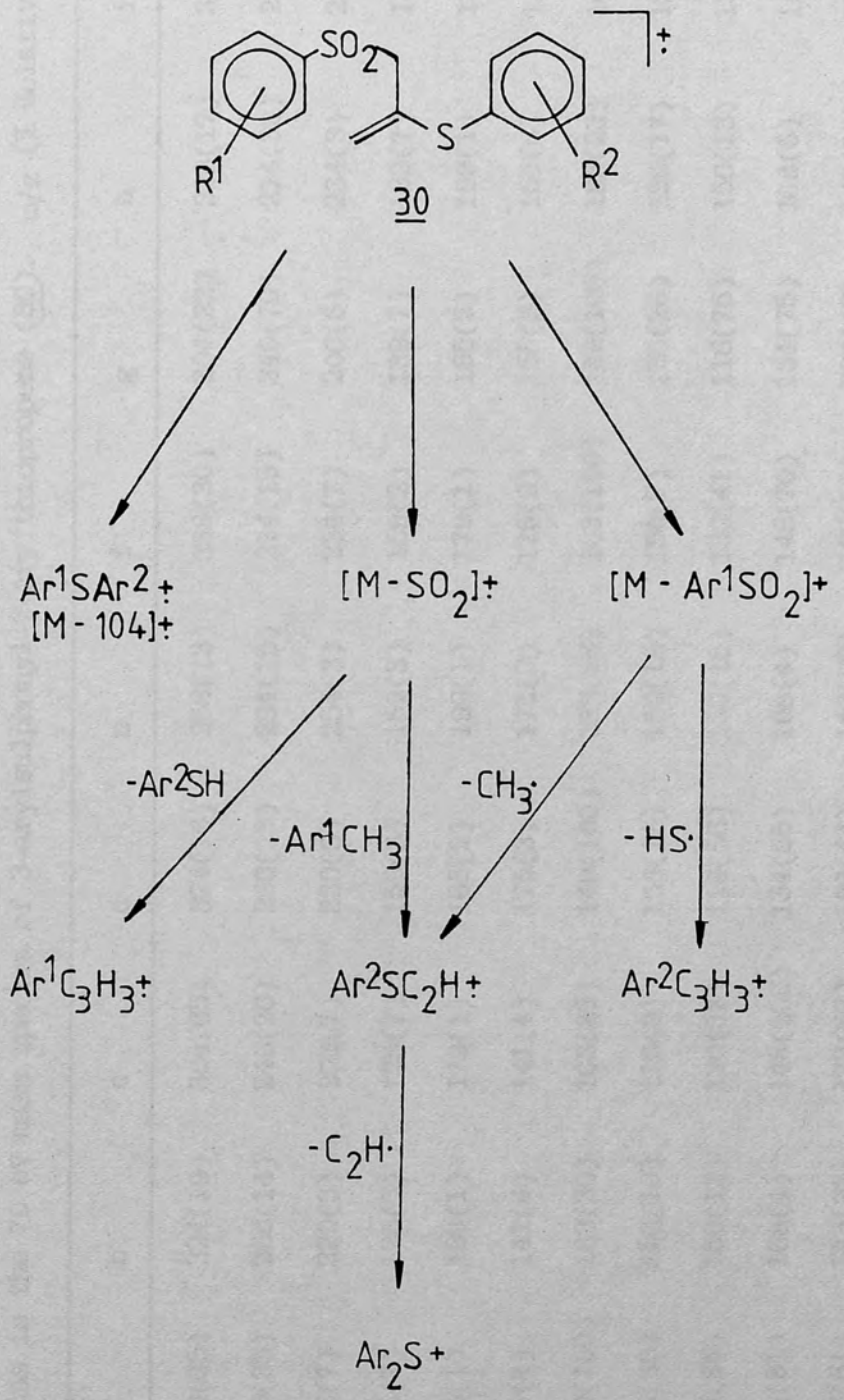
SO2
S
R1
R2
30
Ar1SAr2+
[M - 104]+
[M - SO2]+
[M - Ar1SO2]+
-Ar2SH
-Ar1CH3
-CH3·
-HS·
Ar1C3H3+
Ar2SC2H+
Ar2C3H3+
-C2H·
Ar2S+

Scheme 2.2 - 1

TABLE 2.2 - 1

Significant ions in the 70 eV mass spectra of 3-arylsulphonyl-2-arylthiopropene (30). m/z (% Relative abundance).

ION	a	b	c	d	e	f	g	h	i	j
$M^{+\cdot}$	290(35)	324(19)	304(65)	324(16)	358(13)	338(30)	304(22)	338(17)	318(42)	392(64)
$\{M-SO_2\}^{+\cdot}$	226(35)	260(14)	240(20)	260(23)	294(15)	274(15)	240(70)	274(33)	254(46)	328(1)
$Ar^1SAr^{2+\cdot}$	186(7)	220(3)	200(7)	220(3)	254(3)	234(7)	200(6)	234(3)	214(8)	288(12)
Ar^1SO^+	125(7)	125(5)	125(7)	159(3)	159(3)	159(2)	139(7)	139(7)	139(6)	197(1)
$\{M-Ar^1SO\}^+$	165(1)	199(1)	179(1)	165(1)	199(1)	179(1)	165(2)	199(1)	179(1)	195(1)
$Ar^1SO_2^+$	141(4)	141(4)	141(4)	175(3)	175(3)	175(2)	155(6)	155(8)	155(3)	213(1)
$\{M-Ar^1SO_2\}^{+\cdot}$	149(100)	183(30)	163(83)	149(100)	183(26)	163(100)	149(100)	183(23)	163(100)	179(32)
$Ar^1C_3H_3^{+\cdot}$	116(86)	116(10)	116(9)	150(16)	150(15)	150(7)	130(28)	130(17)	130(63)	189(0.1)
$Ar^2C_3H_3^{+\cdot}$	116(86)	150(12)	130(57)	116(56)	150(15)	130(41)	116(75)	150(13)	130(63)	146(4)
$Ar^2SC_2H^{+\cdot}$	134(81)	168(4)	148(100)	134(55)	168(4)	148(70)	134(75)	168(5)	148(83)	164(20)
Ar^2S^+	109(61)	143(23)	123(62)	109(44)	143(22)	123(10)	109(48)	143(25)	123(44)	139(100)
$R^1C_7H_6^+$	91(14)	91(2)	91(21)	125(3)	125(5)	125(4)	105(19)	105(4)	105(11)	163(3)

TABLE 2.2 - 2

Metastable peaks in the 70 eV mass spectra of 3-arylsulphonyl-2-arylthiopropenes (30).

Derivative	Metastable peak (m/z)	Transition	Neutral lost
30a	176.5	290 → 226	SO_2
	120.5	226 → 134	$CH_3\cdot$
	90.3	226 → 116	HS·
	88.7	134 → 109	$C_2H\cdot$
	76.5	290 → 149	$Ar^1SO_2\cdot$
30b	208.6	324 → 260	SO_2
	121.9	168 → 143	$C_2H\cdot$
	119.6	183 → 148	Cl·
	103.3	324 → 183	$Ar^1SO_2\cdot$
30c	189.4	304 → 240	SO_2
	134.5	163 → 148	$CH_3\cdot$
	103.6	163 → 130	HS·
	102.2	148 → 123	$C_2H\cdot$
	87.3	304 → 163	$Ar^1SO_2\cdot$
30d	208.6	324 → 260	SO_2
	120.5	175 → 134	$CH_3\cdot$
	90.3	175 → 116	HS·
	88.6	134 → 109	$C_2H\cdot$
	68.5	324 → 149	$Ar^1SO_2\cdot$
30e	241.4	358 → 294	SO_2
	119.7	183 → 148	Cl·
30f	222.1	338 → 274	SO_2
	134.4	163 → 148	$CH_3\cdot$
	103.7	163 → 130	HS·
	102.2	148 → 123	$C_2H\cdot$
	78.6	338 → 163	$Ar^1SO_2\cdot$

TABLE 2.2 - 2 (continued)

Derivative	Metastable peak (m/z)	Transition	Neutral lost
30g	189.4	304 → 240	SO_2
	120.5	149 → 134	$CH_3\cdot$
	90.3	149 → 116	$HS\cdot$
	88.7	134 → 109	$C_2H\cdot$
	73.3	304 → 149	$Ar^1SO_2\cdot$
	70.4	240 → 130	Ar^2SH
30h	222.1	338 → 274	SO_2
	119.6	183 → 148	$Cl\cdot$
	61.7	183 → 130	Ar^2SH
30i	202.8	318 → 254	SO_2
	134.3	163 → 148	$CH_3\cdot$
	103.6	163 → 130	$HS\cdot$
	102.2	148 → 123	$C_2H\cdot$
	83.5	318 → 163	$Ar^1SO_2\cdot$
	66.5	254 → 130	Ar^2SH
30j	274.4	392 → 328	SO_2
	211.6	392 → 288	$SO_2C_3H_4$
	150.2	179 → 164	$CH_3\cdot$
	119.1	179 → 146	$HS\cdot$
	81.7	392 → 179	$Ar^1SO_2\cdot$

TABLE 2.2 - 3

Product ions identified by B/E linked scanning of selected ions in the mass spectrum of 30a

Precursors scanned			Product ion
m/z	Assignment	Neutral lost	m/z
290	$M^{+\cdot}$	SO_2	226
		$C_3H_4SO_2$	186
		$Ar^1SO_2\cdot$	149
226	$\{M-SO_2\}^{+\cdot}$	$CH_3\cdot$	211
		H_2S	192
		$CH_3C_6H_6$	134
		Ar^2SH	116
149	$\{M-Ar^1SO_2\}^{+}$	$CH_3\cdot$	134
		$HS\cdot$	116

TABLE 2.2 - 4

Product ions identified by B/E linked scanning of selected ions in the mass spectrum of 30i.

Precursor scanned			Product ion
m/z	Assignment	Neutral lost	m/z
318	$M^{+\cdot}$	SO_2	254
		$C_3H_4SO_2$	214
		$Ar^1SO_2\cdot$	163
254	$\{M-SO_2\}^{+\cdot}$	$CH_3\cdot$	239
		H_2S	220
		$CH_3C_6H_4CH_3$	148
		Ar^2SH	130
163	$\{M-Ar^1SO_2\}^{+}$	$CH_3\cdot$	148
		$HS\cdot$	130

TABLE 2.2 - 5

Product ions identified by B/E linked scanning of selected ions in the mass spectrum of 30j.

Precursor scanned			Product ion
m/z	Assignment	Neutral lost	m/z
392	$M^{+\cdot}$	SO_2	328
		$C_3H_4SO_2$	288
		$Ar^1SO_2\cdot$	179
179	$\{M-Ar^1SO_2\}^+$	$CH_3\cdot$	164
		$HS\cdot$	146

Exact mass measurements were obtained for the $\{M-104\}^{+\cdot}$ ions in the mass spectra of 30a, i and j (see Table 2.2 - 6). The results were in excellent agreement with calculated values, assuming the loss of $C_3H_4SO_2$ from the molecular ion.

TABLE 2.2 - 6

Exact masses of the M-104 ions in the mass spectra of 30a, i and j.

Derivative	Ion Composition	Exact mass Calc.	Found
30a	$C_{12}H_{10}S$	186.0503	186.0498
30i	$C_{14}H_{14}S$	214.0816	214.0813
30j	$C_{13}H_8F_4S$	288.0232	288.0227

The electron impact mass spectra of 30h and the tetrafluoro derivative 30j were also obtained at the lower nominal electron energies of 20, 15, 10 and 5 eV. The variation in the abundances (% Σ_{40}) of the $M^{+\cdot}$, $\{M-SO_2\}^{+\cdot}$, $Ar^1SAr^{2+\cdot}$ and $\{M-ArSO_2\}^+$ ions as a function of nominal electron energy are shown in Graphs 2.2 - 1 and 2.2 - 2 for 30h and 30j, respectively.

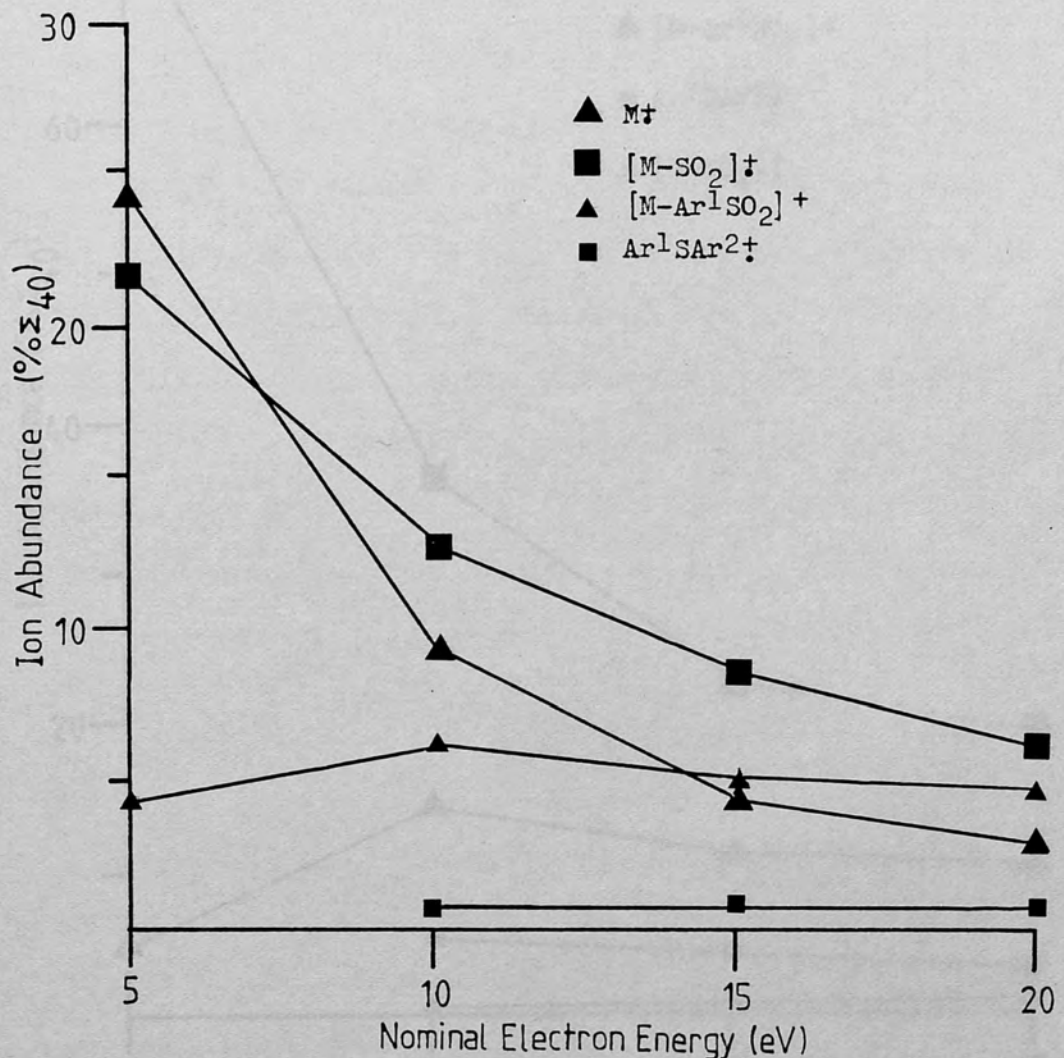

Graph 2.2-1 : Abundance of selected ions in the low electron energy mass spectra of 30h.

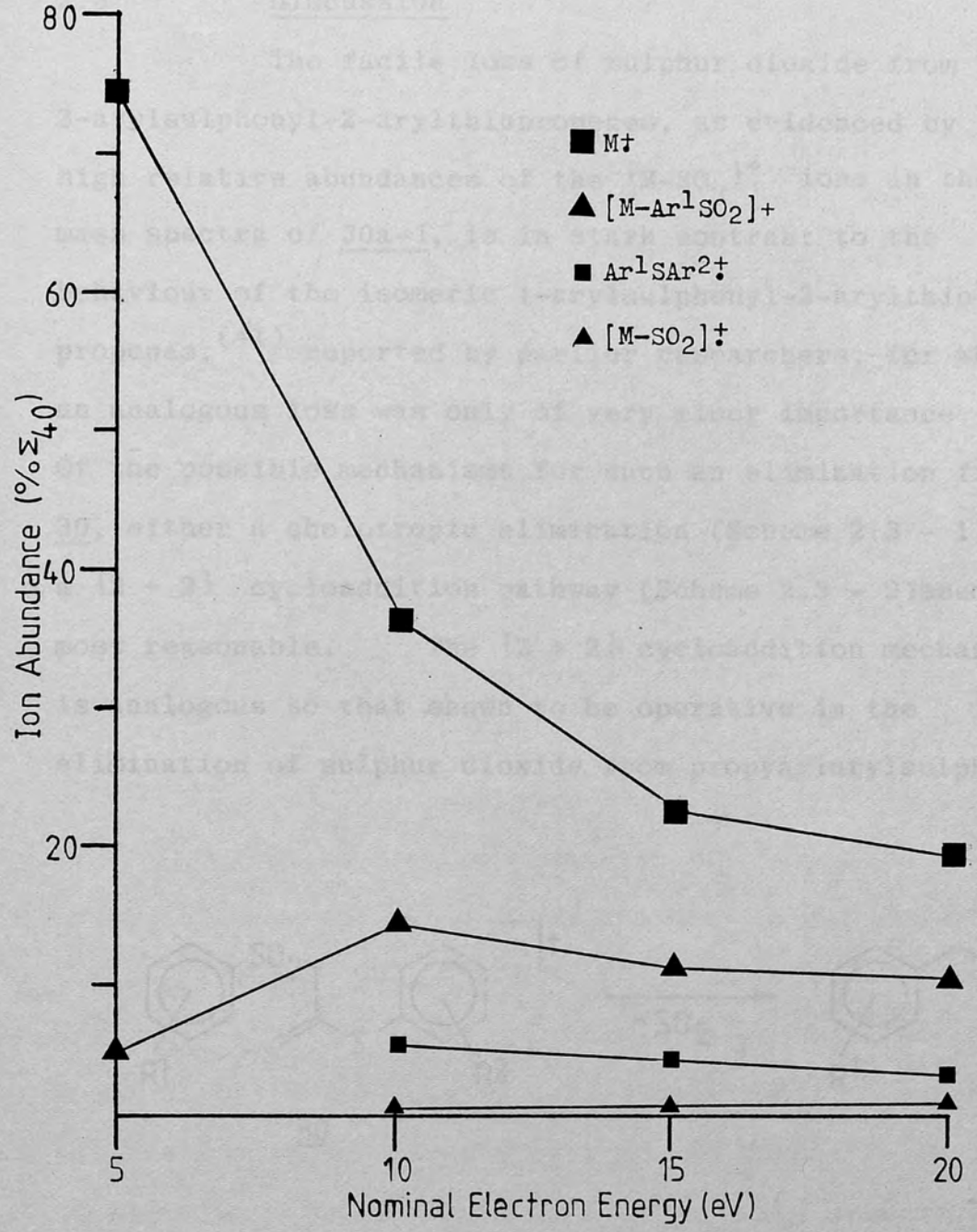

Graph 2.2-2 : Abundance of selected ions in the low electron energy mass spectra of 30j.

2.3 Discussion

The facile loss of sulphur dioxide from 3-arylsulphonyl-2-arylthiopropenes, as evidenced by the high relative abundances of the $\{M-SO_2\}^{+\cdot}$ ions in the mass spectra of 30a-i, is in stark contrast to the behaviour of the isomeric 1-arylsulphonyl-2-arylthio-trans-propenes,[41] reported by earlier researchers, for which an analogous loss was only of very minor importance. Of the possible mechanisms for such an elimination from 30, either a chelotropic elimination (Scheme 2.3 - 1) or a {2 + 2} cycloaddition pathway (Scheme 2.3 - 2)seem the most reasonable. The {2 + 2} cycloaddition mechanism is analogous to that shown to be operative in the elimination of sulphur dioxide from propynylarylsulphones.[33,34]

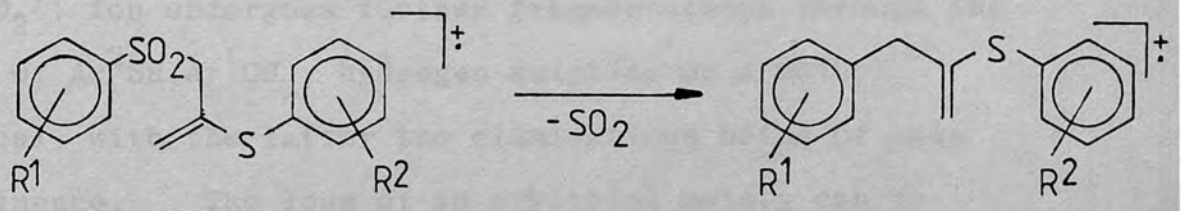

30 33

Scheme 2.3 - 1

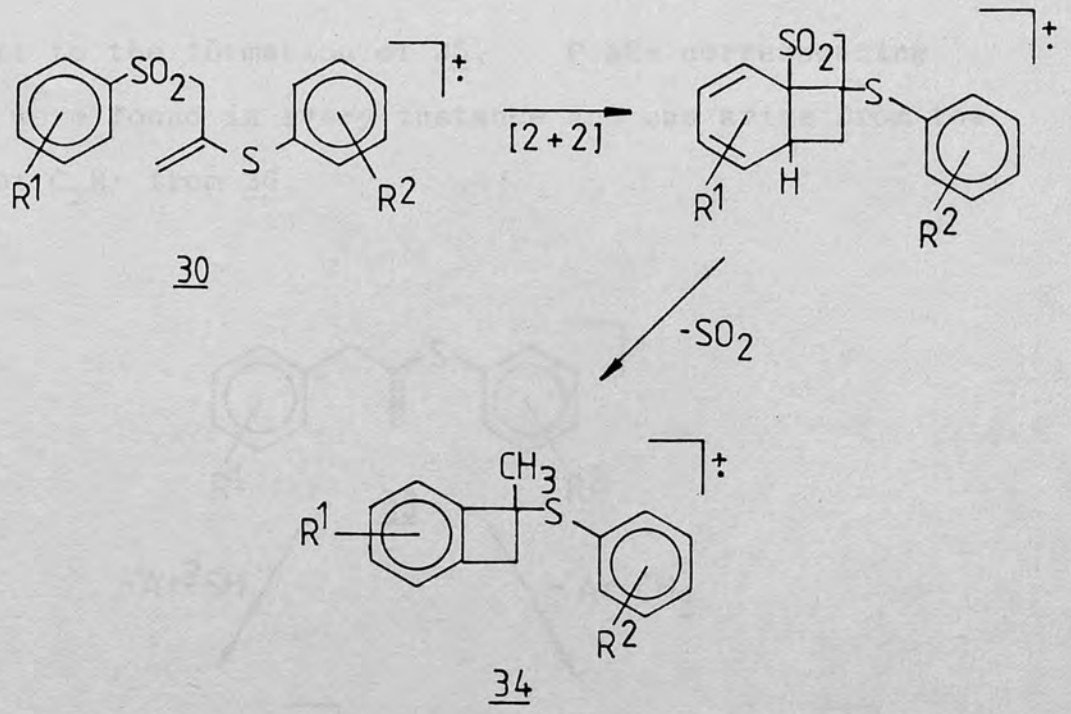

30 34

Scheme 2.3 - 2

The B/E linked scanning data showed that the $\{M-SO_2\}^{+\cdot}$ ion undergoes further fragmentations through the loss of Ar^2SH, Ar^1CH_3, hydrogen sulphide or a methyl radical, with the latter two eliminations being of less prominence. The loss of an arylthiol moiety can be easily rationalised from either an ion formed by chelotropic elimination, e.g. from ion 33, or 34, resulting from {2 + 2} cycloaddition in ion 30 (Schemes 2.3 - 3 and 2.3 - 4 respectively). However the loss of a methylarene species is more easily accommodated by 33 (Scheme 2.3 - 3) to give an ethynylarylsulphide ion, 35. The further loss of $C_2H\cdot$, which was substantiated by corresponding metastable peaks in many instances, lends

support to the formation of 35. Peaks corresponding to 37 were found in every instance and can arise from the loss of $C_2H\cdot$ from 36.

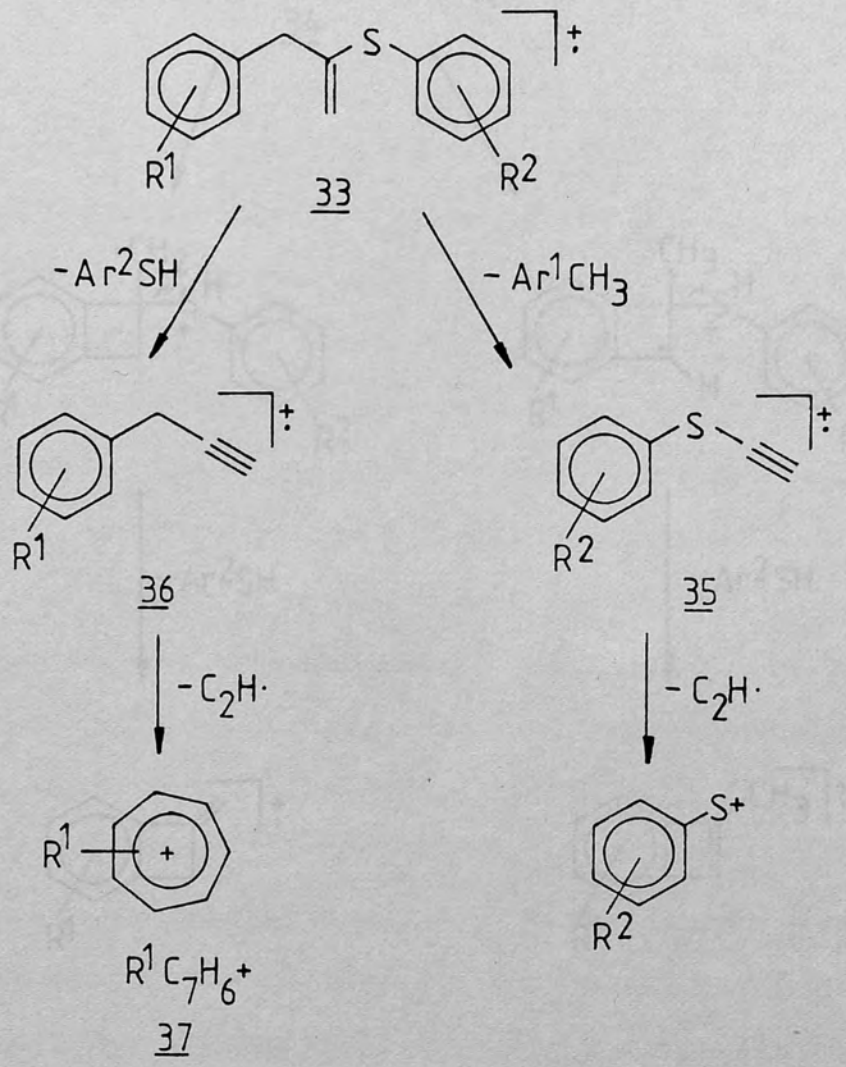

Scheme 2.3 - 3

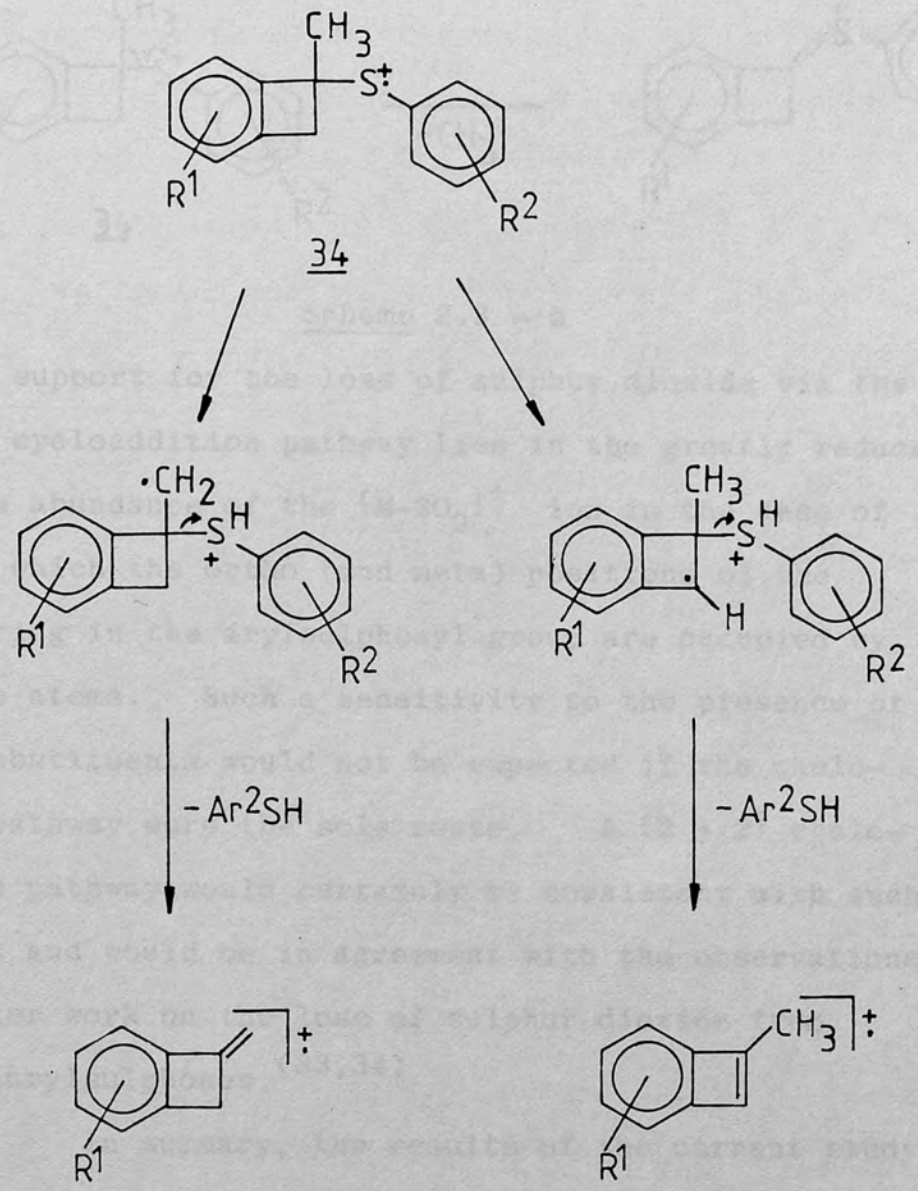

Scheme 2.3 - 4

The observed loss of a methyl radical from the $\{M-SO_2\}^{+\cdot}$ ion can, however, be more easily interpreted from ion 34, via alpha cleavage:

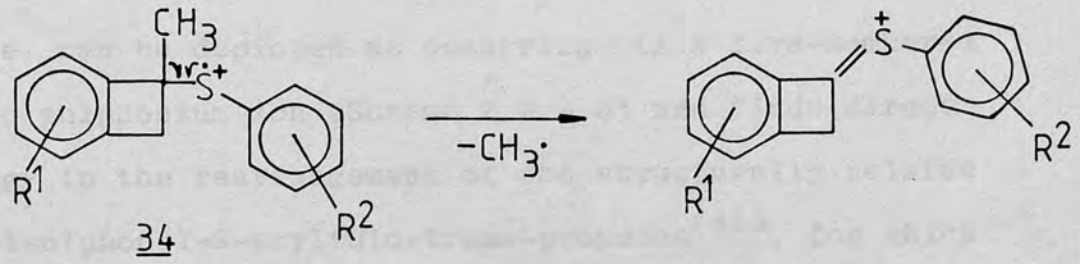

34

Scheme 2.3 - 5

Further support for the loss of sulphur dioxide via the {2 + 2} cycloaddition pathway lies in the greatly reduced relative abundance of the $\{M-SO_2\}^{+\cdot}$ ion in the case of 30j, in which the ortho (and meta) positions of the phenyl ring in the arylsulphonyl group are occupied by fluorine atoms. Such a sensitivity to the presence of ortho substituents would not be expected if the chelotropic pathway were the sole route. A {2 + 2} cycloaddition pathway would certainly be consistent with such a result and would be in agreement with the observations in earlier work on the loss of sulphur dioxide from propynylarylsulphones.[33,34]

In summary, the results of the current study indicate that both the chelotropic and {2 + 2} cycloaddition pathways are available for the elimination of sulphur dioxide from the molecular ions of 3-arylsulphonyl-2-arylthiopropenes 30, except in the case of the tetrafluoro derivative, in which the latter is precluded for the reasons mentioned above.

The elimination of the elements of $C_3H_4SO_2$ from the 3-arylsulphonyl-2-arylthiopropenes, either as

2-methylenethiirane-1,1-dioxide or as sulphur dioxide and allene, can be depicted as occurring via a five-membered cyclic sulphonium ion (Scheme 2.3 - 6) and finds direct analogy in the rearrangement of the structurally related 1-arylsulphonyl-2-arylthio-trans-propenes[41], for which a similar mechanism has been proposed (see Section 1.3.2.3).

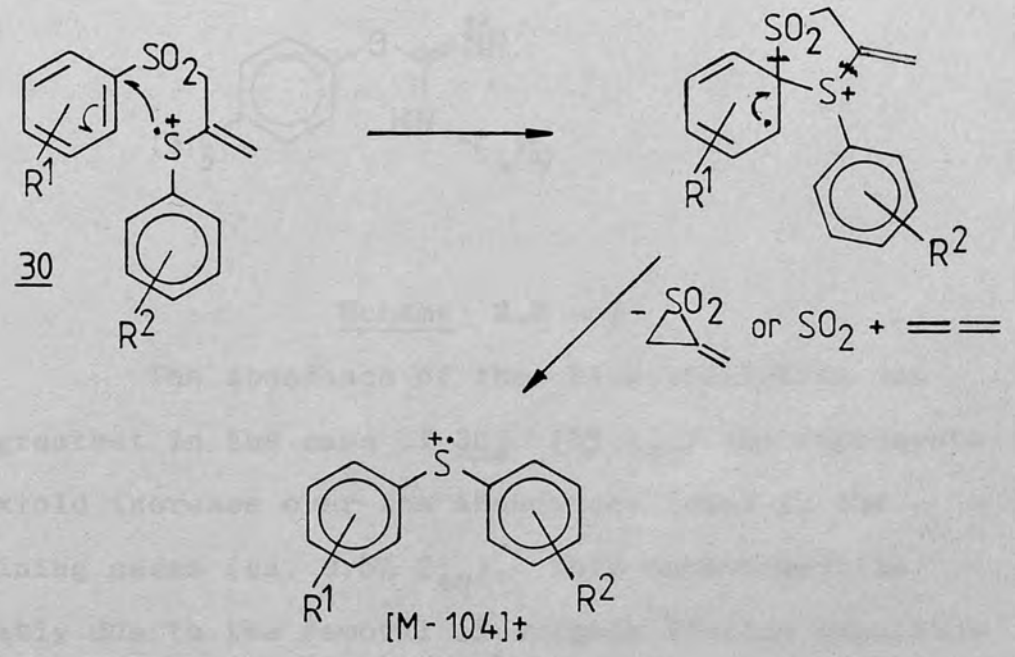

Scheme 2.3 - 6

A mechanistic resemblance is found in the elimination of sulphur dioxide from N-n-butyl-N'-p-toluene-sulphonylurea. Exact mass analysis and deuterium labelling techniques established the presence of two competitive pathways.[72] One of these, the formation of a five-membered cyclic sulphone ion and subsequent explusion of sulphur dioxide (Scheme 2.3 - 7), was shown to predominate over a three-membered cyclic rearrangement pathway.

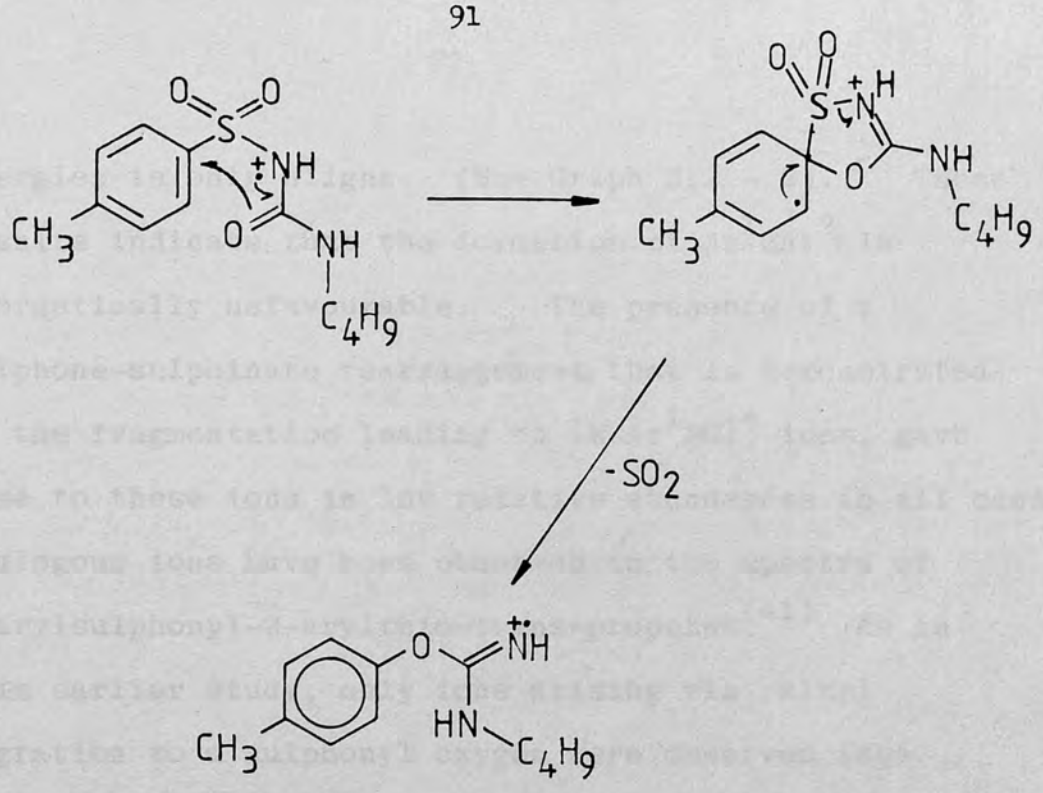

Scheme 2.3 - 7

The abundance of the bisarylsulphide ion was greatest in the case of 30j (3% Σ_{40}) and represents a sixfold increase over the abundances found in the remaining cases (ca. 0.5% Σ_{40}). This enhancement is probably due to the removal of sulphur dioxide expulsion as a competitive pathway, as a result of the presence of ortho substituents. In the large majority of cases, the formation of the bisarylsulphide ion does not compete successfully with the elimination of sulphur dioxide. At lower energies, the enhancement of the abundance of the $\{M-SO_2\}^{+\cdot}$ ion is observed to be much greater than the increase in abundance of the $Ar^1SAr^2{}^{+\cdot}$ ion (see Graph 2.2 - 1). Even when the elimination of sulphur dioxide is removed as a competitive pathway, (as in the case of 30j) the increase in the abundance of $Ar^1SAr^2{}^{+\cdot}$ at lower

energies is only slight. (See Graph 2.2 - 2). These results indicate that the formation of Ar^1SAr^2+ is energetically unfavourable. The presence of a sulphone-sulphinate rearrangement, that is demonstrated by the fragmentation leading to $\{M-Ar^1SO\}^+$ ions, gave rise to these ions in low relative abundances in all cases. Analogous ions have been observed in the spectra of 1-arylsulphonyl-2-arylthio-trans-propenes.[41] As in this earlier study, only ions arising via alkyl migration to a sulphonyl oxygen were observed (see Scheme 2.3 - 8).

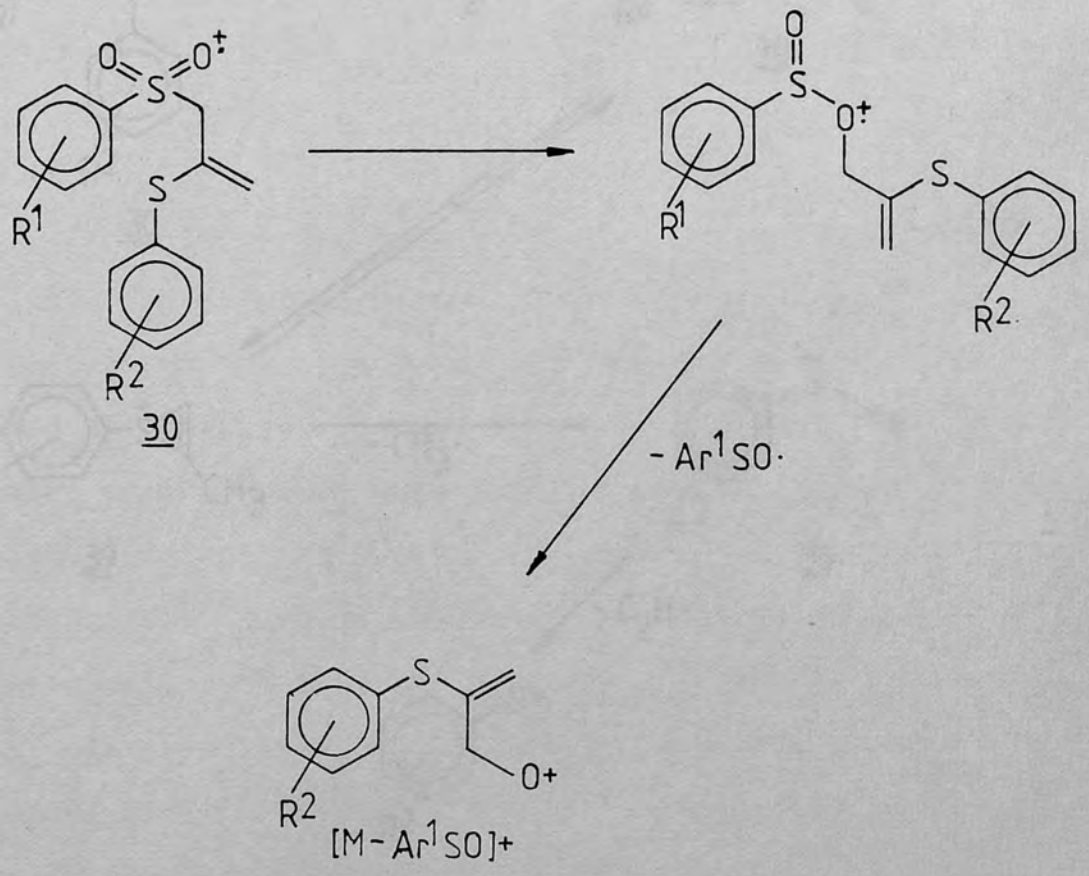

Scheme 2.3 - 8

The elimination of a methyl group from the $\{M-Ar^1SO_2\}^+$ ion, supported by metastable peaks in many instances and also by B/E linked scanning, gives rise to an ion of the same nominal mass as that derived by the elimination of a methylarene from the $\{M-SO_2\}^{+\cdot}$ ion. The same ion, 35 can be formed by both routes. Scheme 2.3 - 9 illustrates its formation from the $\{M-Ar^1SO_2\}^{+\cdot}$ ion.

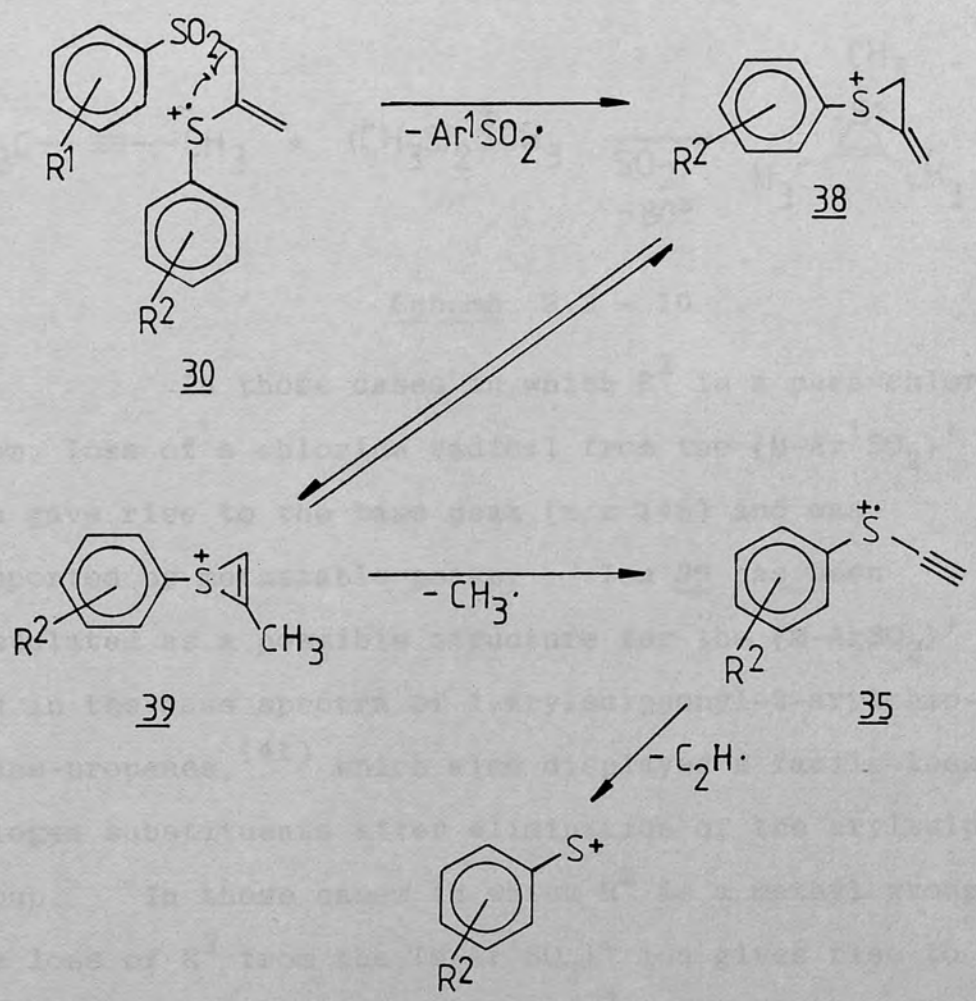

Scheme 2.3 - 9

A {1,3} hydrogen shift occurring in 38 gives rise to the 2-methylthiirenium ion 39, which can then undergo ring opening with concomitant loss of a methyl radical to give 35, followed by the loss of C_2H·. Molecular orbital calculations have shown the thiirenium ion to be slightly (1-14 Kcal mol^{-1}) more stable than an acyclic β-vinylthio cation.(73) Stable thiirenium ions have been observed in the reaction of 2-butyne with a dimethylthiomethyl-sulphonium salt at -80° in liquid sulphur dioxide.(74)

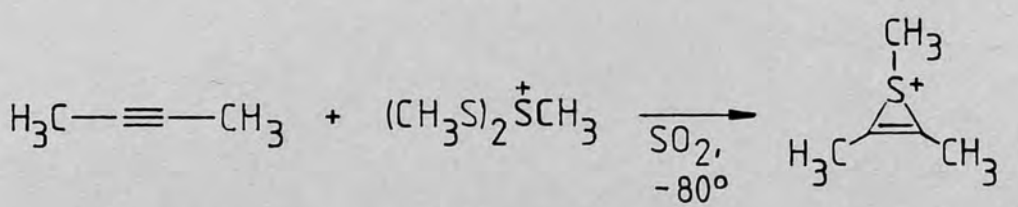

Scheme 2.3 - 10

In those cases in which R^2 is a para-chlorine atom, loss of a chlorine radical from the $\{M-Ar^1SO_2\}^+$ ion gave rise to the base peak (m/z 148) and was supported by metastable peaks. Ion 39 has been postulated as a possible structure for the $\{M-ArSO_2\}^+$ ion in the mass spectra of 1-arylsulphonyl-2-arylthio-trans-propenes,(41) which also displayed a facile loss of halogen substituents after elimination of the arylsulphonyl group. In those cases in which R^2 is a methyl group, the loss of R^2 from the $\{M-Ar^1SO_2\}^+$ ion gives rise to an ion of the same nominal mass as $Ar^2SC_2H^+$.

The loss of HS· from the $\{M-ArSO_2\}^+$ ion was supported by B/E linked scanning studies and by metastable

peaks. A mechanism for the elimination of HS· from a cyclic ion such as 39 or 38 is difficult to imagine and indicates that the $\{M-ArSO_2\}^+$ ion undergoes other modes of rearrangement.

3. 1-ARYLSULPHONYL-4-ARYLTHIO-2-BUTYNES

3.1 Synthesis

Eight derivatives of the title compounds, 40, were synthesised by the route illustrated in Scheme 3.1 - 1.

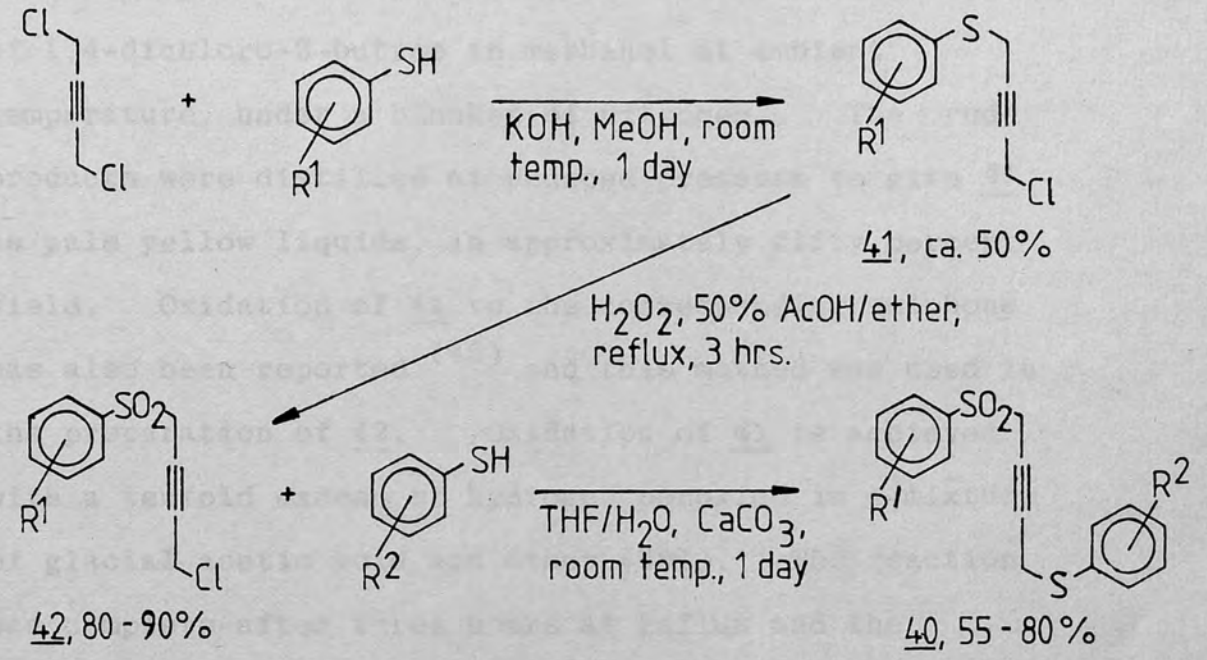

40a: $R^1=R^2=H$

40b: $R^1=H, R^2=4\text{-}Cl$

40c: $R^1=H, R^2=2,5\text{-}Cl$

40d: $R^1=R^2=4\text{-}Cl$

40e: $R^1=4\text{-}Cl, R^2=4\text{-}CH_3$

40f: $R^1=4\text{-}CH_3, R^2=4\text{-}Cl$

40g: $R^1=4\text{-}CH_3, R^2=4\text{-}Br$

40h: $R^1=4\text{-}CH_3, R^2=3\text{-}CH_3, 4\text{-}Br$

Scheme 3.1 - 1

The 1-chloro-4-arylthio-2-butynes, 41, were prepared by following a published procedure.[45] Here, the appropriate potassium arenethiolate, prepared *in situ* by dissolution of the arenethiol in methanol containing an equimolar amount of potassium hydroxide, is reacted with an excess of 1,4-dichloro-2-butyne in methanol at ambient temperature, under a blanket of nitrogen. The crude products were distilled at reduced pressure to give 41 as pale yellow liquids, in approximately fifty percent yield. Oxidation of 41 to the corresponding sulphone has also been reported [45] and this method was used in the preparation of 42. Oxidation of 41 is achieved with a tenfold excess of hydrogen peroxide in a mixture of glacial acetic acid and ether (50%). The reaction was complete after three hours at reflux and the sulphones were obtained as white solids (~ 80% yield) by pouring the reaction mixture into water. The products obtained in this manner were pure enough for use in the final step, after drying *in vacuo*.

In having regard to the conditions for the base catalysed reaction of 42 with arenethiols,the possibility of dehydrochlorination must be considered. Whereas 1,4-dichloro-2-butyne reacts with alkali to give chlorobutatriene and 1,3-butadiyne[75] (Scheme 3.1 -2), triethylamine causes hydrogen chloride to be eliminated from (2-chloroethyl)sulphonyl derivatives to yield vinylsulphonyl compounds[76] (Scheme 3.1 -3).

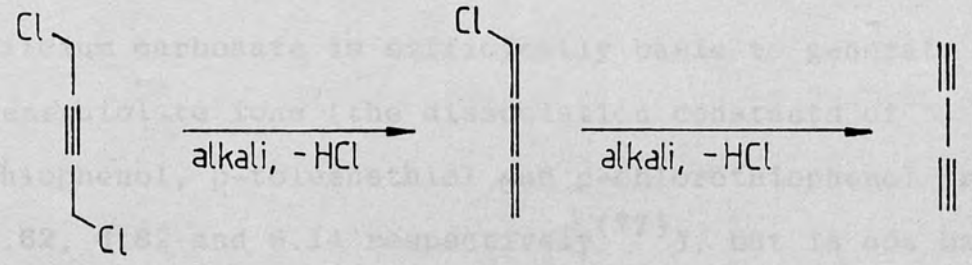

Scheme 3.1 - 2

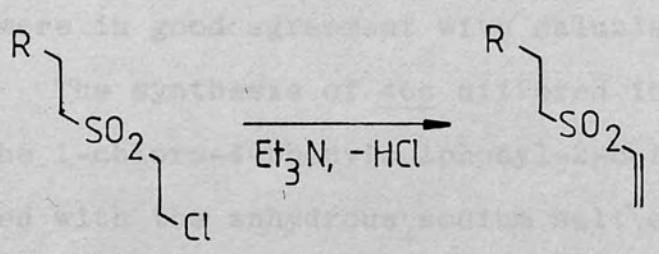

Scheme 3.1 - 3

Mild conditions must therefore be employed to avoid the formation of an arylsulphonylbutatriene from 42 as follows:

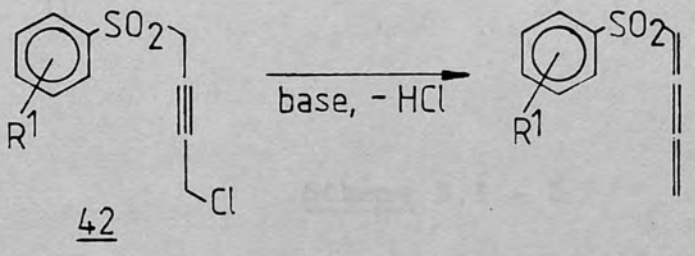

42

Scheme 3.1 - 4

The use of a strong base to generate arenethiolate ions was avoided by means of a two-phase reaction system. A solution in tetrahydrofuran of 42 and the desired arenethiol was stirred for one day with a slurry of calcium carbonate in water, at ambient temperature.

Calcium carbonate is sufficiently basic to generate arenethiolate ions (the dissociation constants of thiophenol, p-toluenethiol and p-chlorothiophenol are 6.62, 6.82 and 6.14 respectively[77]), but is not basic enough to isomerise 42. The products obtained in this manner were white solids and were characterised by their NMR and mass spectra. The results of elemental analyses were in good agreement with calculated values.

The synthesis of 40a differed in the final step. The 1-chloro-4-phenylsulphonyl-2-butyne (42, R^1=H) was reacted with the anhydrous sodium salt of thiophenol in refluxing acetonitrile for one day:

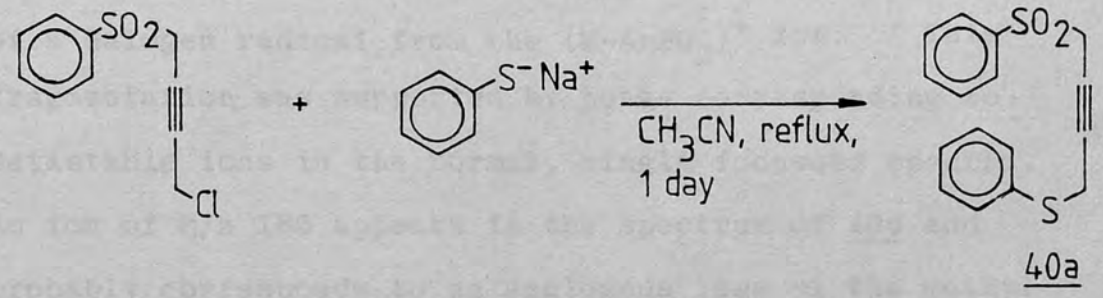

40a

Scheme 3.1 - 5

The crude product was chromatographed on silica gel to give 40a in 38% yield as a pale yellow oil. The thin layer chromatogram displayed a single spot and spectral data were entirely consistent with the expected structure.

3.2 E.I. induced fragmentation results.

Abundant molecular ions are present in the 70 eV spectra of all of the derivatives of 40 which were investigated. In general, loss of an arylsulphonyl radical ($Ar^1SO_2\cdot$) greatly overshadows elimination of an arylthio radical ($Ar^2S\cdot$). The relative abundances of the $\{M-Ar^2S\}^+$ ion were, on the average, approximately one percent, whereas the relative abundances of the $\{M-Ar^1SO_2\}^+$ ion ranged from 3-100%. Loss of an arylsulphonyl radical concomitant with hydrogen migration to a sulphonyl oxygen was also observed. Base peaks at m/z 160 in the spectra of 40b, 40d, 40f, and 40g, m/z 194 in the spectrum of 40c and m/z 174 in the spectrum of 40h corresponded to loss of a halogen radical from the $\{M-ArSO_2\}^+$ ion. This fragmentation was supported by peaks corresponding to metastable ions in the normal, singly focussed spectra. An ion of m/z 160 appears in the spectrum of 40e and probably corresponds to an analogous loss of the methyl substituent from the $\{M-Ar^1SO_2\}^+$ ion, although here no supporting metastable peak is apparent. Exact mass analyses of m/z 160 in the mass spectra of 40b, 40d, 40f and 40g confirm the composition of this ion to be $C_{10}H_8S$ (see Table 3.2 - 4).

Two skeletal rearrangements of 40 were also observed, resulting in the formation of $\{M-Ar^1SO\}^+$ and a bisarylsulphide ion ($Ar^1SAr^{2+}\cdot$). These ions were present in the normal mass spectra in all cases and were also detected by B/E linked scanning of the molecular ions

of 40f and 40b, respectively.

Scheme 3.2 - 1 illustrates the electron impact induced fragmentation of 40. The formation of the ions shown in Scheme 3.2 - 1 from the molecular ions of the 1-arylsulphonyl-4-arylthio-2-butynes was supported by the presence of corresponding metastable peaks and/or by B/E linked scanning of selected ions in the mass spectra of 40b and 40f. The relative abundances of significant ions, metastable peak data, B/E linked scanning data and results of exact mass analyses are presented in Tables 3.2 - 1 to 3.2 - 4 respectively.

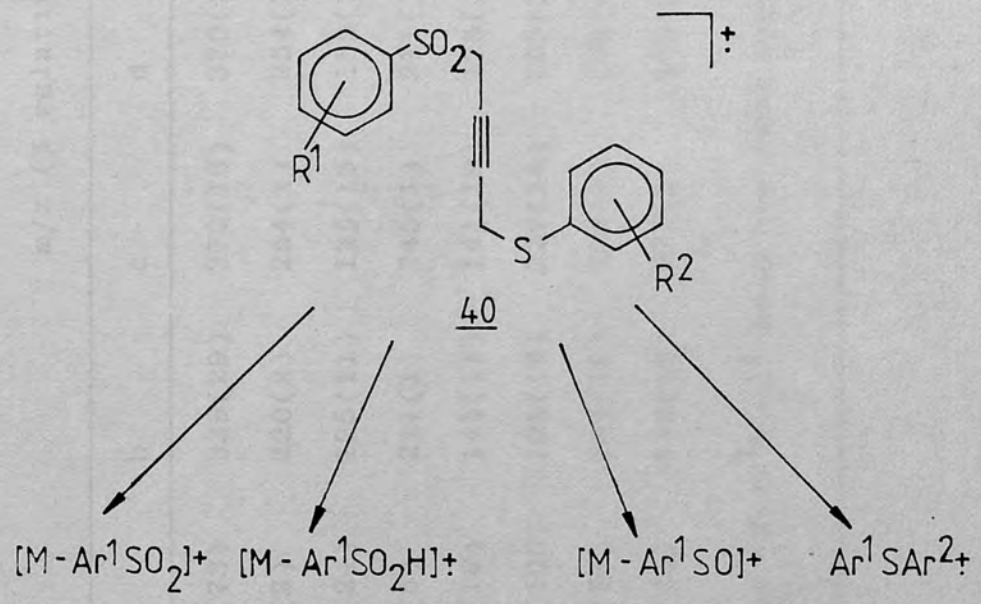

Scheme 3.2 - 1

TABLE 3.2 - 1

Significant ions in the 70 eV mass spectra of 1-arylsulphonyl-4-arylthio-2-butynes (40)

m/z (% relative abundance)

ION	a	b	c	d	e	f	g	h
$M^{+\cdot}$	302(73)	336(29)	370(16)	370(22)	350(47)	350(55)	394(52)	408(22)
$Ar^1SAr^{2+\cdot}$	186(2)	220(2)	254(1)	254(1)	234(1)	234(2)	278(1)	292(1)
Ar^1SO^+	125(24)	125(11)	125(16)	159(14)	159(16)	139(15)	139(11)	139(12)
$\{M-ArSO\}^+$	177(5)	211(1)	245(1)	211(1)	191(1)	211(1)	255(0.4)	269(0.4)
$Ar^1SO_2^+$	141(16)	141(11)	141(19)	175(10)	175(100)[a]	155(21)	155(12)	155(10)
$\{M-Ar^1SO_2\}^+$	161(100)	195(18)	229(16)	195(20)	175(100)[a]	195(17)	239(3)	253(3)
$\{M-Ar^1SO_2H\}^{+\cdot}$	160(77)	194(10)	228(9)	194(9)	174(20)	194(8)	238(7)	252(7)
Ar^2S^+	109(76)	143(19)	177(9)	143(23)	123(55)	143(19)	187(7)	201(6)

[a] $Ar^1SO_2^+$ and $\{M-Ar^1SO_2\}^+$ have the same nominal mass, in this case.

TABLE 3.2 - 2

Peaks corresponding to metastable ions in the 70 eV mass spectra of 1-arylsulphonyl-4-arylthio-2-butynes (40).

Derivative	Metastable peak	Transition	Neutral Lost
40a	85.8	302 → 161	$Ar^1SO_2\cdot$
40b	131.3	195 → 160	Cl·
	113.2	336 → 195	$Ar^1SO_2\cdot$
40c	164.3	229 → 194	Cl·
	141.7	370 → 141	$Ar^1SO_2\cdot$
40d	131.3	195 → 160	Cl·
	102.8	370 → 195	$Ar^1SO_2\cdot$
40e	146.2	175 → 160	$CH_3\cdot$
	104.2	350 → 191	$Ar^1SO\cdot$
	87.5	350 → 175	$Ar^1SO_2\cdot$
40f	131.3	195 → 160	Cl·
	108.6	350 → 195	$Ar^1SO_2\cdot$
40g	145.0	394 → 239	$Ar^1SO_2\cdot$
	107.1	239 → 160	Br·
40h	156.9	408 → 253	$Ar^1SO_2\cdot$
	119.7	253 → 174	Br·

TABLE 3.2 - 3

Product ions determined by the B/E linked scanning spectra of selected ions in the mass spectra of 40b and 40f

Ion scanned				Product ions detected
Derivative	m/z	Assignment	Neutral lost	m/z
40b	376	$M^{+}\cdot$	$Ar^{1}SO_2\cdot$	195
			$Ar^{1}SO_2H$	194
	195	$\{M-Ar^{1}SO_2\}^{+}$	Cl·	160
40f	350	$M^{+}\cdot$	$C_4H_4SO_2$	234
			$Ar^{1}SO\cdot$	211
			$Ar^{1}SO_2\cdot$	195
			$Ar^{1}SO_2H$	194
	195	$\{M-Ar^{1}SO_2\}^{+}$	Cl·	160

TABLE 3.2 - 4

Exact mass analyses of m/z 160 in the mass spectra of 40b, 40d, 40f and 40g

		Exact Mass	
Derivative	Composition	Calc.	Found
40b	$C_{10}H_8S$	160.0347	160.0354
40d	$C_{10}H_8S$	160.0347	160.0354
40f	$C_{10}H_8S$	160.0347	160.0354
40g	$C_{10}H_8S$	160.0347	160.0347

3.3 Discussion

In contrast to the behaviour of 1,4-bis(arylthio)-2-butynes[62] and 1,4-bis(arylsulphonyl)-2-butynes[43], which eliminated a four carbon cumulene moiety upon electron impact, no such elimination from any of the 1-arylsulphonyl-4-arylthio-2-butynes 40 was observed nor was the elimination of sulphur or sulphur dioxide detected. One of the skeletal rearrangements which was observed, the elimination of the elements of $C_4H_4SO_2$ to yield a bisarylsulphide ion, is notable in view of the intervening distance between the arylthio group and the arylsulphonyl group. Since the elimination of $C_4H_4SO_2$ from 40 appears unlikely, because of the rigidity of the butynyl system, it is probable that rearrangement occurs prior to the formation of the bisarylsulphide ion. A {1,3} arylthio shift enables the arylthio group and arylsulphonyl group to come into close proximity in 43, as illustrated in Scheme 3.3 - 1.

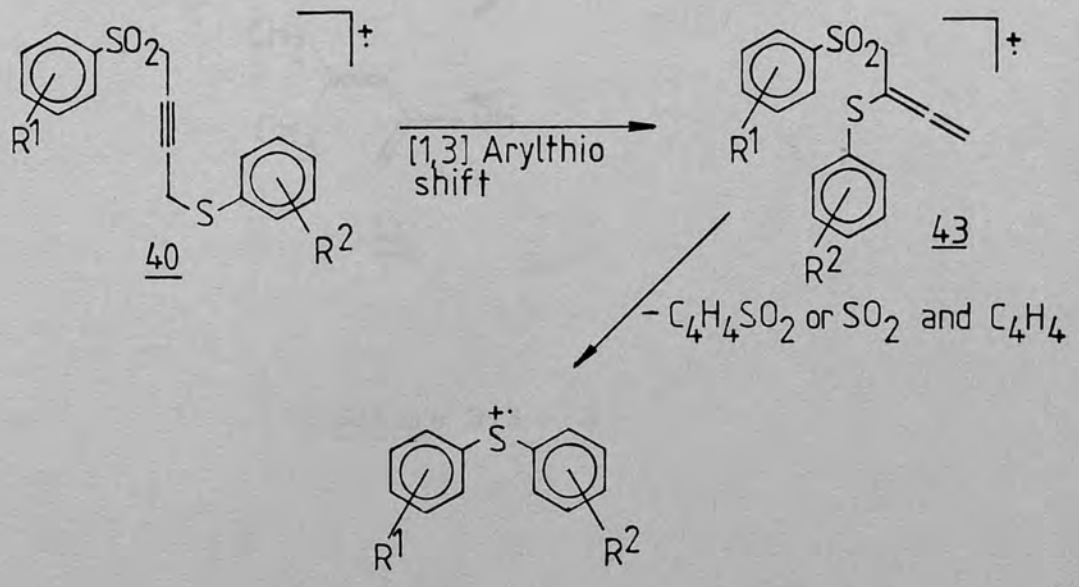

Scheme 3.3 - 1

Such {1,3} arylthio migrations have been postulated in both the electron impact induced rearrangements and thermal rearrangements of compounds containing a triple bond α to an arylthio group (see Section 1.3.3.3). The electron impact induced rearrangements of some alkynyl and allenyl alcohols have been reported[78] and provide further examples of {1,3} migration to an sp hybridised carbon by groups other than hydrogen (e.g. 44 → 45 → 46, Scheme 3.3 - 2 and 47 → 48, Scheme 3.3 - 3).

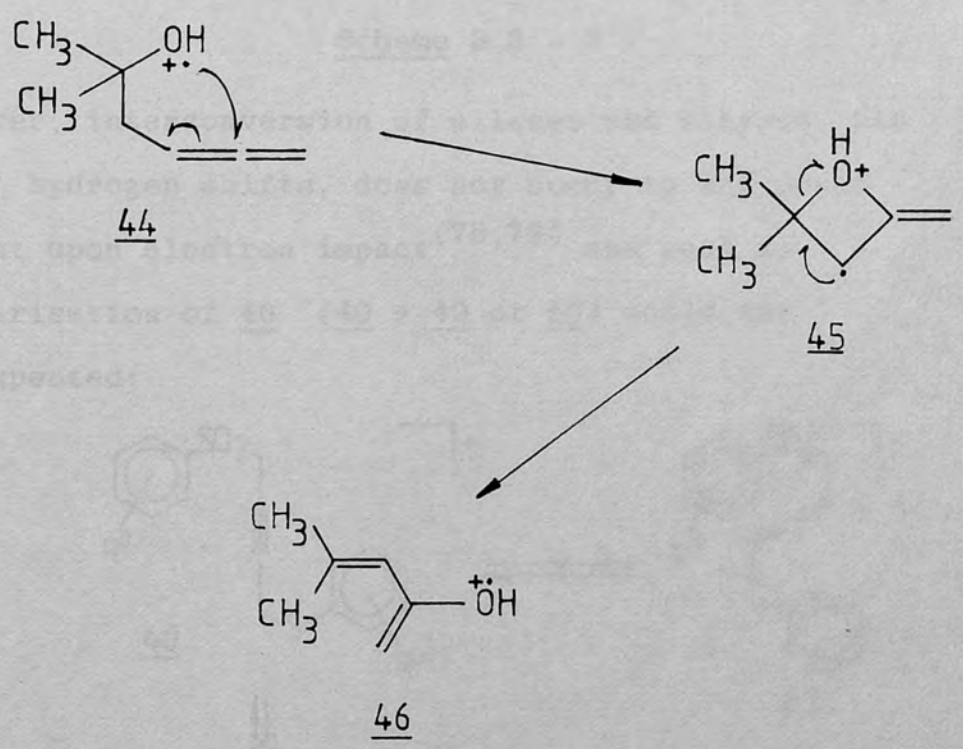

Scheme 3.3 - 2

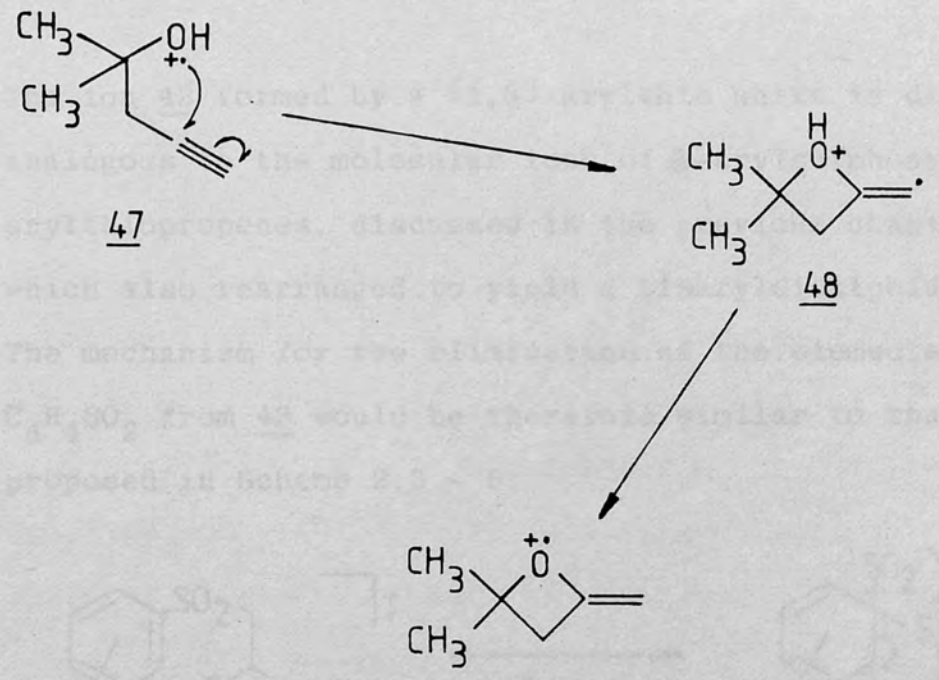

Scheme 3.3 - 3

However, interconversion of allenes and alkynes, via {1,3} hydrogen shifts, does not occur to any great extent upon electron impact[78,79] and such an isomerisation of 40 (40 → 49 or 50) would not be expected:

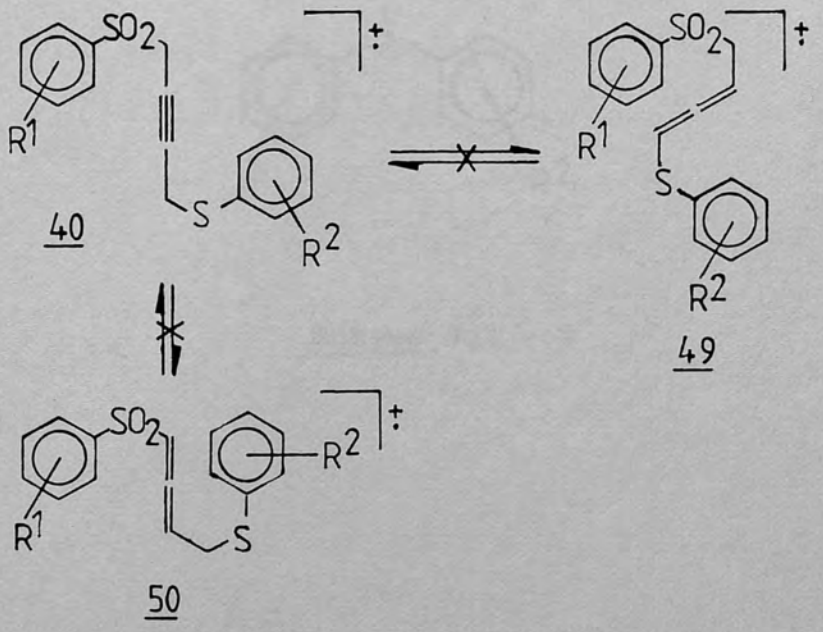

Scheme 3.3 - 4

The ion 43 formed by a {1,3} arylthio shift is directly analogous to the molecular ions of 3-arylsulphonyl-2-arylthiopropenes, discussed in the previous chapter, which also rearranged to yield a bisaryldisulphide ion. The mechanism for the elimination of the elements of $C_4H_4SO_2$ from 43 would be therefore similar to that proposed in Scheme 2.3 - 5:

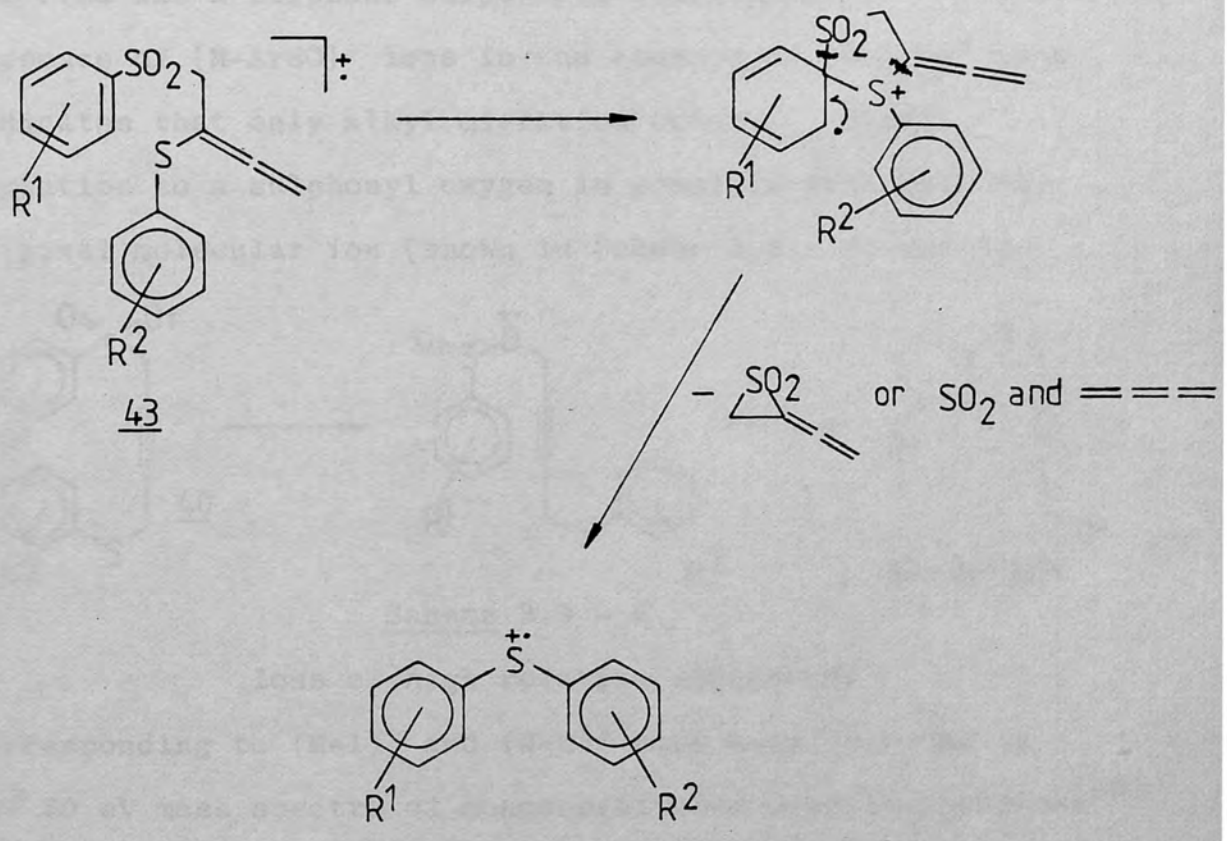

Scheme 3.3 - 5

The reader is directed to Section 2.3, as the arguments concerning the mechanism shown in Scheme 3.3 - 5 would be the same as those for Scheme 2.3 - 5. The eliminated neutral portion could be either a thiirane-1,1-dioxide or sulphur dioxide and a four carbon cumulene.

The only other skeletal rearrangement observed was a sulphone-sulphinate rearrangement. The presence of $\{M-ArSO\}^+$ ions in the absence of $\{M-ArO\}^+$ ions indicates that only alkyl migration occurs. Alkyl migration to a sulphonyl oxygen is possible with both the original molecular ion (shown in Scheme 3.3 - 6) and 43.

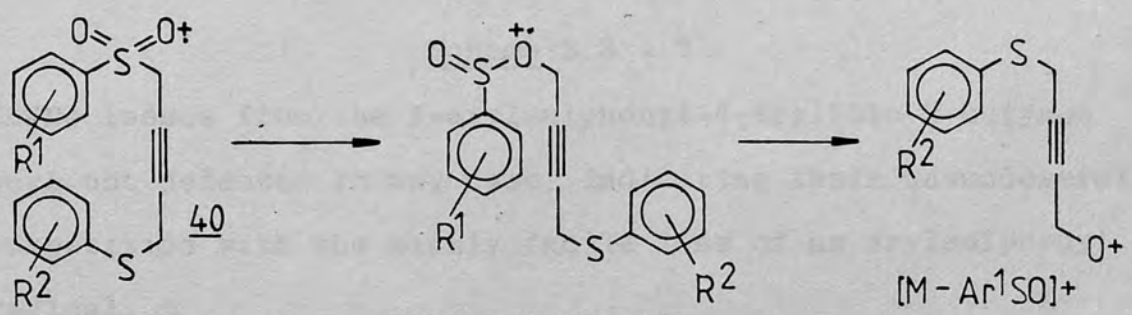

Scheme 3.3 - 6

Ions of high relative abundances corresponding to $\{M-1\}^+$ and $\{M-R\}^+$ have been observed in the 70 eV mass spectra of monosubstituted 3-aryloxypropynes[80] (51a, Scheme 3.3 - 7) and one might expect the 1-arylsulphonyl-4-arylthio-2-butynes (51b) to behave as sulphur analogues.

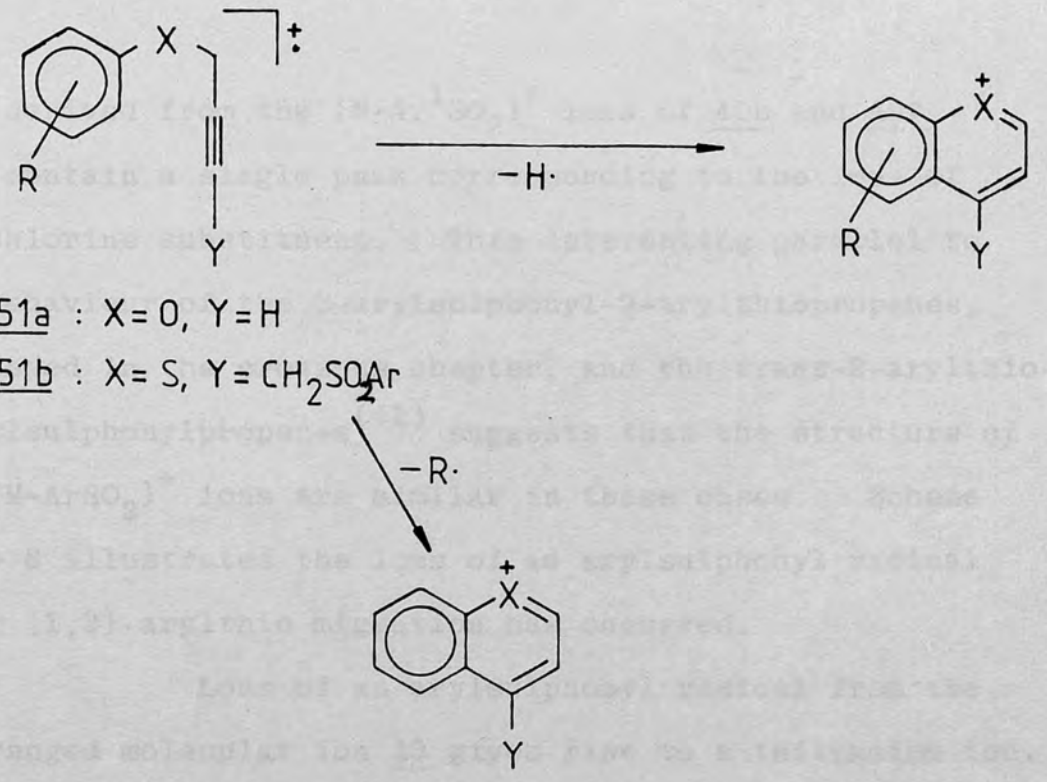

Scheme 3.3 - 7

These losses from the 1-arylsulphonyl-4-arylthio-2-butynes were not detected in any case, indicating their unsuccessful competition with the highly facile loss of an arylsulphonyl radical.

The loss of a substituent from the aryl group of the $\{M-Ar^1SO_2\}^+$ ion was observed to be highly facile and the resulting ions corresponded to the base peak in those cases in which Ar^2 contained a bromine or chlorine substituent. In the case of 40h, in which Ar^2 is 4-bromo-3-methylphenyl, the loss of a bromine radical from the $\{M-Ar^1SO_2\}^+$ ion occurs exclusively. Loss of the methyl substituent from the $\{M-Ar^1SO_2\}^+$ ion of 36e was also observed , however, and a corresponding metastable peak was present. B/E linked scanning spectra of the

ions derived from the $\{M-Ar^1SO_2\}^+$ ions of 40b and 40f each contain a single peak corresponding to the loss of the chlorine substituent. This interesting parallel to the behaviour of the 3-arylsulphonyl-2-arylthiopropenes, discussed in the previous chapter, and the trans-2-arylthio-/-arylsulphonylpropenes[41] suggests that the structure of the $\{M-ArSO_2\}^+$ ions are similar in these cases. Scheme 3.3 - 8 illustrates the loss of an arylsulphonyl radical after {1,3} arylthio migration has occurred.

Loss of an arylsulphonyl radical from the rearranged molecular ion 43 gives rise to a thiiranium ion. Isomerisation is then possible to give the thiirenium ion 52 (the stability of these ions has been mentioned in Section 2.3) which is analogous to the $\{M-Ar^1SO_2\}^+$ ions derived from the trans-2-arylthio-/-arylsulphonylpropenes.[41] The loss of a ring substituent can occur from 52, as shown, or from the thiiranium ion.

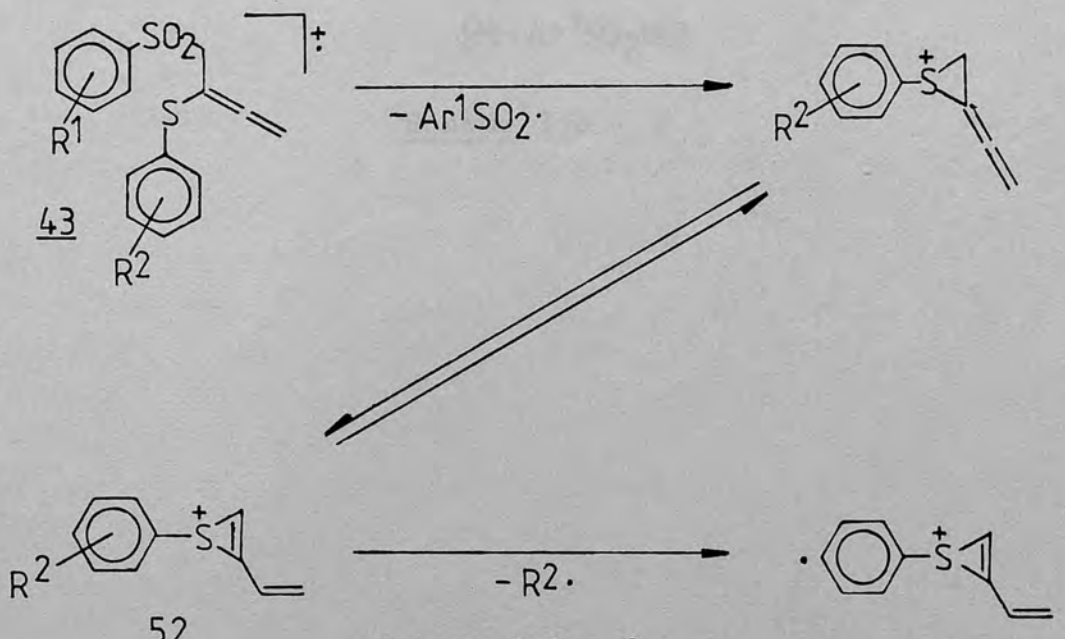

Scheme 3.3 - 8

Hydrogen migration to the departing arylsulphonyl group was observed in all cases to give rise to the $\{M-ArSO_2H\}^{+\cdot}$ ion. Donation from the 4-position to give an arylthiocumulene is illustrated in Scheme 3.3 - 9. Donation from the 1-position would result in the less favourable formation of a carbene.

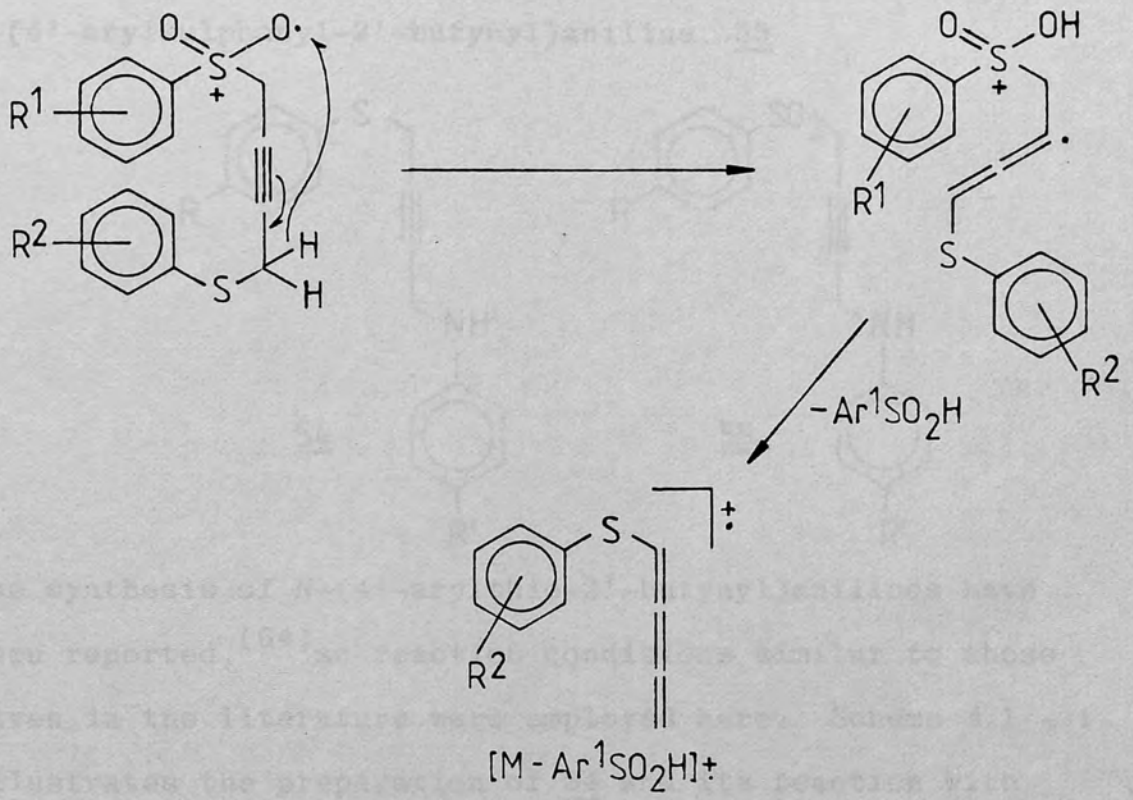

Scheme 3.3 - 9

4. N-(4'-ARYLSULPHONYL-2'-BUTYNYL)-N-(4''-ARYLTHIO-2''-BUTYNYL)ANILINES.

4.1 Synthesis

Obvious choices for synthetic intermediates in the preparation of the title compounds, 53, include N-(4'-arylthio-2'-butynyl)anilines, 54, and N-(4'-arylsulphonyl-2'-butynyl)aniline, 55

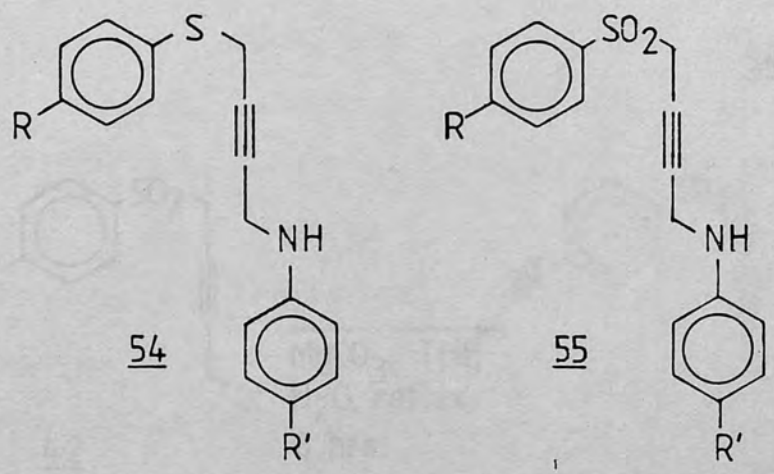

54 55

The synthesis of N-(4'-arylthio-2'-butynyl)anilines have been reported,[64] so reaction conditions similar to those given in the literature were employed here. Scheme 4.1 - 1 illustrates the preparation of 54 and its reaction with 4-arylsulphonyl-1-chloro-2-butyne to give the title compounds.

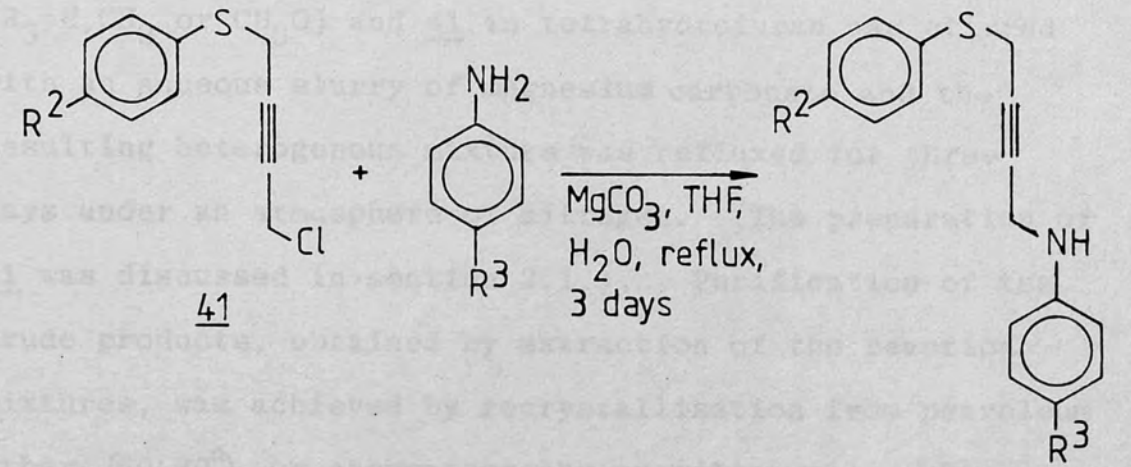

54, 20 - 70%

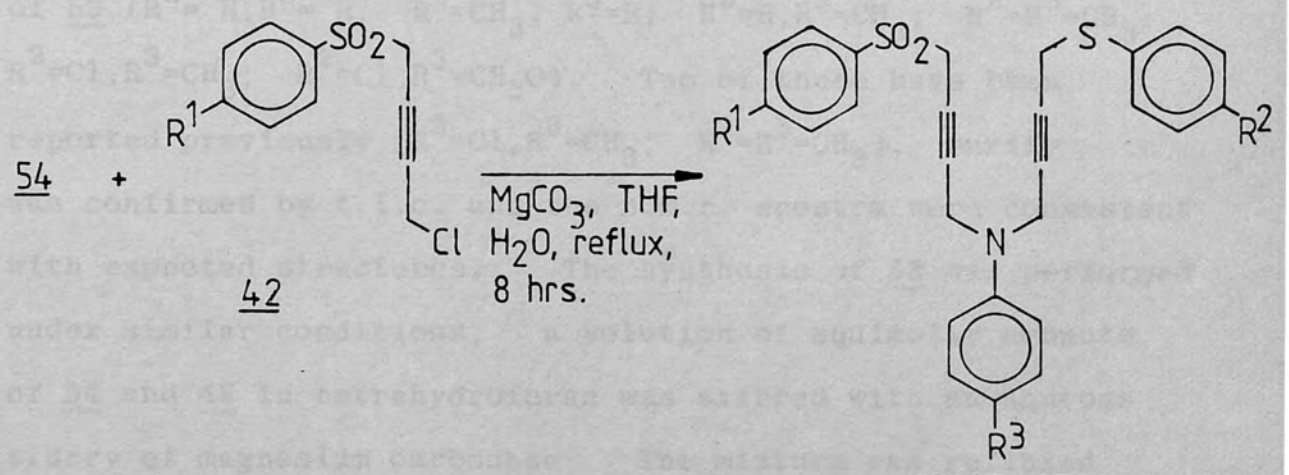

53, 27 - 85%

53a: R^1=Cl, R^2=H, R^3=H
53b: R^1=Cl, R^2=CH_3, R^3=H
53c: R^1=Cl, R^2=H, R^3=CH_3
53d: R^1=Cl, R^2=R^3=CH_3
53e: R^1=R^2=Cl, R^3=CH_3
53f: R^1=H, R^2=Cl, R^3=CH_3
53g: R^1=R^2=Cl, R^3=CH_3O
53h: R^1=H, R^2=Cl, R^3=CH_3O

Scheme 4.1 - 1

A solution of the desired arylamine (R_3=H,CH_3 or CH_3O) and 41 in tetrahydrofuran was stirred with an aqueous slurry of magnesium carbonate and the resulting heterogenous mixture was refluxed for three days under an atmosphere of nitrogen. (The preparation of 41 was discussed in section 2.1.). Purification of the crude products, obtained by extraction of the reaction mixtures, was achieved by recrystallisation from petroleum ether (60-80°), or chromatography on silica gel. Six derivatives of 54 were prepared for use in the synthesis of 53 (R^2= H,R^3= H; R^2=CH_3, R^3=H; R^2=H,R^3=CH_3; R^2=R^3=CH_3; R^2=Cl,R^3=CH_3; R^2=Cl,R^3=CH_3O). Two of these have been reported previously (R^2=Cl,R^3=CH_3; R^2=R^3=CH_3). Purity was confirmed by t.l.c. and the n.m.r. spectra were consistent with expected structures. The synthesis of 53 was performed under similar conditions; a solution of equimolar amounts of 54 and 42 in tetrahydrofuran was stirred with an aqueous slurry of magnesium carbonate. The mixture was refluxed for eight hours under a blanket of nitrogen and the organic layer was separated, dried, and the solvent removed *in vacuo* to give the crude products. Solids obtained by this procedure were triturated with hot petroleum spirit and analytical samples were recrystallised from a methylene chloride/petroleum spirit mixture. Oily crude products were chromatographed on silica gel and recrystallised as above. Yields after trituration or chromatography were in the range of 27-85%. The n.m.r. and mass spectra of these

compounds were in accordance with their expected structures, and the results of elemental analyses were in good agreement with calculated values.

4.2 E.I. induced fragmentation results.

Moderately high relative abundances of molecular ions were observed in the 70 eV mass spectra of 53a-h . Correlation of metastable ions (Table 4.2 -2) and B/E linked scanning studies (Tables 4.2 - 3 and 4.2 - 4) established the principal fragmentation routes to be those depicted in Scheme 4.2 - 1 (Ar^1 and Ar^2 are defined as before. $Ar^3=R^3C_6H_4$). Predictably, the facile loss of $Ar^1SO_2\cdot$, Ar^1SO_2H and $Ar^2S\cdot$ from the molecular ion was observed in all cases. Simple C-N bond fission and C-N bond fission accompanied by proton rearrangement were also evident. (For the sake of simplicity, ions arising by C-N bond cleavage with concomitant hydrogen rearrangement are not shown).

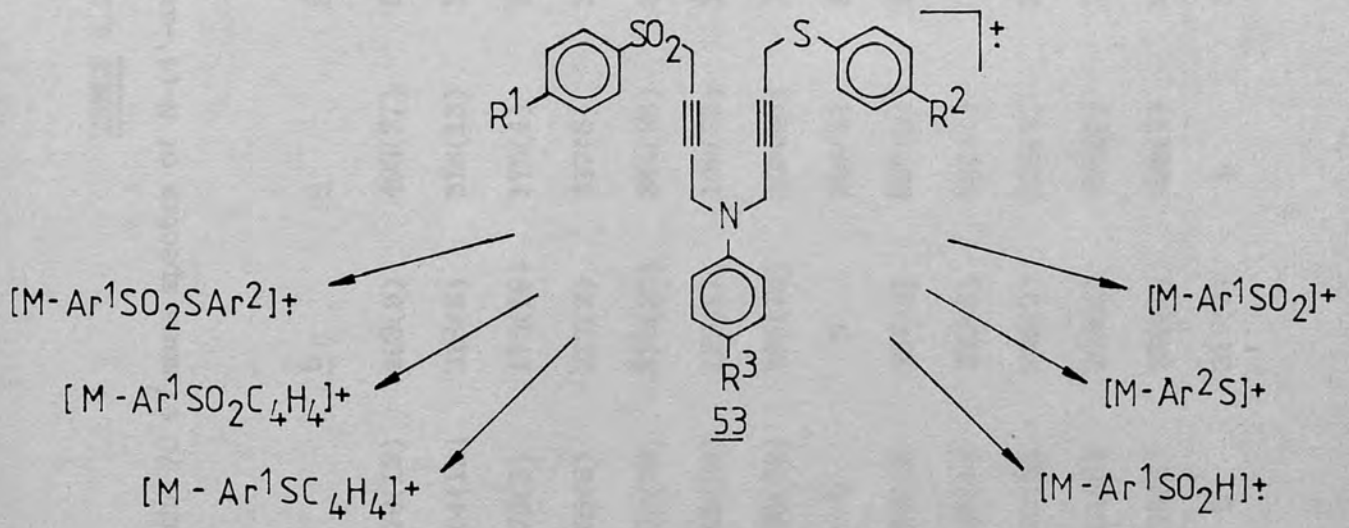

Scheme 4.2 - 1

TABLE 4.2 - 1

Significant ions in the 70 eV mass spectra of N-(4'-arylsulphonyl-2-butynyl)-N-(4''-arylthio-2''-butynyl)anilines (53).

	m/z (% Relative abundance)							
Ion	a	b	c	d	e	f	g	h
$M^{+\cdot}$	479(13)	493(9)	493(27)	507(26)	527(19)	493(15)	543(16)	509(24)
$\{M-Ar^1SO_2\}^+$	304(12)	318(8)	318(13)	332(11)	352(13)	352(14)	368(8)	368(9)
$Ar^1SO_2^+$	175(3)	175(19)	175(4)	175(26)	175(16)	141(11)	175(23)	141(24)
$\{M-Ar^1SO_2H\}^{+\cdot}$	303(6)	317(2)	317(6)	331(4)	351(9)	351(12)	367(7)	367(13)
$\{M-Ar^2S\}^+$	370(29)	370(25)	384(26)	384(28)	384(22)	350(52)	400(9)	366(23)
Ar^2S^+	109(20)	123(17)	109(23)	123(25)	143(15)	143(11)	143(27)	143(100)
$\{M-Ar^1SSO_2Ar^2\}^{+\cdot}$	195(72)	195(75)	209(86)	209(99)	209(56)	209(93)	225(48)	225(56)
$Ar^1SSO_2Ar^{2+\cdot}$	b	b	284(1)	298(1)	318(2)	284(2)	318(6)[a]	284(9)
$\{M-Ar^1SO_2C_4H_3\}^{+\cdot}$	253(3)	267(2)	267(2)	281(4)	301(22)	301(6)	317(42)	317(29)
$Ar^1SO_2C_4H_3^{+\cdot}$	226(1)	226(1)	226(1)	226(1)	226(1)	192(6)	226(10)	192(4)
$\{M-Ar^1SO_2C_4H_4\}^+$	252(3)	266(2)	266(3)	280(4)	300(12)	300(4)	316(10)	316(17)
$\{M-Ar^1SO_2C_4H_5\}^{+\cdot}$	251(6)	265(4)	265(6)	279(9)	299(46)	299(10)	315(35)	315(75)
$Ar^1SO_2C_4H_5^{+\cdot}$	228(2)	228(1)	228(1)	228(2)	228(11)	194(21)	228(4)	194(8)
$\{M-Ar^2SC_4H_3\}^{+\cdot}$	b	319(3)	b	333(4)	333(2)	299(10)	349(5)	315(75)

/ continued ..

TABLE 4.2 - 1 (continued)

Ion	a	b	c	d	e	f	g	h
$Ar^2SC_4H_3^+$	160(5)	174(3)	160(5)	174(2)	194(12)	194(21)	194(5)	194(8)
$\{M-Ar^2SC_4H_4\}^{+\cdot}$	b	318(8)	b	332(11)	332(2)	298(2)	348(8)	314(5)
$Ar^2SC_4H_4^+$	161(21)	175(19)	161(22)	175(26)	195(6)	195(6)	195(5)	195(17)
$\{M-Ar^2SC_4H_5\}^{+\cdot}$	b	317(2)	b	331(4)	331(3)	297(1)	347(7)	313(9)
$Ar^2SC_4H_5^{+\cdot}$	162(3)	176(4)	162(4)	176(4)	196(3)	196(2)	196(2)	196(7)
$Ar^3NC_8H_7^+$	194(100)	194(100)	208(100)	208(99)	208(58)	208(100)	224(48)	224(73)
$Ar^3NC_6H_5^+$	168(6)	168(5)	182(5)	182(5)	182(4)	182(4)	198(3)	198(6)
$Ar^3NC_4H_5^+$	144(17)	144(14)	158(15)	158(19)	158(22)	158(19)	174(23)	174(76)
$Ar^3NC_4H_4^{+\cdot}$	143(63)	143(58)	157(16)	157(100)	157(62)	157(96)	173(61)	173(56)
$Ar^3NC_4H_3^+$	142(27)	142(25)	156(92)	156(34)	156(100)	156(55)	172(100)	172(36)
$C_6H_4NC_8H_8^+$	194(100)	194(100)	194(20)	194(20)	194(12)	194(21)	194(5)	194(8)
Ar^1SO^+	159(14)	159(11)	159(13)	159(15)	159(78)	125(24)	159(65)	125(57)

a) Approximately 50% contribution from $C_{17}H_{15}Cl^{37}NOS$ ($\{M-Ar^1SO_2C_4H_4\}^{+\cdot}$).

b) Present in less than 1% relative abundances.

TABLE 4.2 - 2

Metastable peaks identified in the 70 eV mass spectra of N-(4'-arylsulphonyl-2'-butynyl)-N-(4"-arylthio-2"-butynyl)anilines (53).

Derivative	Metastable peak (m/z)	Transition	Neutral lost
53a	211.1	479 → 318	$Ar^2SC_4H_4\cdot$
	192.9	479 → 304	$Ar^1SO_2\cdot$
	132.5	479 → 252	$Ar^1SO_2C_4H_4\cdot$
	125.1	304 → 195	$Ar^2S\cdot$
	123.8	304 → 194	Ar^2SH
	102.8	370 → 195	$Ar^1SO_2\cdot$
53b	203.8	493 → 317	$Ar^1SO_2\cdot$
	119.9	317 → 195	$Ar^2S\cdot$
	118.7	317 → 194	Ar^2SH
	102.7	370 → 195	$Ar^1SO_2\cdot$
	96.6	317 → 175	$Ar^3NC_4H_4$
53c	299.1	493 → 384	$Ar^2S\cdot$
	205.1	493 → 318	$Ar^1SO_2\cdot$
	144.6	493 → 266	$Ar^1SO_2C_4H_4\cdot$
	137.3	318 → 209	$Ar^2S\cdot$
	113.7	384 → 209	$Ar^1SO_2\cdot$

/ continued ..

TABLE 4.2 - 2 (continued)

Derivative	Metastable peak (m/z)	Transition	Neutral lost
53d	290.8	507 → 384	$Ar^2S\cdot$
	217.4	507 → 332	$Ar^1SO_2\cdot$
	154.6	507 → 280	$ArSO_2C_4H_4\cdot$
	131.6	332 → 209	$Ar^2S\cdot$
	130.3	332 → 208	Ar^2SH
	113.7	384 → 209	$Ar^1SO_2\cdot$
	64.2	384 → 157	$Ar^1SO_2C_4H_4\cdot$
53e	279.8	527 → 384	$Ar^2S\cdot$
	235.1	527 → 352	$Ar^1SO_2\cdot$
	124.1	352 → 209	$Ar^2S\cdot$
	113.7	384 → 209	$Ar^1SO_2\cdot$
	82.8	527 → 209	$Ar^1SO_2SAr^2$
	69.1	352 → 156	$Ar^2SC_4H_5$
53f	251.3	493 → 352	$Ar^1SO_2\cdot$
	248.5	493 → 350	$Ar^2S\cdot$
	180.1	493 → 298	$Ar^2SC_4H_4$
	124.8	350 → 209	Ar^1SO_2
	124.1	352 → 209	$Ar^2S\cdot$
	88.6	493 → 209	$Ar^1SO_2SAr^2$

/ continued ..

TABLE 4.2 - 2 (continued)

Derivative	Metastable peak (m/z)	Transition	Neutral lost
53g	294.6	543 → 350	$Ar^2S\cdot$
	249.4	543 → 368	Ar^1SO_2
	80.4	368 → 172	$Ar^2SC_4H_4$
53h	266.1	509 → 368	$Ar^1SO_2\cdot$
	263.2	509 → 366	$Ar^2S\cdot$
	138.3	366 → 225	$Ar^1SO_2\cdot$
	137.6	368 → 225	$Ar^2S\cdot$
	99.5	509 → 225	$Ar^1SO_2SAr^2$
	81.7	366 → 172	$ArSO_2C_4H_4\cdot$
	80.4	368 → 172	$Ar^2SC_4H_4\cdot$

TABLE 4.2 - 3

Product ions identified by B/E linked scanning of selected ions in the mass spectrum of 53f.

Precursors scanned			Product ion
m/z	Assignment	Neutral lost	m/z
493	$M^{+\cdot}$	$Ar^1SO\cdot$	352
		$Ar^2S\cdot$	350
		$Ar^1SO_2C_4H_4\cdot$	300
		$Ar^1SO_2C_4H_5$	299
		$Ar^1SO_2SAr^2$	209
352	$\{M-Ar^1SO_2\}^+$	$Ar^2S\cdot$	209
		Ar^2SH	208
		$Ar^3NC_4H_4$	195
		$Ar^2SC_4H_4\cdot$	157
		$Ar^2SC_4H_5$	156
350	$\{M-Ar^2S\}^+$	$Ar^1SO_2\cdot$	209
		Ar^1SO_2H	208
		$Ar^3NC_4H_4$	193
		$Ar^1SO_2C_4H_4\cdot$	157
		$Ar^1SO_2C_4H_5$	156
209	$\{M-Ar^1SO_2SAr^2\}^{+\cdot}$	$H\cdot$	208
		$CH_3\cdot$	194
		$C_2H_3\cdot$	182
		C_4H_4	157

TABLE 4.2 - 4

Product ions identified by B/E linked scanning of selected ions in the mass spectra of 53h.

Precursors scanned			Product ion
m/z	Assignment	Neutral lost	m/z
509	$M^{+\cdot}$	$Ar^1SO_2\cdot$	368
		$Ar^2S\cdot$	366
		$Ar^1SO_2C_4H_4\cdot$	316
		$Ar^1SO_2C_4H_5$	315
		$Ar^2SC_4H_4\cdot$	314
		$Ar^2SC_4H_5$	313
		$Ar^1SO_2SAr^2$	225
368	$\{M-Ar^1SO_2\}^+$	$Ar^2S\cdot$	225
		Ar^2SH	224
		$Ar^3NC_4H_4$	195
366	$\{M-Ar^2S\}^+$	$Ar^1SO_2\cdot$	225
		Ar^1SO_2H	224
		$Ar^1SO_2C_4H_4\cdot$	173
		$Ar^1SO_2C_4H_5$	172
225	$\{M-Ar^1SO_2SAr^2\}^{+\cdot}$	$H\cdot$	224
		$CH_3\cdot$	210
		$C_2H_3\cdot$	198
		$CH_3O\cdot$	194
		C_4H_4	173

The loss of sulphur dioxide or sulphur was not observed from any of the eight molecular ions. In every case however, an ion was present which arises from elimination of an $Ar^1SO_2SAr^2$ moiety. This loss was substantiated by metastable peaks in several instances and by the presence of ions corresponding to $\{M-Ar^1SO_2SAr^2\}^+$ in the B/E linked scanning spectra obtained by focusing on the molecular ions of 53f and 53h.

B/E linked scans, focusing on the $\{M-Ar^1SO_2\}^+$ and $\{M-Ar^2S\}^+$ ions in the mass spectra of 53f and 53h, showed that ions of the same nominal mass as the $\{M-Ar^1SO_2SAr^2\}^+$ ions were formed by the losses of $Ar^2S\cdot$ from $\{M-Ar^1SO_2\}^+$ and $Ar^1SO_2\cdot$ from $\{M-Ar^2S\}^+$. (Schemes 4.2 - 2 and 4.2 - 3 illustrate these and other fragmentations undergone by the $\{M-Ar^1SO_2\}^+$ and $\{M-Ar^2S\}^+$ ions). Exact mass anlayses of the m/z 209 and m/z 225 ions arising from 53f and 53h, respectively, confirmed their compositions to be $C_{15}H_{15}N$ and $C_{15}H_{15}NO$, also respectively (see Table 4.2 - 5).

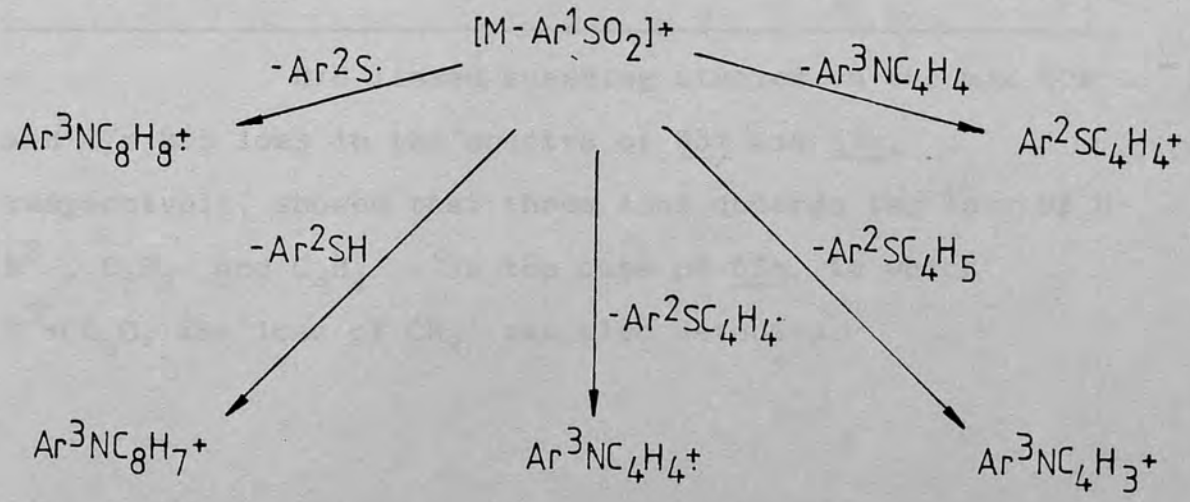

Scheme 4.2 - 2

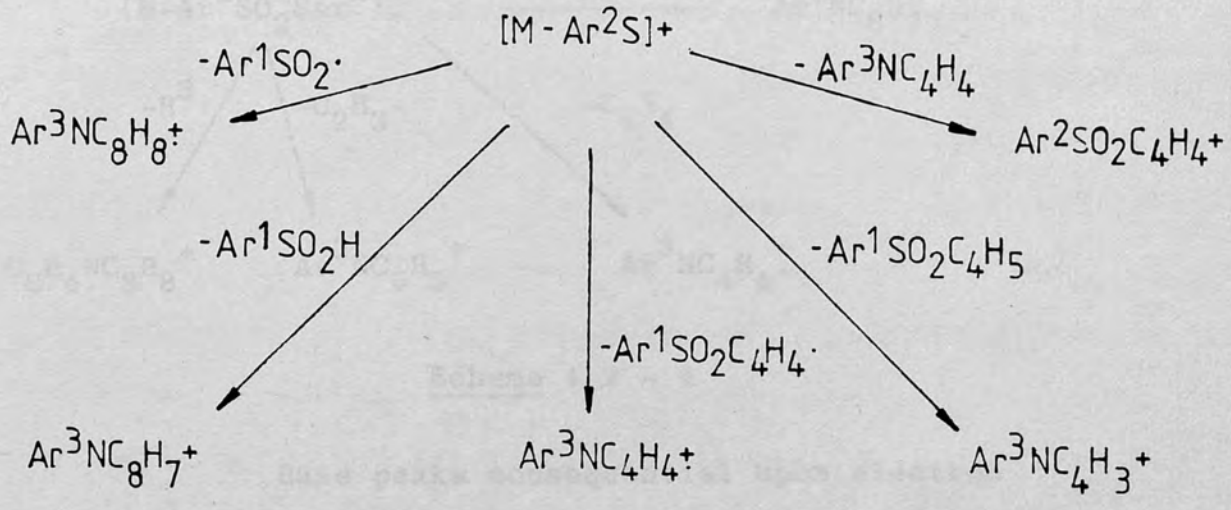

Scheme 4.2 - 3

TABLE 4.2 - 5

Exact mass analysis of selected ions in the mass spectra of 53f and 53h.

Derivative	Nominal mass (m/z)	Composition	Exact mass Calc.	Found
53f	209	$C_{15}H_{15}N$	209.1205	209.1185
53h	225	$C_{15}H_{15}NO$	225.1154	225.1152

B/E linked scanning studies on the m/z 209 and m/z 225 ions in the spectra of 53f and 53h, respectively, showed that these ions undergo the loss of H·, R^3·, C_2H_3· and C_4H_4. In the case of 53h, in which R^3=CH_3O, the loss of CH_3· was also detected.

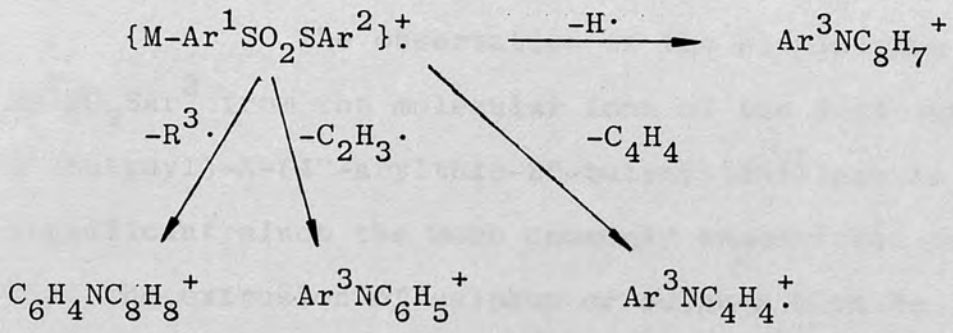

Scheme 4.2 - 4

Base peaks consequential upon electron impact of four of the compounds correspond to $Ar^3C_8H_7^+$, arising from the losses of Ar^2SH from $\{M-Ar^1SO_2\}^+$, Ar^1SO_2H from $\{M-Ar^2S\}^+$ and H· from $Ar^3C^8H_8^+$·. The $Ar^3NC_4H_3^+$ ions give the base peaks in the spectra of 53e and 53g and the ion of greatest abundance in the spectrum of 53d is $Ar^3NC_4H_4^+$·. The $Ar^3NC_4H_3^+$ and $Ar^3NC_4H_4^+$· ions may result from fragmentation of either the $\{M-Ar^2S\}^+$ or $\{M-Ar^1SO_2\}^+$ ions but $Ar^3NC_4H_4^+$· may also arise from fragmentation of the $\{M-Ar^1SO_2SAr^2\}^+$· ion. A peak corresponding to Ar^2S^+ has the highest intensity in the spectrum of 53h.

4.3 Discussion

The observation of the elimination of $Ar^1SO_2SAr^2$ from the molecular ions of the N-(4'-arylsulphonyl-2'-butynyl)-N-(4"-arylthio-2"-butynyl)anilines is highly significant since the more commonly encountered rearrangements viz. the extrusion of sulphur or sulphur dioxide, or a sulphone-sulphinate rearrangement were not observed. The related N,N-bis(4'-arylthio-2'-butynyl)anilines 27 and N,N-bis(4'-arylsulphonyl-2'-butynyl)aniline 13 have been shown to undergo the analogous losses of Ar^1SSAr^2 and $Ar^1SO_2SO_2Ar^2$, respectively[45] (see Scheme 4.3 - 1). The formation of 29 was postulated for both these systems and the possibility of its formation here from 53 exists also.

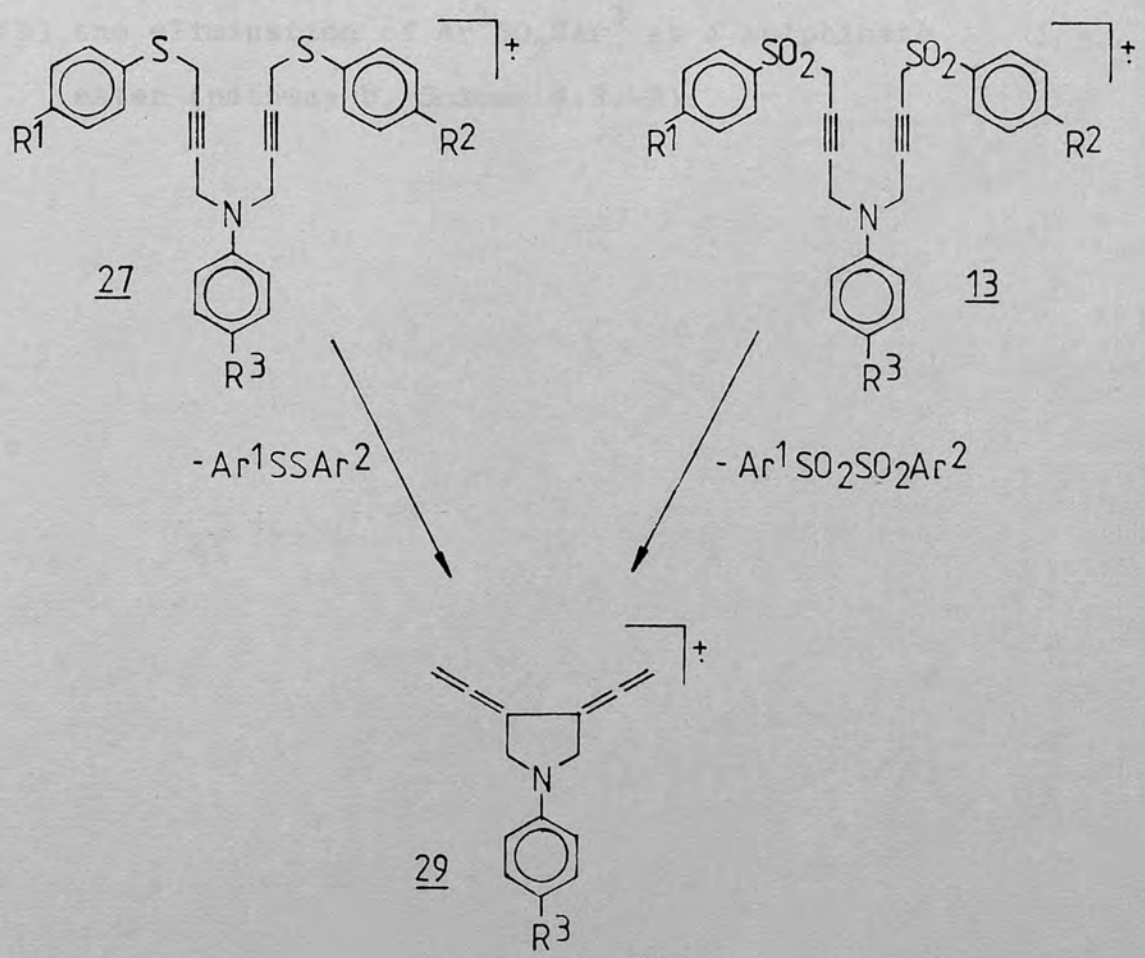

Scheme 4.3 - 1

Since electron induced or thermal {1,3} rearrangements of arylsulphonyl groups are not known, the elimination of $Ar^1SO_2SO_2Ar^2$ from 13 was postulated to occur from the unrearranged molecular ion. The possibility of{1,3} arylthio shifts in 27 is present, however, and elimination of a bisaryl disulphide moiety can occur from the unrearranged molecular ion or a rearranged molecular ion formed after the {1,3} migration of both arylthio groups[45], as discussed in Section 1.3.3.3.

Two possible mechanisms for the elimination of the elements of $Ar^1SO_2SAr^2$ from 53 are:

(a) the formation of a neutral bisaryl(thiosulphonate) fragment (pathway a, Scheme 4.3.-2) and

(b) the elimination of $Ar^1SO_2SAr^2$ as a sulphinate ester (pathway b, Scheme 4.3.-2).

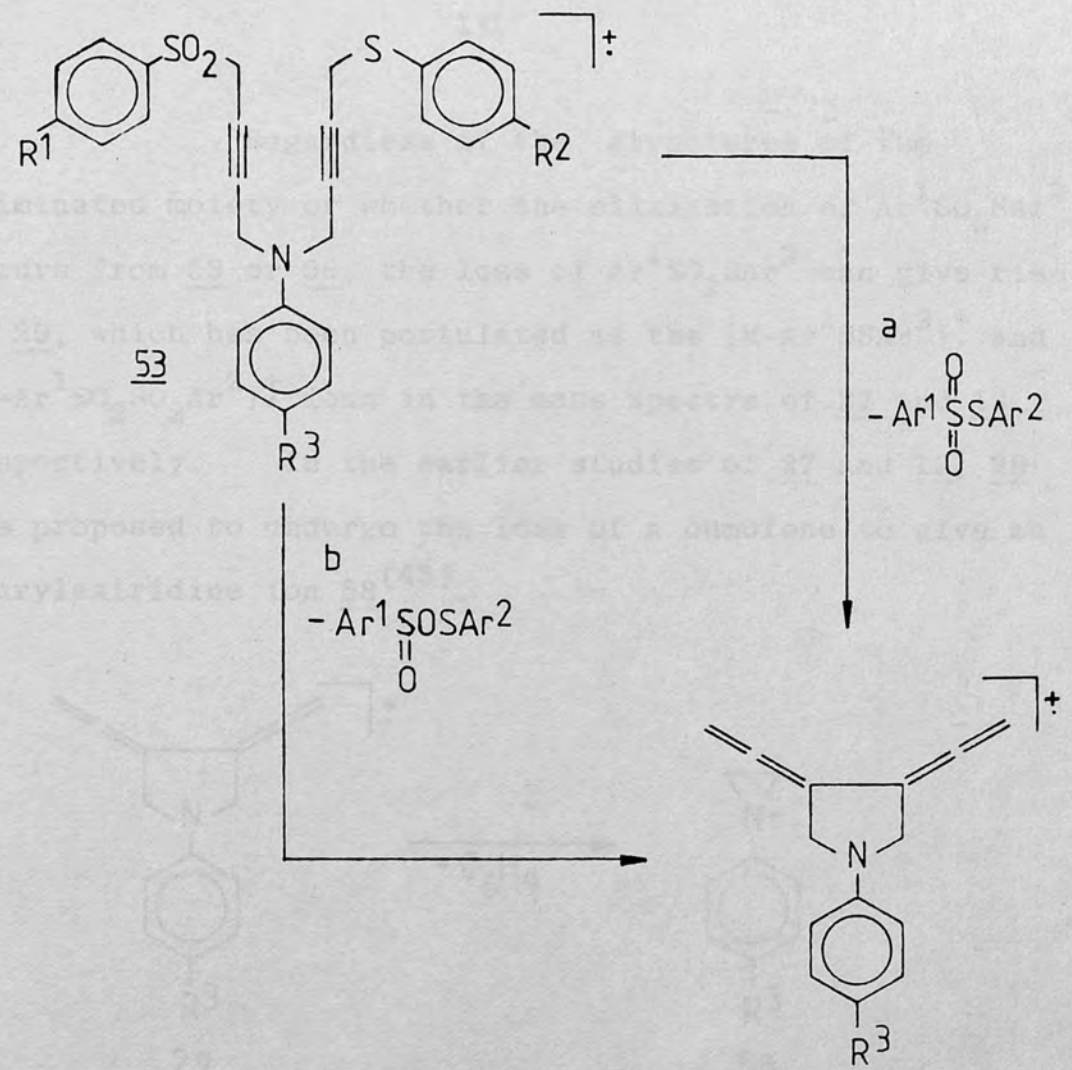

Scheme 4.3 - 2

The possibility of a {1,3} arylthio shift in 53 is also present and the elimination of $Ar^1SO_2SAr^2$ from an ion such as 56 cannot be dismissed entirely. However, since the elimination of $Ar^1SO_2SAr^2$ from 57 has not been observed[81], such a loss appears unlikely.

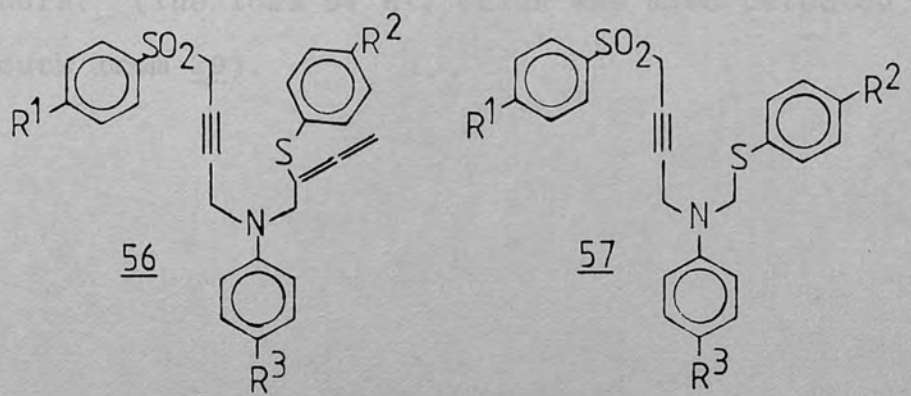

Regardless of the structures of the eliminated moiety or whether the elimination of $Ar^1SO_2SAr^2$ occurs from 53 or 56, the loss of $Ar^1SO_2SAr^2$ can give rise to 29, which has been postulated as the $\{M-Ar^1SSAr^2\}^{+\cdot}$ and $\{M-Ar^1SO_2SO_2Ar^2\}^{+\cdot}$ ions in the mass spectra of 27 and 13, respectively. In the earlier studies of 27 and 13, 29 was proposed to undergo the loss of a cumulene to give an N-arylaziridine ion 58[45].

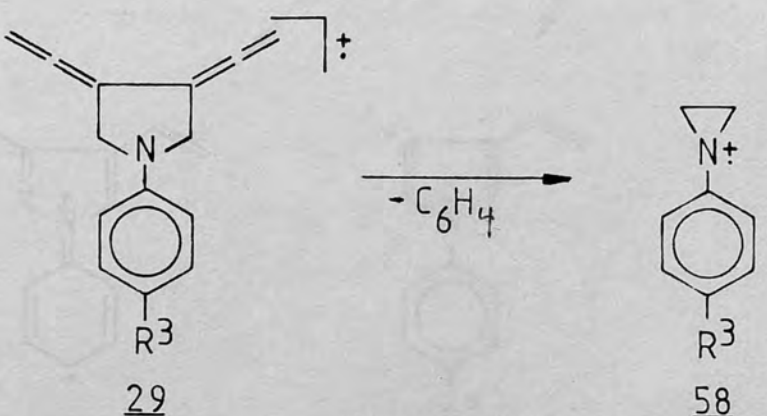

29 58

Scheme 4.3 - 3

However, B/E linked scanning studies of the $\{M-Ar^1SO_2SAr^2\}^{+\cdot}$ ion in the spectra of 53f and 53h indicated that the loss of C_6H_4 does not occur. Instead, the losses of $R^{3\cdot}$, $C_2H_3\cdot$ and C_4H_4 from the $\{M-Ar^1SO_2SAr^2\}^{+\cdot}$ ion were observed. These losses can be easily rationalised by the rearrangement of 29 to 59, before fragmentation occurs. (The loss of H·, which was also detected, probably occurs from 29).

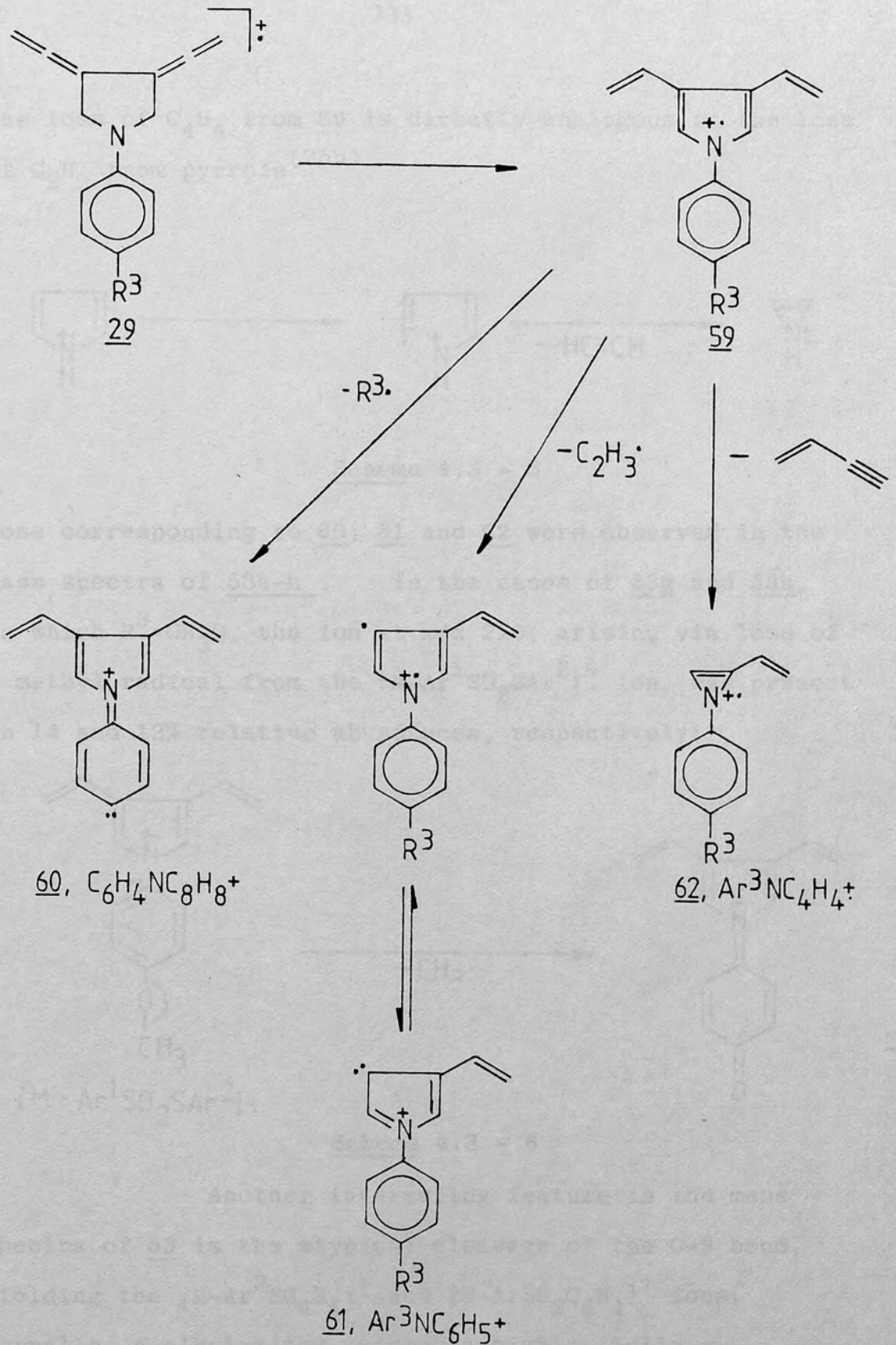

Scheme 4.3 - 4

The loss of C_4H_4 from 59 is directly analogous to the loss of C_2H_2 from pyrrole[25b].

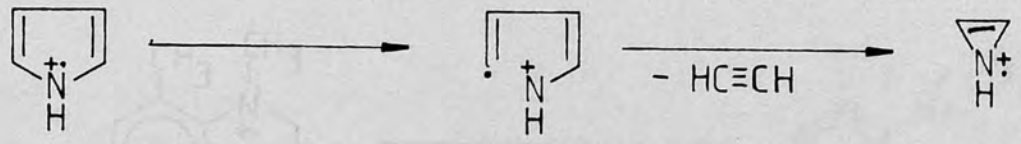

Scheme 4.3 - 5

Ions corresponding to 60, 61 and 62 were observed in the mass spectra of 53a-h . In the cases of 53g and 53h, in which $R^3=CH_3O$, the ion at m/z 210, arising via loss of a methyl radical from the $\{M-Ar^1SO_2SAr^2\}^+$. ion, was present in 14 and 12% relative abundances, respectively:

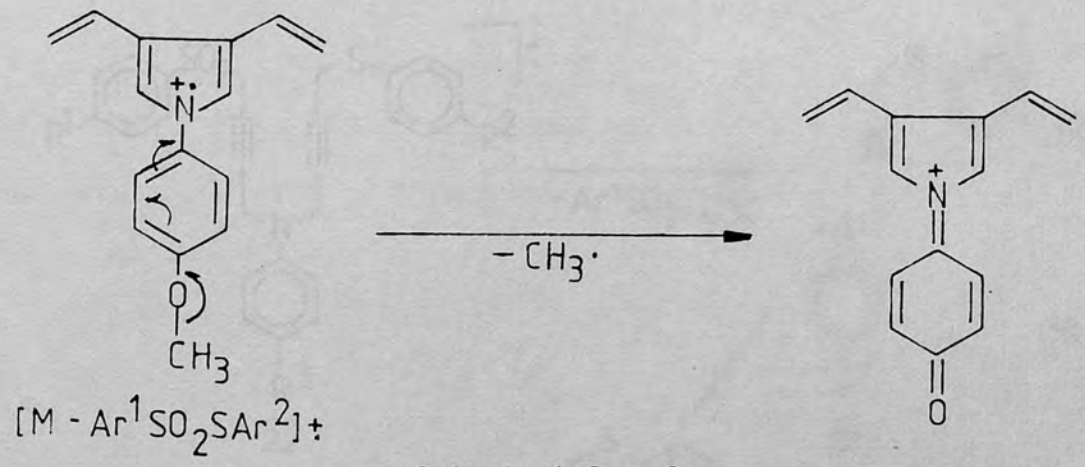

Scheme 4.3 - 6

Another interesting feature in the mass spectra of 53 is the atypical cleavage of the C-N bond, yielding the $\{M-Ar^2SC_4H_4\}^+$ and $\{M-ArSO_2C_4H_4\}^+$ ions. Normally, n-alkylamines undergo a highly facile α-cleavage[82]:

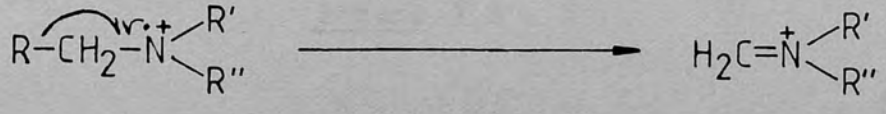

Scheme 4.3 - 7

However, the presence of sp hybridised carbons at the β-positions preclude α-cleavage, as exemplified by the loss of a propynyl group from 63, which gives rise to the base peak in its mass spectrum[83].

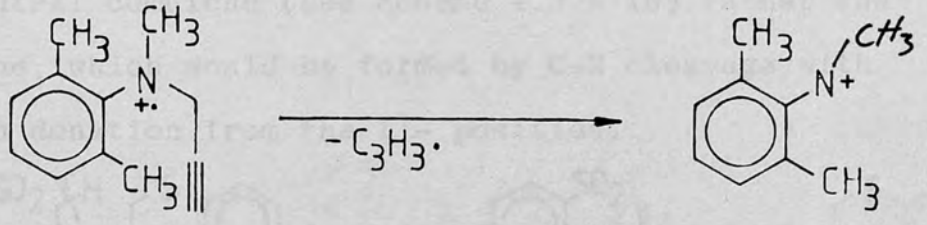

63

Scheme 4.3 - 8

Fission of one of the C-N bonds in 53 leads to 64, although the ion probably exists as an immonium ion such as 65:

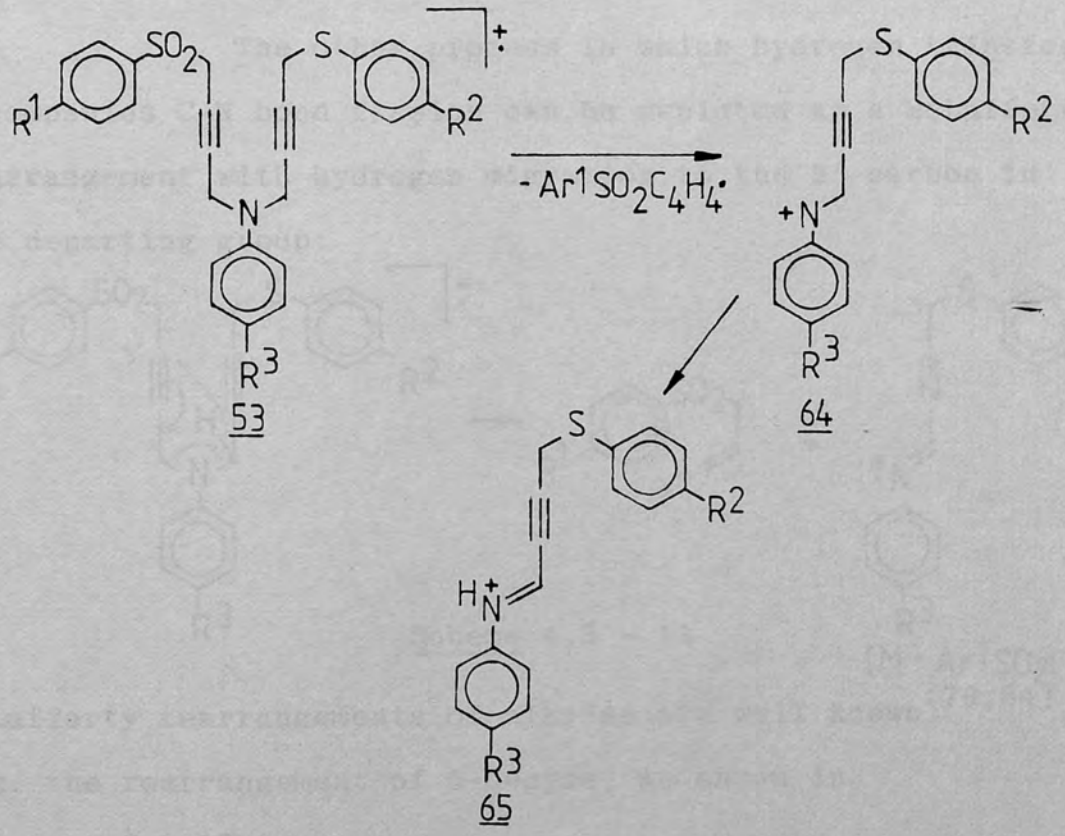

53 64 65

Scheme 4.3 - 9

The loss of fragments such as $Ar^1SO_2C_4H_3$ can readily be explained by a hydrogen migration from the 4'-position to the nitrogen. Donation of a hydrogen from this position results in the more favourable elimination of a neutral cumulene (see Scheme 4.3 - 10) rather than a carbene, which would be formed by C-N cleavage with hydrogen donation from the 1'- position.

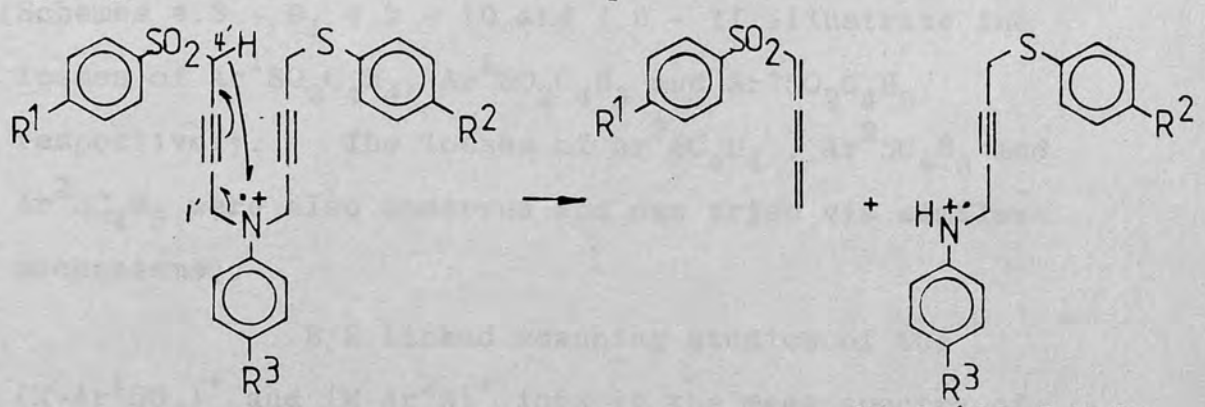

Scheme 4.3 - 10 $[M-Ar^1SO_2C_4H_3]^+$

The other process in which hydrogen transfer accompanies C-N bond fission can be depicted as a McLafferty rearrangement with hydrogen migration to the 3'-carbon in the departing group:

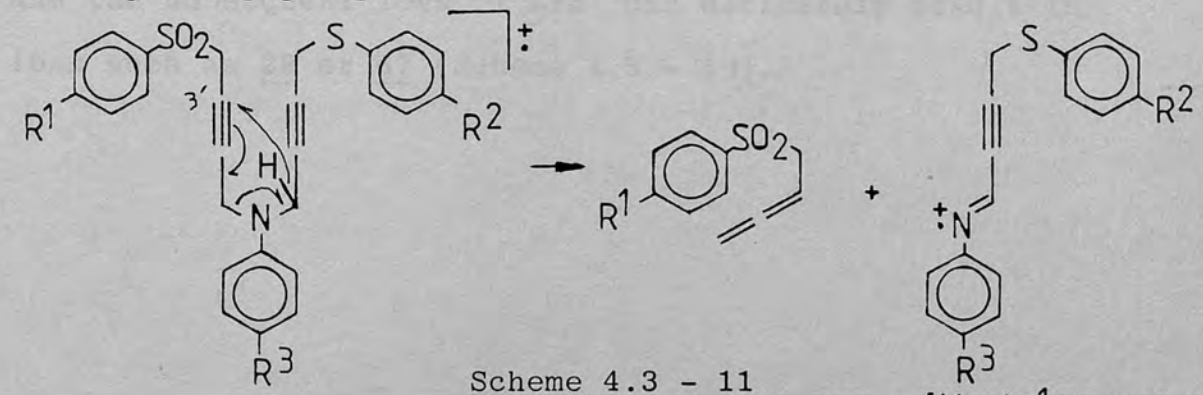

Scheme 4.3 - 11 $[M-Ar^1SO_2C_4H_5]^+$

McLafferty rearrangements of alkynes are well known[79,84], e.g. the rearrangement of 5-decyne, as shown in Scheme 4.3 - 12.

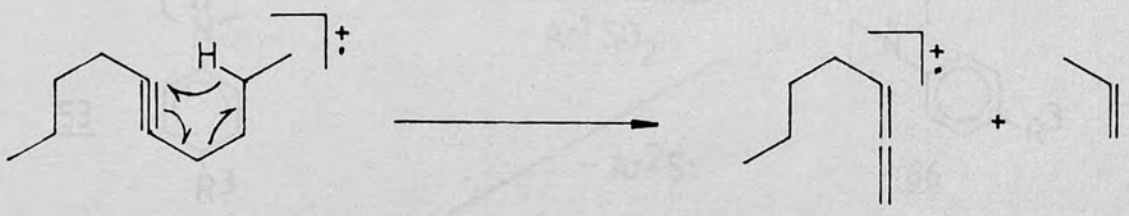

Scheme 4.3 - 12

(Schemes 4.3 - 9, 4.3 - 10 and 4.3 - 11 illustrate the losses of $Ar^1SO_2C_4H_4$; $Ar^1SO_2C_4H_3$ and $Ar^1SO_2C_4H_5$, respectively. The losses of $Ar^2SC_4H_4\cdot$, $Ar^2SC_4H_3$ and $Ar^2SC_4H_5$ were also observed and can arise via similar mechanisms).

B/E linked scanning studies of the $\{M-Ar^1SO_2\}^+$ and $\{M-Ar^2S\}^+$ ions in the mass spectra of 53f and 53h indicate that these ions fragment to give rise to an ion of the same nominal mass as the $\{M-Ar^1SO_2SAr^2\}^{+\cdot}$ ion. For example, the loss of $Ar^1SO_2\cdot$, stabilisation of the charge via the formation of a cyclic ammonium ion 66 and the subsequent loss of ArS· can ultimately result in ions such as 29 or 67 (Scheme 4.3 - 13).

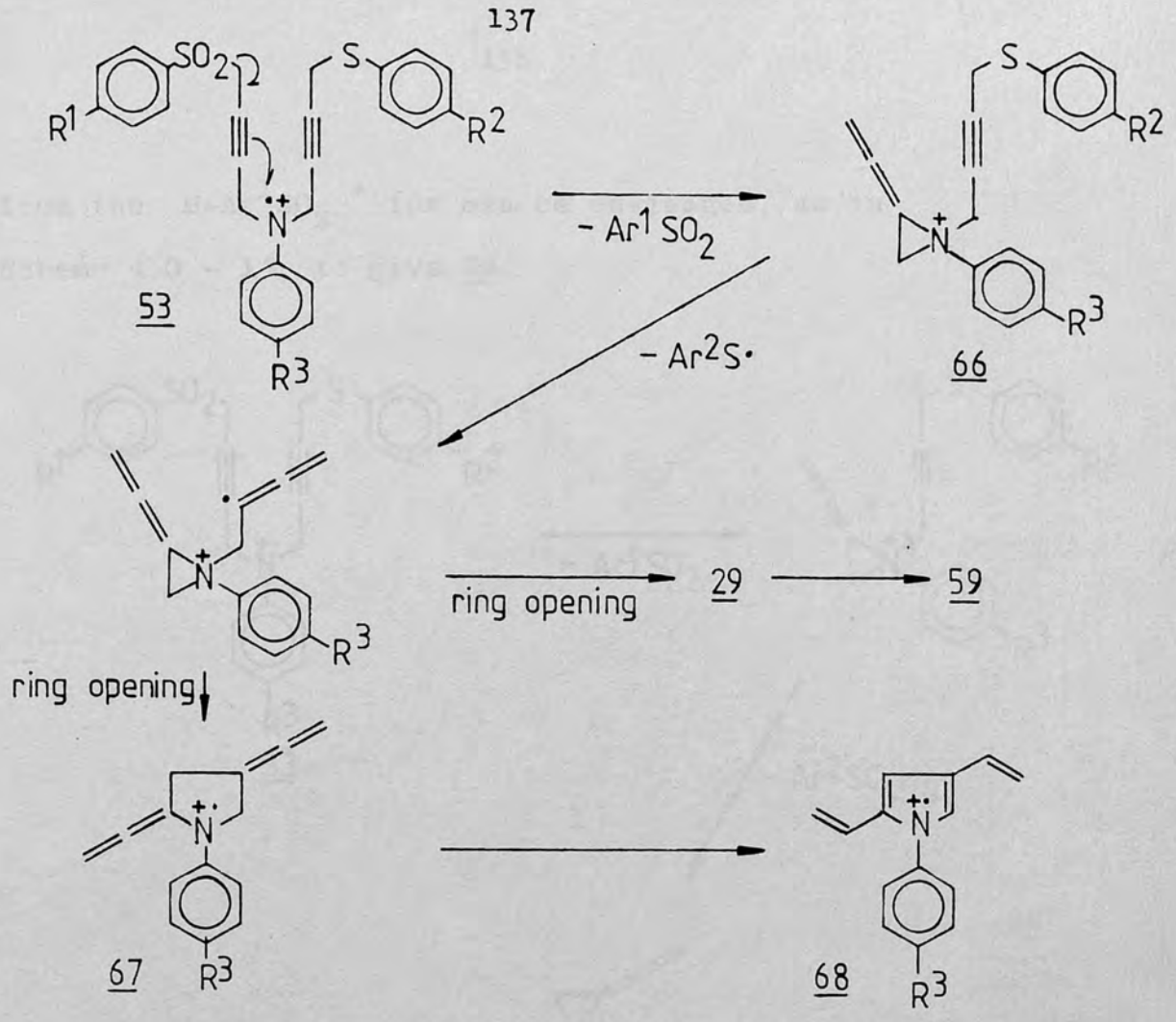

Scheme 4.3 - 13

Ion 29 is the same ion as that formed by the loss of $Ar^1SO_2SAr^2$ from the molecular ion and its fragmentation would be similar. The presence of 67 cannot be ascertained, since its rearrangement to an N-arylpyrrole 68 and subsequent fragmentation would result in the same losses shown to occur from the $\{M-Ar^1SO_2SAr^2\}^{+\cdot}$ ion. Also, 29 and 67 can be formed from the $\{M-Ar^2S\}^+$ ion via similar routes and have the same fates.

As proven by B/E linked scanning studies the $Ar^3NC_4H_4^{+\cdot}$ ion arises from the fragmentation of more than one ion (i.e. $\{M-Ar^2S\}^+$, $\{M-Ar^1SO_2\}^+$ and $\{M-Ar^1SO_2SAr^2\}^{+\cdot}$) and thus ions other than 62 probably contribute to its relative abundance. For example, loss of $Ar^1SC_4H_4\cdot$

from the $M-Ar^1SO_2^+$ ion can be envisaged, as in Scheme 4.3 - 14, to give 69.

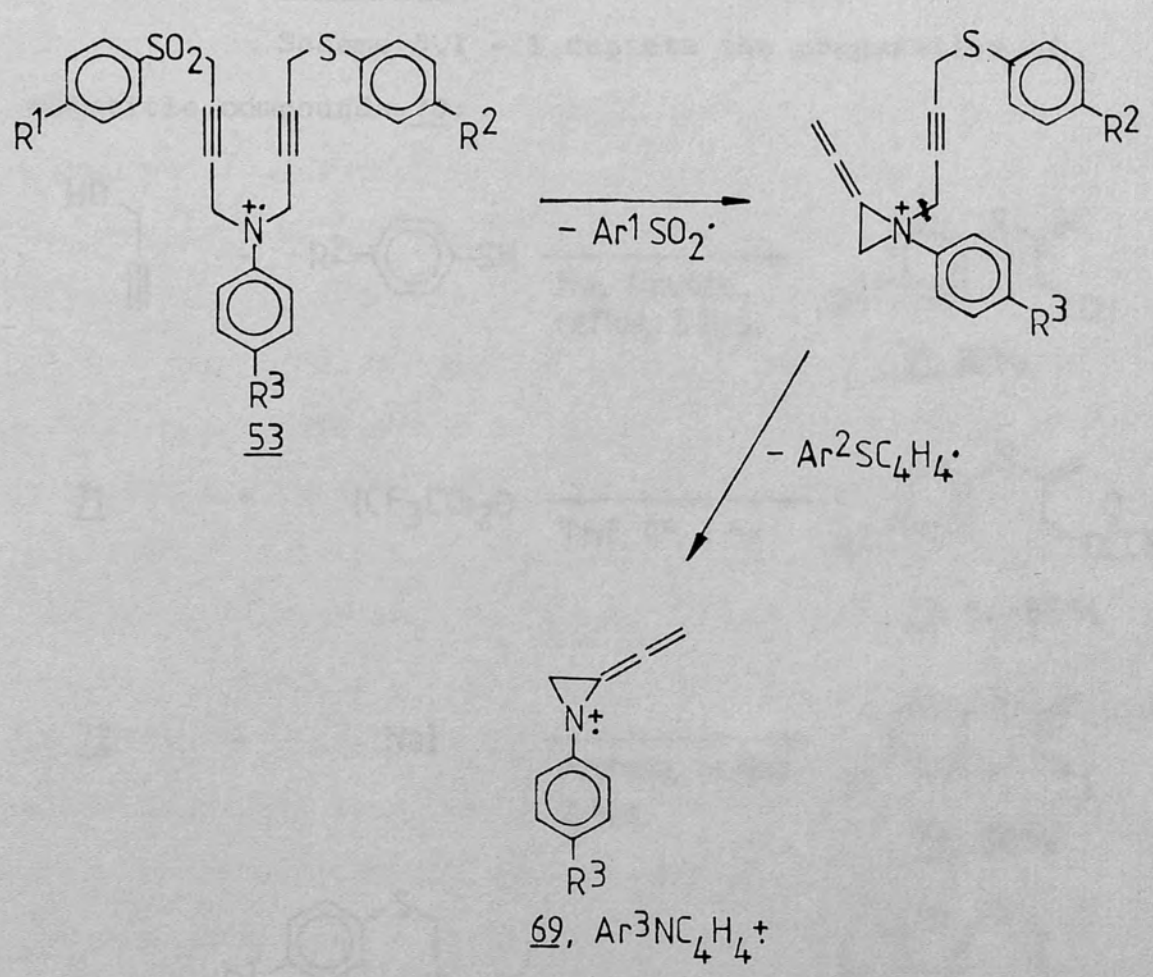

Scheme 4.3 - 14

5. N-(4'-ARYLTHIO-2'-BUTYNYL)-N-(4''-ARYLTHIO-2''-PROPENYL)-p-TOLUIDINES.

5.1 Synthesis

Scheme 5.1 - 1 depicts the preparation of the title compounds 70:

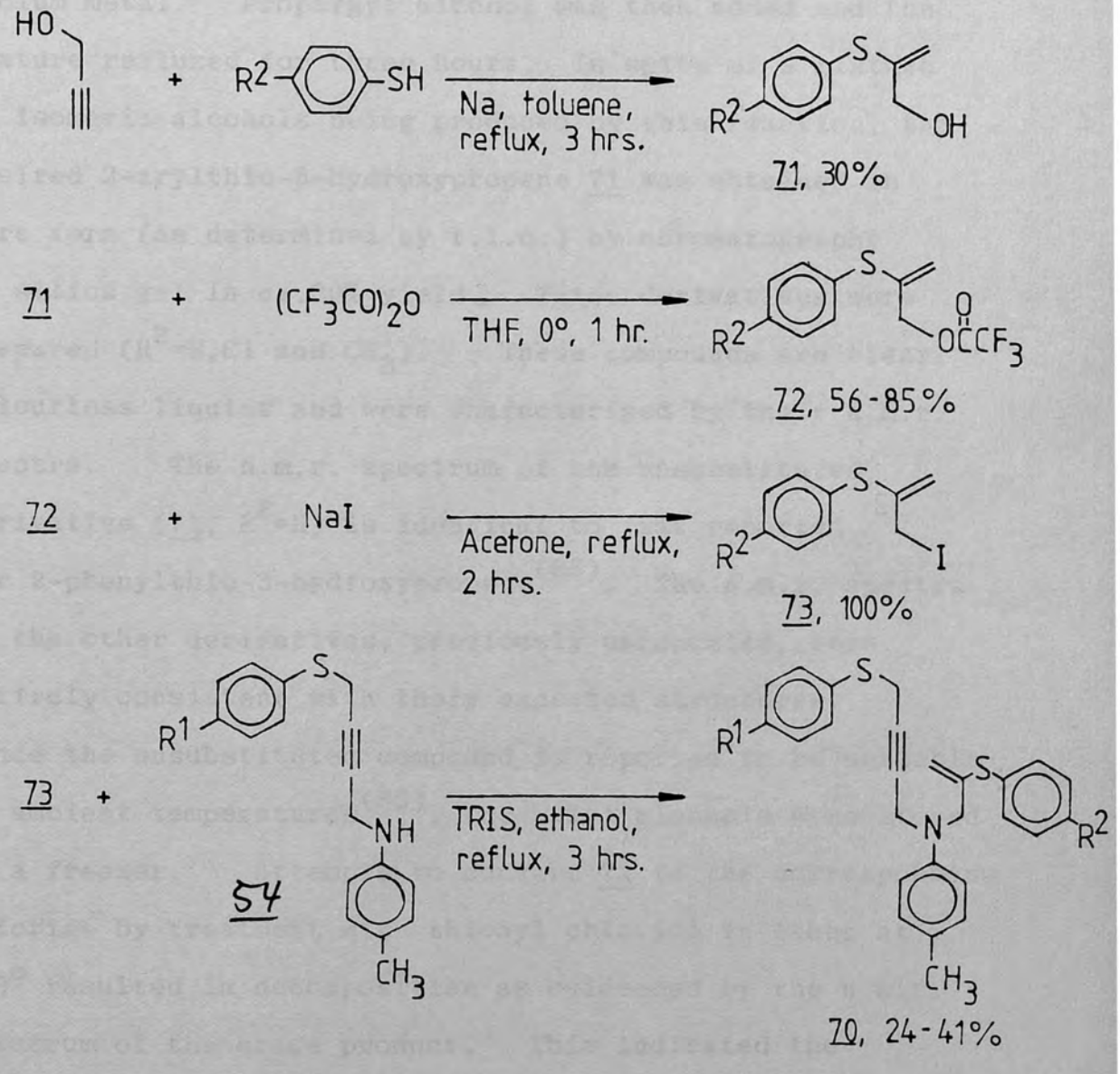

70a	$R^1=R^2=H$	70f	$R^1=Cl, R^2=CH_3$
70b	$R^1=H, R^2=Cl$	70g	$R^1=CH_3, R^2=H$
70c	$R^1=H, R^2=CH_3$	70h	$R^1=CH_3, R^2=Cl$
70d	$R^1=Cl, R^2=H$	70i	$R^1=R^2=CH_3$
70e	$R^1=R^2=Cl$		

Scheme 5.1 - 1

The base catalysed addition of thiophenol to propargyl alcohol has been reported[85] and a method similar to the published procedure was employed. The appropriate arenethiol in refluxing toluene was partially converted to the sodium salt by the addition of 0.1 equivalents of sodium metal. Propargyl alcohol was then added and the mixture refluxed for three hours. In spite of a mixture of isomeric alcohols being produced by this reaction, the desired 2-arylthio-3-hydroxypropene 71 was obtained in pure form (as determined by t.l.c.) by chromatography on silica gel in ca.30% yield. Three derivatives were prepared (R^2=H,Cl and CH_3). These compounds are clear, colourless liquids and were characterised by their n.m.r. spectra. The n.m.r. spectrum of the unsubstituted derivative (71, R^2=H) is identical to that reported for 2-phenylthio-3-hydroxypropene[86]. The n.m.r. spectra of the other derivatives, previously unreported, were entirely consistent with their expected structures. Since the unsubstituted compound is reported to be unstable at ambient temperatures[85], the allyl alcohols were stored in a freezer. Attempts to convert 71 to the corresponding chloride by treatment with thionyl chloride in ether at -70^{o} resulted in decomposition as evidenced by the n.m.r. spectrum of the crude product. This indicated the complete absence of unsaturation:

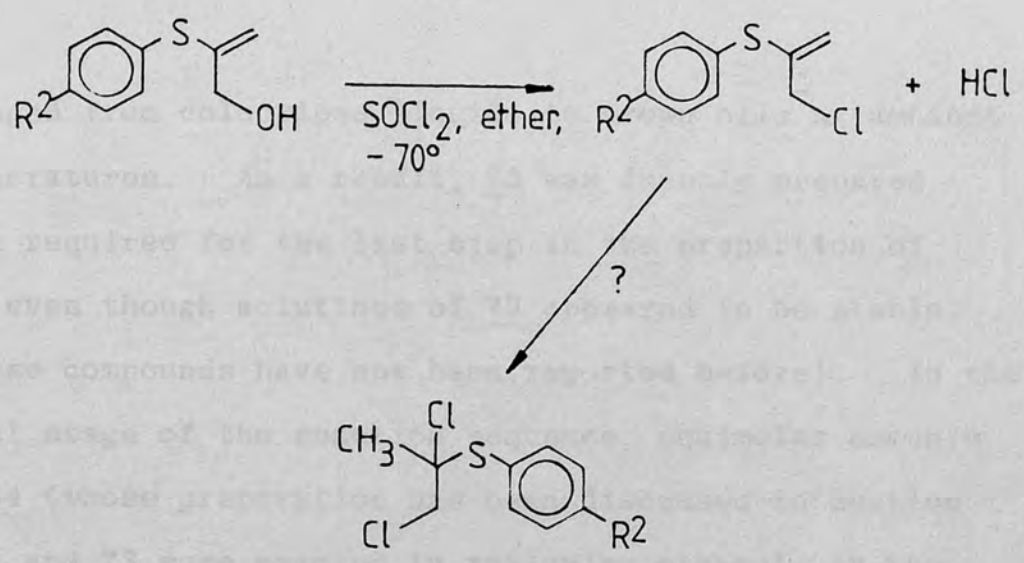

Scheme 5.1 - 2

To avoid the problem of hydrogen halide addition to the double bond, 71 was converted to the corresponding trifluoroacetate 72 by reaction with trifluoroacetic anhydride in tetrahydrofuran at ice bath temperature. The crude product was distilled at high vacuum to give the pure ester in moderate yields. These previously unknown compounds were obtained as clear colourless liquids (single spot by t.l.c.) and were characterised by their boiling points and n.m.r. spectra. The n.m.r. spectra of the three derivatives of 72 thereby prepared (R^2=H,R^2=Cl,R^2=CH_3) indicated that no other isomer was present.

The reaction of 72 with a tenfold excess of sodium iodide in refluxing acetone proceeded quantitatively to give the pure (t.l.c) allyl iodide 73. No other isomers were detected by n.m.r., confirming the structure of 73 to be 2-arylthio-3-iodopropene. The neat iodides (R^2=H, R^2=Cl, R^2=CH_3) were highly unstable and rapidly

changed from colourless liquids to brown oils at ambient temperatures. As a result, 73 was freshly prepared when required for the last step in the prepartion of 70, even though solutions of 73 appeared to be stable. (These compounds have not been reported before). In the final stage of the reaction sequence, equimolar amounts of 54 (whose preparation has been discussed in Section 4.1) and 73 were reacted in refluxing ethanol, in the presence of tris-(hydroxymethyl)-aminomethane (TRIS) for 3 hours. The product mixtures were chromatographed on silica gel to give the desired compounds 70, in 24-41% yields as colourless liquids which displayed a single spot in their thin layer chromatograms. Attempts to crystallise 70 from several solvents failed. These products, previously unknown, were characterised by their n.m.r. and mass spectra, which were entirely consistent with their proposed structures. Nine derivatives of 70 were prepared by the reaction sequence shown in Scheme 5.1 - 1. Due to their tendency to darken at ambient temperature, 70a-i were stored in a refrigerator.

5.2 E.I. induced fragmentation results.

Apart from the presence of prominent molecular ions, a feature which is common to the mass spectra of 70a-i is an intense peak (22-100% R.A.) appearing at m/z 197, which arises from the loss of the two arylthio groups, both sequentially and as a bisaryl-disulphide unit. Peaks corresponding to metastable ions were found in several instances in support of both routes of formation.(Metastable peaks confirming the loss of $Ar^2S\cdot$ from the $\{M-Ar^1S\}^+$ ion were observed in the spectra of 70a,b,c,d,f,h and i. The elimination of Ar^1SSAr^2 was supported by metastable peaks in the spectra of 70a,g,h and i.)

Peaks corresponding to $Ar^1SSAr^{2+\cdot}$ were present in most cases, but the elimination of sulphur, $HS\cdot$ or hydrogen sulphide was not observed in any of the spectra.

Expectedly, the loss of $Ar^1S\cdot$, which was supported by metastable peaks in most cases, predominates over the loss of the vinylic arylthio group. These. and the other principal fragmentations of the title compounds are summarised in Scheme 5.2 - 1.

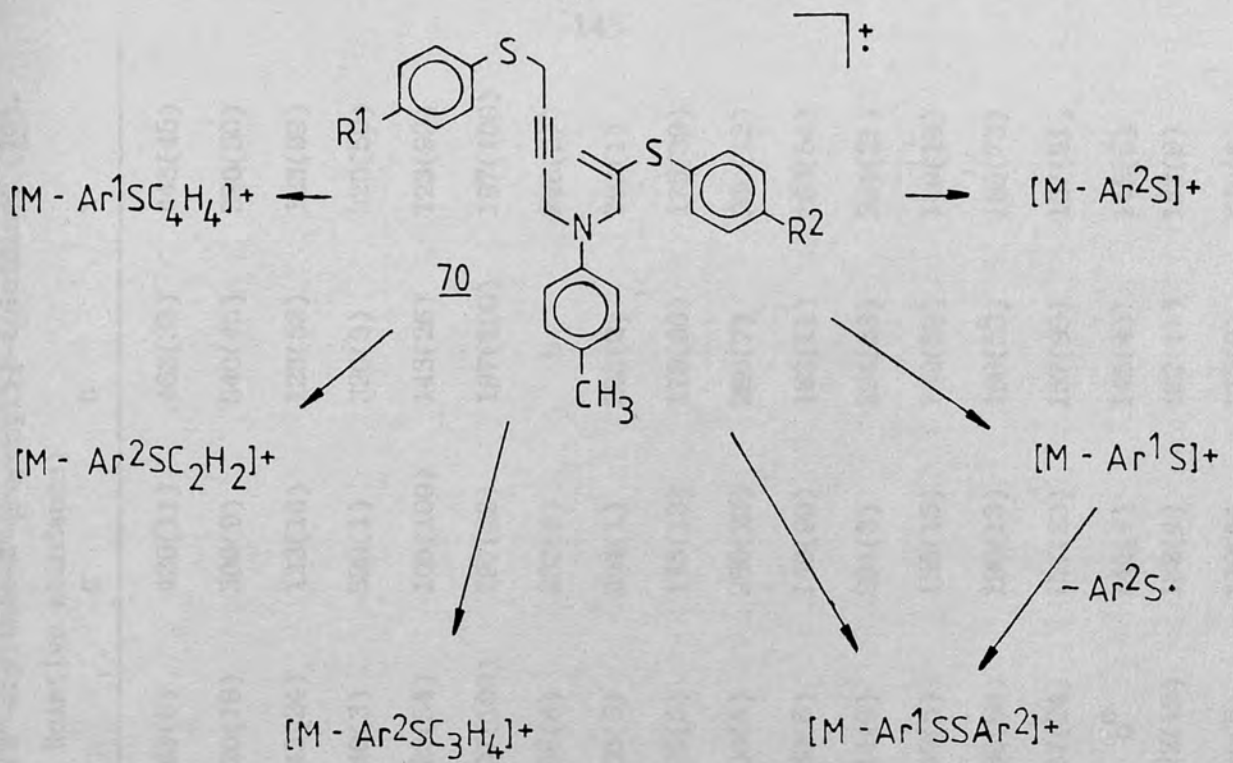

Scheme 5.2 - 1

Ions formed via C-N bond cleavage (i.e. $[M-Ar^1SC_4H_4]^+$ and $[M-Ar^2SC_3H_4]^+$) and alpha cleavage (i.e. $[M-Ar^2SC_2H_2]^+$) were also present. Those cases in which the base peak did not appear at m/z 197 displayed base peaks corresponding to Ar^2S^+, with the exception of 70e. The peak of greatest intensity in the spectrum of 70e appears at m/z 160 and can arise via loss of a chlorine radical ($R^1\cdot$) from the $Ar^1SC_4H_4^+$ ion. A peak at m/z 160 appears in the spectra of all nine cases, but is most significant when R^1=Cl and is not included in Table 5.2 - 1, which contains the relative abundances of significant ions in the mass spectra of 70a-i.

TABLE 5.2 - 1

Significant ions in the 70 eV mass spectra of N-(4'-arylthio-2'-butynyl)-N-(2''-arylthio-2''-propenyl)-p-toluidines (70).

ION[a]	m/z (% Relative abundance)								
	a	b	c	d	e	f	g	h	i
$M^{+\cdot}$	415(39)	449(6)	429(20)	449(32)	483(8)	463(6)	429(11)	463(33)	443(45)
$\{M-Ar^1S\}^+$	306(45)	340(2)	320(20)	306(58)	340(15)	320(18)	306(9)	340(45)	320(50)
Ar^1S^+	109(25)	109(26)	109(16)	143(18)	143(67)	143(24)	123(16)	123(52)	123(92)
$\{M-Ar^2S\}+$	306(45)	306(1)	306(3)	340(4)	340(15)	340(3)	320(1)	320(3)	320(50)
Ar^2S^+	109(25)	143(100)	123(100)	109(22)	143(67)	123(54)	109(100)	143(26)	123(92)
$\{M-Ar^1SSAr^2\}^{+\cdot}$	197(100)	197(86)	197(80)	197(100)	197(95)	197(100)	197(22)	197(100)	197(100)
$Ar^1SSAr^{2\ +\cdot}$	218(10)	252(29)	232(6)	252(1)	286(15)	266(8)	232(6)	b	246(27)
$\{M-Ar^1SC_4H_4\}^+$	254(1)	288(21)	268(2)	254(1)	288(13)	268(5)	254(1)	288(2)	268(1)
$Ar^1SC_4H_4^+$	161(22)	161(19)	161(37)	195(13)	195(10)	195(5)	175(13)	175(66)	175(39)
$\{M-Ar^2SC_3H_4\}^+$	266(6)	266(13)	266(5)	300(16)	300(10)	300(4)	280(22)	280(7)	280(12)
$Ar^2SC_3H_4^+$	149(10)	183(10)	163(83)	149(15)	183(19)	163(6)	149(99)	183(11)	163(56)
$\{M-Ar^2SC_2H_2\}^+$	280(14)	280(2)	280(10)	314(39)	314(33)	314(6)	294(3)	294(33)	294(21)
$Ar^2SC_2H_2^+$	135(6)	169(1)	149(25)	135(10)	169(7)	149(5)	135(15)	169(59)	149(14)
$Ar^3NC_7H_7^+$	196(63)	196(10)	196(40)	196(53)	196(58)	196(68)	196(13)	196(53)	196(73)
$Ar^3NC_4H_4^{+\cdot}$	157(32)	157(33)	157(32)	157(84)	157(83)	157(24)	157(23)	157(99)	157(51)
$Ar^3NC_3H_4^{+\cdot}$	145(4)	b[c]	145(11)	145(2)[c]	145(7)[c]	b[c]	145(4)	145(4)[c]	145(5)
$C_6H_4NC_7H_8^{+\cdot}$	182(7)	182(7)	182(9)	182(9)	182(11)	182(12)	182(4)	182(11)	182(9)
$Ar^3NC_5H_5^{+\cdot}$	170(4)	170(4)	170(5)	170(18)	170(11)	170(5)	170(5)	170(9)	170(6)

a) $Ar^1 = R^1C_6H_4$, $Ar^2 = R^2C_6H_4$, $Ar^3 = CH_3C_6H_4$

b) Less than 1% R.A.

c) Corrected for contribution from $C_5H_4Cl^{37}S$ (Ar^2S+ and/or Ar^1S+).

5.3 Discussion

The formation of bisaryldisulphide ions from N,N- bis(4'-arylthio-2'-butynyl) anilines[45] has been discussed in Section 1.3.3.3 and mentioned again in the proceeding chapter. These compounds also displayed prominent peaks in their mass spectra corresponding to $\{M-Ar^1SSAr^2\}^{+\cdot}$. While the elimination of bisaryldisulphide from the original molecular ion of 27 finds indirect support in the parallel behaviour of the corresponding bis-sulphones[45], the rearrangement pathway invoking two {1,3} arylthio migrations has not been substantiated to date. To test this hypothesis, a number of derivatives of 70 were prepared, since the structure of its molecular ion is analogous to the ion which would be obtained upon a single [1,3] arylthio shift having occurred in 27 (see also Scheme 1.3.3.3 - 10).

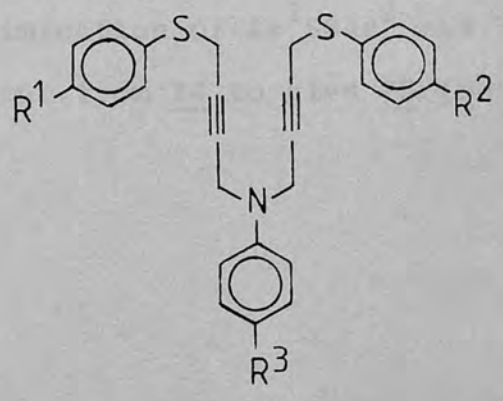

27

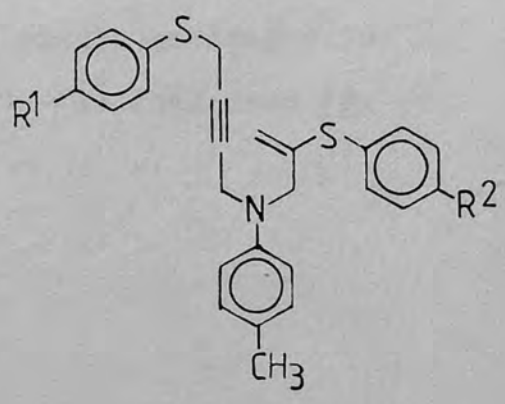

70

The appearance of an intense peak at m/z 197 in the mass spectrum of each of the nine derivatives of 70 and the presence of supporting metastable peaks in several instances, proving its formation via the elimination of

Ar^1SSAr^2, substantiates the intermediacy of an ion analogous to 70 in the rearrangement of 27. If such an analogous ion is formed prior to the elimination of Ar^1SSAr^2 from 27, the relative abundances of the $\{M-Ar^1SSAr^2\}^{+\cdot}$ ions should be comparatively higher in the spectra of 70a-i. Although m/z 197 is the base peak in the spectra of five of the cases, one cannot draw a conclusion from the intensity of m/z 197, since it is also formed via the stepwise loss of the arylthio groups. However, a comparison of the relative abundances of the $Ar^1SSAr^{2\,+\cdot}$ ions in the spectra of 70 and 27 should provide the same information, since these ions can arise only from rearrangement of the molecular ion. The two sulphur atoms in 70 can come into much closer proximity after an {1,3} shift of Ar^1S has occurred to give 74 (this is demonstrated easily by molecular models) and the elimination of Ar^1SSAr^2 can be more easily envisaged to occur from 74 to give 75 (Scheme 5.3 - 1) than from 70.

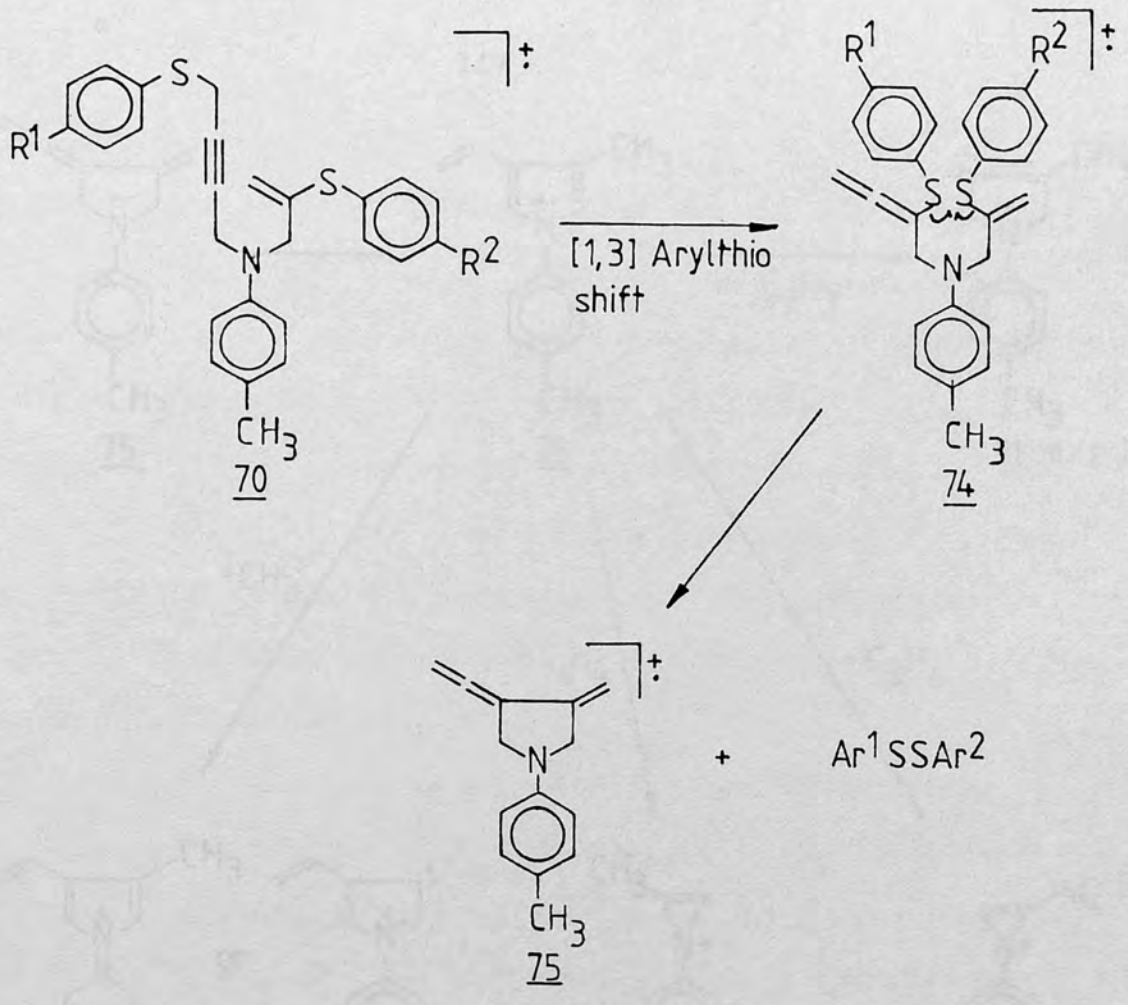

Scheme 5.3 - 1

The higher relative abundances of $Ar^1SSAr^{2+\cdot}$ observed in the spectra of 70a-i in general, as compared to those in the spectra of the N,N-bis-(4'-arylthio-2'-butynyl)anilines, thus strengthens further the postulation of an ion analogous to 70 being formed by an [1,3] arylthio shift in 27.

The fragmentation of 75 should be analogous to that of the $[M-ArSO_2SAr^2]^{+\cdot}$ ions in the mass spectra of the N-(4'-arylsulphonyl-2'-butynyl)-N-(4''-arylthio-2''-butynyl)anilines, discussed in the proceeding chapter. Thus, 75 should rearrange to the N-arylpyrrole ion 76 and undergo the losses illustrated in Scheme 5.3 - 2.

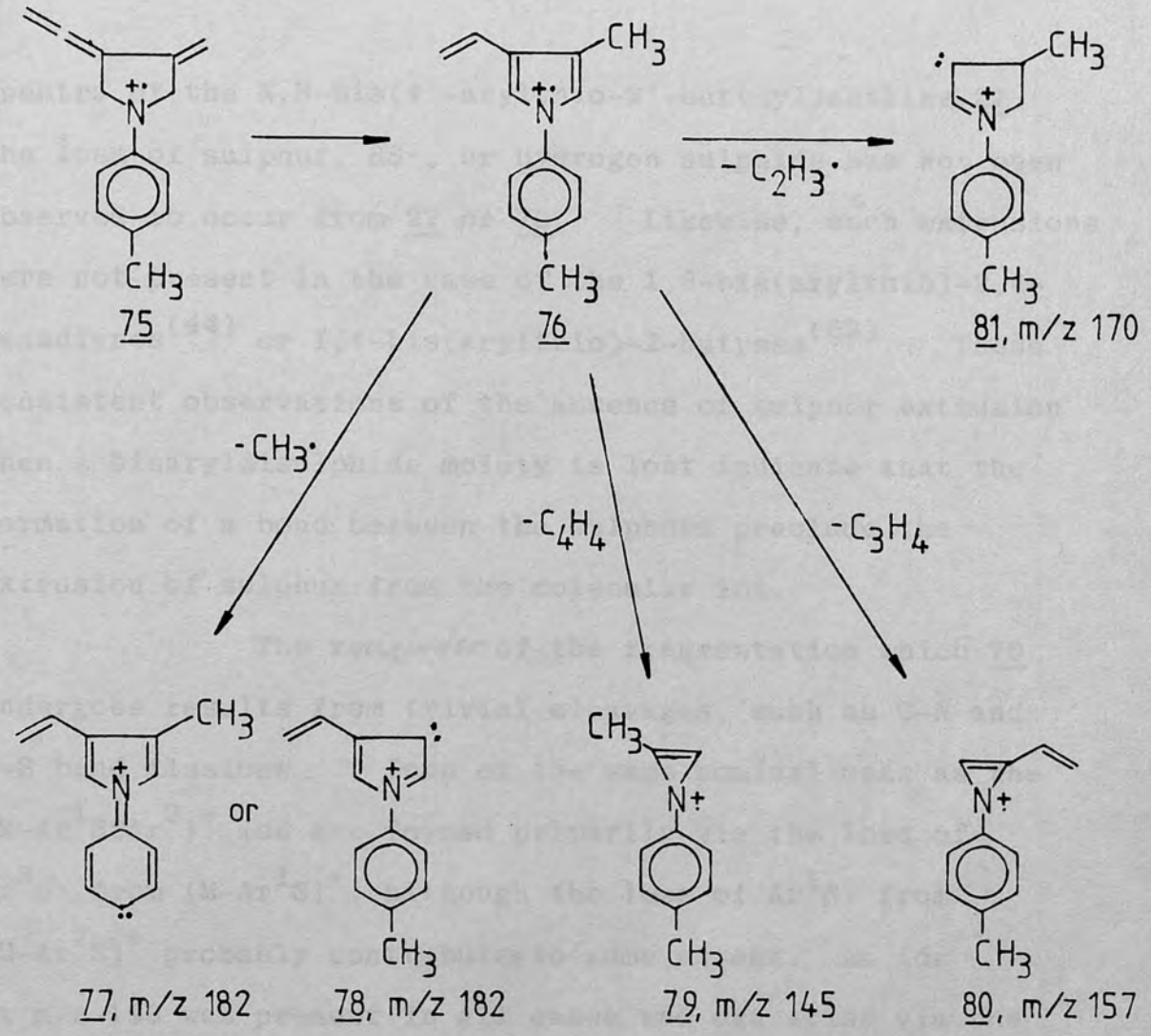

Scheme 5.3 - 2

Indeed, peaks at m/z 182, m/z 170, m/z 157 and m/z 145 are common in the spectra of 70a-j (although the contribution of 79 to m/z 145 is overshadowed by the presence of $Cl^{37}C_6H_4S^+$ in two instances). The presence of these peaks in the mass spectra of 70a-j supports the assumption that the $\{M-Ar^1SSAr^2\}^{+\cdot}$ ion is analogous to the $\{M-Ar^1SO_2SAr^2\}^{+\cdot}$ ion arising from the N-(4'-arylsulphonyl-2'-butynyl)-N-(4''-arylthio-2''-butynyl)anilines. This analogy can logically be extended to the $\{M-Ar^1SSAr^2\}^{+\cdot}$ ion in the

spectra of the N,N-bis(4'-arylthio-2'-butynyl)anilines 27. The loss of sulphur, HS·, or hydrogen sulphide has not been observed to occur from 27 or 70. Likewise, such extrusions were not present in the case of the 1,6-bis(arylthio)-2,4-hexadiynes[44] or 1,4-bis(arylthio)-2-butynes[62]. These consistent observations of the absence of sulphur extrusion when a bisaryldisulphide moiety is lost indicate that the formation of a bond between the sulphurs preclude the extrusion of sulphur from the molecular ion.

The remainder of the fragmentation which 70 undergoes results from trivial cleavages, such as C-N and C-S bond fissions. Ions of the same nominal mass as the $\{M-Ar^1SSAr^2\}^+$ ion are formed primarily via the loss of $Ar^2S\cdot$ from $\{M-Ar^1S\}^+$, although the loss of $Ar^1S\cdot$ from $\{M-Ar^2S\}^+$ probably contributes to some extent. An ion at m/z 196 was present in all cases and can arise via the loss of an arenethiol moiety from the $\{M-Ar^1S\}^+$ and $\{M-Ar^2S\}^+$ ions or H· from $Ar^3NC_7H_8^{+\cdot}$. Of interest is the presence of ions corresponding to $[M-Ar^2SC_2H_2]^+$. Although these ions can result from α-cleavage, which is a prominent process in amines[82], they are unusual in that the normally unfavourable cleavage of a vinyl bond is required here for their formation (Scheme 5.3 - 3).

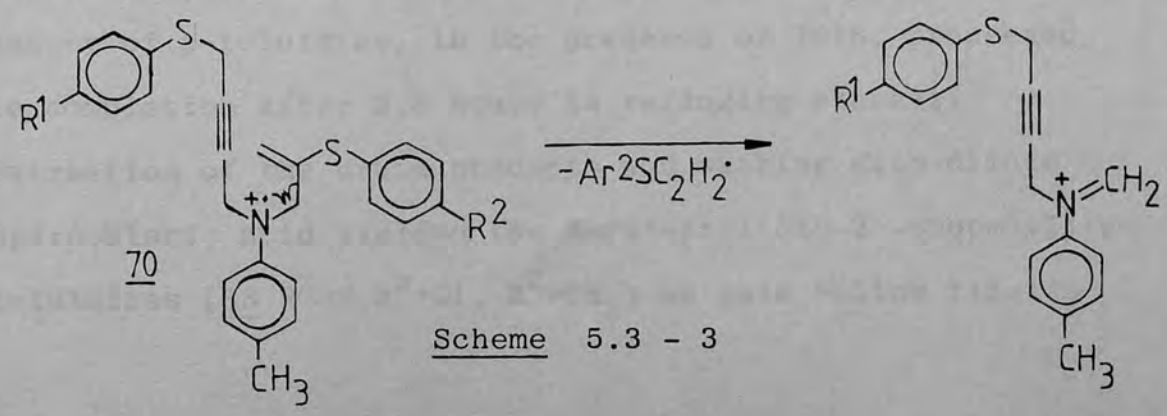

70

Scheme 5.3 - 3

6. N.N-BIS(2'-ARYLTHIO-2'-PROPENYL)-p-TOLUIDINES

6.1 Synthesis

A two step synthesis was employed in the preparation of the N,N-bis(2'-arylthio-2'-propenyl)-p-toluidines 82.

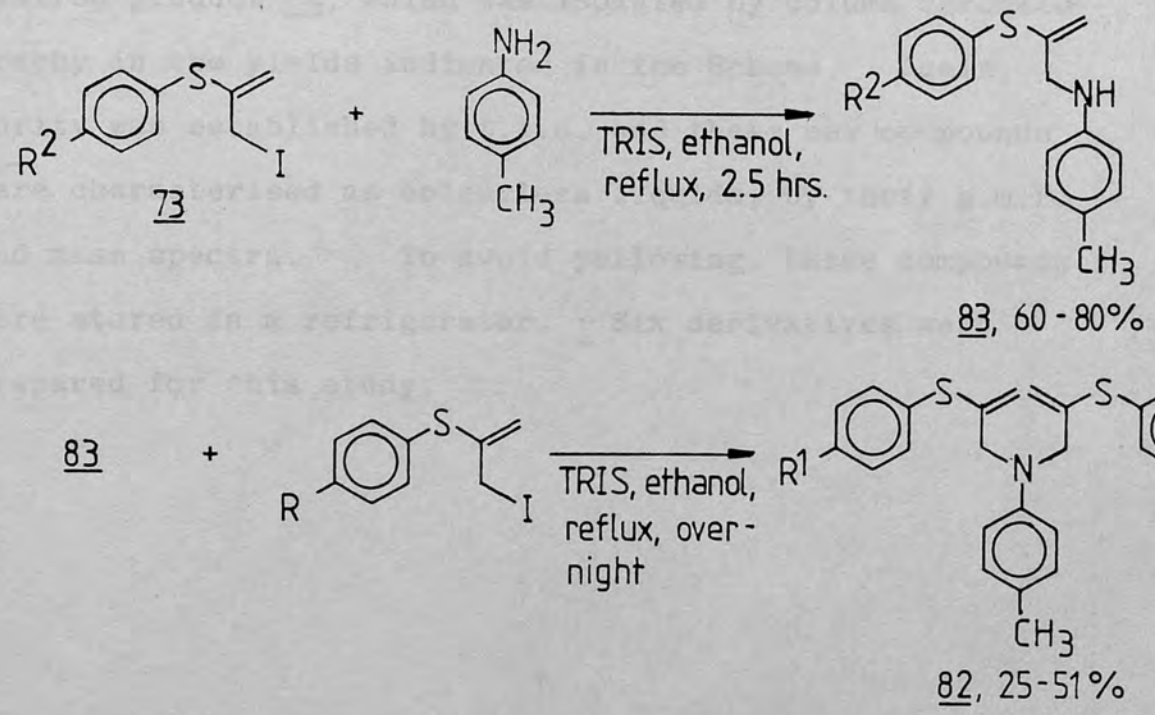

82a : $R^1=R^2=H$ 82d : $R^1=R^2=Cl$
82b : $R^1=H, R^2=Cl$ 82e : $R^1=Cl, R^2=CH_3$
82c : $R^1=H, R^2=CH_3$ 82f : $R^1=R^2=CH_3$

Scheme 6.1 - 1

The preparation of 73 has been described in Section 5.1. The reaction of 73 with an equimolar amount of p-toluidine, in the presence of TRIS, proceeded to completion after 2.5 hours in refluxing ethanol. Extraction of the crude products and washing with dilute hydrochloric acid yielded the N-(2'-arylthio-2'-propenyl)-p-toluidines (83 $R^2=H, R^2=Cl$, $R^2=CH_3$) as pale yellow liquids

in 60-80% yield upon removal of solvents. The purity of these previously unreported compounds were ascertained by t.l.c. and their n.m.r. spectra provided structural confirmation. A second equivalent of allyl iodide and 83 were reacted overnight under similar conditions to give the desired product 82, which was isolated by column chromatography in the yields indicated in the Scheme. Again, purity was established by t.l.c. and these new compounds were characterised as colourless liquids, by their n.m.r. and mass spectra. To avoid yellowing, these compounds were stored in a refrigerator. Six derivatives were prepared for this study.

6.2 E.I. induced fragmentation results.

The fragmentation of the N,N-bis(2'-arylthio-2'-propenyl)-p-toluidines were established by B/E linked scanning studies of the molecular ion, $\{M-Ar^1S\}^+$, $\{M-Ar^2S\}^+$ and m/z 185 ions in the spectra of 82a, 82e and 82f, as well as metastable peak correlation. Scheme 6.2 - 1 illustrates the fragmentation of 82.

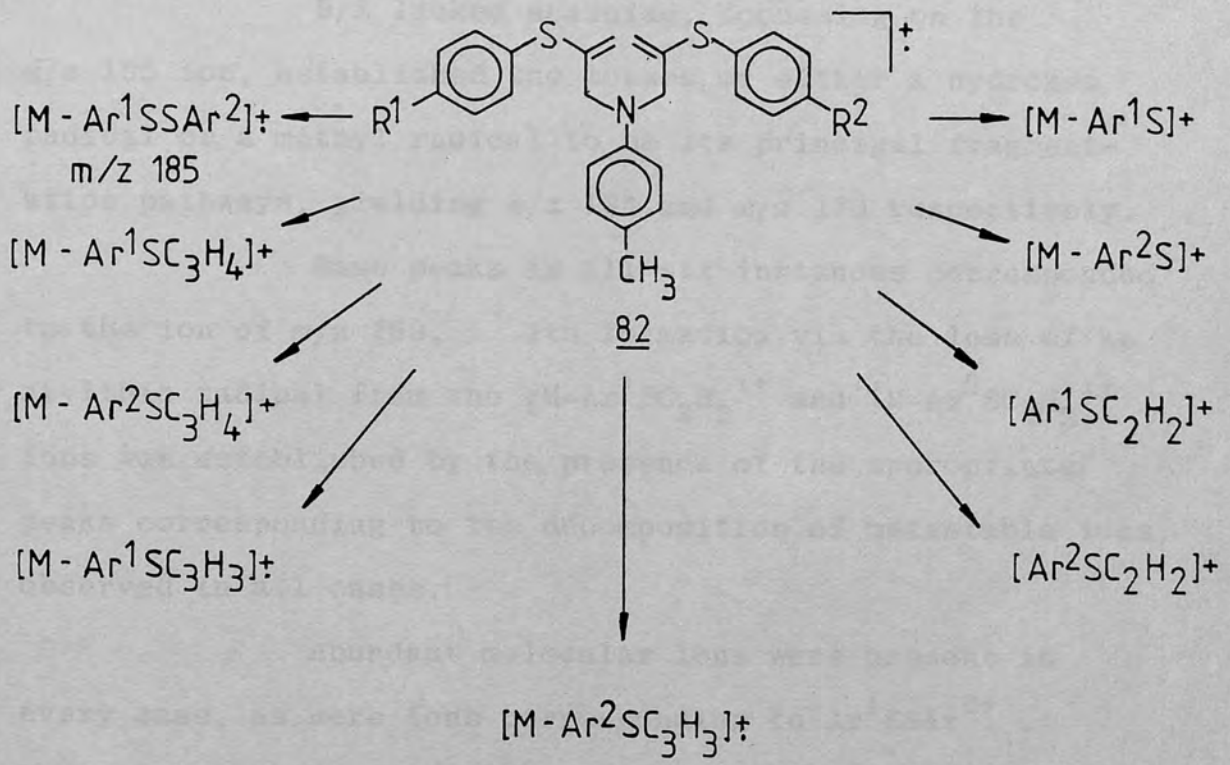

Scheme 6.2 - 1

A skeletal rearrangement was observed in each instance, involving the loss of a bisaryldisulphide molecule from the molecular ion and resulting in a peak

at m/z 185. Ions arising from the extrusion of sulphur were not observed.

The m/z 185 ion is also formed by the loss of the arylthio radicals ($Ar^2S\cdot$ and $Ar^1S\cdot$) from the $\{M-Ar^1S\}^+$ and $\{M-Ar^2S\}^+$ ions respectively. These ions, in addition, eliminate the corresponding arenethiols to give m/z 184.

B/E linked scanning, focussing on the m/z 185 ion, established the losses of either a hydrogen radical or a methyl radical to be its principal fragmentation pathways, yielding m/z 184 and m/z 170 respectively.

Base peaks in all six instances corresponded to the ion of m/z 159. Its formation via the loss of an arylthio radical from the $\{M-Ar^1SC_2H_2\}^+$ and $\{M-Ar^2SC_2H_2\}^+$ ions was established by the presence of the appropriate peaks corresponding to the decomposition of metastable ions, observed in all cases.

Abundant molecular ions were present in every case, as were ions corresponding to $Ar^1SSAr^{2+}\cdot$. The relative abundances of these and other significant ions are presented in Table 6.2 - 1. Table 6.2 - 2 indicates the metastable peaks observed and Tables 6.2 - 3. -4 and -5 contain the B/E linked scanning data for 82a, 82e and 82f , respectively. Exact mass analyses were obtained for the m/z 185 and $Ar^1SSAr^{2+}\cdot$ ions in the spectra of these same three derivatives and the results are collected in Table 6.2 - 6.

TABLE 6.2 - 1

Significant ions in the 70 eV mass spectra of N,N-bis(2'-arylthio-2'-propenyl)-p-toluidines (82).

	m/z (Relative abundance)					
Ion[a]	a	b	c	d	e	f
$M^{+\cdot}$	403(49)	437(29)	417(46)	471(23)	451(32)	431(51)
$Ar^1SSAr^{2+\cdot}$	218(10)	252(13)	232(25)	286(2)	266(10)	246(43)
$\{M-Ar^1SSAr^2\}^{+\cdot}$	185(19)	185(65)	185(19)	185(22)	185(76)	185(16)
Ar^1S^+	109(28)	109(59)	109(71)	143(18)	143(25)	123(92)
$\{M-Ar^1S\}^+$	294(14)	328(7)	308(8)	328(6)	308(11)	308(19)
Ar^2S^+	109(28)	143(46)	123(80)	143(18)	123(80)	123(92)
$\{M-Ar^2S\}^+$	294(14)	294(13)	294(10)	328(6)	328(7)	308(19)
$Ar^1SC_3H_4^+$	149(38)	149(40)	149(99)	183(7)	183(2)	163(94)
$\{M-Ar^1SC_3H_4\}^+$	254(5)	288(2)	268(14)	288(4)	268(10)	268(6)
$\{M-Ar^1SC_3H_3\}^{+\cdot}$	255(3)	289(3)	269(3)	289(2)	269(8)	269(38)
$Ar^2SC_3H_4^+$	149(38)	183(40)	163(27)	183(7)	163(17)	163(94)
$\{M-Ar^2SC_3H_4\}^+$	254(5)	254(11)	254(2)	288(4)	288(4)	268(6)
$\{M-Ar^2SC_3H_3\}^{+\cdot}$	255(3)	255(6)	255(2)	289(2)	289(15)	269(38)
$Ar^1SC_2H_2^+$	135(22)	135(6)	135(22)	169(1)	169(3)	149(19)
$\{M-Ar^1SC_2H_2\}^+$	268(21)	302(6)	282(11)	302(18)	282(8)	282(19)
$Ar^2SC_2H_2^+$	135(22)	169(2)	149(99)	169(1)	149(14)	149(19)
$\{M-Ar^2SC_2H_2\}^+$	268(21)	268(14)	268(14)	302(18)	302(7)	282(19)
$Ar^3NC_6H_7^+$	184(17)	184(58)	184(24)	184(23)	184(76)	184(19)
$C_6H_4NC_6H_8^{+\cdot}$	170(1)	170(4)	170(2)	170(2)	170(6)	170(4)
$Ar^3NHCH_2^{+\cdot}$	120(12)	120(18)	120(12)	120(9)	120(50)	120(70)
$Ar^3NC_4H_6^{+\cdot}$	159(100)	159(100)	159(100)	159(100)	159(100)	159(100)

a) $Ar^1 = R^1C_6H_4$, $Ar^2 = R^2C_6H_4$, Ar^3 = p-tolyl.

TABLE 6.2 - 2

Metastable peaks in the mass spectra of 82a-f.

Derivative	Metastable peak (m/z)	Transition	Neutral lost
82a	214.5	403 → 294	$Ar^{1,2}S\cdot$
	178.2	403 → 268	$Ar^{1,2}SC_2H_2\cdot$
	160.0	403 → 254	$Ar^{1,2}SC_3H_4\cdot$
	116.4	294 → 185	$Ar^{1,2}S\cdot$
	94.3	266 → 159	$Ar^{1,2}S\cdot$
82b	247.8	437 → 328	$Ar^{1}S\cdot$
	199.1	437 → 294	$Ar^{2}S\cdot$
	148.7	437 → 254	$Ar^{2}SC_3H_4$
	116.4	294 → 185	$Ar^{2}S\cdot$
	104.3	328 → 185	$Ar^{1}S\cdot$
	94.3	268 → 159	$Ar^{1}S\cdot$
	83.7	302 → 159	$Ar^{2}S\cdot$
82c	227.5	417 → 308	$Ar^{1}S\cdot$
	207.3	417 → 294	$Ar^{2}S\cdot$
	94.3	268 → 159	$Ar^{2}S\cdot$
	89.6	282 → 159	$Ar^{1}S\cdot$
82d	228.4	471 → 328	$Ar^{1,2}S\cdot$
	104.3	328 → 185	$Ar^{1,2}S\cdot$
	83.7	302 → 159	$Ar^{1,2}S\cdot$

/ continued ..

TABLE 6.2 - 2 (continued)

Derivative	Metastable peak (m/z)	Transition	Neutral lost
82e	238.5	451 → 328	$Ar^2S\cdot$
	210.3	451 → 308	$Ar^1S\cdot$
	183.9	451 → 288	$Ar^2SC_3H_4\cdot$
	159.2	451 → 268	$Ar^1SC_3H_4\cdot$
	111.1	308 → 185	$Ar^2S\cdot$
	104.3	328 → 185	$Ar^1S\cdot$
	89.6	282 → 159	$Ar^2S\cdot$
	83.7	302 → 159	$Ar^1S\cdot$
82f	220.1	431 → 308	$Ar^{1,2}S\cdot$
	166.6	431 → 268	$Ar^{1,2}SC_3H_4\cdot$
	111.1	308 → 185	$Ar^{1,2}S\cdot$
	89.6	282 → 159	$Ar^{1,2}S\cdot$

TABLE 6.2 - 3

Product ions identified by B/E linked scanning of selected ions in the mass spectrum of 82a.

Precursors scanned			Product ion
m/z	Assignment	Neutral lost	m/z
403	$M^{+\cdot}$	$Ar^{1,2}S\cdot$	294
		$Ar^{1,2}SC_2H_2\cdot$	268
		$Ar^{1,2}SC_3H_3$	255
		$Ar^{1,2}SC_3H_4\cdot$	254
		Ar^1SSAr^2	185
294	$\{M-Ar^{1,2}S\}^+$	$Ar^{1,2}S\cdot$	185
		$Ar^{1,2}SH$	184
185	$\{M-Ar^1SSAr^2\}^{+\cdot}$	$H\cdot$	184
		$CH_3\cdot$	170

TABLE 6.2 - 4

Product ions identified by B/E linked scanning of selected ions in the mass spectrum of 82e.

Precursors scanned			Product ion
m/z	Assignment	Neutral lost	m/z
451	$M^{+\cdot}$	$Ar^2S\cdot$	328
		$Ar^1S\cdot$	308
		$Ar^2SC_2H_2\cdot$	302
		$Ar^2SC_3H_3$	289
		$Ar^2SC_3H_4\cdot$	288
		$Ar^1SC_2H_2\cdot$	282
		$Ar^1SC_3H_3$	269
		$Ar^1SC_3H_4\cdot$	268
		Ar^1SSAr^2	185
308	$\{M-Ar^1S\}^+$	$Ar^2S\cdot$	185
		Ar^2SH	184
328	$\{M-Ar^2S\}^+$	$Ar^2S\cdot$	185
		Ar^2SH	184
185	$\{M-Ar^1SSAr^2\}^{+\cdot}$	$H\cdot$	184
		$CH_3\cdot$	170

TABLE 6.2 - 5

Product ions identified by B/E linked scanning of selected ions in the mass spectrum of 82f

Precursor scanned			Product ion
m/z	Assignment	Neutral lost	m/z
431	$M^{+\cdot}$	$Ar^{1,2}S\cdot$	308
		$Ar^{1,2}SC_2H_2\cdot$	282
		$Ar^{1,2}SC_3H_3$	269
		$Ar^{1,2}SC_3H_4\cdot$	268
		Ar^1SSAr^2	185
308	$\{M-Ar^{1,2}S\}^+$	$Ar^{1,2}S\cdot$	185
185	$\{M-Ar^1SSAr^2\}^{+\cdot}$	$H\cdot$	184
		$CH_3\cdot$	170

TABLE 6.2 - 6

Results of exact mass analysis.

Derivative	Nominal mass m/z	Composition	Exact mass Calc.	Found
82a	218	$C_{12}H_{10}S_2$	218.0224	218.0230
	185	$C_{13}H_{15}N$	185.1205	185.1186
82e	266	$C_{13}H_{11}ClS_2$	265.9991	266.0035
	185	$C_{13}H_{15}N$	185.1205	185.1186
82f	246	$C_{14}H_{14}S_2$	246.0537	246.0550
	185	$C_{13}H_{15}N$	185.1205	185.1186

6.3 Discussion

The molecular ions of the title compounds are similar to the rearranged molecular ions of 27, postulated in earlier work to be formed via {1,3} migration of both arylthio groups prior to elimination of a bisaryldisulphide moiety[45] (see Scheme 1.3.3.3 - 10).

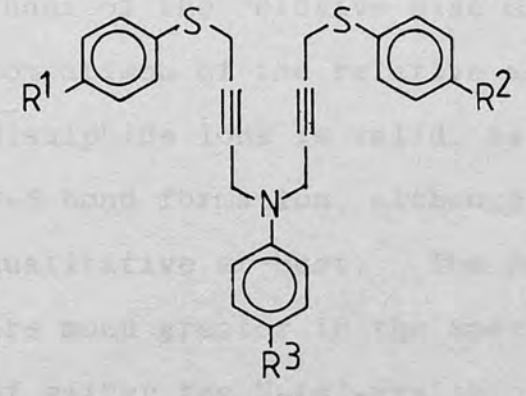

27

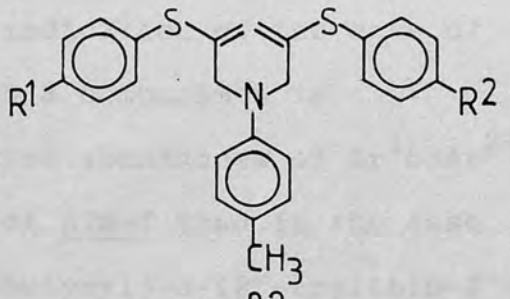

82

The six derivatives of 82 were prepared in order to determine whether elimination of Ar^1SSAr^2 occurs and thus substantiate or disprove the formation of an ion analogous to the molecular ion of 82 from electron impact of 27. Elimination of a bisaryldisulphide unit does in fact occur in every case to give m/z 185 and was supported by B/E linked scanning studies. Additionally, peaks corresponding to $Ar^1SSAr^{2+\cdot}$ were observed in all cases. Confirmation of the composition of the $\{M-Ar^1SSAr^2\}^{+\cdot}$ and $Ar^1SSAr^{2+\cdot}$ ions was obtained by exact mass analyses of these ions in the mass spectra of 82a, 82e and 82f. Owing to the contribution of the ion current of m/z 185 by the ions formed by the stepwise loss

of the arylthio groups, comparison of the relative abundance of $\{M-Ar^1SSAr^2\}^{+\cdot}$ ions in the spectra of 82a-f to those encountered in the mass spectra of the N-(4'-arylthio-2'-butynyl)-N-(2"-arylthio-2"-propenyl)-p-toluidines, discussed in Chapter 5, or the N,N-bis(4'-arylthio-2'-butynyl)anilines[45] cannot be used as an index of the relative ease of elimination of Ar^1SSAr^2. Comparison of the relative abundances of the bisaryldisulphide ions is valid, as an indication of the ease of S-S bond formation, although such a comparison is qualitative at best. The relative abundances of $Ar^1SSAr^{2+\cdot}$ are much greater in the spectra of 82a-f than in the case of either the N-(4'-arylthio-2'-butynyl)-N-(2"-arylthio-2"-propenyl)-p-toluidines or N,N-bis(4'-arylthio-2'-butynyl) anilines. This is to be expected if ions analogous to 82 are formed via {1,3} migrations of the two arylthio groups in 27, prior to the formation of $Ar^1SSAr^{2+\cdot}$ (i.e. if the rearrangement of 27 shown in Scheme 6.3 - 1 occurs to a significant extent, the formation of $Ar^1SSAr^{2+\cdot}$ from ions analogous to 29, which does not require any rearrangement in order for S-S bond formation to occur, should be more facile than from ions having a configuration analogous to 28).

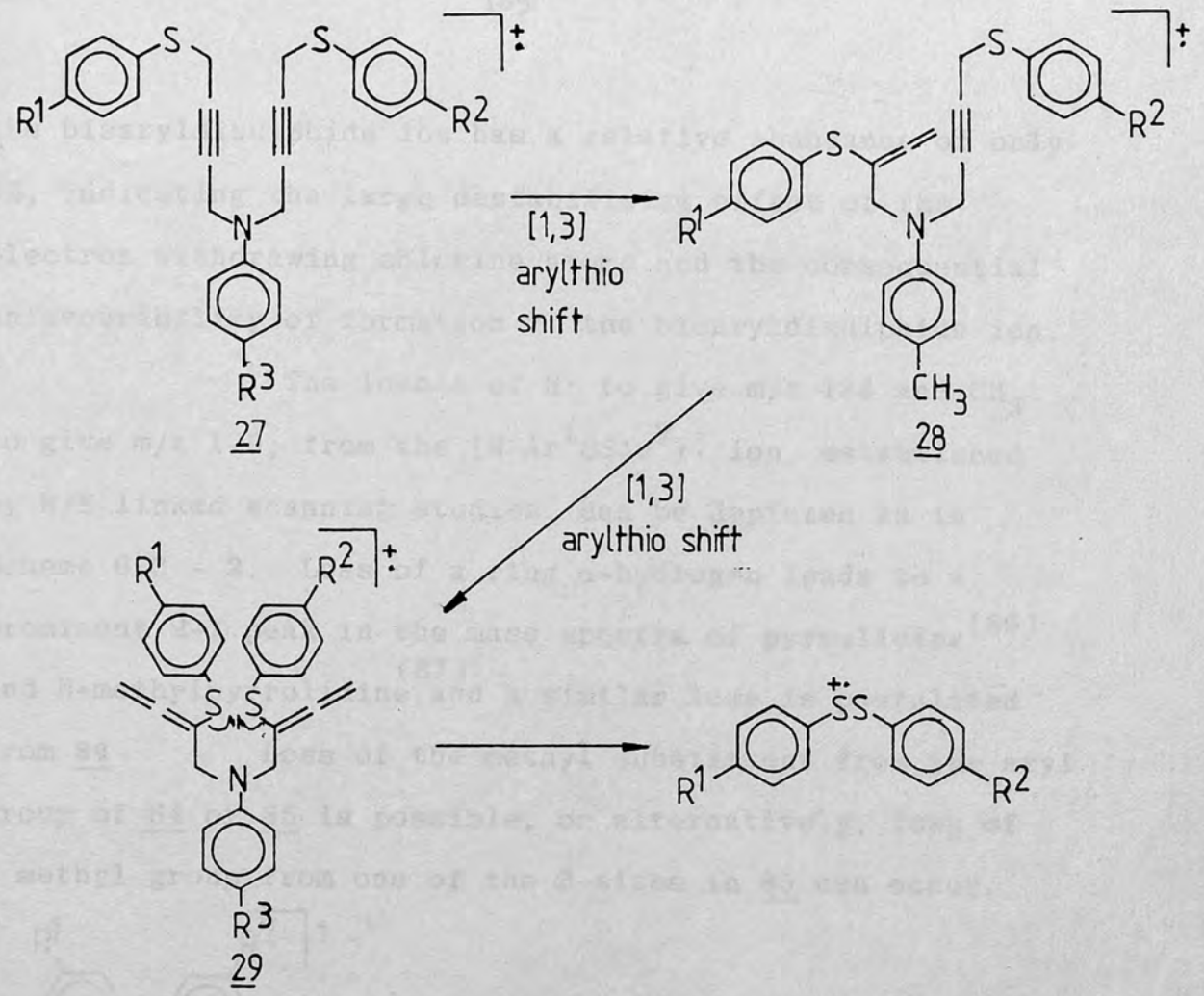

27 28 29

Scheme 6.3 - 1

The results of this work are entirely consistent with the rearrangement of 27 proposed previously.[45] By ranking the derivatives of 82 with respect to the relative abundance of the bisaryldisulphide ions in their spectra, the following order is observed:

(R^1,R^2) (CH_3,CH_3) > > (H,CH_3) > (H,Cl) ≈ (H,H) =

Cl,CH_3 > > (Cl,Cl)

Thus, a qualitative substituent effect is observed in which electron donating groups in Ar^1 and Ar^2 stablise the charge on the bisaryldisulphide product ion and makes its formation more favourable. In 82d, in which R^1=R^2=Cl,

the bisaryldisulphide ion has a relative abundance of only 2%, indicating the large destabilising effect of the electron withdrawing chlorine atoms and the consequential unfavourability of formation of the bisaryldisulphide ion.

The losses of H· to give m/z 184 and CH_3· to give m/z 170, from the $\{M-Ar^1SSAr^2\}^{+}$· ion, established by B/E linked scanning studies, can be depicted as in Scheme 6.3 - 2. Loss of a ring α-hydrogen leads to a prominent M-1 peak in the mass spectra of pyrrolidine[86] and N-methylpyrrolidine[87] and a similar loss is postulated from 84. Loss of the methyl substituent from the aryl group of 84 or 85 is possible, or alternatively, loss of a methyl group from one of the β-sites in 85 can occur.

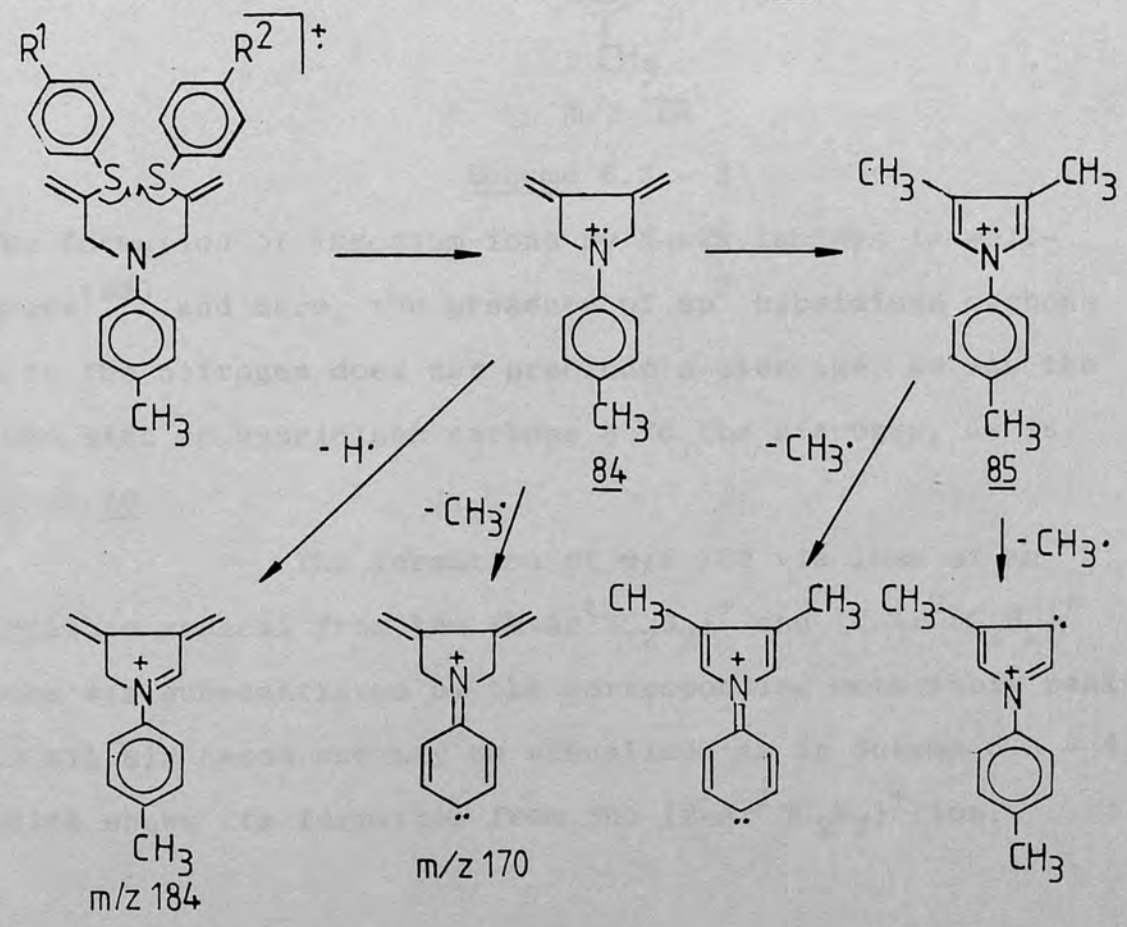

Scheme 6.3 - 2

The m/z 120 ion gave rise to a peak common to the spectra of 82a-f. It can arise via α-cleavage to give $\{M-Ar^1SC_2H_2\}^+$ (or $[M-Ar^2SC_2H_2]^+$) followed by C-N bond cleavage concomitant with hydrogen migration.

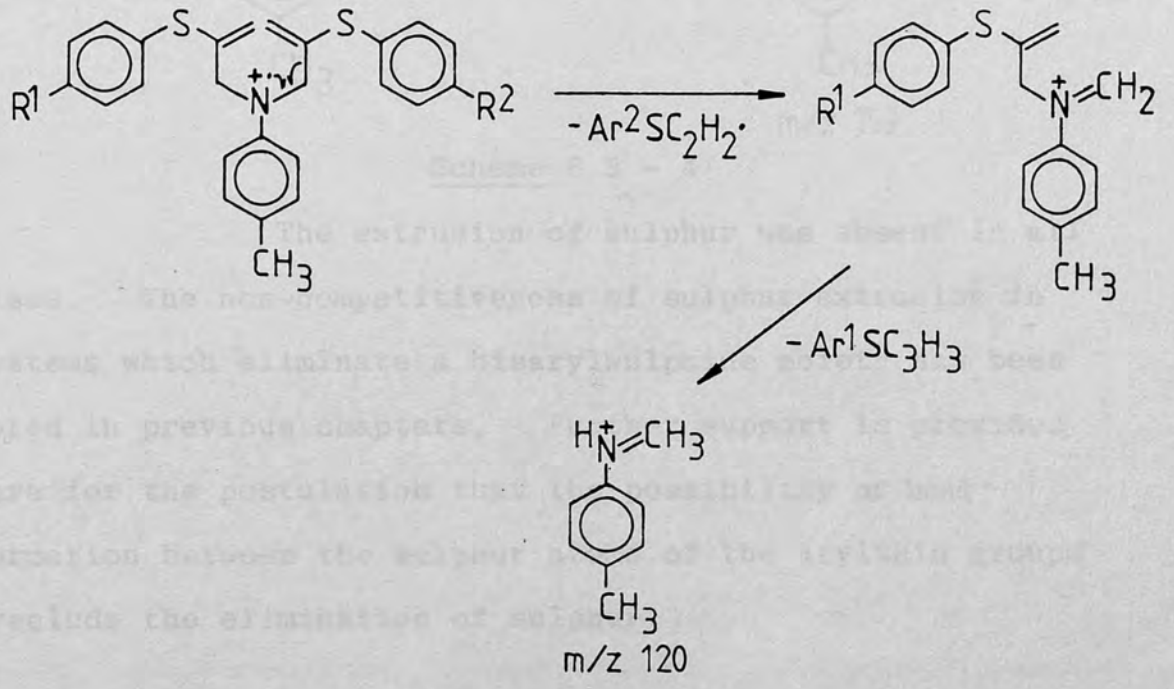

Scheme 6.3 - 3

The formation of immonium ions by N-alkylamines is well-known[82] and here, the presence of sp^2 hybridised carbons β to the nitrogen does not preclude α-cleavage, as was the case with sp hybridised carbons β to the nitrogen, as in 53 or 70.

The formation of m/z 159 via loss of an arylthio radical from the $\{M-Ar^1SC_2H_2\}^+$ and $\{M-Ar^2SC_2H_2\}^+$ ions was substantiated by the corresponding metastable peaks in all six cases and may be visualised as in Scheme 6.3 - 4, which shows its formation from the $\{M-Ar^1SC_2H_2\}^+$ ion.

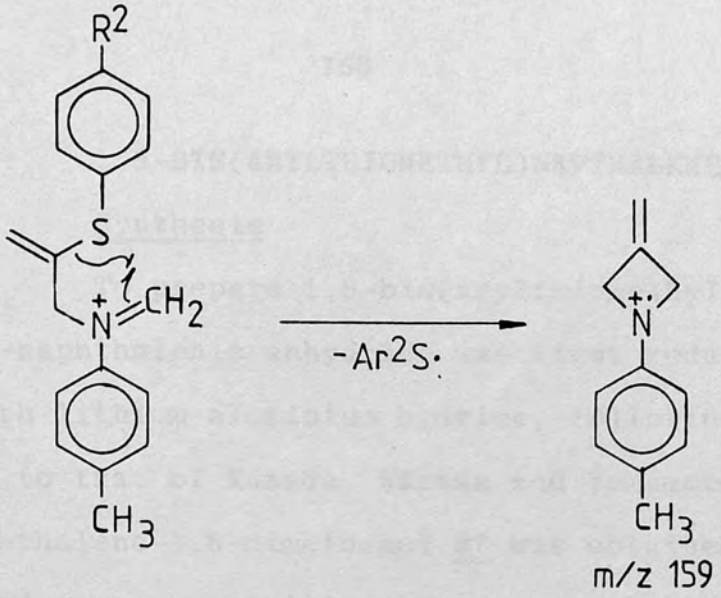

Scheme 6.3 - 4

The extrusion of sulphur was absent in all cases. The non-competitiveness of sulphur extrusion in systems which eliminate a bisarylsulphide moiety has been noted in previous chapters. Further support is provided here for the postulation that the possibility of bond formation between the sulphur atoms of the arylthio groups preclude the elimination of sulphur.

7. 1,8-BIS(ARYLTHIOMETHYL)NAPTHALENES.

7.1 Synthesis

To prepare 1,8-bis(arylthiomethyl)napthalenes 86, 1,8-naphthalenic anhydride was first reduced to the diol with lithium aluminium hydride, following a procedure similar to that of Kamada, Wasada and Yamamoto[88]. The naphthalene-1,8-dimethanol 87 was obtained in 85% yield and was recrystallised from acetone prior to use in the next step (m.p. 156-157°, lit.[88] 157-158°). Reaction of 87 with concentrated hydrochloric acid at 0°, according to the procedure of Boekelheide and Vick,[89] gave the dichloride 88 in 58% yield (recrystallised from petroleum spirit, m.p. 90-91°, lit.[89] 87-90°). Scheme 7.1 - 1 indicates a route for the preparation of the symmetrical derivatives 86a, 86d and 86f and a different route for the three asymmetrical derivatives. The symmetrical compounds were prepared in one step by the addition of a twofold excess of the appropriate potassium arenethiolate in methanol (prepared *in situ*) to a 50% ether/methanol solution of 88 at ambient temperature. After 0.5 hours, the precipitated solid, a mixture of potassium chloride and product, was collected, extracted with chloroform and any unreacted starting material removed by washing its chloroform solution with aqueous potassium hydroxide. Removal of solvent gave the product in 56-74% yields as a white solid.

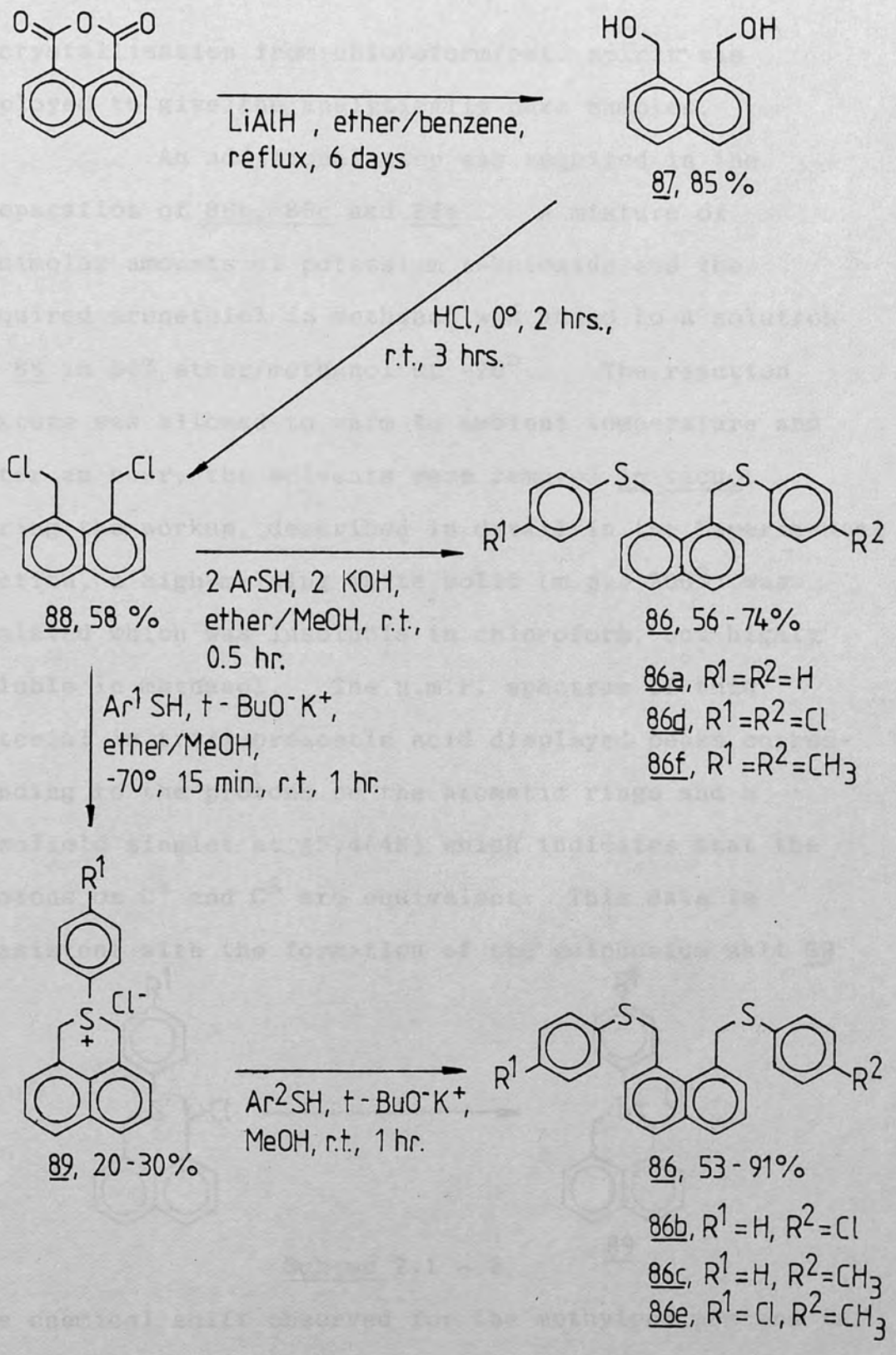
LiAlH , ether/benzene,
reflux, 6 days
87, 85 %
HCl, 0°, 2 hrs.,
r.t., 3 hrs.
88, 58 %
2 ArSH, 2 KOH,
ether/MeOH, r.t.,
0.5 hr.
86, 56 - 74%
86a, R1=R2=H
86d, R1=R2=Cl
86f, R1=R2=CH3
Ar1 SH, t - BuO⁻K⁺,
ether/MeOH,
-70°, 15 min., r.t., 1 hr.
89, 20-30%
Ar2SH, t - BuO⁻K⁺,
MeOH, r.t., 1 hr.
86, 53 - 91%
86b, R1=H, R2=Cl
86c, R1=H, R2=CH3
86e, R1=Cl, R2=CH3

Scheme 7.1 - 1

Recrystallisation from chloroform/pet. spirit was employed to give the analytically pure samples.

An additional step was required in the preparation of 86b, 86c and 86e. A mixture of equimolar amounts of potassium t-butoxide and the required arenethiol in methanol was added to a solution of 88 in 50% ether/methanol at -70°. The reaction mixture was allowed to warm to ambient temperature and after an hour, the solvents were removed in vacuo. During the workup, described in detail in the Experimental section, a high-melting white solid (m.p. > 200°) was isolated which was insoluble in chloroform, but highly soluble in methanol. The n.m.r. spectrum of this material in trifluoroacetic acid displayed peaks corresponding to the protons on the aromatic rings and a downfield singlet at δ5.4(4H) which indicates that the protons on C^1 and C^8 are equivalent. This data is consistent with the formation of the sulphonium salt 89:

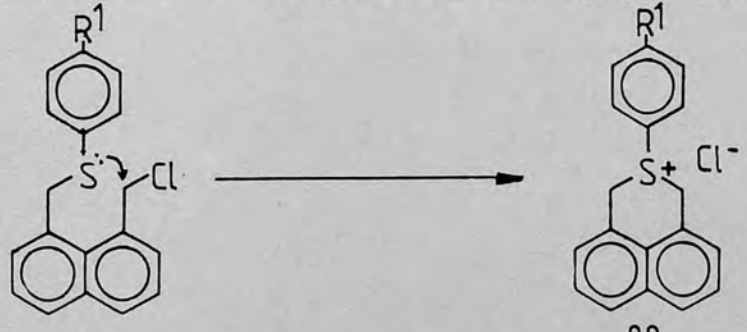

89

Scheme 7.1 - 2

The chemical shift observed for the methylene protons is similar to that reported for the benzylic protons of 90, which absorb at δ4.79 in trifluoroacetic acid(90)

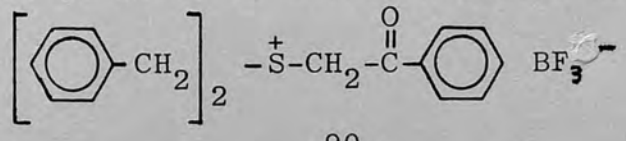

90

Two derivatives of 89 were made (R^1=H and R^1=Cl). Although 89 has not been reported previously, cyclic sulphonium salts are well known and documented.[91]

Reaction of 89 with the desired potassium arenethiolates (prepared *in situ*) in methanol gave the desired products 86b, 86c and 86e as white solids in 53-91% yield. Analytical samples were prepared by recrystallisation from chloroform/pet. ether.

The six derivatives of 86 were characterised by their n.m.r. and mass spectra and gave excellent results upon elemental analysis. None had been previously reported.

7.2 E.I. induced fragmentation results.

The majority of the ions in the spectra of 86a-f arise from cleavage occuring after loss of an arylthio radical. The facility of this loss is so great that it is the sole fragmentation pathway observed for the molecular ion. B/E linked scans of the molecular ions and the $\{M-Ar^{1(2)}S\}^+$ ions in the spectra of 86a, 86d and 86f established the fragmentations shown in Scheme 7.2 - 1.

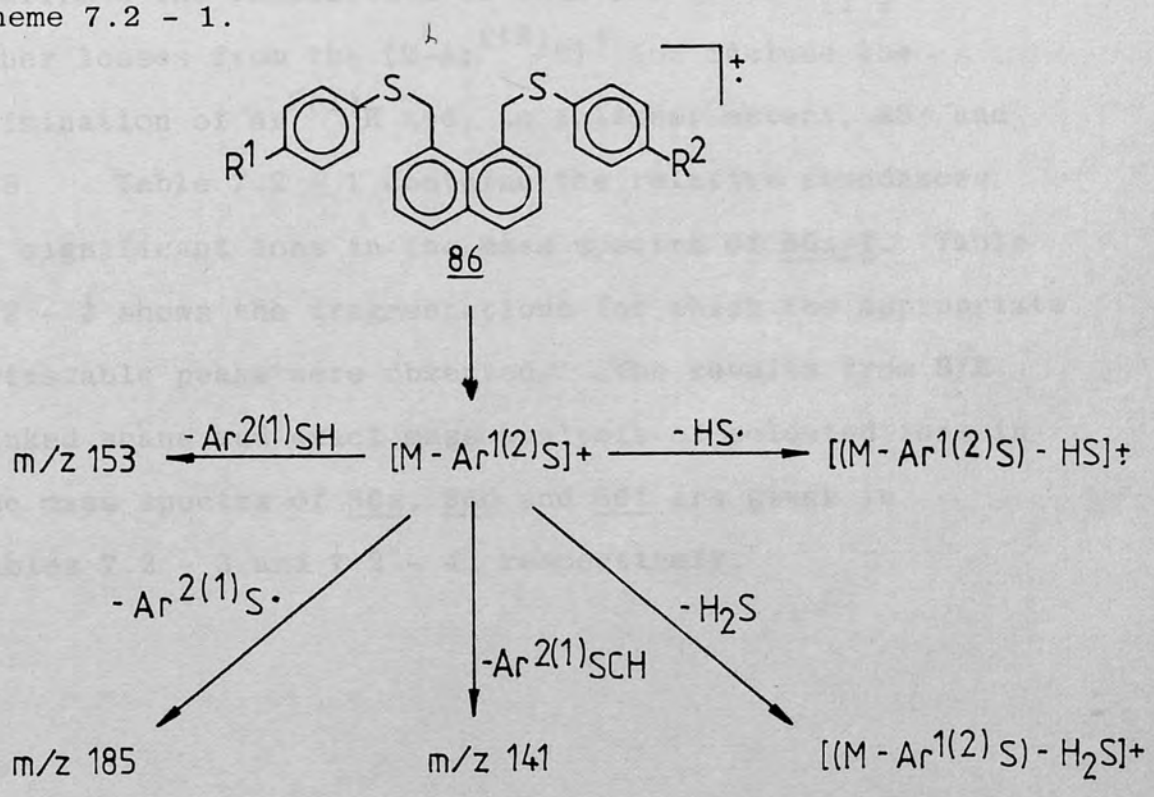

Scheme 7.2 - 1

The base peaks in the mass spectra of 86a and 86f correspond to $\{M-Ar^{1(2)}S\}^+$. In the remainder of cases, the m/z 153 ion gives rise to the base peak and is formed by the loss of $Ar^{2(1)}SH$ from the $\{M-Ar^{1(2)}S\}^+$ ion. Another major process is the formation of m/z 141 via the loss of the elements of $Ar^{2(1)}SCH$ from $\{M-Ar^{1(2)}S\}^+$. Exact mass analyses of the m/z 141 ion in the spectra of 86a, 86d and 86f confirmed the composition of this ion to be $C_{11}H_9$. Other losses from the $\{M-Ar^{1(2)}S\}^+$ ion include the elimination of $Ar^{2(1)}H$ and, to a lesser extent, HS· and H_2S. Table 7.2 - 1 contains the relative abundances of significant ions in the mass spectra of 86a-f. Table 7.2 - 2 shows the fragmentations for which the appropriate metastable peaks were observed. The results from B/E linked scans and exact mass analysis of selected ions in the mass spectra of 86a, 86d and 86f are given in Tables 7.2 - 3 and 7.2 - 4, respectively.

TABLE 7.2 - 1

Significant ions in the mass spectra of 1,8-bis(arylthiomethyl)naphthalenes 86.

	m/z (relative abundance)					
Ion	a	b	c	d	e	f
$M^{+\cdot}$	372(7)	406(4)	386(6)	440(2)	420(7)	400(7)
Ar^1S^+	109(4)	109(5)	109(4)	143(5)	143(4)	123(8)
$\{M-Ar^1S\}^+$	263(100)	297(38)	277(28)	297(44)	277(51)	277(100)
Ar^2S	109(4)	143(5)	123(4)	143(5)	123(5)	123(8)
$\{M-Ar^2S\}^+$	263(100)	263(65)	263(75)	297(44)	297(69)	277(100)
$\{(M-Ar^1S)-HS\}^{+\cdot}$	230(4)	264(13)	244(1)	264(1)	244(2)	244(3)
$\{(M-Ar^1S)-H_2S\}^+$	229(4)	263(65)[a]	243(1)	263(1)	243(2)	243(3)
$\{(M-Ar^2S)-HS\}^{+\cdot}$	230(4)	230(3)	230(4)	264(1)	264(1)	244(3)
$\{(M-Ar^2S)-H_2S\}^+$	229(4)	229(5)	229(6)	263(1)	263(2)	243(3)
$\{(M-ArS)-Ar'SH\}^+$	153(59)	153(100)	153(100)	153(100)	153(100)	153(80)
$\{(M-ArS)-Ar'H\}^+$	185(5)	185(7)	185(7)	185(6)	185(9)	185(8)
$C_{11}H_9^+$	141(27)	141(44)	141(50)	141(46)	141(42)	141(41)
$C_9H_7^+$	115(1)	115(3)	115(2)	115(2)	115(2)	115(2)

[a] Same nominal mass as $[M-Ar^2S]^+$

TABLE 7.2 - 2

Metastable peaks in the mass spectra of 1,8-bis(arylthiomethyl)naphthalenes.

Derivative	Metastable peak	Transition	Neutral lost
86a	201.1	263 → 230	HS·
	185.9	372 → 263	$Ar^{1(2)}S$·
	89.0	263 → 153	$Ar^{1(2)}SH$
	75.6	263 → 141	$Ar^{1(2)}SCH$
86b	234.7	297 → 264	HS·
	201.1	263 → 230	HS·
	170.4	406 → 263	$Ar^{2}S$·
	75.6	263 → 141	$Ar^{1}SCH$
	66.9	297 → 141	$Ar^{2}SCH$
86c	214.9	277 → 244	HS·
	201.1	263 → 230	HS·
	179.2	386 → 263	$Ar^{2}S$·
	75.6	263 → 141	$Ar^{1}SCH$
	71.8	277 → 141	$Ar^{2}SCH$
86d	234.7	297 → 264	HS·
	280.5	440 → 297	$Ar^{1(2)}S$·
	66.9	297 → 141	$Ar^{1(2)}SCH$

/continued ..

TABLE 7.2 - 2 (continued)

Derivative	Metastable peak	Transition	Neutral lost
86e	234.7	297 → 264	HS·
	214.9	277 → 244	HS·
	210.0	420 → 297	Ar^2S·
	182.7	420 → 277	Ar^1S·
	123.6	277 → 185	Ar^2H
	115.2	297 → 185	Ar^1H
	71.8	277 → 141	Ar^2SCH
	66.9	297 → 141	Ar^1SCH
86f	214.9	277 → 244	HS·
	191.8	400 → 277	$Ar^{1(2)}S$·
	123.6	277 → 185	$Ar^{1(2)}H$
	84.5	277 → 153	$Ar^{1(2)}SH$
	71.8	277 → 141	$Ar^{1(2)}SCH$

TABLE 7.2 - 3

Product ions detected in B/E linked scanning spectra of selected ions in the mass spectra of 86a, 86d and 86f.

Derivative	Precursor scanned m/z	Assignment	Neutral lost	Product ion m/z
86a	372	$M^{+\cdot}$	$Ar^{1(2)}S\cdot$	263
	263	$\{M-Ar^{1(2)}S\}^+$	$HS\cdot$	230
			H_2S	229
			$Ar^{2(1)}H$	185
			$Ar^{2(1)}SH$	153
			$Ar^{2(1)}SCH$	141
86d	440	$M^{+\cdot}$	$Ar^{1(2)}S\cdot$	297
	297	$\{M-Ar^{1(2)}S\}^+$	$HS\cdot$	264
			H_2S	263
			$Ar^{2(1)}H$	185
			$Ar^{2(1)}SH$	153
			$Ar^{2(1)}SCH$	141
86f	400	$M^{+\cdot}$	$Ar^{1(2)}S\cdot$	277
	277	$\{M-Ar^{1(2)}S\}^+$	$HS\cdot$	244
			H_2S	243
			$Ar^{2(1)}H$	185
			$Ar^{2(1)}SH$	153
			$Ar^{2(1)}SCH$	141

TABLE 7.2 - 4

Results of exact mass analysis of selected ions in the mass spectra of 86a, 86d and 86f.

Derivative	Nominal mass (m/z	Composition	Exact mass Calc.	Found
86a	141	$C_{11}H_9$	141.0704	141.0713
86d	141	$C_{11}H_9$	141.0704	141.0711
86f	141	$C_{11}H_9$	141.0704	141.0713

7.3 Discussion

The loss of an arylthio group from 86 predominates to such an extent, that skeletal rearrangement of the molecular ion is completely absent. Thus, even though the sulphur atoms of the two arylthio groups can come into close proximity no elimination of a bisaryldisulphide to give 91 occurs:

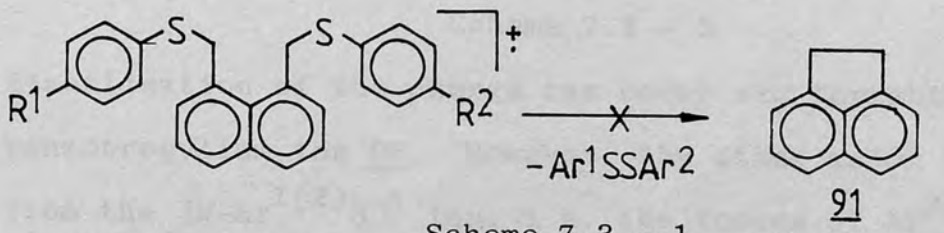

91

Scheme 7.3 - 1

nor was the elimination of sulphur observed. However, the mass spectra of 86a-f do contain some interesting features which are worthy of discussion.

Several structures for the $\{M-Ar^{1(2)}S\}^+$ ion can be postulated with the most reasonable being the benzylic carbonium ion 92, the sulphonium ion 93, and a benzotropylium ion 94.

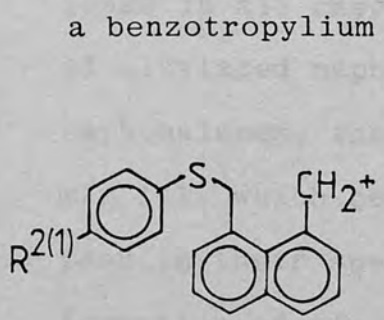

92

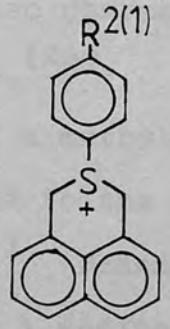

93

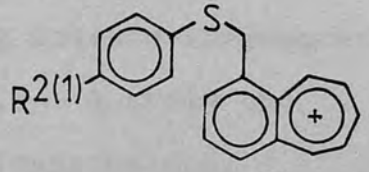

94

The sulphonium ion 93 is identical to the cation of the sulphonium salt isolated during the synthesis of 86. Furthermore, the loss of $Ar^{2(1)}H$ from the $\{M-Ar^{1(2)}S\}^+$ ion to give m/z 185, which was encountered in every case and substantiated by both the B/E linked scanning studies

and metastable peaks in some instances, can be easily rationalised to occur from 93 to give 95

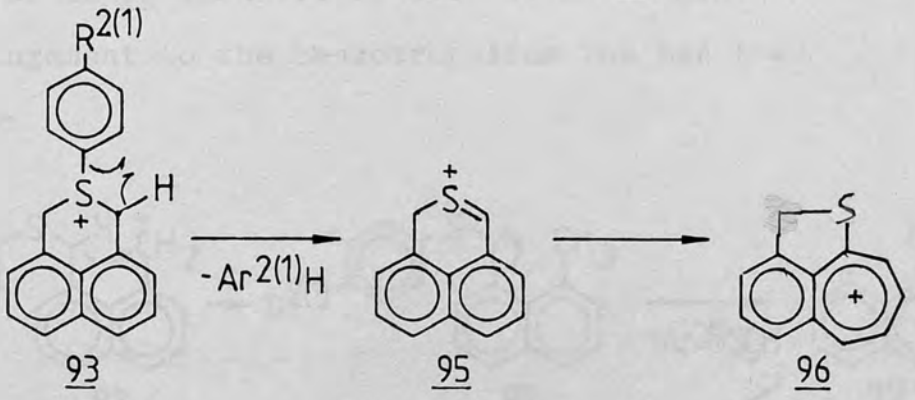

93 95 96

Scheme 7.3 - 2

Stabilisation of the charge can occur via formation of a benzotropylium ion 96. However, the other major losses from the $\{M-Ar^{1(2)}S\}^+$ ion, i.e. the losses of $Ar^{2(1)}SH$ and $Ar^{2(1)}SCH$, are difficult to visualise from the cyclic sulphonium ion 93.

The presence of an intense peak at m/z 141 corresponding to the benzotropylium ion (whose formation from the $\{M-Ar^{1(2)}S\}^+$ ion was proven by B/E linked scanning studies and the presence of supporting metastable peaks in all cases) is also characteristic of the spectra of alkylated naphthalenes.[25c] In the case of dimethylnaphthalenes, the loss of a methyl group gives rise to m/z 141, which corresponds to the only intense fragmentation peak in their spectra.[92] Scheme 7.3 - 3 shows the formation of m/z 141 from 1,8-dimethylnaphthalene.

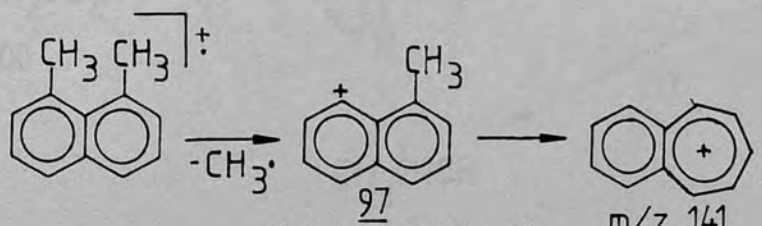

97 m/z 141

Scheme 7.3 - 3

The intermediate ion 97 can also be formed via hydride transfer in 92 followed by loss of $Ar^{2(1)}SCH$. Rearrangement to the benzotropylium ion can then follow:

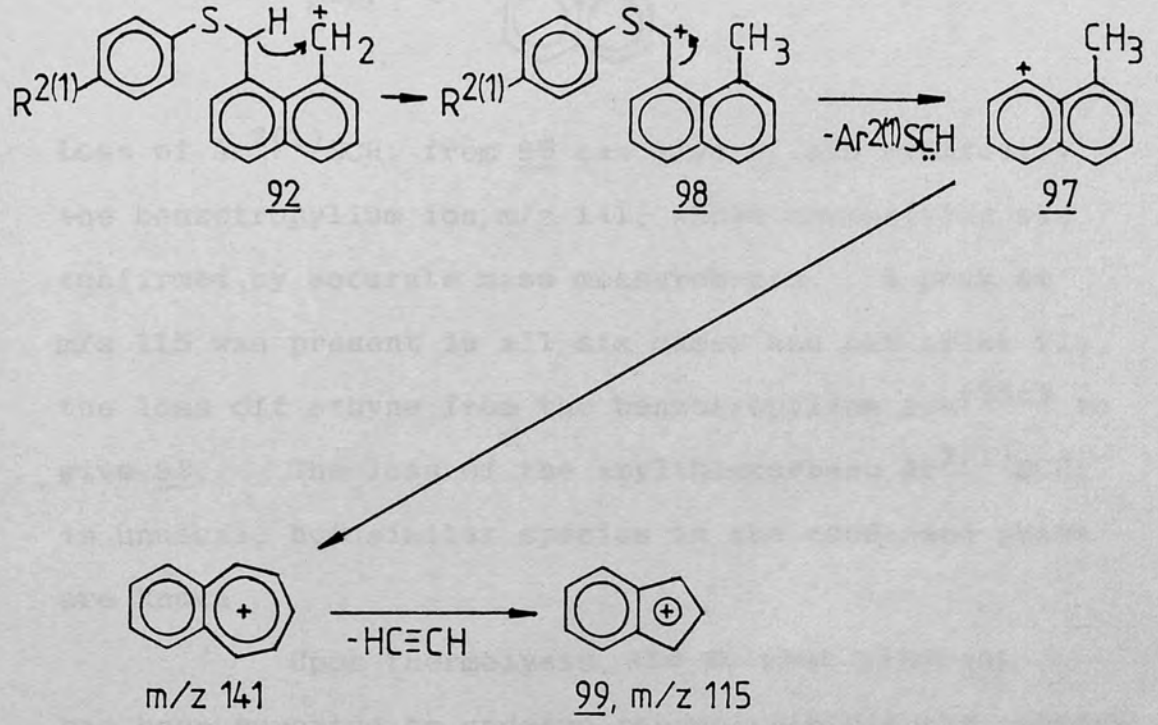

Scheme 7.3 - 4

A hydride shift has also been postulated to account for the loss of carbon monoxide from the $\{M-X\}^+$ ion in the mass spectra of the β-halo acids 100 (x = Cl or Br).[25d]

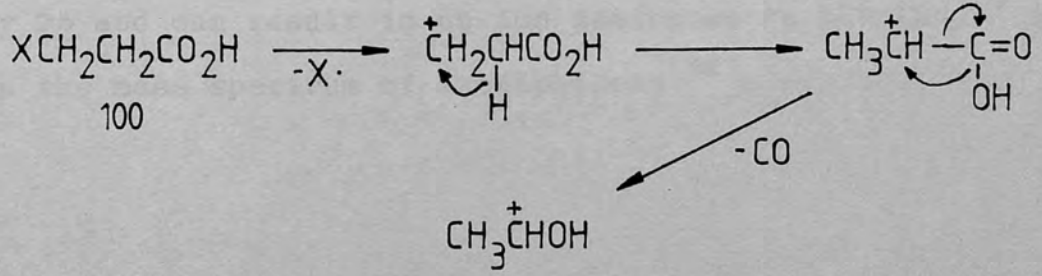

Scheme 7.3 - 5

Although 92 and 98 are both benzylic carbonium ions, 98 can be stabilised to a greater extent by the presence of the sulphur atom adjacent to the charge, i.e.:

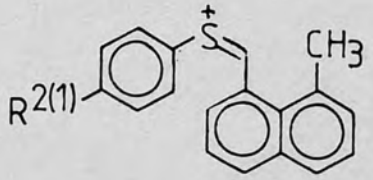

Loss of $Ar^{2(1)}SCH$: from 98 can give 97 and eventually the benzotropylium ion, m/z 141, whose composition was confirmed by accurate mass measurements. A peak at m/z 115 was present in all six cases and can arise via the loss off ethyne from the benzotropylium ion[25c] to give 99. The loss of the arylthiocarbene $Ar^{2(1)}SCH$: is unusual, but similar species in the condensed phase are known.

Upon thermolysis, the sulphur ylide 101 has been reported to undergo thermolysis via the carbene 102[93] (Scheme 7.3 - 6).

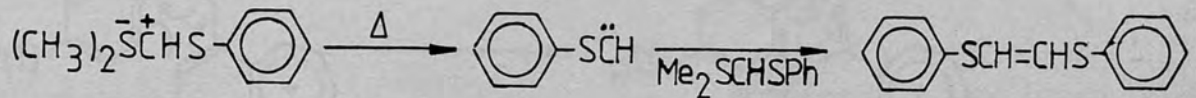

101 102

Scheme 7.3 - 6

The loss of $Ar^{2(1)}SH$ can also be accommodated by 98 and can result in an ion analogous to the $\{M-1\}^+$ ion in the mass spectrum of acenaphthene[94], m/z 153.

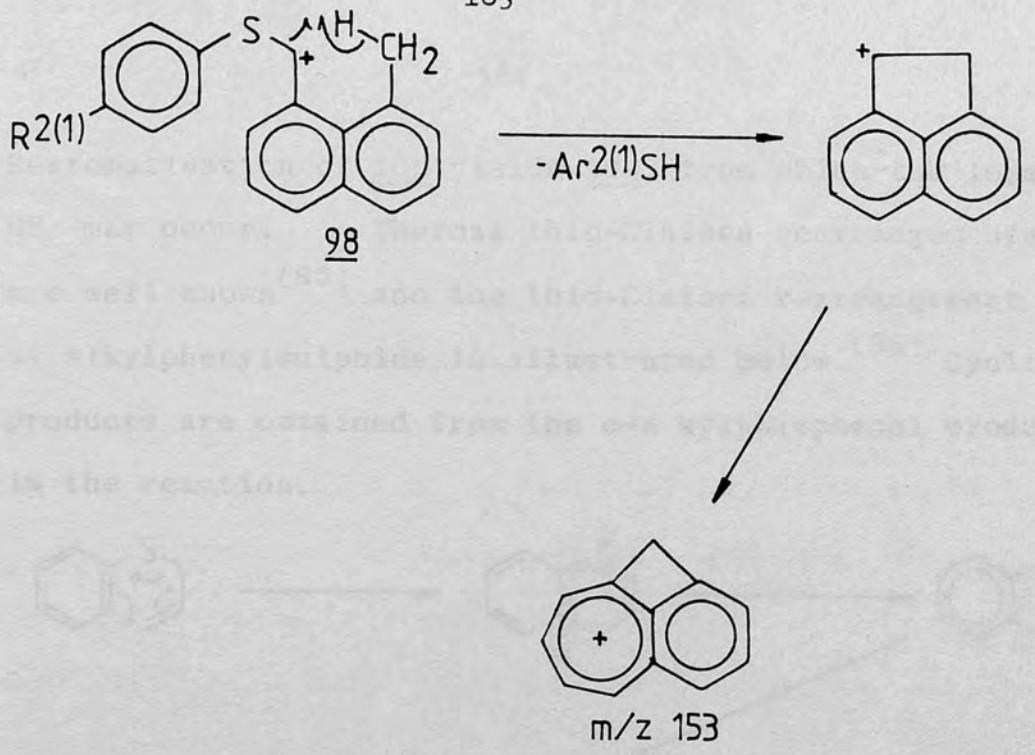

Scheme 7.3 - 7

The stability of the m/z 153 ion is indicated by its correspondence to the base peak in both the mass spectrum of acenaphthene[94] and in the mass spectra of four of the 1,8-bis(arylthiomethyl)naphthalenes.

One possible mechanism for the loss of HS· from the $\{M-Ar^{1(2)}S\}^+$ ions, giving ions of low abundance, invokes the thio-Claisen rearrangement of 94 to 103:

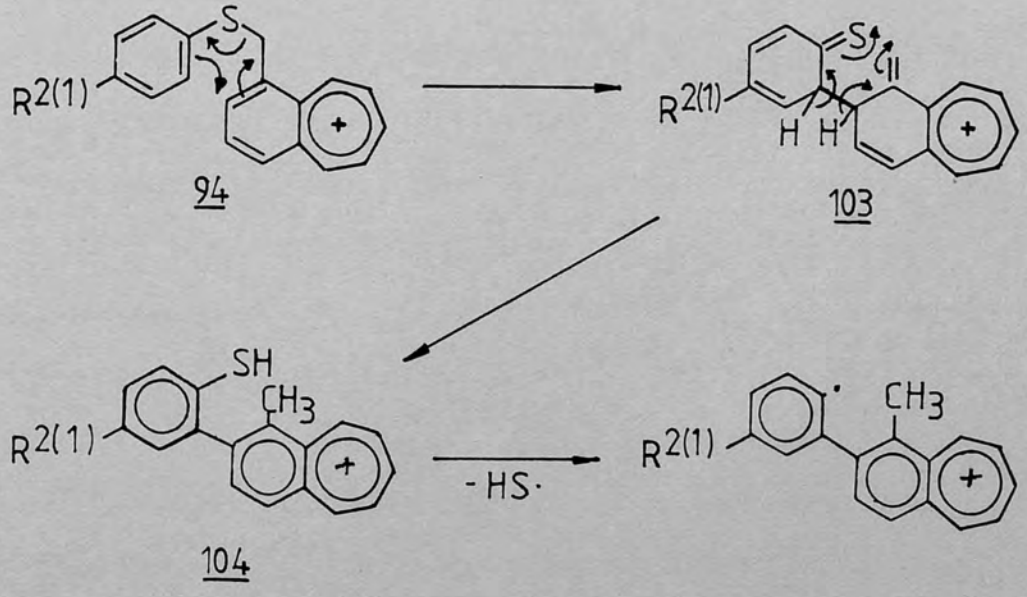

Scheme 7.3 - 8

Rearomatisation of 103 yields 104, from which the loss of HS· may occur. Thermal thio-Claisen rearrangements are well known[95] and the thio-Claisen rearrangement of alkylphenylsulphide is illustrated below.[96] Cyclised products are obtained from the o-alkylthiophenol produced in the reaction.

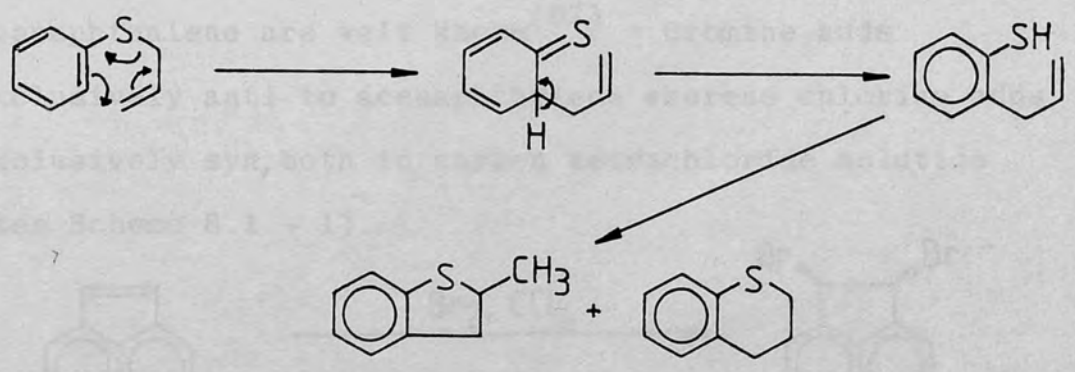

Scheme 7.3 - 9

In summary, the fragmentation of the 1,8-bis(arylthiomethyl)naphthalenes is dominated by the loss of an arylthio radical to the exclusion of other processes and further fragmentation of the $\{M-Ar^{1(2)}S\}^+$ ion appears to occur via several modes of rearrangement.

8. 1,2-BIS(ARYLTHIO)ACENAPHTHENES.

8.1 Synthesis

A synthetic approach to 1,2-bis(arylthio)acenaphthenes can be envisaged in which 1,2-dihaloacenaphthenes would be easily obtained intermediates. The stereospecific additions of bromine and chlorine to acenaphthalene are well known[97]. Bromine adds exclusively anti to acenaphthylene whereas chlorine adds exclusively syn, both in carbon tetrachloride solution (see Scheme 8.1 - 1).

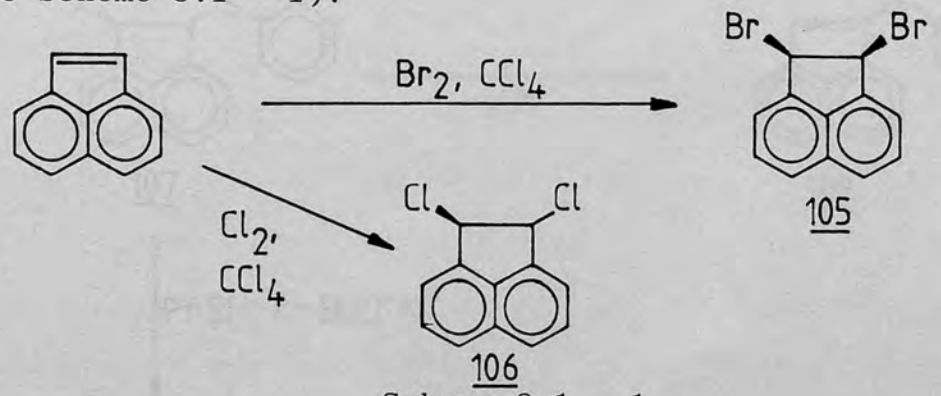

Scheme 8.1 - 1

Compounds 105 and 106 were prepared by known procedures[97]. The dibromide 105 was reacted with 2.2 equivalents of methanolic potassium thiophenolate (prepared *in situ*) in hopes of obtaining the 1,2-bis-(phenolthio)acenaphthene directly. The n.m.r. spectrum of the crude product mixture contained peaks solely in the region of δ7.15 - 8.0, indicating the absence of the desired compound but supporting the formation of elimination products. These would arise from the loss of hydrogen bromide from either 105 or from the phenylthio product, 107. The reaction of the dichloride, 106, under similar conditions yielded a similar product mixture.

Scheme 8.1 - 2 summarises these various reaction paths (X = Cl or Br).

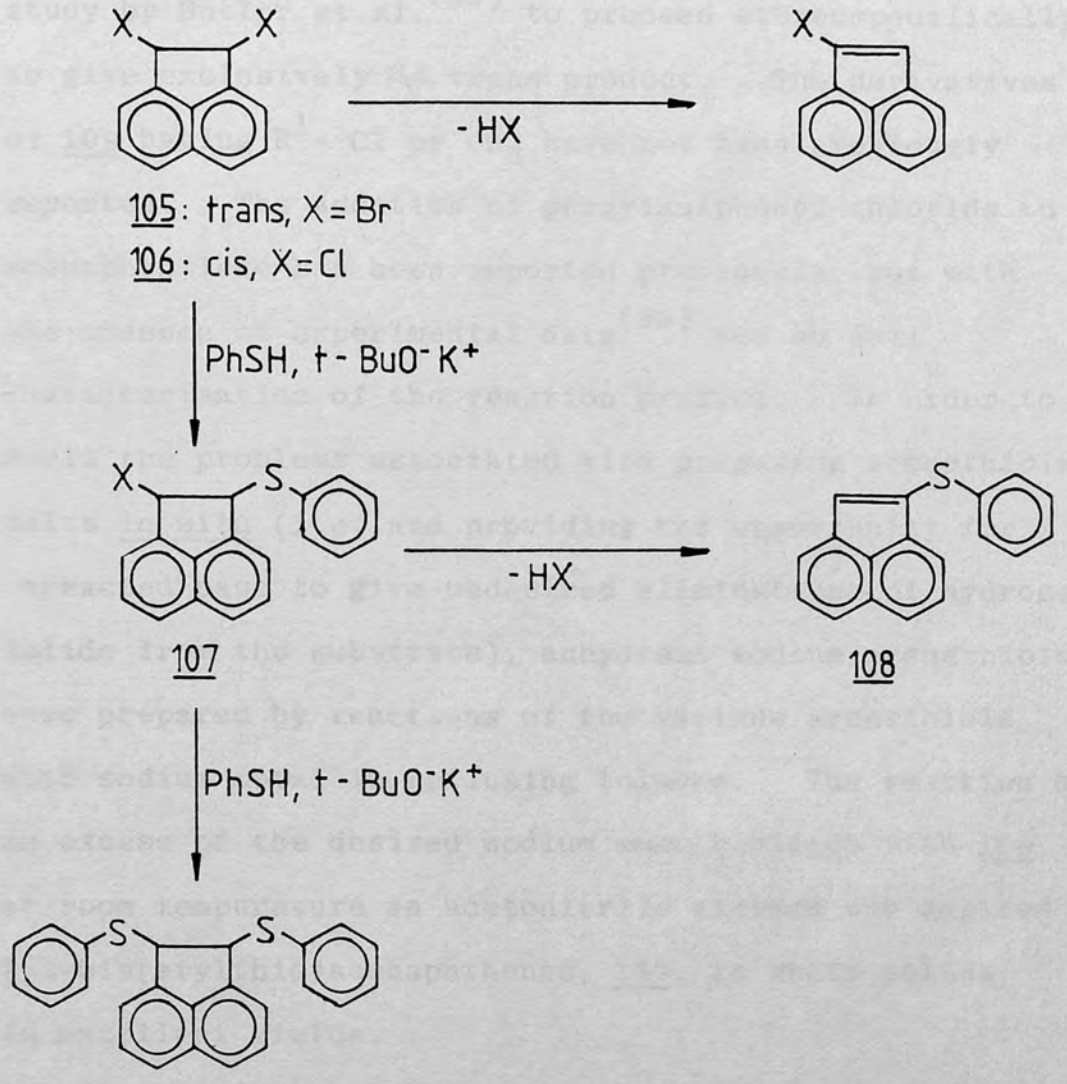

Scheme 8.1 - 2

In order to avoid the facile elimination of hydrogen halide, a second preparative route was employed. 2-Arylthio-1-chloro-acenaphthenes, 107, were prepared in nearly quantitative yields as pale yellow solids by the addition of arenesulphenyl chlorides to acenaphthylene in glacial acetic acid (see Scheme 8.1 - 3), following

the method of Kharasch[98]. The addition of sulphenyl chlorides to acenaphthylene has been shown in an n.m.r. study by Butler et.al.[99] to proceed stereospecifically to give exclusively the trans product. The derivatives of 109 having R^1= Cl or CH_3 have not been previously reported. The addition of phenylsulphenyl chloride to acenaphth lene has been reported previously, but with the absence of experimental data[99] and no full characterisation of the reaction product. In order to avoid the problems associated with preparing arenethiolate salts in situ (i.e. and providing the opportunity for unreacted base to give undesired eliminations of hydrogen halide from the substrate), anhydrous sodium arenethiolates were prepared by reactions of the various arenethiols with sodium metal in refluxing toluene. The reaction of an excess of the desired sodium arenethiolates with 109 at room temperature in acetonitrile yielded the desired 1,2-bis(arylthio)acenaphthenes, 110, as white solids in excellent yields.

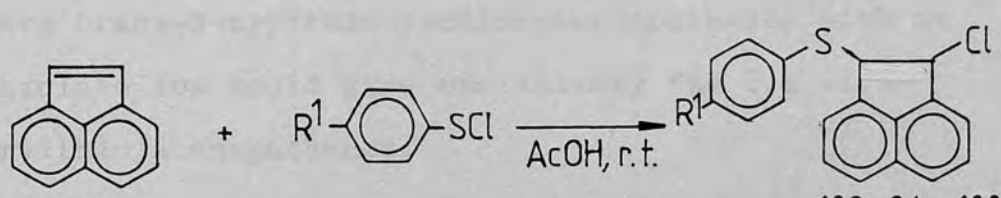

109, 96 - 100%

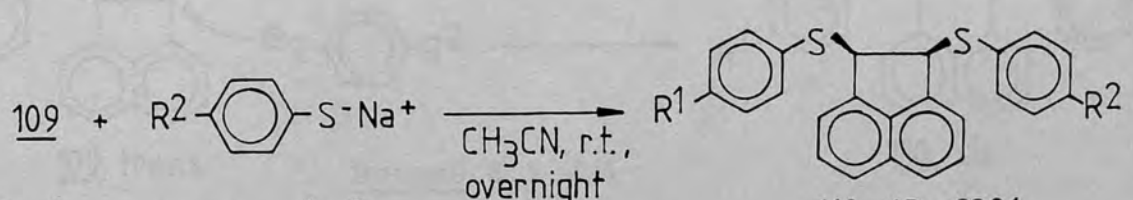

110, 63 - 99%

110a: R^1=R^2=H 110d: R^1=R^2=Cl
110b: R^1=H, R^2=Cl 110e: R^1=Cl, R^2=CH_3
110c: R^1=H, R^3=CH_3 110f: R^1=R^2=CH_3

Scheme 8.1 -3

Analytical samples were obtained by recrystallisation from chloroform/petroleum spirit. Analysis of the recrystallised samples by t.l.c. indicated that a single product was formed in the reaction. The conclusion was substantiated by the appearance of a single sharp downfield singlet in their n.m.r. spectra corresponding to the methine protons (ca. δ5.55).

Sternhall and Westerman have reported the chemical shifts (100 MHz) of the methine protons in a number of cis and trans isomers of 1,2-disubstituted acenaphthenes.[100] The 90 MHz. n.m.r. spectrum of 110 a showed a single singlet (2H) at 5.46 ppm.

Should a mixture of isomers have been formed in this reaction, the n.m.r. spectrum would be expected to contain two downfield singlets corresponding to the two different methine protons.

The production of a single isomer by this reaction suggests that the reaction is proceeding via an S_N2 mechanism with inversion at C_1. Thus, reaction of the pure trans-2-arylthio-1-chloroacenaphthenes with an arenethiolate ion would give exclusively the cis -1,2-bis(arylthio)acenaphthenes.

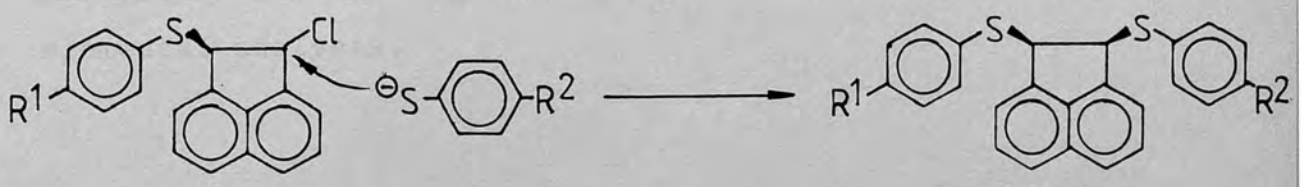

109, trans

Scheme 8.1 - 4

110, cis

Another possible mechanism in which only one isomer would be produced is the formation of a sulphonium intermediate, prior to nucleophilic attack:

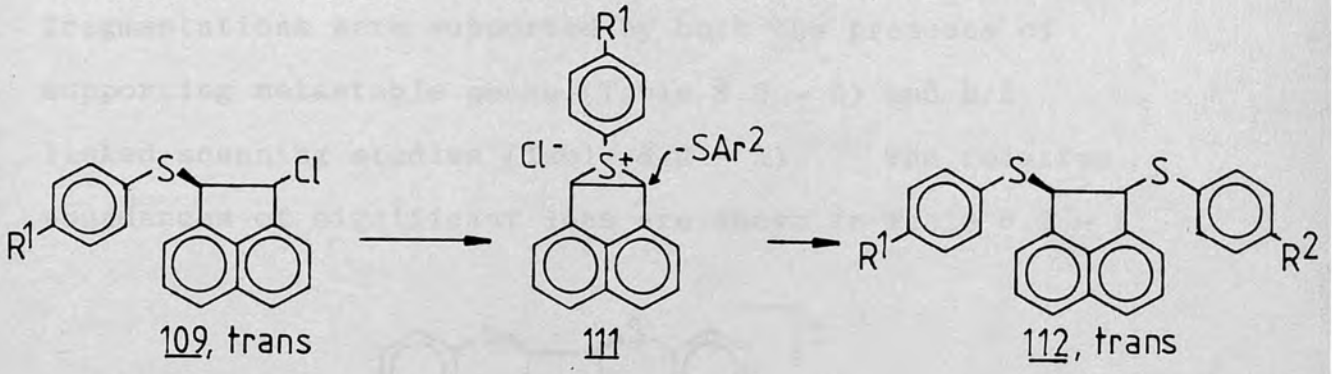

Scheme 8.1 - 5

Such a mechanism would result in the formation of solely the trans- isomer[112]. However, 109 was found to be unreactive towards a tenfold excess of sodium iodide in acetone solution at room temperature (only starting material and 108 were recovered). This would appear to rule out the formation of 111 and any anchimeric assistance to the displacement reaction. Based upon these mechanistic considerations, the six derivatives of 110 have been tentatively designated cis. They were characterised by their n.m.r. and mass spectra. These previously unknown compounds gave excellent results upon elemental analysis.

8.2 E.I. induced fragmentation results

The fragmentation of the cis- 1,2-bis(arylthio)-acenaphthenes is illustrated in Scheme 8.2 - 1. These fragmentations were supported by both the presence of supporting metastable peaks (Table 8.2 - 2) and B/E linked scanning studies (Table 8.2 - 3). The relative abundances of significant ions are shown in Table 8.2 - 1.

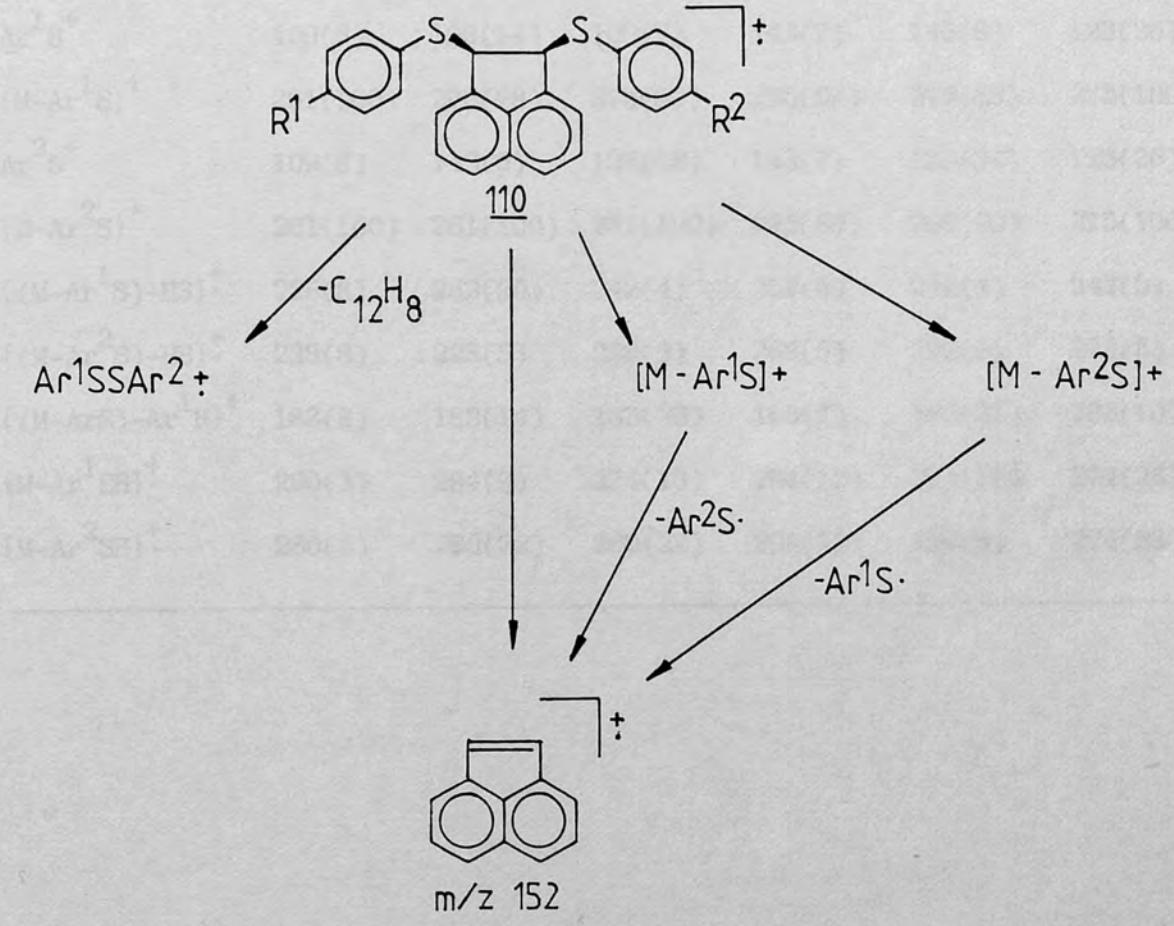

Scheme 8.2 - 1

TABLE 8.2 - 1

Significant ions in the 70 eV mass spectra of cis-1,2-bis(arylthio)acenaphthenes (110)

Ions	m/z (Relative abundance) a	b	c	d	e	f
$M^{+\cdot}$	370(12)	404(5)	384(20)	438(3)	418(11)	398(10)
$Ar^1SSAr^2{}^{+\cdot}$	218(8)	252(5)	232(23)	286(3)	266(16)	246(11)
$\{M-Ar^1SSAr^2\}^{+\cdot}$	152(62)	152(51)	152(66)	152(100	152(100)	152(66)
Ar^1S^+	109(6)	109(14)	109(7)	143(7)	143(6)	123(26)
$\{M-Ar^1S\}^+$	261(100)	295(28)	275(89)	295(69)	275(88)	275(100)
Ar^2S^+	109(6)	143(6)	123(28)	143(7)	123(34)	123(26)
$\{M-Ar^2S\}^+$	261(100)	261(100)	261(100)	295(69)	295(90)	275(100)
$\{(M-Ar^1S)-HS\}^{+\cdot}$	228(8)	262(20)	242(4)	262(5)	242(4)	242(5)
$\{(M-Ar^2S)-HS\}^{+\cdot}$	228(8)	228(5)	228(9)	262(5)	262(3)	242(5)
$\{(M-ArS)-Ar^1H\}^+$	183(8)	183(14)	183(23)	183(7)	183(21)	183(10)
$\{M-Ar^1SH\}^{+\cdot}$	260(3)	294(9)	274(13)	294(12)	274(12)	274(28)
$\{M-Ar^2SH\}^{+\cdot}$	260(3)	260(22)	260(22)	294(12)	294(8)	274(28)

TABLE 8.2 - 2

Metastable transitions in the mass spectra of cis-1,2-bis(arylthio)acenaphthenes (110).

	m^*	Transition	Neutral lost
110a	199.2	261 → 228	HS·
	184.1	370 → 261	ArS·
	128.5	370 → 218	acenaphthylene
	88.5	261 → 152	ArS·
110b	168.6	404 → 261	Ar^2S·
	199.1	261 → 228	HS·
	128.3	261 → 183	Ar^1H
110c	196.9	384 → 275	Ar^1S·
	177.4	384 → 261	Ar^2S·
	213.0	275 → 242	HS·
	199.1	261 → 228	HS·
	140.2	384 → 232	acenaphthylene
	121.8	275 → 183	Ar^2S
	128.3	261 → 183	Ar^1H
	84.0	275 → 152	Ar^2S·
110d	198.2	438 → 295	ArS·
	113.5	295 → 183	HS·
	78.3	295 → 152	ArS·
110e	208.2	418 → 295	Ar^2S·
	180.9	418 → 275	Ar^1S·
	169.3	418 → 266	acenaphthylene
	213.0	275 → 242	HS·
	121.8	275 → 183	Ar^2S·
110f	190.0	398 → 275	ArS·
	121.8	275 → 183	ArH

TABLE 8.2 - 3

Product ions identified by B/E linked scanning of selected ions in the mass spectra of 110a, 110c and 110e.

Derivative	Precursor scanned m/z	Assignment	Neutral lost	Product ion m/z
110a	370	$M^{+\cdot}$	ArS·	261
			ArSH	260
			$C_{12}H_8$	218
			ArSSAr	152
	261	$\{M-ArS\}^+$	HS·	228
			ArH	183
			ArS·	152
110c	384	$M^{+\cdot}$	Ar^1S·	275
			Ar^2S·	261
			$C_{12}H_8$	232
	275	$\{M-Ar^1S\}^+$	HS·	242
			Ar^2H	183
			Ar^2S·	152
	261	$\{M-Ar^2S\}^+$	HS·	228
			Ar^1H	183
			Ar^1S·	152
110e	418	$M^{+\cdot}$	Ar^2S·	295
			Ar^1S·	275
			$C_{12}H_8$	266
			Ar^1SSAr^2	152
	295	$\{M-Ar^2S\}^+$	HS·	262
			Ar^1H	183
			Ar^1S·	152
	275	$\{M-Ar^1S\}^+$	HS·	242
			Ar^2H	183
			Ar^2S·	152

The base peak corresponded to $M-Ar^1S^+$ or $\{M-Ar^2S\}^+$ in four of the six cases, with the remaining two cases, viz 110d and 110e, having base peaks corresponding to m/z 152. The $\{M-Ar^1S\}^+$ and $\{M-Ar^2S\}^+$ ions underwent the loss of the remaining aryl group, with concomitant hydrogen migration to the departing group, to give m/z 183. These ions also eliminated HS· and gave rise to m/z 152 via the loss of an arylthio radical. The loss of Ar^1SH and Ar^2SH from the molecular ion was detected in every case. The formation of a bisaryldisulphide ion and the formation of m/z 152 via the elimination of a bisaryldisulphide from the molecular ion were present in all cases. These were the only ions formed by skeletal rearrangement of the molecular ion.

8.3 Discussion

The stepwise loss of two arylthio radicals from the molecular ions of 1,2-bis(arylthio)acenaphthenes parallels the photolytic and thermolytic decomposition of 1,2-bis(phenylthio)ethane 113a, and 2,3-bis(phenylthio)butanes 113b and 113c which eliminate two phenylthio groups to produce alkenes[101].

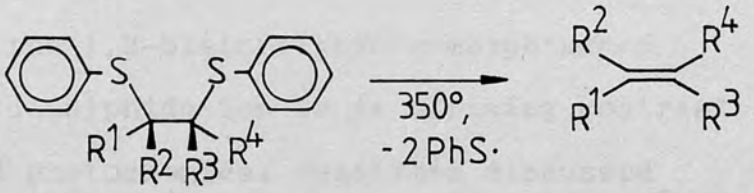

113a: $R^1=R^2=R^3=R^4=H$

113b: $R^2=R^3=H, R^1=R^4=CH_3$

113c: $R^2=R^4=H, R^1=R^3=CH_3$

Scheme 8.3 - 1

The elimination of two arylthio groups from 110 can be regarded as occurring via a similar process to form the m/z 152 ion, corresponding to the molecular ion of acenaphthylene.

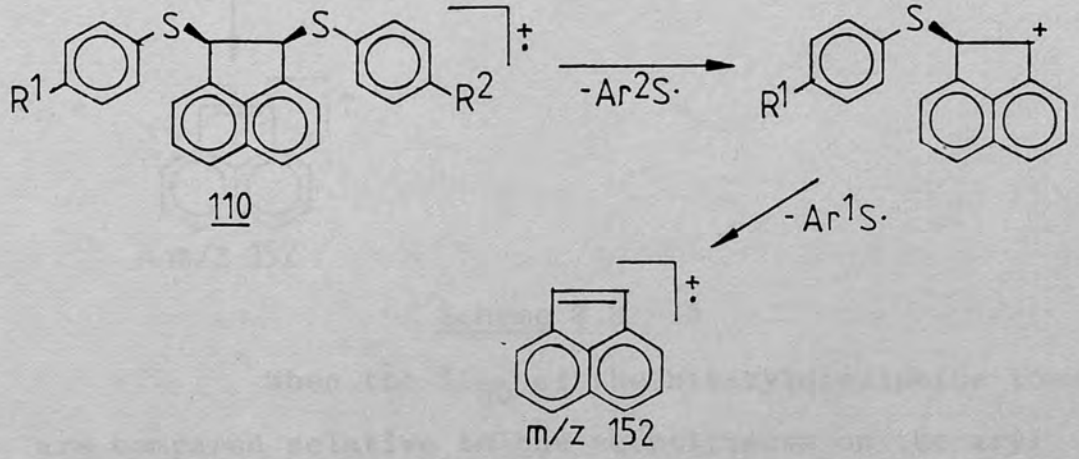

Scheme 8.3 - 2

The mass spectrum of acenaphthylene is dominated by the molecular ion (m/z 152), which corresponds to the base

peak, and contains very few fragment ions[92], indicating a high stability for the acenaphthylene radical cation. The appearance of a base peak corresponding to m/z 152 in two cases and its high abundance in the remainder is consistent with the m/z 152 ion being equivalent to the acenaphthylene molecular ion.

The elimination of acenaphthylene from the molecular ions of the 1,2-bis(arylthio)acenaphthenes to yield a bisaryldisulphide ion is in striking contrast to the thermal and photochemical reactions discussed above. Thus, the m/z 152 ion can also be formed directly by the elimination of a neutral bis(arylthio)-disulphide, as in Scheme 8.3 - 3.

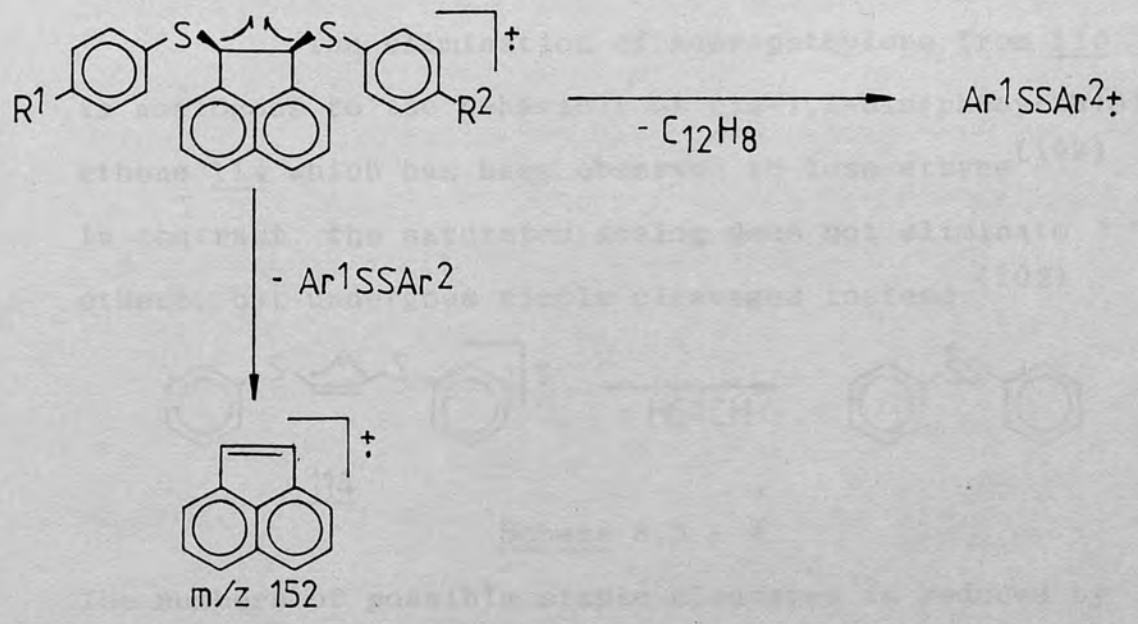

Scheme 8.3 - 3

When the $\%\Sigma_{50}$ of the bisaryldisulphide ions are compared relative to the substituents on the aryl groups, the following patterns emerge:

(R^1,R^2)	(H,Me)	>	(H,H)	>	(H,Cl)
$\%\Sigma_{50}$	3.5		2.8		0.94
(R^1,R^2)	(Cl,Me)	>	(H,Cl)	>	(Cl,Cl)
$\%\Sigma_{50}$	1.7		0.9		0.4
(R^1,R^2)	(H,Me)	>	(Me,Me)	>	(Cl,Me)
$\%\Sigma_{50}$	3.5		2.9		1.7

These trends, which, it must be emphasised, should be interpreted in only a general qualitative way, seem to reflect the stabilisation of the charge on the bisaryldisulphide ion by electron donating methyl groups and/or destabilisation by the electron withdrawing chlorines. From this viewpoint, the $\%\Sigma_{50}$ of the bisaryldisulphide ion bearing R^1=R^2= methyl would seem to be anomalously low.

The elimination of acenaphthylene from 110 is analogous to the behaviour of cis-1,2-bis(phenylthio) ethene 114 which has been observed to lose ethyne[102]. In contrast, the saturated analog does not eliminate ethene, but undergoes simple cleavages instead.[102]

114

Scheme 8.3 - 4

The numbers of possible simple cleavages is reduced by the presence of the double bond in 114, whereas the acenaphthylene skeleton performs the same function in the 1,2-bis(arylthio)acenaphthenes, increasing the probability of skeletal rearrangement.

The molecular ions of 110 also eliminated Ar^1SH and Ar^2SH, which may result from the migration of

the hydrogen on the β carbon to the sulphur of the departing arylthio group.

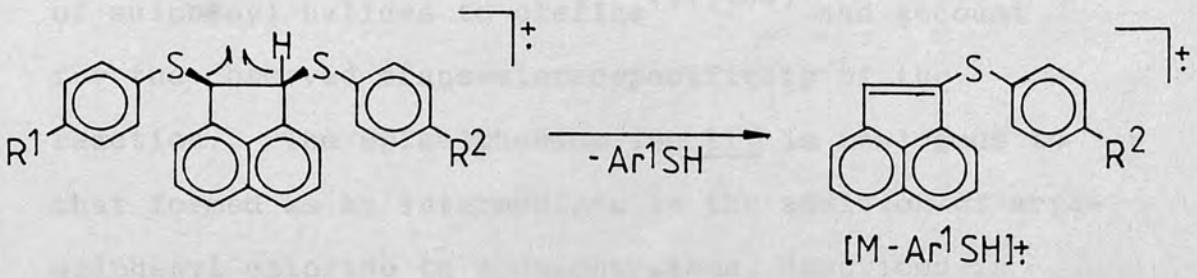

Scheme 8.3 -5

The $\{M-Ar^1S\}^+$ and $\{M-Ar^2S\}^+$ ions decompose further via loss of HS· and this loss is supported by metastable peaks in most cases as well as linked scanning data. This loss can arise via a thio-Claisen rearrangement mechanism similar to that proposed for the loss of HS· from the $\{M-ArS\}^+$ ion in the mass spectra of the 1,8-bis(arylthiomethyl)naphthalenes (see Scheme 7.3 - 8).

The loss of Ar^1H and Ar^2H from $\{M-Ar^2S\}^+$ and $\{M-Ar^1S\}^+$, respectively, suggests that these ions might exist as cyclic sulphonium ions.

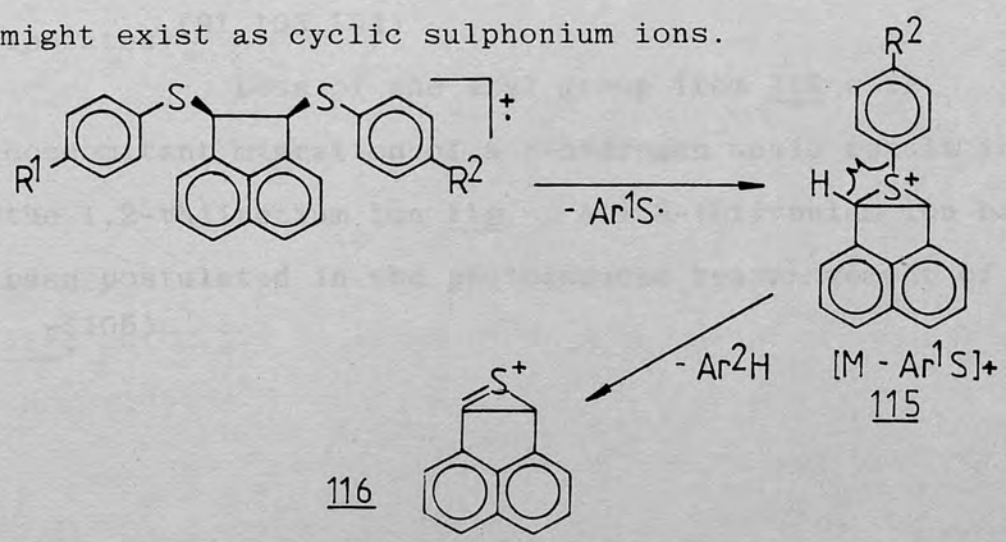

Scheme 8.3 - 6

Episulphonium (thiiranium) ions have been clearly established as reaction intermediates in the addition of sulphenyl halides to olefins[91,103] and account for the observed trans-stereospecificity of the reaction. The episulphonium ion 115 is analogous to that formed as an intermediate in the addition of aryl-sulphenyl chloride to acenaphthylene, described in Section 8.1:

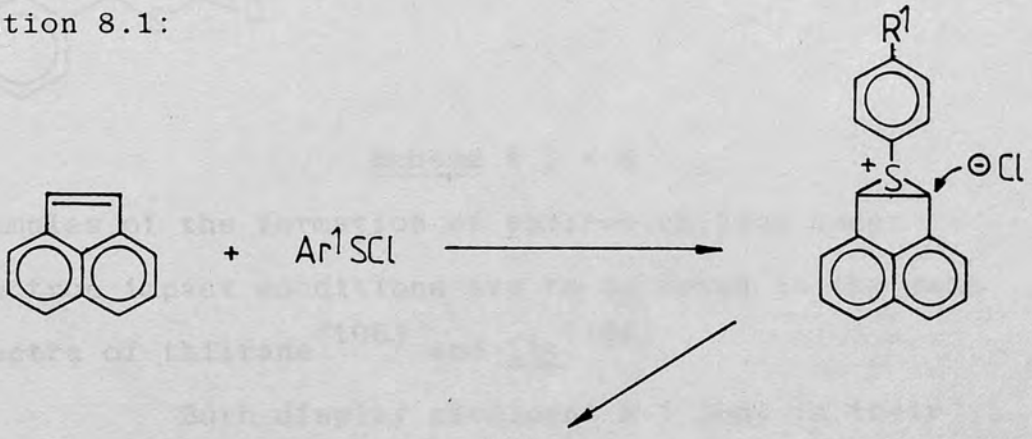

109

Scheme 8.3 - 7

Many stable episulphonium salts are known and have been isolated.[91,103,104]

Loss of the aryl group from 112 with concomitant migration of a β-hydrogen would result in the 1,2-thiirenium ion 116. A 1,2-thiirenium ion has been postulated in the photoinduced rearrangement of 117.[105]

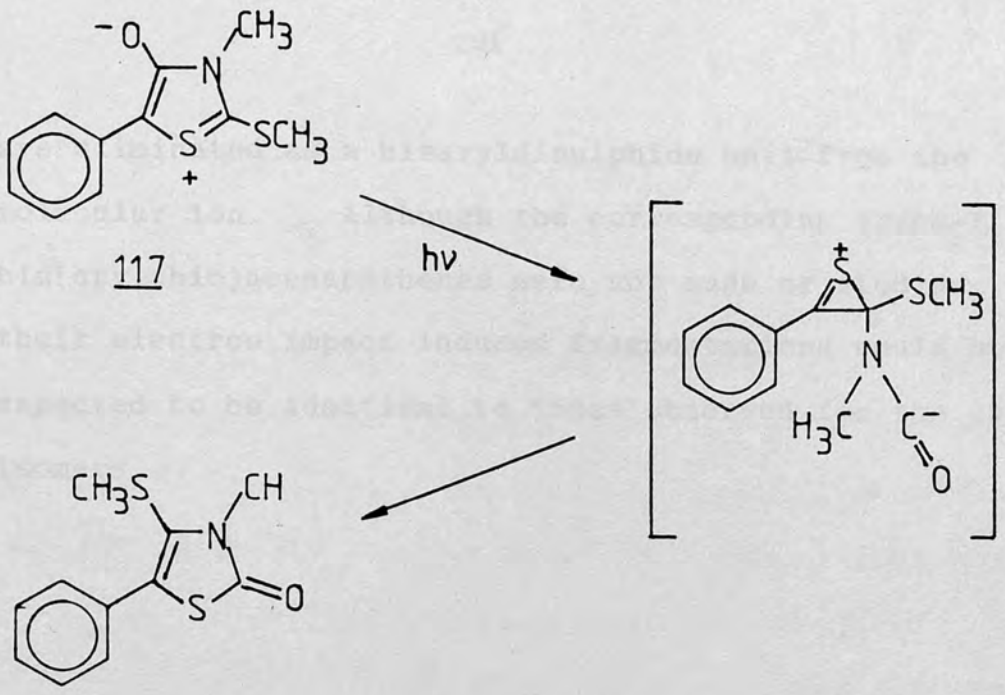

Scheme 8.3 - 8

Examples of the formation of thiirenium ions under electron impact conditions are to be found in the mass spectra of thiirane[106] and 118.[106]

Both display prominent M-1 ions in their mass spectra. In the case of 118, the base peak corresponds to the M-1 ion, indicating the stability of the conjugated ion 119.

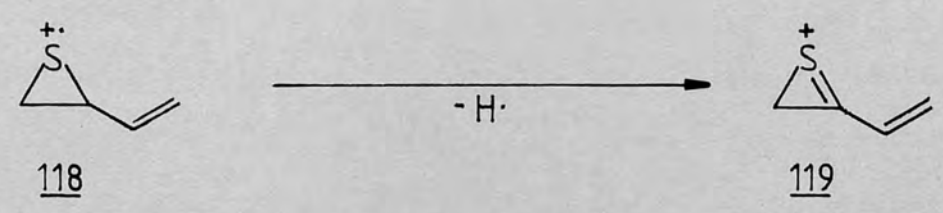

Scheme 2.7.3 - 9

Similarly, 116 should also be stabilised by charge delocalisation.

The loss of sulphur, HS· or hydrogen sulphide from the molecular ion was not observed in any of the cases studied. The absence of such eliminations is in agreement with the behaviour of other systems (discussed previously) having two arylthio groups which

are eliminated as a bisaryldisulphide unit from the molecular ion. Although the corresponding trans-1,2-bis(arylthio)acenaphthenes were not made or studied, their electron impact induced fragmentations would be expected to be identical to those observed for the cis isomers.

9. FACTORS IN THE ELIMINATION OF BISARYLDISULPHIDE MOIETIES FROM BIS(ARYLTHIOETHERS)

9.1 Derivatives of N,N-bis(alkyl)anilines.

In the earlier study of the electron impact induced fragmentation of N,N-bis(4'-arylthio-2'-butynyl) anilines[45] the elimination of a bisaryldisulphide moiety from the molecular ions of these compounds was observed and the complimentary bisaryldisulphide ions were also formed. Although these compounds may undergo rearrangement via {1,3} arylthio migrations, the elimination of a bisaryldisulphide molecule from the original molecular ion was supported by the behaviour of N,N-bis(4'-arylsulphonyl -2'-butynyl) anilines,[45] which underwent a concerted elimination of the two arylsulphonyl groups in the absence of possible {1,3} arylsulphonyl migrations. Further support for the elimination of the bisaryldisulphide moiety from the unrearranged molecular ion of the N,N-bis(4'-arylthio-2'-butynyl) anilines was obtained by a study of N-(4'-arylsulphonyl-2'-butynyl)-N-(4''-arylthio-2''-butynyl)anilines, in the current work. These derivatives eliminated an $Ar^1SO_2SAr^2$ moiety from their molecular ions. This elimination is less likely to occur after the arylthio group has undergone an {1,3} migration.

The N,N-bis(4'-arylthio-2'-butynyl)anilines can also eliminate a bisaryldisulphide moiety after both arylthio groups have migrated and such a rearrangement pathway had been proposed earlier.[45]

To substantiate this pathway, study

was undertaken of two systems, analogous to the intermediates formed by one and two {1,3} arylthio shifts in the N,N-bis(4'-arylthio-2'-butynyl)anilines, respectively. N-(4'-Arylthio-2'-butynyl)-N-(2''-arylthio-2''-propenyl)-p-toluidines were found to readily eliminate a bisaryldisulphide moiety, thus supporting the formation of an analogous ion (via a single {1,3} arylthio shift) in the rearrangement of the bis-butynyl system. A bisaryldisulphide unit was also eliminated from N,N-bis(2'-arylthio-2'-propenyl)-p-toluidines and substantiates the rearrangement of the N,N-bis(4'-arylthio-2'-butynyl)anilines to an analogous ion prior to the loss of Ar^1SSAr^2. Bisaryldisulphide ions were also present in generally higher abundances in the mass spectra of the N-(4'arylthio-2'-butynyl)-N-(2''arylthio-2''-propenyl)-p-toluidines and in ever higher abundances with the N,N-bis(2'-arylthio-2'-propenyl)-p-toluidines, as compared with the spectra of the bis-butynylanilines.

These observations are fully consistent with the proposed elimination of a bisaryldisulphide moiety from the N,N-(4'-arylthio-2'-butynyl)anilines via the {1,3} migration of both arylthio groups. The behaviour of the compounds studied in this work is also consistent with earlier studies in that the elimination of sulphur was not observed to compete successfully with the loss of a bisaryldisulphide molecule. Neither the N-(4'-arylthio-2'-butynyl)-N-(2''-arylthio-2''-propenyl)-p-toluidines or the N,N-bis(2'-arylthio-2'-propenyl)-p-toluidines eliminated sulphur. Thus, formation of the sulphur-sulphur bond

appears to preclude the extrusion of sulphur from the systems discussed above.

9.2 1,2-Bis(arylthio)acenaphthenes.

The electron impact mass spectra of the title compounds inter alia display peaks corresponding to the skeletal rearrangement ions $\{M-Ar^1SSAr^2\}^{+\cdot}$ and $Ar^1SSAr^{2+\cdot}$. A qualitative relationship between substituents on the aryl groups and relative abundance of the bisaryldisulphide ions was observed in which electron donating groups on Ar^1 and Ar^2 appear to enhance the formation of $Ar^1SSAr^{2+\cdot}$. The elimination of sulphur was again found to be non-competitive with the elimination of Ar^1SSAr^2.

10. EXPERIMENTAL

10.1 Materials, instrumentation and analysis.

All reagents, with a few exceptions, were obtained commercially. Bisaryldisulphides, prepared from the corresponding thiols by the method of Yiannios and Karabinos[107], were reacted with sulphuryl chloride to give the corresponding arenesulphenyl chlorides.[108] The addition of bromine or chlorine to acenaphthylene, to give the corresponding 1,2-dihalo acenaphthenes, was performed according to known procedures.[97] Acenaphthylene, supplied by Aldrich, was purified by dissolution in petroleum spirit and treatment with decolourising charcoal.

Melting points were obtained on a Thomas-Hoover Capillary Melting Point Apparatus and are uncorrected. Mass spectra were obtained with a VG Micromass 12F single-focussing mass spectrometer at 70eV electron energy (unless stated otherwise) and an ion-source temperature of ca.200^{o}. Representative mass spectra are presented in the Appendix. Linked-scanning B/E spectra and accurate mass measurements of selected samples were provided by Mr D Carter (School of Pharmacy, University of London) using a VG ZAB double-focusing mass spectrometer. N.m.r. spectra were recorded using either a Varian EM 360, Varian A60, or a Hitachi Perkin Elmer R24B spectrometer. Chemical shifts are reported in p.p.m. from TMS (TMS = 0.0δ, $CDCl_3$ solution, unless stated otherwise).

Elemental analyses were provided by Galbraith Laboratories Inc., U.S.A., Butterworth

Laboratories Ltd., U.K., and in this department by Mrs E Whitaker.

10.2 3-Arylthiopropynes (31)

A solution of the desired arenethiol (0.042 moles) and an equimolar amount of KOH (2.36g) in methanol(50 cm^3) was added dropwise with stirring to a solution of propargyl bromide (5g, 0.042 moles) in methanol (50 cm^3) under N_2 at ambient temperature. After stirring overnight, the precipitated KBr was filtered off and the solvent removed in vacuo. The crude product was dissolved in chloroform (100 cm^3) and washed with 0.2N KOH (3 x 100 cm^3) and water (1 x 100 cm^3), dried ($MgSO_4$) and solvent removed in vacuo to give a pale yellow liquid which was distilled at reduced pressure to yield the pure product in ca.50% yield. Physical and spectral data were as follows:

3-Phenylthiopropyne - b.p.54° (0.2mm), lit.[68] 104-110°(10mm); n.m.r. δ = 2.3 (t,1H), 3.65 (d,2H), 7.2-7.8 (m,5H) ppm,

3-p-tolylthiopropyne - b.p.64°(0.2mm), lit.[68] 124°(15mm); n.m.r. δ =2.3 (t,1H), 3.65 (d,2H) 7.42 (q,4H) ppm,

3-(4-chlorophenyl)thiopropyne - b.p. 76°(0.18mm). lit.[69] 58° (0.1mm); n.m.r. δ =2.3 (t,1H), 3.65 (d,2H), 7.5 (s,4H) ppm,

3-(2,3,5,6-tetrafluorophenyl)thiopropyne - b.p. 44°(0.02mm), n.m.r. δ =2.28 (t,1H), 3.75 (d,2H), 7.0-7.55 (m,1H)ppm.

The tetrafluorophenyl derivative had not been previously reported.

10.3 3-Arylsulphonylpropynes(32)

Oxidation of the 3-arylthiopropynes with 86% hydrogen peroxide in a mixture of glacial acetic acid and ether gave the corresponding sulphones in high yields.[34] In a typical reaction, 0.0213 moles of the arylthiopropyne was dissolved in 1:1 glacial acetic acid and ether (100 cm^3).

A tenfold excess of hydrogen peroxide was added to the mixture and the reaction mixture refluxed for 3 hours. The mixture was then poured into ice-water (500 cm^3) with stirring and the precipitated white solid was collected and washed with water. The product was then dried in a vacuum dessicator containing an open beaker of KOH pellets. The products obtained in this manner were pure and able to be used without further purification. Yields and melting points are presented below. The tetrafluorophenyl derivative had not been described previously.

3-Phenylsulphonylpropyne - 99% ; m.p. 92-93°, lit.[70] 93°,

3-p-Tolylsulphonylpropyne - 90% ; m.p.101-103°, lit.[71] 99-100°,

3-(4-Chlorophenyl)sulphonylpropyne - 85% ; m.p. 114-115°, lit.[34] 116-117°,

3-(2,3,5,6-tetrafluorophenyl)sulphonylpropyne- 65%; m.p. 69-71; n.m.r. δ= 2.57 (t,1H),4.39 (d,2H), 7.38-7.97 (m,1H) ppm.

10.4 3-Arylsulphonyl-2-arylthiopropenes (30)

The method of Stirling[67] was followed for the synthesis of the title compounds. He had only described the unsubstituted derivative. A general procedure is described below.

The sulphone (0.5g) and an equimolar amount of the required arenethiol were dissolved in methanol (10 cm^3) and stirred for 105 minutes at ambient temperature in the presence of triethylamine (0.025 cm^3). Removal of the solvent in vacuo gave the products as solids in yields of 94-100% (with the exception of '30j', which was chromatographed on 30g of silica gel (50% ether/pet.ether) to give 0.1g of clear colourless oil which crystallised upon dissolution in ether/pet. ether and cooling. Analytical samples were prepared by recrystallisation from ether/pet.ether (Rf ≃0.45, 50% ether/petroleum ether, silica gel). The unsubstituted compound was identical to that described by Stirling (m.p. 61-62°, lit.[67] 60-61°). Physical and analytical data are presented in Table 10.4-1. These compounds were characteristed by n.m.r., m.s. and elemental analysis.

TABLE 10.4 - 1 3-Arylsulphonyl-2-arylthiopropenes (30)[a]: physical and anlytical data.

Derivative	M.P. (°C)	Yield (%)	Elemental Analysis (%) $C_{calc.}$	$H_{calc.}$	C_{Found}	H_{Found}	N.M.R (δ /ppm)
30a	61-62	94	(b)	(b)	(b)	(b)	3.99(s,2H), 5.32(s,1H), 5.55(s,1H) 7.49(s,5H), 7.70-8.30(m,5H)
30b	64-66	95	55.46	4.03	55.37	4.06	3.99(s,2H), 5.32(s,1H), 5.55(s,1H) 7.45(q,4H). 7.70-8.30 (m,5H)
30c	81-83	95	63.12	5.30	63.06	5.34	2.35(s,3H), 3.99(s,2H), 5.20(s,1H), 5.48(s,1H), 7.33(s,4H), 7.70-8.30(s,5H)
30d	49-50	100	55.46	4.03	55.35	4.04	3.99(s,2H), 5.32(s,1H), 5.55(s,1H), 7.49(s,5H), 7.90(q,4H)
30e	103-104	100	50.14	3.37	50.07	3.50	4.02(s,2H), 5.35(s,1H), 5.60(s,1H) 7.52(q,4H), 7.90(q,4H)
30f	94-96	99	56.71	4.46	56.44	4.47	2.37(s,3H), 3.99(s,2H), 5.25(s,1H), 5.48(s,1H), 7.33(s,4H), 7.90(q,4H)
30g	84-86	96	63.13	5.30	63.04	5.15	2.52(s,3H), 3.99(s,2H), 5.30(s,1H), 5.54(s,1H), 7.50(s,5H), 7.76(q,4H)
30h	85-86	95	56.71	4.46	56.68	4.48	2.52(s,3H), 3.98(s,2H), 5.30(s,1H), 5.54(s,1H), 7.45(s,4H), 7.76(s,4H)
30i	76-77	100	64.12	5.70	63.66	5.40	2.38(s,3H), 2.52(s,3H), 3.95(s,2H), 5.19(s,1H), 5.42(s,1H), 7.31(s,4H), 7.75(q,4H)
30j	118-120	13	48.97	3.08	49.03	3.09	3.89(s,3H), 4.25(s,2H), 5.25(s,1H), 5.61(s,1H), 6.9-7.85(m,5H).

(a) See Page 71.

(b) Described by Stirling, ref.67.

10.5 4-Arylthio-1-chloro-2-butynes (41)

An earlier, published procedure[45] was followed in the preparation of the title compounds. A methanolic solution of 0.22 moles KOH in 150 cm^3 was added dropwise to a solution of an equimolar amount of the required arenethiol in methanol (150 cm^3) over a period of 30 minutes, with stirring under an atmosphere of N_2, at room temperature. The potassium arenethiolate solution was then added dropwise, with stirring to a solution of 1,4-dichloro-2-butyne in methanol (600 cm^3) over a 3 hour period under N_2, also at room temperature. After stirring overnight, the reaction mixture was filtered and the methanol removed *in vacuo*. The crude product was then dissolved in chloroform (300 cm^3) and washed with 0.2N KOH (2 x 150 cm^3) and water (1 x 150 cm^3). Removal of solvent and distillation at high vacuum gave the pure products in ca. 40% yield; spectral and physical data are given below:

4-Phenylthio-1-chloro-2-butyne - b.p. 117°(0.07mm);
n.m.r. δ = 3.5 (t,2H), 4.02 (t,2H), 7.3 (m,5H) ppm,

4-(4-Chlorophenyl)thio-1-chloro-2-butyne - b.p. 135°(0.15mm);
n.m.r. δ = 3.58 (t,2H), 4.02 (t,2H), 7.2 (s,4H) ppm,

4-p-Tolylthio-1-chloro-2-butyne - b.p. 125° (0.05 mm);
n.m.r. δ = 2.3 (s,3H), 3.57 (t,2H), 4.05 (t,2H), 7.2(q.4H) ppm,

4-(4-Bromophenyl)thio-1-chloro-2-butyne - b.p. 130°(0.1 mm);
n.m.r. δ = 3.6 (t,2H), 4.1 (t,2H) 7.25 (q,4H) ppm.

These products were identical to those reported in the literature[34,45].

10.6 4-Arylsulphonyl-1-chloro-2-butynes (42)

Oxidation of the 4-arylthio-1-chloro-2-butnes with hydrogen peroxide was performed according to a published procedure.(45) A mixture of ether (100 cm^3) and glacial acetic acid (100 cm^3) was used to dissolve 0.036 moles of the sulphide. A tenfold excess of 30% hydrogen peroxide was refluxed for 3 hours and then poured into ice-water (500 cm^3) with stirring. After allowing the ice to melt, the mixture was then dried in a vacuum desiccator containing an open beaker of KOH pellets. The sulphones were prepared in ca.80% yields in this manner and needed no further purification. The physical and spectral data are as follows:-

4-Phenylsulphonyl-1-chloro-2-butyne - m.p. 88-90°, lit.(34) 91-92°; n.m.r. δ=4.16 (m,4H), 7.7-8.33 (m,5H) ppm,

4-p-Tolylsulphonyl-1-chloro-2-buryne - m.p. 80-82°, lit.(34) 79-81°; n.m.r. δ=2.45 (s,3H), 4.1 (m,4H), 7.59 (q,4H) ppm,

4-(4-Chlorophenyl)sulphonyl-1-chloro-2-butyne - m.p. 105-106°, lit.(34) 105-106°; n.m.r. δ=4.1 (m,4H), 7.73 (q,4H) ppm,

4-(4-Bromophenyl)sulphonyl-1-chloro-2-butyne - m.p. 112-114°, lit.(45) 112-114°; n.m.r. δ=4.1 (m,4H), 7.9 (q,4H) ppm.

10.7 1-Arylsulphonyl-4-arylthio-2-butynes (40)

The following general procedure was used:

To a solution of 0.0165 moles of the appropriate 4-arylsulphonyl-1-chloro-2-butynes in THF (50 cm^3) was added an equimolar amount of the required arenethiol. The resulting mixture was then stirred with a slurry of calcium carbonate (0.0165 moles) in water (100 cm^3) under N_2 at room temperature overnight. The organic layer was separated and solvent removed in vacuo. The residue was then taken up in CH_2Cl_2 (100 cm^3) and washed with 0.2N KOH (2 x 100 cm^3) and water (100 cm^3). Drying over magnesium sulphate and removal of solvents in vacuo gave the desired compounds in moderate yields. Analytical samples were obtained by recrystallisation from CH_2Cl_2 petroleum ether (Rf = 0.45, toluene, silica gel).

The synthesis of the unsubstituted derivative differed from the general procedure given above and was prepared as follows:

A solution of 4-phenylsulphonyl-1-chloro-2-butyne (1g, 0.00439 moles) in acetonitrile (20 cm^3) and an equimolar amount of the anhydrous sodium salt of thiophenol (prepared by the reaction of thiophenol with metallic sodium in refluxing toluene) was refluxed for 1 day. The solvent was removed in vacuo and the residue taken up in CH_2Cl_2 (100 cm^3) and washed with 0.1N Na_2CO_3(2 x 100cm^3), water (1 x 100 cm^3) and dried ($MgSO_4$). Removal of the solvent in vacuo gave a brown oil which was chromatographed on 50g of silica gel (30% ether/petroleum ether) to give a 0.5g of the desired compound.

Spectral, physical and analytical data for the derivatives studied are collected in Table 10.7-1.

TABLE 10.7 - 1 1-Arylsulphonyl-4-arylthio-3-butynes (40)[a] : spectral, physical and analytical data

Derivative	M^+	M.P. (°C)	Yield (%)	Elemental Analysis (%) $C_{Calc.}$	$H_{Calc.}$	C_{Found}	H_{Found}	N.M.R (δ/ppm)
40 a	302	-	38	63.54	4.67	-	-	3.64 (t,2H), 4.0 (t,2H), 7.40-8.20 (m,10H)
40 b	336	91-92	74	57.04	3.90	57.14	3.98	3,49 (t,2H), 3.90 (t,2H), 7.20-7.9 (m,9H)
40 c	370	85-86	58	51.76	3.26	51.51	3.15	3.60 (t,2H), 3.96 (t,2H), 6.95-7.95 (m,8H)
40 d	370	125-126	64	51.75	3.23	51.84	3.26	3.54 (t,2H), 3.94 (t,2H), 7.33 (s,4H), 7.68 (q,4H)
40 e	350	129-130	70	58.19	4.32	58.22	4.62	2.33 (s,3H), 3.54 (t,2H), 3.95 (t,2H), 7.20 (q,4H), 7.65, (q,4H)
40 f	350	124-125	69	58.19	4.32	58.37	4.26	2.40 (s,3H), 3.55 (t,2H), 3.92 (t,2H), 7.28 (s,4H), 7.53 (q,4H)
40 g	394	132-133	68	51.77	3.81	51.72	3.72	2.45 (s,3H), 3.55 (t,2H), 3.90 (t,2H), 7.29 (q,4H), 7.52 (q,4H)
40 h	408	88-90	80	52.81	4.19	52.23	4.10	2.32 (s,3H), 2.39 (s,3H), 3.50 (t,2H), 3.95 (t,2H), 6.83-7.43 (m,3H),7.45 (q,4H)

(a) See page 96.

10.8 N-(4'-Arylthio-2'-butynyl)anilines (54)

The synthesis of some N-(4'-arylthio-2'-butynyl)anilines has been reported previously.[64] and a similar procedure was employed in this work. A solution of 4-arylthio-1-chloro-2-butyne (0.0476 moles) and the desired aryl amine (0.119 moles) in refluxing THF (200 cm^3) was stirred with a slurry of magnesium carbonate (0.0476 moles) in water (100 cm^3) for three days under an atmosphere of nitrogen. The organic layer was separated and the solvent removed *in vacuo* to give a brownish oil. The crude product was taken up in chloroform (10 cm^3) and washed with 1.ON HCL (2 x 100 cm^3), 0.2N KOH (1 x 100 cm^3) and water (1 x 100 cm^3). Drying the solution over sodium sulphate and removal of the solvent under vacuum gave abrown oil which solidified upon standing in some cases. The crude product was dissolved in refluxing petroleum spirit (b.p. 60-80^{o}), filtered and cooled to give the pure products (Rf ≃ 0.56, 50% ether pet.ether, silica gel) as pale yellow crystals in moderate yields (35-70%). Recrystallisation from petroleum spirit gave the analytical samples. The N-(4'-phenylthio-2'-butynyl)aniline and N-(4'-p-tolylthio-2'-butynyl)aniline were liquids and were purified by chromatography on silica gel, using toluene as the eluting solvent.

N-(4'-p-tolylthio-2'-butynyl)-p-toluidine - m.p. 49-50°, lit.[64] 49°; n.m.r. δ=2.3 (s,3H),2.38 (s,3H),3.92(t,2H), 3.2-3.7 (m,3H), 6.86 (q,4H), 7.38 (q,4H) ppm,

N-(4'-phenylthio-2'-butynyl)-p-toluidine - m.p. 43-45°; n.m.r. δ=2.3 (s,3H), 3.43 (m,3H), 3.93 (t,2H), 6.9 (q,4H), 7.5 (m,5H) ppm,

N-(4'-phenylthio-2'-butynyl)aniline - n.m.r. δ= 3.64 (m,3H), 3.94 (t,2H), 6.7-7.8 (m,10H) ppm,

N-(4'-p-tolylthio-2'-butynyl)aniline - n.m.r. δ= 2.34 (s,3H), 3.58 (t,2H), 3.9 (m,3H), 6.68-7.58 (m,9H) ppm,

N-(4'-(4-chlorophenyl)thio-2'-butynyl)-p-touidine - m.p. 61-62°, lit.[64] 61°; n.m.r.δ=2.26 (s,3H), 3.4 (br. s,1H) 3.57 (t,2H), 3.85 (t,2H), 6.78 (q,4H), 7.21 (q,4H) ppm,

N-(4'-(4-chlorophenyl)thio-2'-butynyl)-p-anisidine- m.p. 52-53°; n.m.r. δ=3.68 (m,3H), 3.9 (m,5H), 6.75 (q,4H), 7.3 (s,4H) ppm.

10.9 <u>N-(4'-Arylsulphonyl-2'-butynyl)-N-(4''-arylthio-2''-butynyl)anilines</u> (<u>53</u>)

The title compounds were synthesised by the following general procedure:

In THF (20 cm^3) were dissolved equimolar amounts of N-(4'-arylthio-2'-butynyl)aniline (1g) and 4-arylsulphonyl-1-chloro-2-butyne. This solution was then added to a round-bottomed flask containing a slurry of water (20 cm^3) and an equimolar amount of magnesium carbonate. The mixture was then stirred at reflux, under an atmosphere nitrogen, for 7.5 hours. The organic layer was separated, dried over sodium sulphate and the solvent removed <u>in vacuo</u>. The product mixture was then

triturated with hot petroleum spirit, if a solid, or chromatographed on silica gel with toluene to give the desired product (Rf ≃ 0.39).

Analytical samples were obtained by recrystallisation from CH_2Cl_2/petroleum spirit. Physical and analytical data are presented in Table 10.9 - 1.

TABLE 10.9 -1 Spectral, physical and analytical data for N-(4'-arylsulphonyl-2'-butynyl)-N-(4''-arylthio-2''-butynyl)anilines (53)[a]

Derivative	M^+	Yield (%)	M.P. (°C)	Elemental Analysis (%) $C_{Calc.}$	$H_{Calc.}$	C_{Found}	H_{Found}	N.M.R (δ/ ppm.)
53a	479	42	92-93	65.05	4.62	65.08	4.73	3.67 (t,2H) 4.08 (m,6H), 6.90-8.08 (m, 14H)
53b	493	85	95-96	65.64	4.90	65.70	4.86	2.43 (s,3H), 3.67(t,2H), 4.1 (m,6H), 6.90-8.04(m,13H)
53c	493	48	99-100	65.64	4.90	65.61	4.99	2.33 (s,3H), 3.67 (t,2H), 4.1(m,6H), 6.78-8.0 (m,13H)
53d	507	39	118-119	66.19	5.16	66.03	5.19	2.33 (s,6H), 3.56 (t,2H), 3.99 (m,6H), 6.75-8.0 (m,12H)
53e	527	27	126-128	61.36	4.37	61.65	4.59	2.34 (s,3H), 3.56 (t,2H), 3.93 (m,6H), 6.65-7.85 (m,12H)
53f	493	40	101-103	65.64	4.90	65.80	4.97	2.36 (s,3H), 3.60 (t,3H), 3.98 (m,6H), 6.68-7.84 (m,13H)
53g	543	41	111-112	59.55	4.26	59.45	4.37	3.55 (t,2H), 3.75 (s,3H), 3.89 (m,6H), 6.75 (s,4H), 7.20-7.80 (m,8H)
53h	509	37	75-76	63.58	4.74	63.68	4.88	3.60 (t,2H), 3.81 (s,3H), 3.95 (m,6H), 6.82 (s,4H), 7.30-7.95 (m,9H)

[a] See page 114.

10.10 2-Arylthio-3-hydroxypropenes (71)

To a solution of 0.1 moles of the appropriate arenethiol in toluene (50 cm^3) was added 0.01 moles of Na (cut into small pieces). The mixture was refluxed under nitrogen, with stirring until all of the sodium had reacted. Propargylalcohol (5g, 0.1 moles) was then added in one portion and the reaction mixture refluxed for 3 hours under an atmosphere of nitrogen, with stirring. After washing the reaction mixture with 0.2N KOH (4 x 100 cm^3), water (1 x 100 cm^3) and drying over magnesium sulphate, the solvent was removed *in vacuo* to give a mixture of the allylic and vinylic alcohols as a brownish liquid. Chromatography on silica gel (50% ether/petroleum ether) yielded the pure allylic alcohol as the fastest running product (Rf $\simeq$ 0.38). Only the unsubstituted derivative had been reported previously[85]; yields and spectral data are given below:

2-Phenylthio-3-hydroxypropene - 30%; n.m.r. δ=3.2 (br.s,1H), 4.23 (s,2H), 5.21 (s,1H), 5.69 (m,1H), 7.15-7.8 (m,5H) ppm,

2-p-Chlorophenylthio-3-hydroxypropene - 28%; n.m.r. δ=2.25 (br. t,1H), 4.25 (d,2H), 5.41 (s,1H), 5.74 (s,1H), 7.55 (s,4H) ppm,

2-p-Tolylthio-3-hydroxypropene - 27%; n.m.r. δ= 2.37 (s,3H), 2.97 (br. t,1H), 4.22 (d,2H), 5.25 (s,1H), 5.56 (s,1H) ppm.

10.11 Reaction of 2-phenylthio-3-hydroxypropene with thionyl chloride.

To 2-phenylthio-3-hydroxypropene (1g, 0.006 moles) in ether (5 cm^3) was added thionyl chloride (o.5 cm^3, 0.007 moles) at -70^o. After 1 hour, the reaction mixture was washed copiously with water, neutralised with solid K_2CO_3 and dried over sodium sulphate. Removal of solvent in vacuo gave 0.85g of a dark brown oil whose n.m.r. spectrum was complex and contained no peaks corresponding to vinylic protons.

10.12 2-Arylthio-3-trifluoroacetylpropenes (72)

The allylic alcohols described in Section 10.10 were converted to the corresponding trifluoroacetates in moderate yields as follows:

The allylic alcohol (5g) was dissolved in THF (25 cm^3) and added dropwise to 1.5 equivalents of trifluoroacetic acid in THF (25 cm^3) at 0^o over a period of 30 minutes with stirring. After an additional 30 minutes, the solution was neutralised with solid sodium bicarbonate at 0^o, filtered, concentrated in vacuo and triturated with petroleum spirit (100 cm^3). Any remaining sodium trifluoroacetate was filtered off and the solvent removed in vacuo to give a clear, colourless liquid which was distilled at high vacuum to give the pure product (Rf $\simeq$ 0.73, 50% ether/pet.ether, silica gel):

2-phenylthio-3-trifluoroacetylpropene - 64%; b.p. 65^o (0.05 mm): n.m.r. δ=4.95 (s,2H), 5.55 (s,1H), 5.22(s,1H), 7.4-7.8 (m,5H) ppm,

2-(4-chlorophenyl)thio-3-trifluoroacetylpropene - 54%; b.p. 79° (0.09 mm); n.m.r. δ=4.94 (s,2H), 5.54 (s,1H), 5.69 (s,1H), 7.58 (s,4H) ppm,

2-(p-tolyl)thio-3-trifluoroacetylpropene - 75%; b.p. 67° (0.1 mm); n.m.r. δ=2.41 (s,3H), 4.94 (s,2H), 5.48 (s,1H), 5.65 (s,1H), 7.46 (q,4H) ppm.

10.13 2-Arylthio-3-iodopropenes (73)

In acetone (20 cm^3), 0.00187 moles of the 2-arylthio-3-trifluoroacetylpropene and NaI (0.02 moles) were dissolved. The mixture was refluxed for 2 hours, after which no starting material was detected by t.l.c. (silica gel, petroleum ether), and only one product was observed (Rf ≃0.40). The reaction mixture was diluted with ether (100 cm^3) and washed with 0.1N sodium thiosulphate (1 x 50 cm^3), dried over calcium chloride and the solvent removed in vacuo at ambient temperature to give a pale yellow liquid. The allyl iodides were unstable in neat form and decomposed to a black oil if left at room temperature. They were stable in solution, however, and were dissolved immediately in ethanol for use in the preparation of N,N-bis-(2'-arylthio-2'-propenyl) anilines and N-(4'-arylthio-2'-butynyl)-N-(2''-arylthio-2''-propenyl)anilines. These compounds have not been described before and were characterised by their n.m.r. spectra (given below):

2-Phenylthio-3-iodopropene - n.m.r. δ=4.08 (s,2H), 5.28 (s,1H), 5.74 (s,1H), 7.35-7.75 (m,5H) ppm,

2-(4-Chlorophenyl)thio-3-iodopropene - n.m.r. δ=4.08 (s,2H), 5.28 (s,1H), 5.74 (s,1H), 7.4 (s,4H) ppm, 2-p-Tolylthio-3-iodopropene - n.m.r. δ= 2.22(s,3H), 4.03 (s,2H), 5.65 (s,1H), 7.33 (q,4H) ppm.

10.14 N-(4'-Arylthio-2'-butynyl)-N-(2''-arylthio-2''-propenyl)anilines (70).

To 0.00187 moles of the appropriate 2-arylthio-3-iodopropene in ethanol (25 cm^3) was added 1 equivalent of tris-(hydroxymethyl)methylamine (TRIS) and an equimolar amount of N-(4'-arylthio-2'-butynyl)toluidine. After refluxing under nitrogen for 3 hours, the reaction mixture was concentrated in vacuo and diluted with chloroform (100 cm^3). The mixture was then washed with water (1 x 100 cm^3), dried over magnesium sulphate and the solvents removed in vacuo. The crude products were chromatographed on silica gel using 25% ether/cyclohexane as the eluting solvent to yield the pure product as a clear, colourless liquid (Rf $\simeq$ 0.54, 25% ether/petroleum ether, silica gel). The derivatives obtained in this manner were characterised by their n.m.r. and mass spectra. These compounds were stored in a freezer, due to their tendency to darken at room temperature. Yields and spectral data are given in Table 10.14 -1. None of these derivatives had been previously described.

TABLE 10.14 - 1 N-(4'-Arylthio-2'-butynyl)-N-(2''-arylthio-2''-propenyl)-p-toluidines(70)[a] :

Derivative	M^{+}	Yield(%)	N.M.R (δ/ppm)
70a	415	26	2.32 (s,3H), 3.62 (t,2H), 4.00 (m,4H), 5.20 (s,1H), 5.50 (s,1H), 7.00 (q,4H), 7.30-7.80 (m,10H).
70b	449	24	2.32 (s,3H), 3.68 (t,2H), 4.00 (m,4H), 5.23(s,1H), 5.55 (s,1H), 7.00 (q,4H), 7.34-7.75 (m, 9H)
70c	429	31	2.32 (s,3H), 2.38 (s,3H), 3.61 (t,2H), 4.00 (m,4H), 5.08 (s,1HO),5.40 (s,1HO),7.00 (q,4H), 7.30-7.75(m,9H)
70d	449	24	2.32 (s,3H), 3.64(t,2H), 4.00(m,4HO),5.18(s,1H), 5.49 (s,1H), 7.00 (q,4H), 7.30-7.80 (m,9H)
70e	483	55	2.32 (s,1H), 3.60 (t,2H), 4.00 (m,4H), 5.24(s,1H), 5.55 (s,1H), 7.00 (q,4H), 7.30-7.70 (m,8H)
70f	463	46	2.32 (s,3H), 2.38 (s,3H), 3.53 (t,2H), 4.00 (m,4H), 5.10 (s,1H), 5.40 (s,1HO), 7.00 (q,4H), 7.3-7.70 (m,8H)
70g	429	25	2.32 (s,3H), 3.60 (t,2H), 4.00 (m,4H), 5.24(s,1H), 5.53 (s,1H), 7.00 (q,4H), 7.30-7.80 (m,9H)
70h	463	46	2.32 (s,3H), 3.58 (t,2H), 4.00 (m,4H), 5.20(s,1H) 5.50 (s,1H), 7.00 (q,4H), 7.30-7.70 (m,8H)
70i	443	36	2.32 (s,3H), 2.38 (s,3H), 3.59 (t,2H), 4.00 (m,4H), 5.11 (s,1H), 5.49 (s,1H), 7.00 (q,4H), 7.30-7.75(m,8H)

[a] See Page 139.

10.15 N-(2'-Arylthio-2'-propenyl)-p-toluidines (83)

Using the procedure described in Section 10.13, the freshly prepared arylthio-3-iodopropene (0.00187 moles) was dissolved in ethanol (25 cm^3), with an equimolar amount of p-toluidine and 0.002 moles of TRIS. The mixture was refluxed for 2.5 hours under nitrogen and concentrated *in vacuo*. The mixture was extracted with CH_2Cl_2 (100 cm^3) and washed with 0.1N HCl (1 x 100cm^3) and o.1N Na_2CO_3 (1 x 100 cm^3) dried ($MgSO_4$) and the solvents removed *in vacuo* to give a ca. 60% yield of a pale yellow liquid which displayed a single component in its t.l.c. (Rf ≃ 0.43, 5% ether/petroleum ether, silica gel). The n.m.r. spectra of these previously unknown compounds were entirely consistent with that of the expected product:

N-(2'-Phenylthio-2'-propenyl)-p-toluidine - δ = 2.27 (s,3H), 3.85 (s,2H), 3.75 (br. s,1H), 5.21 (s,1H), 5.55 (s,1H), 6.85 (q,4H), 7.43 (m,5H) ppm,

N-(2'-(4-Chlorophenyl)thio-2'-propenyl-p-toluidine - δ = 2.27 (s,3H), 3.85 (s,2H), 3.75 (br. s,1H), 5.19 (s,1H), 5.50 (s,1H), 6.82 (q,4H), 7.38 (s,4H) ppm,

N-(2'-p-tolylthio-2'-propenyl)-p-toluidine - δ = 2.27 (s,3H), 2.40 (s,3H), 3.75 (br. s,1H), 3.90 (s,2H) 5.21 (s,1H), 5.55 (s,1H) 6.90 (q,4H), 7.48 (q,4H) ppm.

10.16 N,N-Bis(2'arylthio-2'-propenyl)-p-toluidines (82)

The N-(2'-arylthio-2'-propenyl)-p-toluidines prepared by the reaction described above were reacted immediately with a second equivalent of 2-arylthio-3-iodopropene according to the following general procedure. The products thus obtained were characterised by their n.m.r. and mass spectra.

The freshly prepared N-(2'-arylthio-2'-propenyl)-p-toluidine (ca. 0.3g) was dissolved in ethanol (20 cm^3) with 2-arylthio-3-iodopropene (0.00187 moles, ca. 40% excess) and 0.00187 moles of TRIS. After refluxing overnight, the ethanol was removed *in vacuo* and the reaction mixture extracted with chloroform (100 cm^3) and washed with 0.1N HCl (1 x 100 cm^3), and 0.1N Na_2CO_3 (1 x 100 cm^3). After drying ($MgSO_4$) and removal of solvent *in vacuo*, a yellow liquid was obtained. The crude product was chromatographed on silica gel (Rf ≃ 0.55, 5% ether/petroleum ether) to give the pure product as a clear colourless liquid which darkened unless it was kept refrigerated. The yields and spectral data of these previously unknown compounds are presented in Table 10.16 - 1.

TABLE 10.16 - 1 N,N-Bis(2'-arylthio-2'-propenyl)-p-toluidines(82)[a] :

Yields and spectral data

Derivative	M^{+}	Yield (%)	N.M.R. (δ/ppm)
82a	403	13	2.30 (s,3H), 4.09 (s,4H), 5.25 (s,2H), 5.37 (s,2H), 6.90 (q,4H), 7.30 - 7.75 (m,10H),
82b	437	12	2.30 (s,3H), 4.08 (s,4H), 5.30 (s,2H), 5.40 (s,2H), 6.9 (q,4H), 7.25 - 7.65 (m,9H)
82c	403	13	2.28 (s,3H), 2.40 (s,3H), 4.08 (s,4H), 5.18-5.40 (m,4H), 6.9 (q,4H), 7.35-7.75 (m,9H)
82d	471	11	2.30 (s,3H), 4.06 (s,4H), 5.28 (s,2H), 5.40 (s,4H), 6.9 (q,4H), 7.55 (s,8H)
82e	451	12	2.30 (s,3H), 2.42 (s,3H), 4.09 (s,4H), 5.18-5.48 (m,4H), 6.9 (q,4H), 7.28-7.70 (m,8H)
82f	431	12	2.25 (s,3H), 2.40 (s,6H), 4.00 (s,4H) 5.10 (s,2H), 5.30 (s,2H), 6.90 (q,4H), 7.38 (q,8H)

[a] See page 151.

10.17 1,8-Naphthalene dimethanol (87)

A procedure similar to that of Kamada[88] was followed for the reduction of 1,8-naphthalic anhydride with lithium aluminium hydride. A three-necked flask was fitted with a double-surface, water cooled condenser and charged with anhydrous ether (480 cm^3), anhydrous benzene (400 cm^3) and 20g (0.53 moles) of lithium aluminium hydride under a nitrogen blanket. To the stirred suspension at ambient temperature, the anhydride (50g, 0.25 moles) was added slowly as a fine powder so as to maintain a gentle relflux. The reaction mixture was refluxed for six days (mercury bubbler, under nitrogen). Excess reducing agent was then destroyed by the slow addition of water and the mixture acidified with 2N HCl (400 cm^3). The solid material was collected and washed with water and triturated with hot acetone (5 x 1000cm^3). The combined extracts were evaporated to dryness *in vacuo* to give 39.52g (85%) of the crude diol which was recrystallised from acetone to give the pure 1,8-naphthalene dimethanol, mp 156-157° (lit.[88] 157-158°).

10.18 1,8-Bis(Chloromethyl)naphthalene (88)

Following the method of Boekelheide and Vick[89] finely powdered 1,8-naphthalene dimethanol (10.45g, 0.056 moles) was added to concentrated HCl (153 cm^3) at 0° and the resulting slurry stirred at 0° for two hours and then for an additional three hours at ambient temperature. The mixture was filtered and the precipitate was washed with water until the

washings were neutral. After drying *in vacuo*, recrystallisation from petroleum ether yielded 7.2g (58%) of the dichloride, mp 90-91°(lit.[89] 87-90°).

10.19 *1,8-Bis(arylthiomethyl)naphthalenes* (*86*)

Table 10.19 -1 contains the yields and physical and analytical data for the six derivatives prepared. The synthetic procedure differed for the symmetrical and asymmetrical compounds in that the symmetrically substituted derivatives were prepared in one step, whereas two separate steps were required for the three asymmetrical cases. Procedures for the two types are given below.

10.19.1 Symmetrically substituted -

A mixture of 1:1 ether : methanol (40 cm^3) was used to dissolve 1,8-bis(chloromethyl)naphthalene (2g, 0.00893 moles) to which a solution of 0.0184 moles of the appropriate arenethiol and an equimolar amount of KOH in methanol (20 cm^3) was added dropwise under nitrogen at room temperature, with stirring, over 15 minutes. After stirring for an additional 0.5 hour at ambient temperature, the precipitated solution was washed with 0.2N KOH (1 x 100 cm^3), water (1 x 100 cm^3), dried ($MgSO_4$) and the solvent removed *in vacuo* to give a white solid. Recrystallisation from petroleum ether/chloroform yielded the analytical samples.

10.19.2 Asymmetrically substituted -

10.19.2.1 Reactions of 1,8-bis(chloromethyl) naphthalene with thiophenol and p-chloro-thiophenol.

The same procedure was used in both cases and the preparation of the unsubstituted derivative is given below as an example.

In methanol (20 cm^3), potassium-t-butoxide (0.25g, 0.00223 moles) and thiophenol (0.24g, 0.00223 moles) were dissolved and the solution was added to 1,8-bis(chloromethyl)naphthalene (0.5g, 0.00223 moles) in ether (20 cm^3) at -70^o, under nitrogen and with stirring over 15 minutes. The reaction mixture was allowed to warm to ambient temperature and stirred for 1 hour. The solvent was removed and the crude product was dissolved in chloroform (50 cm^3), washed with water (1 x 50 cm^3) and dried ($MgSO_4$). The solvent was removed <u>in vacuo</u> to give a white solid. The solid was dissolved in methanol (50 cm^3) and filtered. Removal of methanol on a rotavapour resulted in a white solid which, when triturated with chloroform, yielded a high melting solid. By repeating the process of removal of solvent and trituration, more product could be obtained. In this manner, 0.2g (30%) of the material was collected, (m.p. 207-209^o, dec.). This product was insoluble in cold chloroform. Its n.m.r. spectrum was obtained by employing trifluoroacetic acid as the solvent:

n.m.r. - δ = 5.40 (s,4H), 7.60-8.40 (m,11H) ppm.

The p-chlorothiophenyl derivative was obtained in 20% yield, m.p. 248-250°(dec.)

n.m.r. - δ = 5.40 (s,4H), 7.60-8.30 (m,10H) ppm.

The n.m.r. spectra of these two compounds indicate that the methylene protons are equivalent. This observation, together with their high melting points and their insolubility in chloroform are consistent with the sulphonium salts 89 rather than the 8-arlythiomethyl-1-chloromethyl naphthalenes.

10.19.2.2 Reaction of arenethiols with 89

Again using the unsubstituted case as an example, the sulphonium salt 89 (0.5g, 0.00223 moles) was dissolved in methanol (20 cm^3) to which an equimolar solution of the appropriate arenethiol and potassium t-butoxide (1 equivalent) in methanol (20 cm^3) was added at ambient temperature under nitrogen. After stirring for 1 hour, the solvent was removed *in vacuo* and the crude product dissolved in chloroform (25 cm^3) and washed with 0.2N KOH (1 x 25 cm) and water (1 x 25cm^3). Drying over magnesium sulphate and removal of solvent *in vacuo* gave the desired compounds in the yields indicated in Table 10.19 -1. Analytical samples were obtained by recrystallisation from $CHCl_3$/petroleum ether.

TABLE 10.19 - 1 1,8-Bis(arylthiomethyl)naphthalenes (86) [a]. Physical and analytical data.

Derivative	M^+	Yield (%)	M.P. (°C)	Elemental Analysis (%) $C_{Calc.}$	$H_{Calc.}$	C_{Found}	H_{Found}	N.M.R (δ / ppm)
86a	372	74	126-128	77.38	5.41	77.33	5.51	4.97(s,4H), 7.20-8.20 (m,16H)
86b	406	91	110-112	70.83	4.70	69.84	4.71	4.97 (s,4H) 7.20 - 8.20 (m,15H)
86c	386	85	126-128	77.67	5.74	77.49	5.86	2.34 (s,3H), 4.94(s,2H), 5.00 (s,2H), 7.10-8.10(m,15H)
86d	440	62	170-172	65.30	4.11	65.12	4.20	4.90 (s,4H), 7.20-8.20 (m,14H)
86e	420	53	133-135	71.32	5.03	71.25	5.12	2.33 (s,3H), 4.86(s,2H), 4.91 (s,2H), 7.20-8.10(m,14H)
86f	400	56	125-126	77.95	6.04	78.10	6.11	2.38 (s,6H), 4.97 (s,4H), 7.10-8.20 (m,14H).

[a] See page 169.

10.20 Reaction of thiophenol with 1,2-dihalo acenaphthenes.

To a solution of thiophenol (0.78g, 0.00706 moles)in methanol (40 cm^3) was added an equimolar amount of potassium t-butoxide. The resulting solution was then added over a period of 40 minutes to 1,2-dibromo-acenaphthene (1g) in ether (20 cm^3) with stirring, under a blanket of nitrogen. After stirring at room temperature for 2 hours, the solvent was removed *in vacuo* and the residue extracted with chloroform (50 cm^3), washed with 0.2N KOH (1 x 50 cm^3), water (1 x 50 cm^3) and dried ($MgSO_4$). Removal of the solvent *in vacuo* gave 1.15g of brown oil whose n.m.r. displayed a singlet at 7.2 ppm and a complex multiplet in the "aromatic" region (7.25-8.0 ppm).

In a similar reaction, in which 1,2-dichloro acenaphthene was substituted for the 1,2-dibromo acenaphthene in the procedure outlined above, the reaction mixture was refluxed for two hours. After working up the reaction mixture as above, a similar yield of brown oil was obtained. The n.m.r. spectrum of this material also contained a singlet at 7.2 ppm and a complex multiplet (7.25-8.0 ppm). Two weak singlets at 5.30 and 5.90 ppm indicated the presence of a small amount of monosubstituted product.

10.21 2-Arylthio-1-chloro acenaphthenes (109)

Arenesulphenyl chlorides were reacted with acenaphthylene in glacial acetic acid in a similar fashion to that of Kharasch.[98]

Acenaphthylene (8.02g, 0.0528 moles) was slowly added as a fine powder to the desired sulphenyl chloride (0.528 moles) in glacial acetic acid (150 cm^3), at ambient temperature, with stirring. Slight warming occurred and the red colour of the sulphenyl chloride disappeared immediately after completion of the addition. The reaction mixture was poured into 1,200 cm^3 of ice-water and the mixture stirred to facilitate solidification of the product. The product was collected and washed with copious amounts of water. Drying in vacuo gave a near quantitative yield of the desired product. The pure compounds were obtained by recrystallisation from petroleum ether (yields and spectral data as follows):

2-Phenylthio-1-chloro acenaphthene: 100%; m.p. 65-67°; δ= 5.44 (s,1H), 5.82 (s,1H), 7.3-8.0 (m,11H) ppm,

2-(4-Chlorophenyl)thio-1-chloro acenaphthene: 96% ; m.p. 137-139°; n.m.r. δ= 5.43 (s,1H), 5.82 (s,1H), 7.3-8.1 (m,10H) ppm,

2-p-tolylthio-1-chloro acenaphthene: 97% ; m.p. 113-115°; n.m.r. δ=2.26 (s,3H), 5.42 (s,1H), 5.82 (s,1H), 7.1-8.0 (m,10H) ppm.

The 4-chlorophenyl and p-tolyl derivatives had not been previously described. Butler et al[99] have reported the addition of benzenesulphenyl chloride to acenaphthylene but

there is an absence of experimental detail.

10.22 Attempted reaction of 2-(4-chlorophenyl)-thio-1-chloro acenaphthene with sodium iodide.

A solution of 2-(4-chlorophenyl)thio-1-chloro acenaphthene (1g, 0.00303 moles) and a tenfold excess of sodium iodide were dissolved in acetone (30 cm^3). The reaction mixture was stirred overnight at ambient temperature. The mixture was filtered and extracted with methylene chloride (100 cm^3). After washing the methylene chloride solution with 0.1N sodium thiosulphate (1 x 100 cm^3) and water (1 x 100 cm^3), the organic layer was dried over magnesium sulphate and the solvents removed in vacuo to give 0.45g of a yellow solid. The n.m.r. spectrum of this crude material indicated it to be a mixture of starting material and 1-(4-chlorophenyl)thio acenaphthylene, i.e. an elimination product.

10.23 cis-1,2-bis(arylthio)acenaphthenes (110).

A general procedure for the synthesis of the title compounds proceeded as follows.

Anhydrous sodium arenethiolate (0.011 moles, prepared by reacting sodium with excess arenethiol in refluxing toluene) was added as a fine powder to the appropriate 2-arylthio-1-chloro acenaphthene (0.01 moles) in acetonitrile (75 cm^3) at ambient temperature and stirred overnight. The reaction mixture was then poured into chloroform (100 cm^3), washed with water (1 x 100 cm^3),

0.1M sodium carbonate (2 x 100 cm^3)and again with water (1 x 100 cm^3). The organic layer was dried (Na_2SO_4) and solvent removed *in vacuo* to give an orange solid. The orange solid was triturated with petroleum ether (70 cm^3) to give the desired product as a light yellow solid. Analytical samples were obtained by recrystallisation from chloroform/petroleum ether (Rf ≃ 0.62, 10% ether/petroleum ether, silica gel). These compounds were previously unknown and were characterised by their n.m.r.† and mass spectra. Their compositions were confirmed by elemental analysis. Physical and analytical data pertaining to these compounds are presented in Table 10.23 - 1.

---

† The 90 MHz n.m.r. spectrum of 110a was obtained on a Joel FX90Q Fourier transform instrument by Mr D.Parkinson in this department.

TABLE 10.23 - 1 1,2-Bis(arylthio)acenaphthenes (110)[a] : Physical and Analytical Data

Derivative	M^+	Yield (%)	M.P. (°C)	Elemental Analysis (%) $C_{Calc.}$	$H_{Calc.}$	C_{Found}	H_{Found}	N.M.R. (δ / ppm)
110a	370	70	144-145	77.79	4.90	77.77	5.04	5.55 (s,2H), 7.30-7.90 (m,16H) [b]
110b	404	64	121-123	71.18	4.23	71.32	4.33	5.55 (s,2H), 7.20-7.90 (m,15H)
110c	384	75	102-104	78.08	5.24	78.04	5.37	2.4 (s,3H), 5.60(s,2H), 7.20-7.95 (m,15H)
110d	438	82	164-166	65.60	3.67	65.62	3.86	5.56 (s,2H) 7.30-8.00 (m,14H)
110e	418	99	132-133	71.66	4.57	71.60	4.70	2.40 (s,3H), 5.50 (s,2H) 7.18-7.95 (m,14H)
110f	398	63	110-111	78.35	5.56	78.07	5.68	2.40 (s,3H), 5.5 (s,2H) 7.18 - 7.90 (m,14H).

[a] See Page 187.

[b] 90 MHz: δ = 5.46 (s,2H), 7.11 - 7.69 (m,16H) ppm.

APPENDIX

Representative Mass Spectra

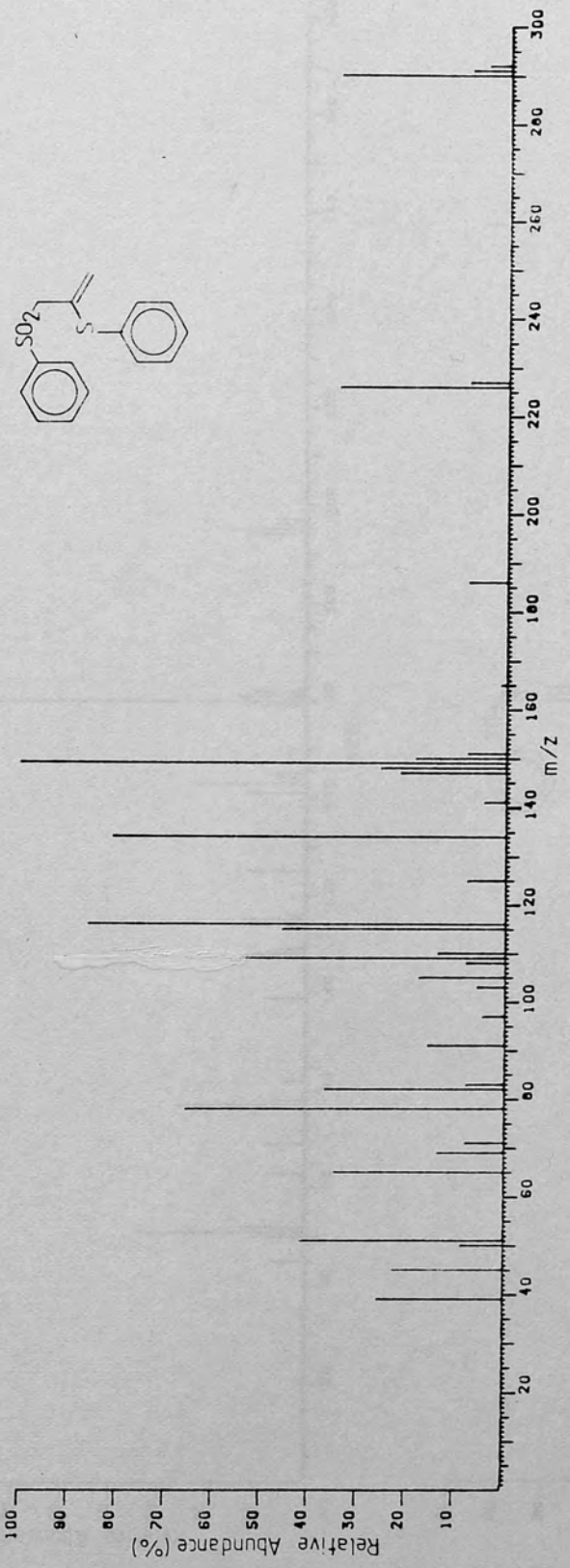
Relative Abundance (%)
m/z
SO2
S

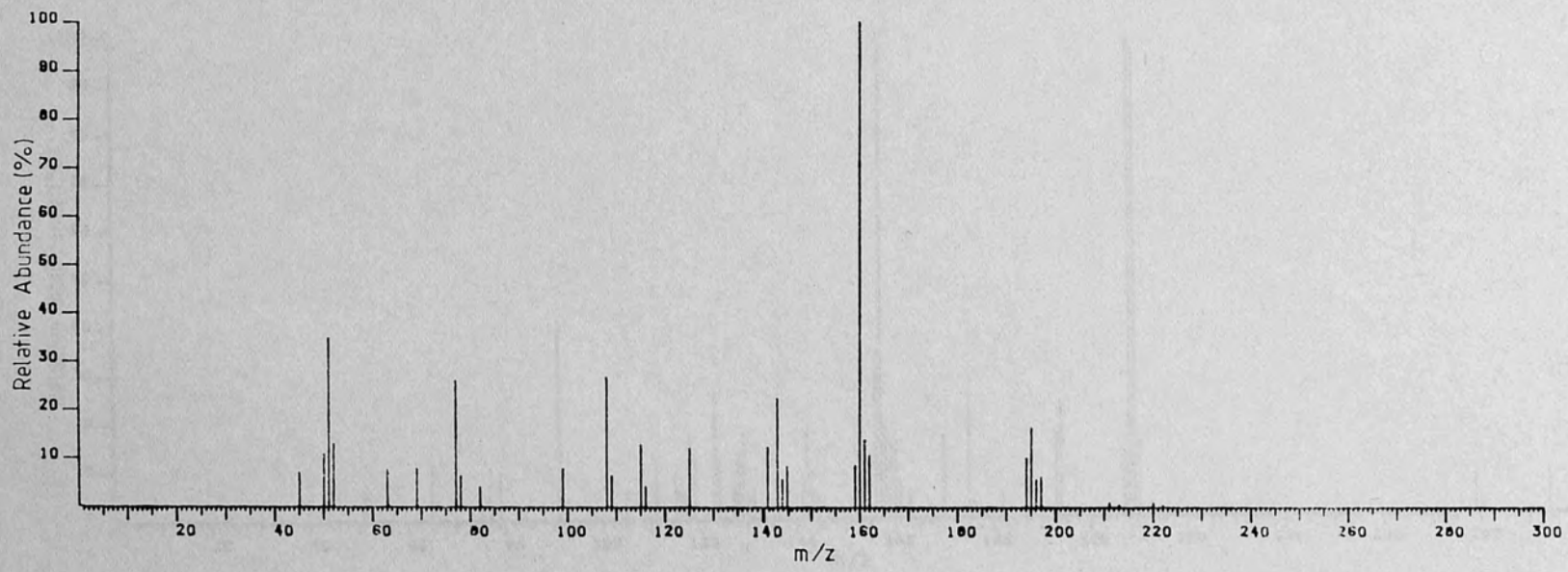
Relative Abundance (%)
100
90
80
70
60
50
40
30
20
10
20
40
60
80
100
120
140
160
180
200
220
240
260
280
300
m/z

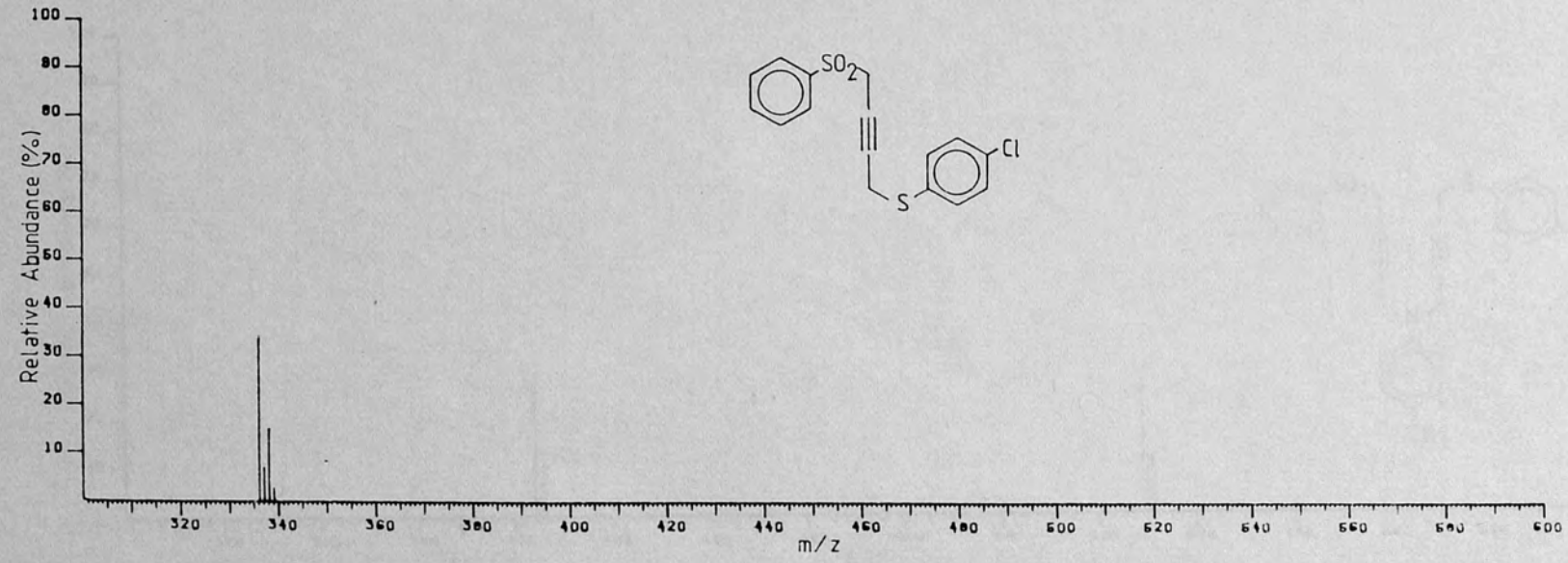
Relative Abundance (%)
100
90
80
70
60
50
40
30
20
10
320
340
360
380
400
420
440
460
480
500
520
540
560
580
600
m/z

SO2
Cl
S

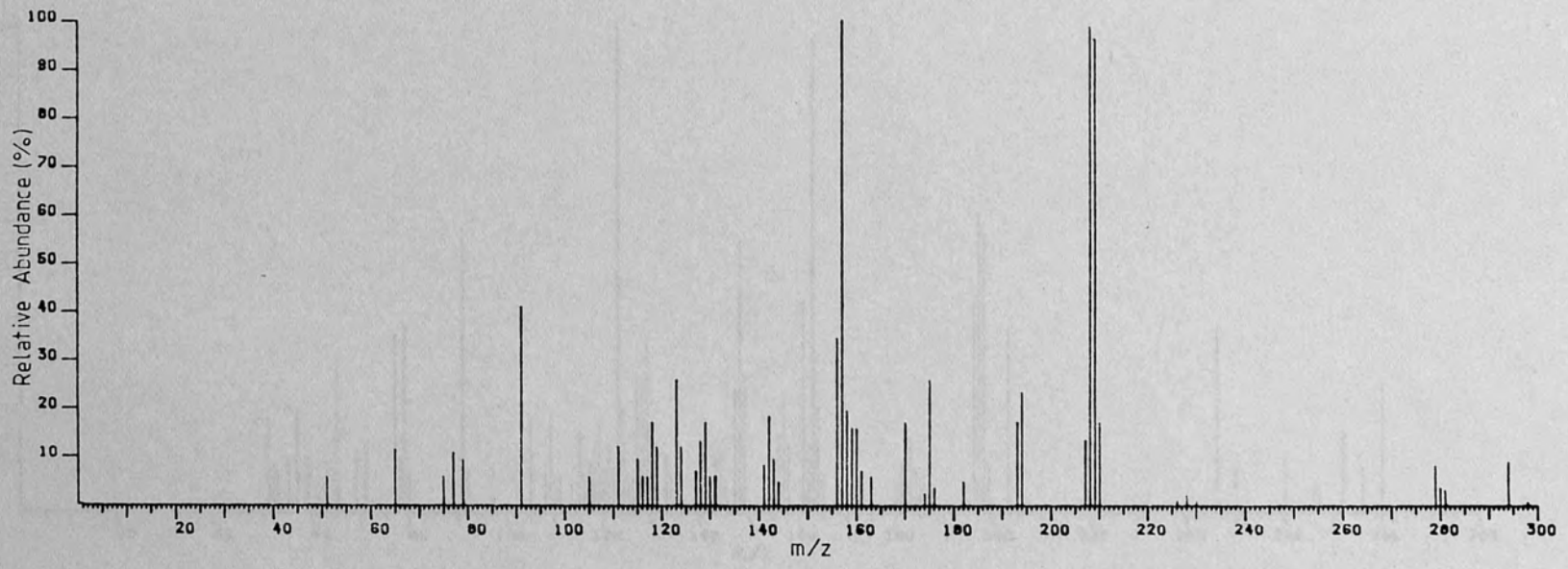
Relative Abundance (%)
100
90
80
70
60
50
40
30
20
10
20
40
60
80
100
120
140
160
180
200
220
240
260
280
300
m/z

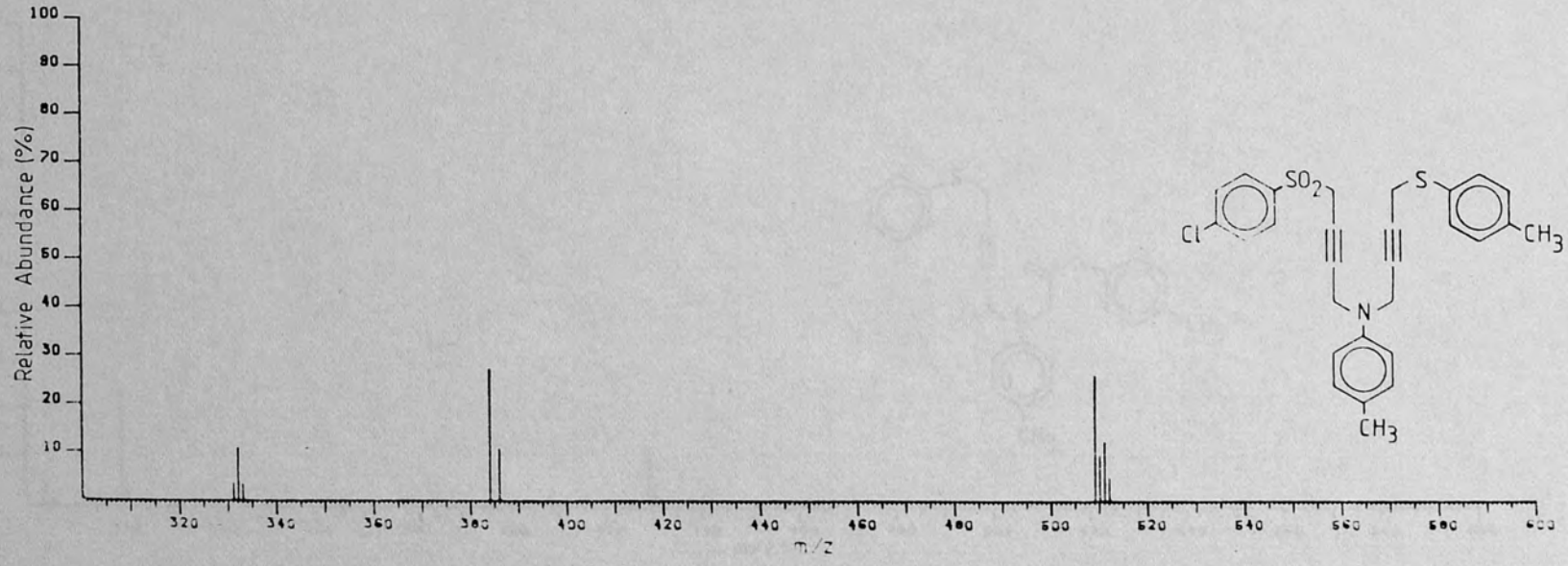
Relative Abundance (%)
100
90
80
70
60
50
40
30
20
10
320
340
360
380
400
420
440
460
480
500
520
540
560
580
600
m/z

Cl
SO2
S
CH3
N
CH3

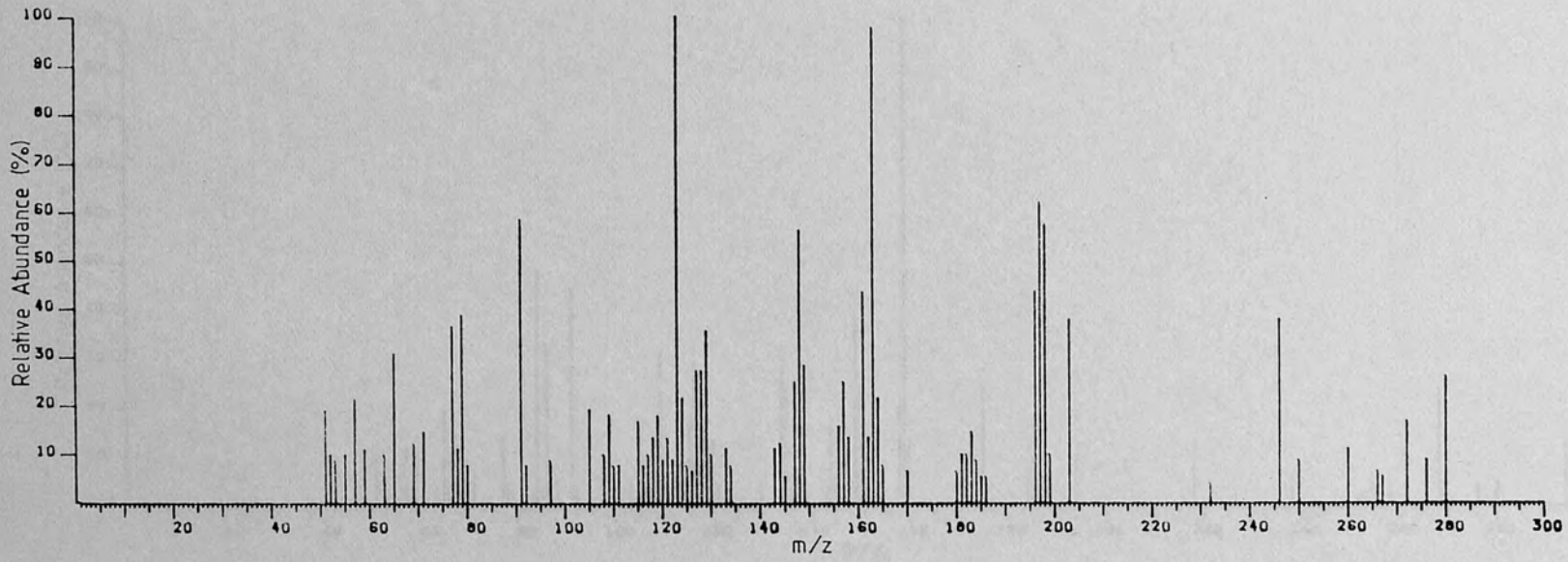
Relative Abundance (%)
100
90
80
70
60
50
40
30
20
10
20
40
60
80
100
120
140
160
180
200
220
240
260
280
300
m/z

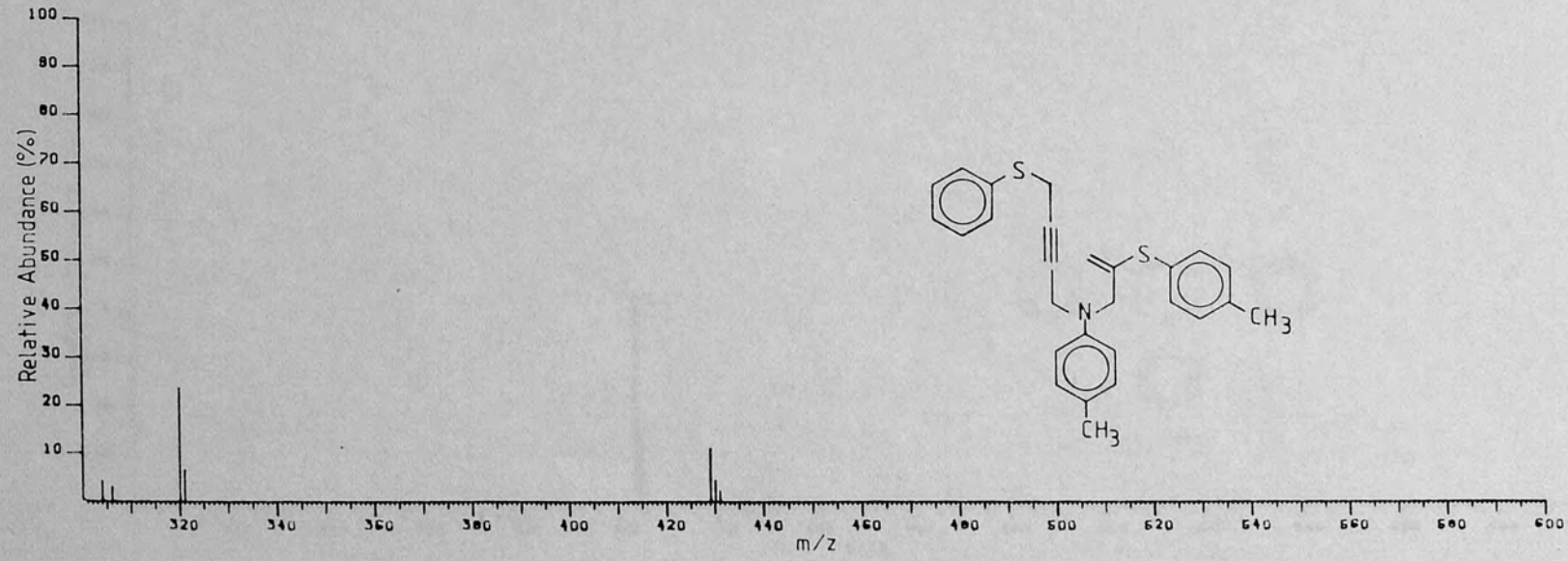
Relative Abundance (%)
100
90
80
70
60
50
40
30
20
10
320
340
360
380
400
420
440
460
480
500
520
540
560
580
600
m/z

S
S
N
CH3
CH3

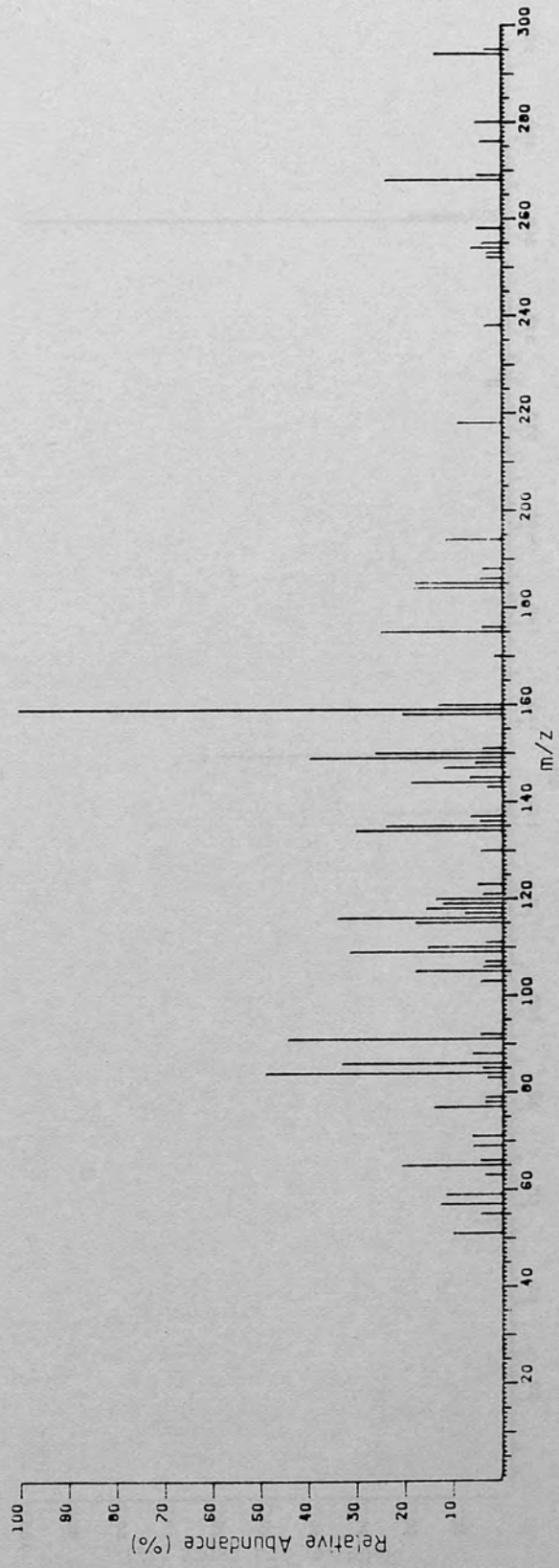
Relative Abundance (%)
m/z

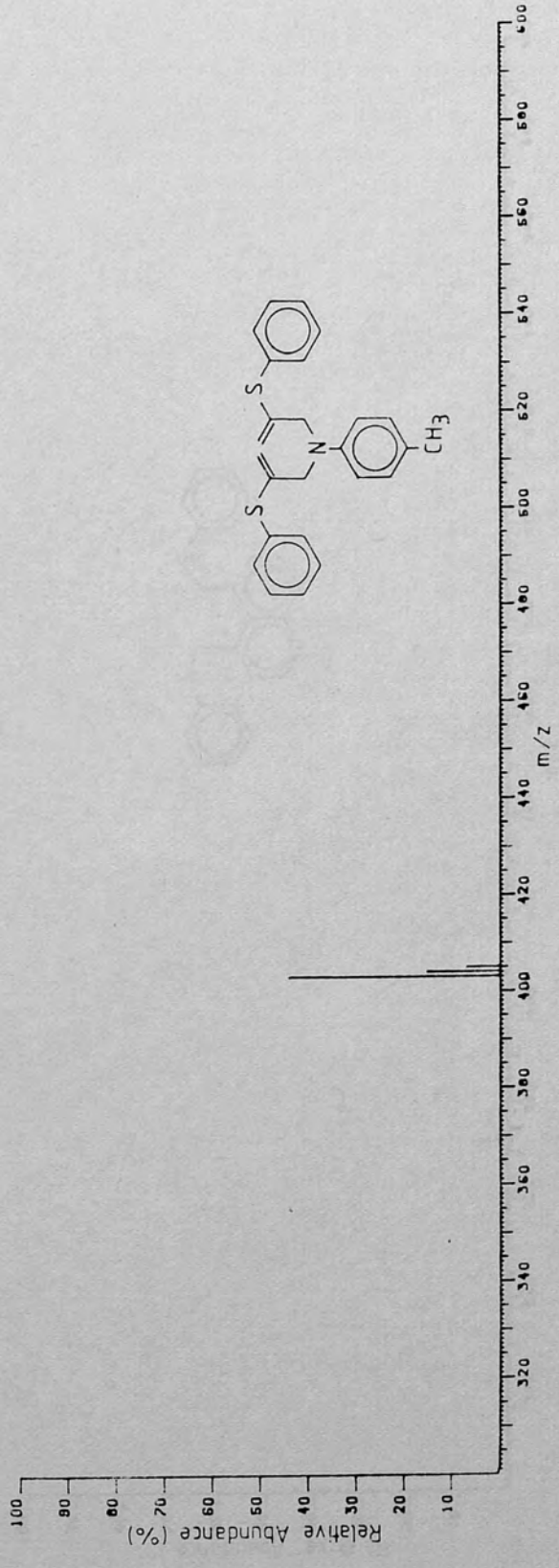
Relative Abundance (%)
m/z
S
S
N
CH3

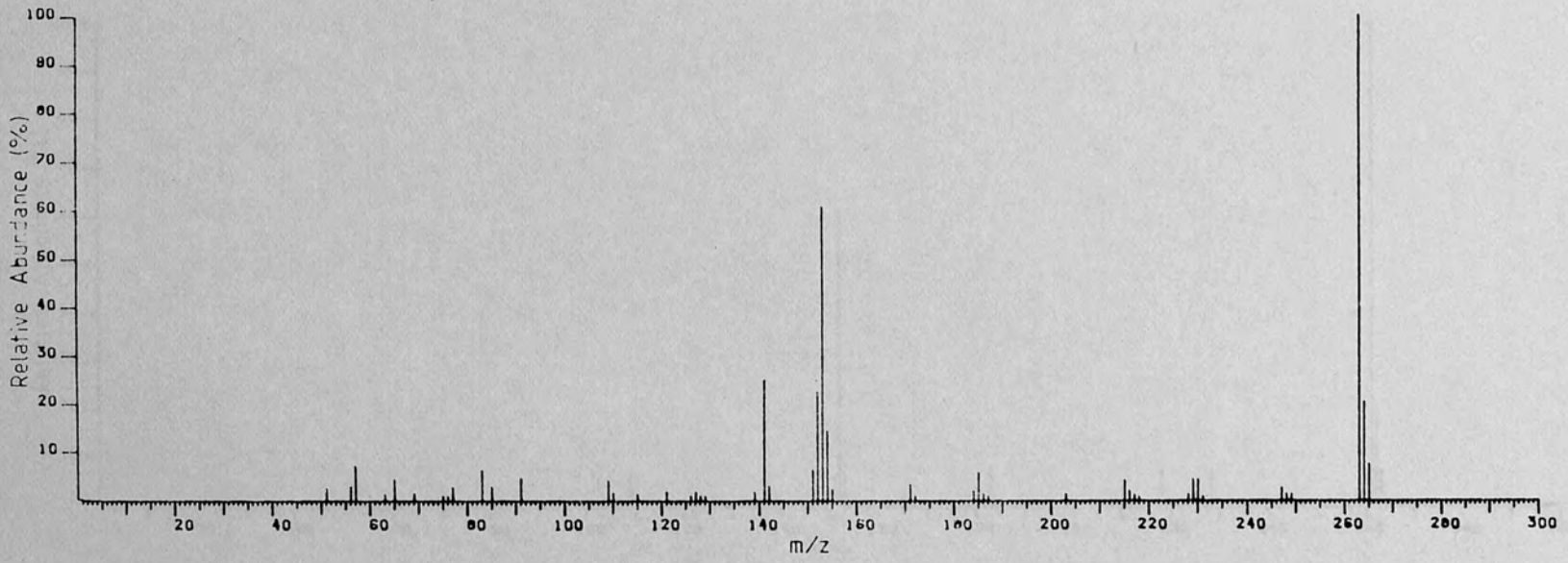
Relative Abundance (%)
100
90
80
70
60
50
40
30
20
10
20
40
60
80
100
120
140
160
180
200
220
240
260
280
300
m/z

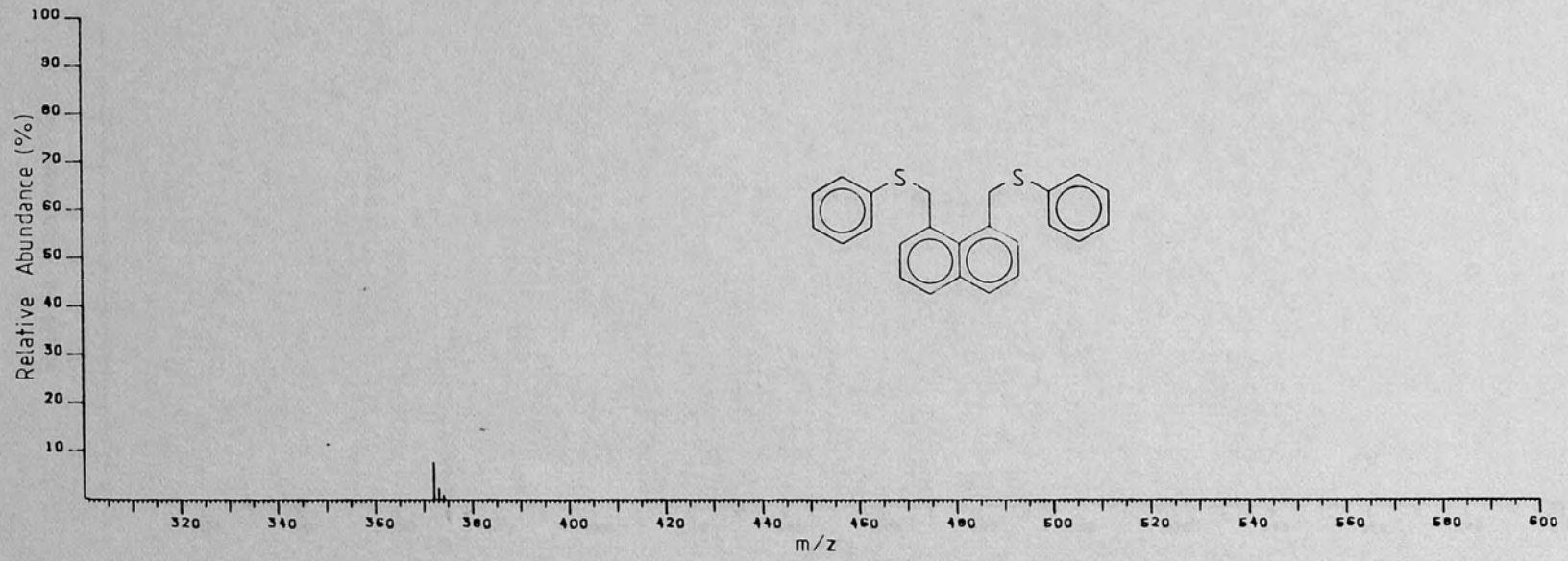
Relative Abundance (%)
100
90
80
70
60
50
40
30
20
10
320
340
360
380
400
420
440
460
480
500
520
540
560
580
600
m/z

S
S

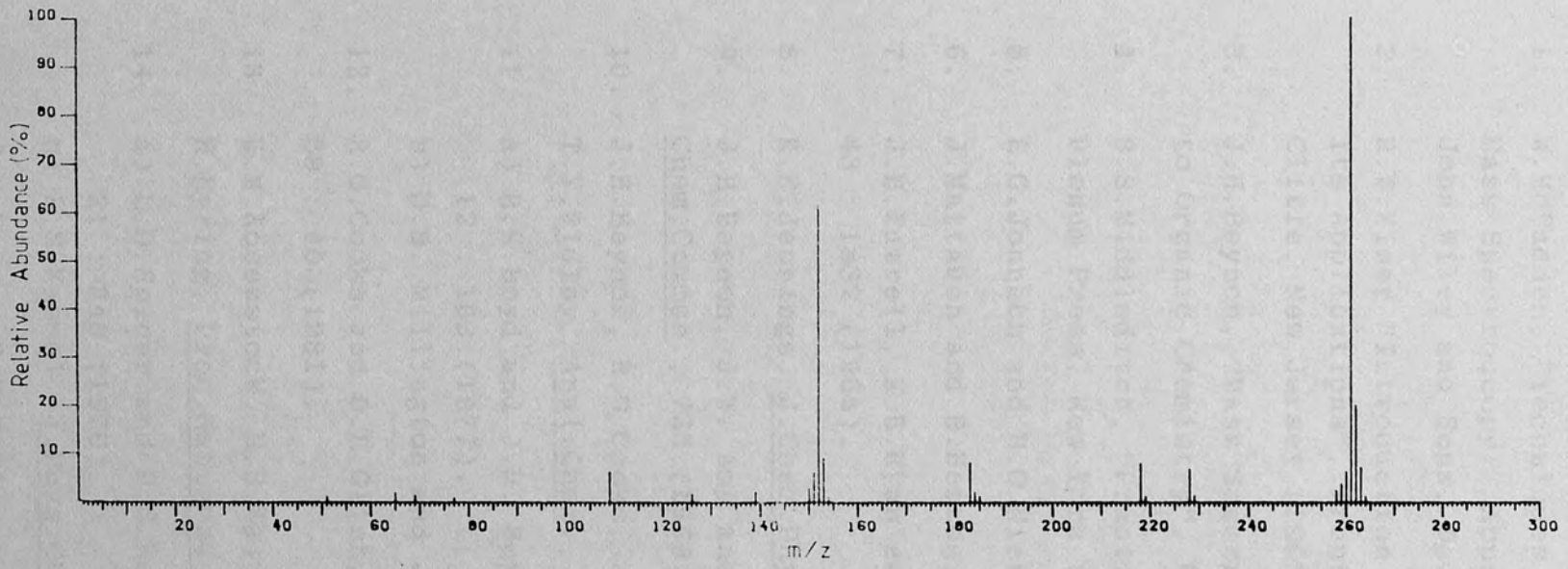
Relative Abundance (%)
100
90
80
70
60
50
40
30
20
10
20
40
60
80
100
120
140
160
180
200
220
240
260
280
300
m/z

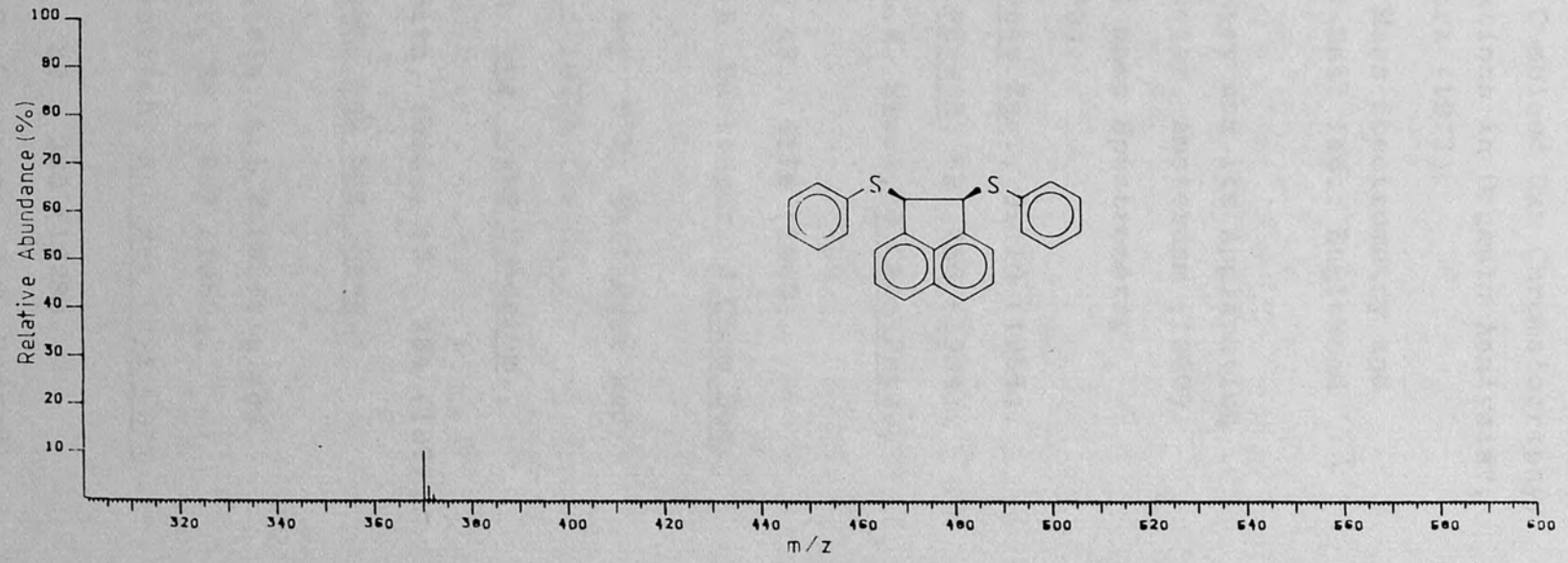
Relative Abundance (%)
100
80
60
70
60
50
40
30
20
10
320
340
360
380
400
420
440
460
480
500
520
540
560
580
600
m/z

S
S

REFERENCES

1. W.McFadden, "Techniques of Combined Gas Chromatography/ Mass Spectroscopy: Applications in Organic Analysis", John Wiley and Sons, New York (1973).

2. R.W.Kiser "Introduction to Mass Spectrometry and its Applications", Prentice-Hall Inc., Englewood Cliffe, New Jersey (1965).

3. J.H.Beynon, "Mass Spectrometry and its Application to Organic Chemistry", Elsevier, Amsterdam (1960).

4. B.S.Middleditch, "Practical Mass Spectrometry", Plenum Press, New York (1979).

5. E.G.Johnson and H.O.Nier, Phys.Rev., 91:10 (1953).

6. J.Mattauch and R.Herzog, Z.Physik, 89: 786 (1934).

7. J.H.Futrell, K.R.Ryan and L.W. Sieck, J.Chem.Phys., 43 : 1832 (1965).

8. K.R.Jennings, J.Chem.Phys., 43 : 4176 (1965).

9. J.H.Beynon, J.W. Amy and W.E. Bartinger, J.Chem.Soc., Chem.Commun., 723 (1969).

10. J.H.Beynon, R.G.Cooks, J.W.Amy, W.E. Baitinger and T.Y.Ridley, Anal.Chem., 45 : 1023A (1973).

11. a) R.K.Boyd and J.H. Beynon, Org. Mass Spectrum., 12 : 163 (1977).
b) D.S. Millington and J.Smith, ibid., 12 : 264 (1977).

12. R.G.Cooks and G.L.Glish, Chem. and Eng. News, 59 : 40 (1981).

13. H.M.Rosenstock, M.B.Wallenstein, A.L.Warhaftig and H.Eyring, Proc.Nat.Acad.Sci., 38 : 667 (1952).

14. a) L.D.Spicer and B.S.Rabinovitch, Ann.Rev.Phys.Chem., 21 : 349 (1970).
b) L.S.Kassel, J.Phys.Chem., 32 : 225 (1928).

15. J.H.Bowie, D.H.Williams, S-O. Lawesson, J.Ø. Madsen, C.Nolde and G.Schroll, Tetrahedron 22 : 3575 (1966).

16. R.Smakman and T.H.DeBoer, Org.Mass Spectrom., 3 : 1561 (1970).

17. R.T.Aplin and K.Bailey, J.Chem.Soc. (B), 513 (1967).

18. R.G.Gillis and J.L.Occolowitz, Tet.Lett.,1997 (1966).

19. A.Quayle, Chimia (Aarau), Colloquium Spectroscopium International VIII, 259 (1959).

20. A.A.Kutz and S.J.Weininger, J.Org.Chem., 33 : 4070 (1968).

21. D.S.Weinberg, C.Stafford and M.W.Scoggins, Tetrahedron, 24 : 5409 (1968).

22. S.Meyerson, H.Drews and E.K.Fields, Anal.Chem., 36 : 1294 (1964).

23. J.Ø.Madsen, C.Nolde, S.-O.Lawesson, G.Schroll, J.H.Bowie and D.H. Williams, Tet.Lett. 4377 (1965).

24. A.I.Khodair, A.A.Swelim and A.A.Abdel-Wahab, Phos. and Sulfur, 2 : 173 (1976).

25. H.Budzikiewicz, C.Djerassi and D.H.Williams, "Mass Spectrometry of Organic Compounds", Holden-Day, Inc., San Francisco (1967),a)p559,b)p597,c)p87,d)p218.

26. J.Heiss, K.-P.Zeller, B.Zeeh, Tetrahedron,24 : 3255 (1968).

27. E.K.Fields and S.Meyerson, J.Am.Chem.Soc., 88 : 2836 (1966).

28. I.W.Jones and J.C.Tebby, Phos. and Sulfur, 5 : 57 (1978).

29. R.J.Soothill and L.R.Williams, Org.Mass Spectrom., 6 : 141 (1972).

30. R.J.Soothill and L.R.Williams, Org.Mass Spectrom., 6 : 1145 (1972).

31. T.H.Kinstle and W.R.Oliver, Org.Mass Spectrom., 6 : 699 (1972).

32. B.S.Thyagarajan, K.C.Majumdar and D.K.Bates, Phos. and Sulfur, 1 : 67 (1976).

33. D.K.Bates and B.S.Thyagarajan, Int.J.Sulfur Chem., 8 : 57 (1973).

34. D.K.Bates, Ph.D. thesis, Univ. of Idaho (1974).

35. Q.N.Porter, Aust. J. Chem., 20 : 103 (1967).

36. A.O.Pederson, G.Schroll and S.-O.Lawesson, Tetrahedron, 26 : 4449 (1970).

37. I Pratanata, L.R.Williams and R.N.Williams, Org.Mass Spectrom., 9 : 418 (1974).

38. I.Pratanata, L.R.Williams and R.N.Williams, Org.Mass Spectrom., 8 : 175 (1974).

39. T.H.Kinstle, W.R.Oliver and L.A.Ochrymowycz, Org.Mass Spectrom., 3 : 241 (1970).

40. L.R.Williams, Org. Mass Spectrom., 1 : 613 (1968).

41. C.V.Hill, B.S.Thyagarajan, D.K. Bates and R.J. Spangler, Org.Mass Spectrom., 12 : 379 (1977).

42. W.J.Evans and S.Smiles, J. Chem. Soc., 181 (1935).

43. B.S.Thyagarajan, D.K.Bates, K.C.Majumdar and P.Brown, Int.J.Sulfur Chem., 4 : 1 (1974).

44. B.S.Thyagarajan, P.E.Glaspy, E.Baker and P.Brown, Org. Mass Spectrom., 15 : 224 (1980).

45. B.S.Thyagarajan, P.E. Glaspy and P.Brown, ibid., 15 : 22 (1980).

46. E.J. Levy and W.A.Stahl, Anal. Chem., 33 : 707 (1961).

47. B.J.Gowenlock, J.Kay and J.R.Majer, Trans.Faraday Soc., 59 : 2463 (1963).

48. S.Sample and C.Djerassi, J.Am.Chem.Soc., 88 : 1937 (1966).

49. B.G.Holbrock and R.W.Kiser, J.Phys.Chem., 66 : 1648 (1962).

50. E.V.Gallegos and R.W.Kiser, J.Phys.Chem., 65 : 1177 (1961).

51. "Catalog of Mass Spectral Data", American Petroleum Institute', Project 44, Carnegie Institute of Technology, Pittsburgh.

52. A.M.Duffield, H.Budzikiewicz and C. Djerassi, J.Am.Chem.Soc., 87 : 2920 (1965).

53. J.H.D.Eland and C.J.Danby, J.Chem.Soc., 5935 (1965).

54. J.H.Bowie, S.-O.Lawesson, G.Schroll and D.H. Williams, J.Chem.Soc. (B), 951 (1966).

55. J.D.Henion and D.G.I.Kingston, J.Am.Chem.Soc., 95 : 8358 (1973).

56. G.Saint-Ruf, J.Servoine-Sidoine and J.P.Coie, J.Het. Chem., 11 : 287 (1974).

57. A.Tatematsu, S.Inoue and T.Goto, Tet. Lett., 4609 (1966).

58. M.Fischer and C.Djerassi, Chem.Ber., 99 : 750 (1966)

59. L.R.Williams, Aust. J.Chem., 21 : 2311 (1968).

60. J.K.McCleod and C.Djerassi, J.Am.Chem.Soc., 88 : 1840 (1966).

61. W.D.Weringa, Tet.Lett., 273 (1969).

62. B.S.Thyagarajan and T.Traugott, unpublished results.

63. H.Kwart and T.J.George, J.Chem.Soc., Chem.Commun., 433 (1970).

64. B.S.Thyagarajan and P.E. Glaspy, J. Chem.Soc ., Chem.Commun., 515 (1979).

65. P.Brown and C.Djerassi, Angew. Chem.Int.Ed.Eng., 6 : 477 (1967).

66. J.H.Bowie, B.K.Simons and S.-O.Lawesson, Rev.Pure App.Chem., 19 : 61 (1969).

67. C.J.M. Stirling, J.Chem.Soc., 5856 (1964).

68. K.Sato and O.Miyamota, Nippon Kagaku Zasshi, 77 : 1409 (1956).

69. L.Skattebøl, B.Boulette and S.Solomon, J.Org.Chem., 32 : 3111 (1967).

70. G.Pouralot, P.Cardiot and A.Willemart, Compt.Rend., 252 : 1630 (1961).

71. S.T.McDowell and C.J.M.Stirling, J.Chem.Soc.(B), 351 (1967).

72. H.F.Grostic, R.J.Wnuk and F.K.Mackellar, J.Am.Chem.Soc., 88 : 4664 (1966).

73. I.G.Csizmadia, A.J.Duke, V.L. Lucchini and G.Modena, J.Chem.Soc., Perkin Trans.II, 1808 (1974).

74. G.Capozzi, O. De Lucchi, V.Luccini and G.Modena, J.Chem.Soc., Chem.Commun., 248 (1975).

75. V.Ragner, A.Borg and T.Lindblom, Acta Chem.Scand., 22 : 685 (1968).

76. A.Etienne, G.Lonchambon, C.R.Acad.Sci., Ser.C., 275 : 375 (1972).

77. P.De Maria, A.Fino and F.M.Hall, J.Chem.Soc., Perkin Trans.II, 1969 (1973).

78. B.Ciommer and H.Schwarz, Z.Naturforsch, B, 34B: 1307 (1979).

79. J.R.Wiersig, A.N.H.Yeo and C.Djerassi, J.Am.Chem.Soc., 99 : 532 (1977).

80. C.Bogentroft, C.Lindberg and U.Swensson, Acta Chem. Scand. B, 30 : 85 (1976).

81. B.S.Thyagarajan, private communication.

82. R.S.Gohlke and F.W. McLafferty, Anal.Chem., 34 : 1281 (1962).

83. C.Bogentroft, Org.Mass Spectrom., 3 : 1527 (1970)

84. P.D.Woodgate, K.K.Mayer and C.Djerassi, J.Am.Chem.Soc., 94 : 3115 (1972).

85. A.Behzadi and L.N.Owen, J.Chem.Soc., Perkin Trans.I, 25 (1974).

86. H.Budzikiewicz, C.Djerassi and D.H.Williams, "Interpretation of Mass Spectra of Organic Compounds", Holden-Day, San Francisco (1964) p.98.

87. A.M.Duffield, H.Budzikiewicz, D.H.Williams and C.Djerassi, J.Am.Chem.Soc., 87 : 810 (1965).

88. T.Kamada, N.Wasada and O.Yamamoto, Bull.Chem.Soc. Japan, 49: 275 (1976).

89. V.Boekelheide and G.C.Vick, J.Am.Chem.Soc., 78 : 653 (1956).

90. K.Kondo and K.Mislow, Tet.Lett., 1325 (1967).

91. D.C.Dittmer and B.H.Patwhardan, in "Chemistry of the Sulphonium Group", vol.2, edited by C.J.M. Stirling, Wiley, Chichester (1981), p.387.

92. "EPA/NIH Mass Spectral Data Base", edited by S.R. Hellner and G.W.A. Milne, U.S. Department of Commerce, National Technical Information Service (1978).

93. Y.Hayasi and H.Nozaki, Bull Chem.Soc.Japan, 45 : 198 (1971).

94. B.Franck, P.Wilmo and D.Randau, Adv.Mass Spectrom., 4 : 167 (1968).

95. E.Block, "Reactions of Organosulfur Compounds", Academic Press, New York (1978), p.256.

96. H.Kwart and C.M.Hackett, J.Am.Chem.Soc., 84 : 1754 (1962).

97. S.V.Cristol, F.R. Stermitz and P.S.Ramley, J.Am.Chem. Soc., 78 : 4939 (1956).

98. N.Kharasch and C.M.Buess, J.Am.Chem.Soc., 71 : 2724 (1949).

99. P.E.Butler, W.H.Mueller and J.J.R.Reed, Environ.Sci. Tech., 1 : 315 (1967).

100. S.Sternhall and P.W.Westerman, J.Org.Chem., 39 : 3795 (1974).

101. P.B.Shevlin and J.L.Green, J.Am.Chem.Soc., 94 : 8447 (1972).

102. C.A.McAuliff, F.P.McCullough, R.D.Sedgwick and W.Levason, Inorg.Chem.Acta., 27 : 185 (1978).

103. C.J.M.Stirling in "Organic Chemistry of Sulfur", edited by S.Oae, Plenum Press, New York (1977), p.473.

104. A.S.Gybin, W.A.Smit, V.S. Bogdanov, M.Z.Krimer and J.B.Kalayan, Tet.Lett., 21 : 383 (1980).

105. O.Buchardt, J.Domanus, N.Harritt, A.Holme, G.Isaksson and J.Sandstrom, J.Chem.Soc., Chem. Commun., 376 (1974).

106. Q.N.Porter and J.Baldas, "Mass Spectrometry of Heterocyclic Compounds", Wiley-Interscience, New York (1971), p.225.

107. C.N.Yiannios and J.V.Karabinos, J.Org.Chem., 28 : 3246 (1963).

108. W.H.Mueller and P.E.Butler, J.Am.Chem.Soc., 90 : 2075 (1968).

PART TWO

1. INTRODUCTION

1.1 General aspects of ion-molecule reactions.

1.1.1 Introduction.

In Part One, Section 1.1.1, several methods (e.g. electron impact, photoionisation, field ionisation, etc.) for the ionisation of vaporised substances leading to the formation of primary ions were discussed. When ions are formed at pressures sufficiently high for numerous collisions between ions and molecules to occur the probability of reactions between ions and molecules (Scheme 1.1.1 -1) is increased.

$$A^+ + B \longrightarrow C^+ + D$$

Scheme 1.1.1 -1

A number of techniques have been developed to study the kinetics of ion-molecule reactions and brief descriptions of some of the more commonly used methods are given below. In all of the methods discussed, the kinetics of ion-molecule reactions are investigated by observation of the changes in ion abundances either as the reaction time or the concentration of the neutral species is varied.

1.1.2 Methods commonly used in the study of gas phase ion-molecule reaction kinetics.

1.1.2.1 Introduction.

Various mass analysers and the principles behind their separation have been described previously (Part One, Section 1.1.2) and an example of a single-

focusing mass spectrometer was illustrated in Part One, Figure 1.1.2.1 -1. Because of their suitability for the determination of relative ion abundances, mass spectrometric techniques (vide infra) have gained wide application in the study of ion-molecule reaction kinetics.

1.1.2.2 Continuous ion-extraction mass spectrometry.

Mass spectrometric techniques in which ions are continuously formed in the ion-source, and continuously removed from the ion-source by an applied electric field, are known as continuous ion-extraction techniques. Such a continuous ion-extraction technique was employed for the determination of rate coefficients in this work.

Rate coefficients obtained by continuous ion-extraction methods are, at best, experimental rate coefficients, k_{exp}, which are time averaged. Such experimental rate coefficients are described by

$$k_{exp} = \frac{1}{\tau} \int_{o}^{\tau} k(t)dt \qquad (1.1.2.2\ -1)$$

where τ is the ion residence time, t is the time elapsed between creation and reaction of the ions and k(t) is a microscopic rate constant at a particular t. In order for equation (1.1.2.2 -1) to be valid, the ions should be formed, having no excess energy, at the same distance from the ion exit slit and drift under the influence of a uniform electric field prior to passing through the

ion exit slit. For the above conditions to be met, when a chemical ionisation ion-source is employed, the following three assumptions must be valid[1]:

(a) the ions are formed in an electron beam which is infinitely narrow;

(b) the ions initially have thermal energies;

(c) the electric field strength in the ion-source is constant.

If statements (a)-(c) are true, then:

$$t = v\tau/v_e \qquad (1.1.2.2\text{ -}2)$$

where v and v_e are the instantaneous and exit velocities of the ion, respectively. Under such conditions, k_{exp} is characteristic of the reaction and is not dependent on the particular conditions of the experiment. The measured rate coefficient is then equal to a velocity averaged rate coefficient, $k(v_e)$, described by:

$$k_{exp} = k(v_e) = \frac{1}{v_e} \int_o^{v_e} k(v)dv \qquad (1.1.2.2\text{ -}3)$$

Thus, the rate coefficients obtained from continuous ion-extraction techniques may be compared with values obtained from other methods if assumptions (a)-(c) are valid and only for identical ion exit velocities. Deviations from these conditions can result in experimental rate coefficients which are dependent on experimental circumstances. Control experiments to test the validity of conditions (a)-(c) have been proposed by Henchman[1].

Further difficulty arises owing to the occurrence of reactions with ions possessing a range of energies, $0 \leq E \leq E_e$, where E_e is the exit energy of the ions. Since the energy distribution is pressure dependent, the effects caused by the reaction of molecules reacting with ions having a range of energies can be minimalised by sampling over a relatively narrow pressure range.

1.1.2.3 Pulsed ion-source mass spectrometry.

Pulsed ion-source mass spectrometry was one of the earliest techniques devised solely for the purpose of the determination of rate coefficients of gas phase ion-molecule reactions.[2] In this method, a beam of electrons of short duration (ca. 0.1 μsec) is passed through a gas in the ion-source. The ions formed by this event are retained in the ion-source for a measurable delay time before being extracted and analysed. The delay can amount to several microseconds. The extraction of the ions is achieved by the application of a dc-voltage pulse of the required polarity to a repeller plate and/or an ion withdrawal plate. The observation of the change in ion abundances as the delay time is varied allows reaction rates to be determined.

The existence of mass discrimination effects caused by the extraction pulse is a problem associated with this method and this effect is magnified as delay times are increased. These effects are partly due to

the differences in the rates of diffusion for different ions moving away from the sampling area. By employing delays of sufficiently short duration (ca. 0-1 μsec) and short ionising pulses ($\leq$ 50 nsec), these mass discrimination effects can be minimalised.[1]

1.1.2.4 Drift-tube mass spectrometry.

Within a drift-tube ion-source[3], ions are formed at one end of a tube, by electron impact ionisation of a gas. The tube (which is several centimetres in length) consists of metal rings that are electrically insulated from each other. By applying progressively lower voltages to the metal rings, the ions formed in the ionisation region are made to drift down the tube and to eventually pass through an exit slit into a mass analyser. By maintaining a sufficiently large pressure in the drift tube and a sufficiently low field strength, the mean energy of collisions between ions and molecules will be low and the rate coefficients obtained will correspond to those for near-thermal conditions.

A great advantage of the drift-tube method is that the drift velocity is defined and thus the spatial and velocity distributions of the ions are well established. In addition, the length of the reaction region can be adjusted to vary the reaction time by means of a movable ion-source.[4] Alternatively, different reaction times can be achieved by the reversal of the electric field.[5] Thus, the separate contributions of drift, diffusion and

reaction to the data obtained by drift-tube technique can be determined by alterting the two parameters mentioned above.

The ability to perform experiments with a wide range of pressures aids the identification of kinetic orders of reaction; at higher pressures, the rates of slow reactions can be determined.

1.1.2.5 Flowing-afterglow mass spectrometry.

This technique was devised in 1969[6] with the intent of investigating ion-molecule reactions at thermal energies. Ions are produced from one of the inert gases by means of electron impact, microwave discharge[7] or cold cathode discharge.[8] The resulting plasma of positive ions and electrons is carried by a stream of the gas through a tube (the flight tube).

A second gas (the ion source gas) is injected downstream, into the afterglow of the discharge, and primary ions (A^+) are formed by reaction with the ions and electrons, rather than by direct electron impact. The ions A^+ come to thermal equilibrium with the carrier gas, after flowing a few centimetres downstream, and a reactant gas (B) is there injected into the stream. By means of a quadrupole mass filter, the ions are sampled and thus the ion-molecule reaction:

$$A^+ + B \longrightarrow \text{products}$$

can be investigated. The temperature of the system is

easily varied and hence its effect on reaction rates can be determined.

1.1.2.6 Selected ion flow tube (SIFT) mass spectrometry.

The SIFT technique, developed by Adams and Smith[9], employs a flow tube similar to that used in the flowing afterglow method. A quadrupole mass filter is used to mass select ions produced by an electron impact ion-source. The selected ions are injected into a flow tube and thermalise in collision with a carrier gas. The carrier gas transports these ions past injection ports, through which a reactant gas is introduced. At the end of the reaction region, the ions are sampled through an orifice and are analysed by a second quadrupole mass filter.

These same researchers have recently constructed an adapted SIFT instrument which incorporates a drift tube (vide supra).[10] This SIFT-DRIFT system allows the parameters of energy and temperature to be varied over a wide range and represents a combination of the advantages of flowing-afterglow, drift tube and SIFT techniques.

1.1.2.7 Ion cyclotron resonance spectrometry.

In an ion cyclotron resonance spectrometer[11], ions are generated by electron impact of a gas at one end of a cell, which typically have the dimensions of 2.5 x 2.5 x 12.5 cm. The ions formed in this manner enter the

cell and drift through it, under the influence of crossed electric and magnetic fields, into a "resonance region" where they are irradiated by an alternating electric field.

An ion in a uniform magnetic field will describe a circular orbit of angular frequency ω_c (the cyclotron frequency) and

$$\omega_c = \frac{zB}{mc} \qquad (1.1.2.7\text{ -}1)$$

where z is the charge of the ion, B is the magnetic field strength, m is the mass of the ion and c is the velocity of light. If an alternating electric field is applied normal to the magnetic field at a frequency equal to ω_c, the ion will absorb energy. Thus, by scanning the magnetic field strength while maintaining the alternating electric field at a constant frequency, a spectrum linear in mass can be obtained.

Considering again the general ion-molecule reaction,

$$A^+ + B \longrightarrow C^+ + D,$$

both A^+ and C^+ can be detected by the above method. Furthermore, if, while observing the energy absorbance of C^+, A^+ is perturbed by an alternating electric field equal to its cyclotron frequency, a resulting change in the absorbance of C^+ will be detected if its formation is derived from A^+. This double-resonance method thus provides a means of unambiguously identifying reactant

ions, even when competing processes are occurring in a reaction mixture. Since ions are detected *in situ*, mass discrimination effects, which can arise during the processes of extraction and anlaysis in the other mass spectrometric methods described previously, are avoided.

1.1.3 Ion-molecule reactions in the gas phase.

In 1916, Dempster reported a peak at m/z 3, corresponding to H_3^+, in the mass spectrum of hydrogen.[12] The formation of H_3^+ from the ion-molecule reaction of hydrogen and the hydrogen molecular ion was later confirmed.[13,14]

$$H_2^{+\cdot} + H_2 \longrightarrow H_3^+ + H\cdot$$

Scheme 1.1.3 -1

Later, in 1928, the ion-molecule reactions of both positive and negative ions derived from iodine vapour were studied.[15] In this study, $I_2^{+\cdot}$ was found to arise from both electron impact ionisation and by a charge transfer reaction from I^+. The formation of I_3^+ was found to occur via the reaction of $I_2^{+\cdot}$ with I_2 :

$$I_2^{+\cdot} + I_2 \longrightarrow I_3^+ + I\cdot$$

Scheme 1.1.3 -2

The charge exchange reaction of I^- with I_2 forms $I_2^{-\cdot}$, which undergoes reaction with I_2, yielding I_3^- : [15]

$$I_2^{-\cdot} + I_2 \longrightarrow I_3^- + I\cdot$$

Scheme 1.1.3 -3

The theoretical treatment of the formation of H_3^+ by Eyring, Hirschfielder and Taylor in 1936,[16] based upon absolute rate theory, represents the first calculation of an ion-molecule rate coefficient. An empirical determination obtained later,[17] was found to be in close agreement with their calculated value.

The formation of CH_5^+ from methane was reported by several groups in the 1950's[18,19,20] and marks the beginning of modern studies of ion-molecule reactions:

$$CH_4^{+\cdot} + CH_4 \longrightarrow CH_5^+ + CH_3^{\cdot}$$

Scheme 1.1.3 -4

Later, instruments were designed to operate at higher pressures, such as the one described by Field[21] which could operate at ion-source pressures of up to 2 Torr. The development of chemical ionisation mass spectrometry (discussed in Section 1.2) was a direct result of the construction of high pressure mass spectrometers.[22]

Ion molecule reactions in the gas phase can be classified according to the following types:

1) Charge-transfer reactions

2) Proton, hydride or atom transfer reactions

3) Clustering reactions

The reactions in Schemes 1.1.3 -1, 1.1.3 -2, and 1.1.3 -3 are examples of proton, atom and charge transfer reactions respectively. Hydride transfers in the reaction of carbenium ions with alkanes were first observed by

Field and Lampe.[23]

$$C_nH_{2n+1}^+ + C_mH_{2m+2} \longrightarrow C_nH_{2n+2} + C_mH_{2m+1}^+$$

Scheme 1.1.3 -5

The transfer of H_2^- in the following reaction (in which C_4H_{10} = iso-butane) is an example of a two atom transfer reaction[24]:

$$C_3D_6^{\cdot+} + C_4H_{10} \longrightarrow C_3D_6H_2 + C_4H_8^{\cdot+}$$

Scheme 1.1.3 -6

Clustering reactions, such as that occurring in water vapour:

$$H(H_2O)_{n-1}^+ + H_2O \longrightarrow H(H_2O)_n^+$$

Scheme 1.1.3 -7

have been investigated extensively by Kebarle[25] and reviewed.[26,27]

The study of some ion-molecule clustering reactions, employing a continuous ion-extraction method, froms the basis of the work described here and, thus, emphasis is placed on these reactions. These are discussed separately in the following section.

1.1.4 Ion-molecule clustering (association) reactions.

1.1.4.1 Mechanistic considerations.

The application of the energy transfer mechanism (first proposed by Rabinowitz[28] for atom recombination reactions) to ion-molecule reactions is generally considered to be valid.[26,29,30,31,32] Thus, the formation of a cluster ion (IM^+) from I^+ and M

occurs via an excited collision complex (IM^{+*}), which is stabilised by the removal of excess excitation energy in a subsequent collision with a neutral third body (M) :

$$I^+ + M \underset{k_b}{\overset{k_f}{\rightleftharpoons}} IM^{+*} + M \xrightarrow{k_s} IM^+ + M^*$$

Scheme 1.1.4.1 -1

Assuming the above mechanism, a steady state treatment for the concentration of the collision complex leads to the following expression for the overall forward rate coefficient, k :

$$k = \frac{k_f k_s \{M\}}{k_b + k_s \{M\}} \qquad (1.1.4.1\ -1)$$

At low pressures, when $k_b >> k_s\{M\}$ the above equation becomes:

$$k = \frac{k_f k_s \{M\}}{k_b} \qquad (1.1.4.1\ -2)$$

and the reaction exhibits third order kinetics with a third order rate coefficient equal to $k_f k_s / k_b$. At higher pressures, $k_s\{M\} >> k_b$ and equation (1.1.4.1 -1) reduces to

$$k = k_f \qquad (1.1.4.1\ -3)$$

Thus, association reactions should display a change from third to second order kinetics over a sufficiently large pressure range and this has indeed been reported for many systems.[33]

For the purpose of this discussion, those reactions in which the cluster ion, M_2H^+, incorporates a solvated proton, i.e.

$$MH^+ + M \longrightarrow MHM^+$$

are most pertinent and are discussed in Section 1.1.4.3.

1.1.4.2 Theoretical approaches to the determination of ion-molecule rate coefficients.

One of the earliest models for the theoretical treatment of a point change approaching a polarisable molecule was Langevin's ion-induced dipole theory for nonpolar molecules,[34] which was developed in 1905 and later elaborated by Gioumousis and Stevenson[35] in 1958. The rate constant for a capture collision is given by:

$$k_c = 2\pi q(\alpha/\mu)^{\frac{1}{2}} \qquad (1.1.4.2\text{ -1})$$

where q is the charge on the ion, α is the polarisability of the molecule and μ is the reduced mass. (By definition a capture collision occurs when the ion-molecule separation is zero). Although the rate constants obtained by equation (1.1.4.2 -1) agree well with some simple low energy ion-molecule rate constants, the rate constants for ion-polar molecule reactions are usually underestimated.[36]

To account for the presence of a permanent dipole on the molecule, the locked-dipole approximation was formulated, in which the angle the dipole makes with the line of the centres of the collision (θ) is assumed to be 0^o.[37,38] Based on this assumption, the locked-dipole capture collision rate constant is defined by:

$$k_{LD} = \frac{2\pi q}{\mu^{\frac{1}{2}}} \left[\alpha^{\frac{1}{2}} + \frac{\mu_D}{v} \right] \qquad (1.1.4.2\text{ -2})$$

with μ_D equal to the dipole moment of the neutral and v is the approach velocity of the ion to the molecule. For thermal velocities, the rate constant (k_{LD}') at an absolute temperature T is

$$k_{LD}' = \frac{2\pi q}{\mu^{\frac{1}{2}}} \left[\alpha^{\frac{1}{2}} + \mu_D \left(\frac{2}{\pi k_B T} \right)^{\frac{1}{2}} \right] \qquad (1.1.4.2\text{ -3})$$

where k_B is Boltzmann's constant.[39] However, equations (1.1.4.2 -2) and (1.1.4.2 -3) grossly overestimate the effect of the permanent dipole[36] (i.e. the degree of "locking in") as evidenced by the rate constants predicted by these equations tending to have large positive errors.

Bowers and Laudenslager assumed that only partial locking of the dipole occurs and introduced a dipole locking constant c, which can vary from 0 to 1, such that

$$k_{PLD} = \frac{2\pi q}{\mu^{\frac{1}{2}}} \left[\alpha^{\frac{1}{2}} + c\mu_D \left(\frac{2}{\pi k_B T} \right)^{\frac{1}{2}} \right] \qquad (1.1.4.2\text{ -4})$$

Experimentally, c was determined by comparing the rate constants for the charge transfer reactions of several rare gas ions with the three geometric isomers of difluoroethene, which have very similar ionisation potentials and angle averaged polarisabilities, but very different dipole moments (trans: 0.0D; cis:2.42D;

1,1:1.38D).[36,40]

The dipole locking constant was determined by

$$c = \Delta k(k_B T\mu/8\pi q^2 \mu_D)^{\frac{1}{2}}$$

with Δk being the observed difference between the rate constants for the polar isomer and the nonpolar isomer. (The rates were obtained using ion cyclotron resonance spectrometry). The degree of locking in for cis and trans difluoroethene was small, with c equal to ca.0.1, and was found to increase with an increase in the dipole moment.[40]

Su and Bowers were led by the above results to postulate the average dipole orientation (ADO) theory, in which an average value for θ (vide supra) is calculated.[41] The ADO theory can be parameterised by means of equation (1.1.4.2 -4) to allow simple calculations of ADO rate constants (k_{ADO}) to be made.[42] Su and Bowers have found that, at constant temperature, c is a function of $\mu_D/\alpha^{\frac{1}{2}}$ only and values for c are acquired easily from their published plot of c versus $\mu_D/\alpha^{\frac{1}{2}}$.[41] Theoretical rate constants obtained by this method have been shown to be generally in excellent agreement with experimental values.[36]

1.1.4.3 Clustering reactions involving proton solvation.

The formation of hydrated proton clusters has been mentioned previously in Section 1.1.3 (see Scheme 1.1.3 -7). The series of hydrated proton equilibria (n=1-4):

$$H^+ (H_2O)_{n-1} + H_2O \underset{}{\overset{k_f}{\rightleftharpoons}} H(H_2O)_n^+$$

have been studied in water vapour[43] and with O_2,[44,45] N_2[46], methane [47, 48, 49]. propane,[50], helium[51] or argon[52] as the major gas. The values for k_f obtained in these studies were of the order of 10^{-27} - 10^{-28} $cm^6 molec^{-2}$ sec^{-1} for n=1,2,3 or 4 and showed variations with different third bodies present (e.g. argon is less efficient than either O_2 or N_2 and the rate coefficients for the O_2 and N_2 systems are larger by ca. an order of magnitude). The corresponding clustering reactions in deuterium oxide have been reported.[53]

The kinetics of the formation of the proton bound dimer of ammonia (n=O, Scheme 1.1.4.3 -1), have been studied with M being oxygen, [54] methane[55] and ammonia.[56]

$$NH_4(NH_3)_n^+ + NH_3 + M \longrightarrow NH_4(NH_3)_{n+1}^+ + M$$

Scheme 1.1.4.3 -1

Higher order clusters, n=1,2, were detected in a study of a nitric oxide/ammonia mixture and the third order rate coefficients for their formation were determined.[27]

In a photoionisation mass spectrometric study of pure methyl, dimethyl and trimethylamine, the clustering reactions shown in Schemes 1.1.4.3 -2, 1.1.4.3 -3 and 1.1.4.3 -4 were observed at pressures of up to 0.5 Torr.[57] For these pressures the maximum value for n was found to be 4,3 and 2 for methyl, dimethyl

and trimethylamine, respectively.

$$CH_3NH_3\ (CH_3NH_2)^+_{n-1} + CH_3NH \longrightarrow (CH_3NH_2)_nH^+$$

Scheme 1.1.4.3 -2

$$(CH_3)_2NH_2((CH_3)_2NH)^+_{n-1} + (CH_3)_2NH \longrightarrow ((CH_3)_2NH)_nH^+$$

Scheme 1.1.4.3 -3

$$(CH_3)_3NH((CH_3)_3N)^+_{n-1} + (CH_3)_3N \longrightarrow ((CH_3)_3N)_nH^+$$

Scheme 1.1.4.3 -4

The formation of proton bound dimers in ethylamine, diethylamine, n-propylamine and i-butylamine has also been reported.(56)

1.2 Chemical ionisation mass spectrometry.

Ion-molecule reactions from the basis of chemical ionisation mass spectrometry,(58) since ionisation of the sample occurs via reaction with ions derived from a reagent gas. The reagent gas is introduced into the source at pressures of ca. 0.1-2 Torr and is ionised by one of the methods discussed previously, with electron impact being the most commonly used technique. At such pressures, reaction of the primary ions with the neutral reagent gas molecules can occur and the secondary ions, so formed, can then react with the sample. The relative concentration (pressure) of the sample is kept sufficiently low to avoid direct ionisation.

Isobutane is one of the most commonly used reagent gases and is illustrative. Fragmentation of the molecule ion leads to primary ions such as $C_3H_7^+$:

$$C_4H_{10}^{+\cdot} \xrightarrow[-CH_3\cdot]{} C_3H_7^+$$

Scheme 1.2 -1

The further reaction of $C_3H_7^+$ with an isobutane molecule produces the $C_4H_9^+$ ion, via hydride transfer:

$$C_3H_7^+ + C_4H_{10} \longrightarrow C_3H_8 + C_4H_9^+$$

Scheme 1.2 -2

The other primary ions of isobutane react similarly such that, at pressures higher than 0.15 Torr, its mass spectrum comprises mainly of a signal corresponding to the ion current due to $C_4H_9^+$. This ion, the reactant ion, acts mainly as a Brønsted acid which protonates the sample molecule AH, as in Scheme 1.2 -3, although hydride transfer and clustering reactions can also occur (Schemes 1.2 -4 and 1.2 -5, respectively).

$$C_4H_9^+ + AH \longrightarrow C_4H_8 + AH_2^+$$

Scheme 1.2 -3

$$C_4H_9^+ + AH \longrightarrow C_4H_{10} + A^+$$

Scheme 1.2 -4

$$C_4H_9^+ + AH \longrightarrow C_4H_9AH^+$$

Scheme 1.2 -5

An advantage of chemical ionisation over electron impact ionisation is the relative simplicity of the mass spectra obtained, which aids the identification of unknowns. Ions having masses close to the relative

molecular mass of the sample (such as AH_2^+ and A^+) are usually present, even in cases where the molecular ion gives very low or zero relative abundance in the electron impact mass spectrum.[59] The fragmentations occurring subsequent to chemical ionisation are usually more easily rationalised than those observed upon ionisation with 70 eV electrons, again aiding analysis.

Numerous other gases besides isobutane have been employed as chemical ionisation reagent gases. Methane[59] and ammonia[60] are widely used. The use of these gases, as well as hydrogen, nitrogen, water, tetramethylsilane and the inert gases have been discussed in several reviews.[61-65]

1.3 Objectives in the investigation of the kinetics of ion-molecule reactions occurring in chemical ionisation reagent gases.

An important feature of chemical ionisation is that different types of reactant ions will undergo different types of reaction with any given sample. Since the product distributions of gas phase ion-molecule reactions are temperature and pressure dependent, differences in the chemical ionisation mass spectra obtained as a result will arise from variations in these two parameters. Although ion-source temperatures are routinely controlled and measured, most mass spectrometers are not fitted with an accurate gauge to determine pressures within the ion-source. This problem can be solved by

estimating pressures via kinetic analysis of the ion-molecule reactions occurring in the reagent gas, as has been shown for isobutane and methane.[66]

The methylamines,[67,68] ammonia-d_3[69,70] and deuterium oxide[71] have been found to be useful chemical ionisation reagent gases and the use of water as a reagent gas has been mentioned in the previous section. The objective of the work described in this Part of the thesis was to investigate the kinetics of the ion-molecule reactions occurring in the above mentioned gases under typical chemical ionisation conditions. At the pressures required for chemical ionisation, these gases undergo clustering reactions and, to date, these reactions have not been studied in a way such that the results would be directly applicable to analytical problems in chemical ionisation mass spectrometry. The current work focuses on these clustering reactions with such an application in mind.

2. EXPERIMENTAL

2.1 Chemicals

Water was distilled, deionised and redistilled prior to use. Deuterium oxide was supplied by the Aldrich Chemical Co. in 99.6 atom % purity. Ammonia-d_3 was obtained in 99 atom % purity from British Oxygen (Specialty Gases Division). Methylamine (98% minimum purity), dimethylamine (99% minimum purity) and trimethylamine (99% minimum purity) were supplied by Matheson Gas Products.

2.2. Instrumentation

The present work employed a V.G. Micromass 12F mass spectrometer which is a 60^{o}, 12.7 cm radius, magnetic sector instrument. Mass analysis is achieved by varying either the magnetic field strength or the accelerating voltage. All spectra reported in this work were obtained by scanning the magnetic field with the accelerating voltage maintained constant.

Figure 2.2 -1 is a schematic cross-section of the ion-source employed in this study. The ion-source chamber is a cavity milled out of a stainless steel block (B). An emission regulated filament (F) is mounted outside of the ion-source block. The electron beam produced by the filament enters the ion-source via a non-standard cylindrical orifice (A) of 2 mm length and 0.5 mm internal diameter. The original electron entrance aperture had been altered by the manufacturers to allow the development of higher pressures within the

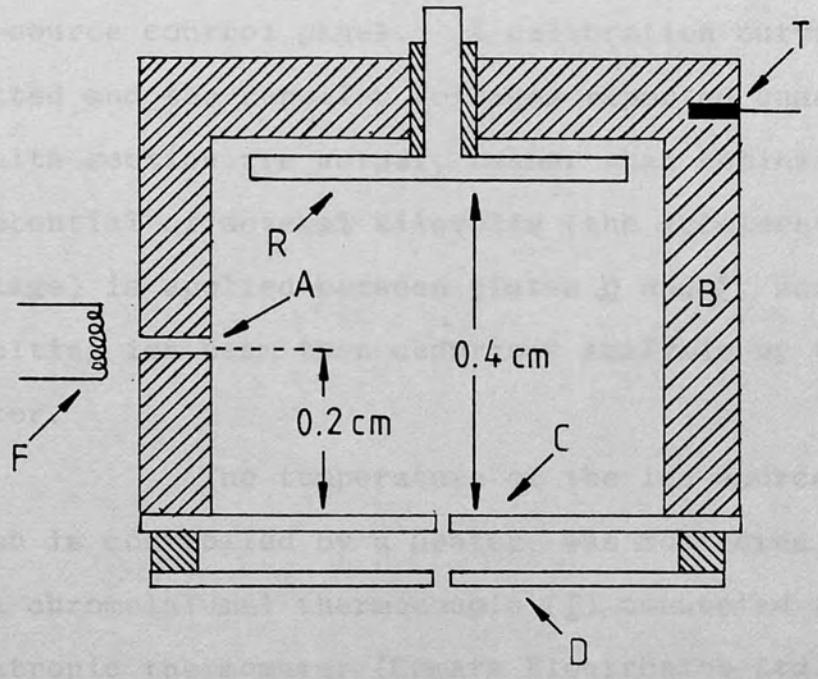

Figure 2.2-1 : Schematic cross-section of the ion-source of the V.G. Micromass 12F mass spectrometer.

ion-source. Ions formed within the ion-source are propelled towards and through the ion exit slit (0.05 x 5 mm) in plate C under the influence of a positive potential on the repeller plate R. (The measured repeller voltages were found to differ by ca. -0.5V in comparison with the value indicated by the meter on the ion-source control panel. A calibration curve was plotted and the repeller voltages reported under the Results section are actual, rather than nominal values). A potential of several kilovolts (the acceleration voltage) is applied between plates D and C, and the resulting ion beam then undergoes analysis by the magnetic sector.

The temperature of the ion-source block, which is controlled by a heater, was monitored by means of a chromelalumel thermocouple (T) connected to an electronic thermometer (Comark Electronics Ltd.), which permitted the temperature to be measured to $\pm$ 1^{o}C. A further modification was the removal of the electron-collimating magnets, normally fitted to the ion-source, to negate the possibility of ion discrimination effects due to the presence of magnetic fields in the ion-source.

After passing through the magnetic analyser, the focused ion-beams pass through a collector slit and are detected by a 17-stage electron multiplier tube. To offset possible mass discrimination effects by the collector slit, it was adjusted to its maximum width (ca.1mm). The lower resolution obtained using a wide collector slit setting did not seriously affect the

spectra below ca. m/z 250. The ions of interest did not have masses greater than this value and hence the widening of the collector slit did not produce adverse effects on the spectra obtained. No corrections can be made for mass discrimination effects arising from the use of an electron multiplier tube as a detector. The response of such tubes are dependent on the mass, kinetic energy, and the elemental composition of the ions striking the first dynode.[72] Sufficient data is not available at present to make general corrections for such discrimination effects.

The signal from the electron multiplier is amplified and then recorded with an S.E. Laboratories 3005 oscillographic recorder. This recorder uses three mirrors, mounted on galvanometers, to reflect U.V. light on to photosensitive paper. The traces produced correspond to attenuation factors of 0.01, 0.1 and 1. For the sake of discussion the galvanometers that correspond to attenuation factors of 0.01, 0.1 and 1 will be designated 1,2 and 3, respectively.

In the sections to follow, the abundance of an ion in the ion source is assumed to be reflected by the height of the corresponding peak in the mass spectrum. Since the abundance of an ion is actually reflected by the area under the corresponding peak, this assumption is an approximation at best. However, since the variation in shape and width of the bases of the peaks is negligible in the mass range of interest ($m/z < 250$), the above assumption is valid. Peak heights are determined

by measurement to the nearest 0.5 mm with a transparent ruler. The deviations of the responses of the galvanometers from the ideal ratio of 1:10:100 had been measured in an earlier study.[73] The heights of the peaks produced by galvanometers (1) and (2), h_1 and h_2 respectively, are corrected to the value that would have been recorded by galvanometer (3) by use of the following equations, which had been determined empirically[73]:

$$h_3 = 10 \times ((1.071 \pm 0.018)h_2 - (0.04 \pm 0.007)) \quad (2.2.-1)$$

$$h_3 = 100 \times ((0.971 \pm 0.025)h_1 - (0.438 \pm 0.008)) \quad (2.2.-2)$$

The spectra reported in this work were obtained by exponentially scanning the magnetic field from high to low field strength. For ions of mass M collected at time t:

$$M = M_o \, e^{(-t/T)} \quad (2.2 -3)$$

where M_o equals the mass of the ions collected initially and T is the time constant (i.e. the time required to scan one decade of mass units). Differentiating equation (2.2 -3) yields

$$dM = -\frac{M_o}{T} \, e^{(-t/T)}dt \quad (2.2 -4)$$

and

$$dM = -Mdt/T \quad (2.2 -5)$$

Rearrangement of equation (2.2 -5) gives

$$dt = -T\frac{dM}{M} \quad (2.2 -6)$$

The entity $\frac{dM}{M}$ is equal to the inverse of the resolving power of the instrument (see Part One, equation 1.1.2.1 -1)) and thus the time spent collecting a given mass is a constant for all masses when T is constant. As a result,

the relative heights of peaks will reflect the relative abundances of the corresponding ions in the ion source if mass discrimination effects are kept minimal. The spectra obtained for this study were recorded with the time constant,T, equal to 30 sec/decade, since better reproducibility of spectra are obtained at slower scan rates. The disadvantage of possible changes in instrument sensitivity occurring during a scan was easily avoided by duplicating scans whenever such a change in sensitivity was suspected.

2.3 Introduction of gases into the ion-source.

The ion-source of the instrument employed in this study has various apertures to accommodate the introduction of samples via a heated inlet system (for liquids), a heated probe (for volatilisation of solids) and a gas-jet interface (for use with a gas chromatograph). In addition, a tube, terminating in the ion-source chamber, allows the introduction of reagent gases directly into the ion-source. Another opening was engineered so as to allow a Baratron gauge-head to be interfaced to the ion-source. A metal tube incorporating a glass insert was used to connect the gauge-head to the ion-source. (The various openings mentioned above are not shown in Figure 2.2 -1 for clarity.) The use of a Baratron gauge to measure pressures in the ion-source is discussed in the next section.

The reagent gas line is connected with the ion-source by a length of silicone rubber tubing.

Reagent gas pressures can be regulated by means of a needle-valve in the reagent gas line. Separate systems were required for the production of pressures in the ion-source in the range 0.005 - 0.4 Torr, depending on the reagent gas of interest.

Methylamine, dimethylamine and trimethylamine are low boiling liquids with boiling points near 0^{o} (-6.3^{o}, 7.4^{o} and 2.87^{o} respectively) and are supplied commercially in "lecture" bottles. To avoid condensation of the gas in the reagent gas line and to maintain a steady head pressure behind the needle valve, the glass inlet system shown in Figure 2.3 -1 was constructed and employed. The valves a - h are high-vacuum "Rotaflow" valves which are constructed of glass and "Teflon". The operation of the system proceeded as follows:

(1) With valves b and h closed, the system was evacuated by means of a rotary high vacuum pump. (The cold trap was kept immersed in liquid nitrogen at all times).

(2) Valves c, d and e were closed and the system was flushed with the given reagent gas by slowly and simultaneously opening the valve on top of the lecture bottle and valve h, which connected the system with a mercury bubbler to prevent the building of excessively high pressures.

(3) These two valves were then shut and the system evacuated again as in step (1).

(4) Valves c, d and e were then shut and the reagent gas allowed to enter the system as in step (2).

By surrounding the liquid sample bulb A with 50% water/ethylene glycol a cold bath (maintained at ca. -15^{o} by a refrigeration unit) and maintaining a slight positive pressure of the appropriate amine reagent gas, approximately $10cm^3$ of the liquid was collected.

(5) The lecture bottle was closed off and valves f and g were shut.

(6) The liquid in volume A was frozen at $-196^{o}C$ and the system evacuated by opening valves e and g. Valve g was closed and the amine allowed to thaw under vacuum. This step was repeated several times in order to de-gas the amine.

(7) After closing valve e, and again immersing volume A in the refrigerated bath, valve g was opened. By opening valves c and d on the arms of the manometer (with the left hand side of the manometer kept under vacuum) the pressure of the reagent gas in the inlet system could be determined to ca. $\pm$ 1mm Hg accuracy.

By maintaining the temperature of the cooled bath constant to within $\pm$ $0.2^{o}C$, extremely stable head pressures, equal to the vapour pressure of the amine at the given temperature were obtained. Typical pressures obtained for methylamine, dimethylamine and trimethylamine were 599 Torr at $-12.5^{o}C$, 316 Torr at $-13.2^{o}C$ and 383 Torr at $-13.0^{o}C$ respectively. The incorporation of a large (2 litre) expansion volume B also aided pressure stability.

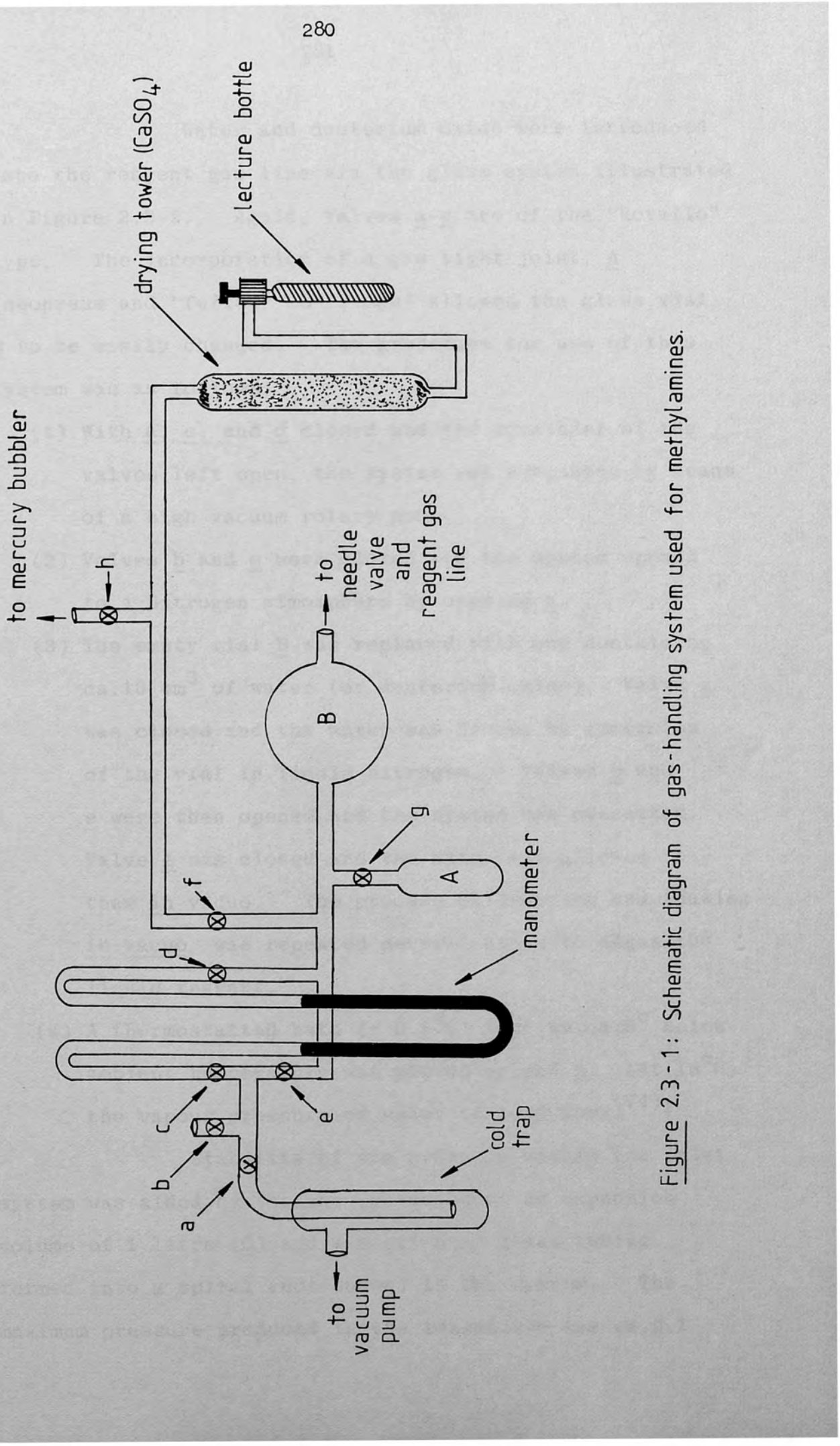

Figure 2.3 - 1 : Schematic diagram of gas-handling system used for methylamines.

Water and deuterium oxide were introduced into the reagent gas line via the glass system illustrated in Figure 2.3-2. Again, valves a-e are of the "Rotaflo" type. The incorporation of a gas tight joint, A (neoprene and "Teflon" "O" rings) allowed the glass vial B to be easily changed. The procedure for use of this system was as follows:

(1) With a, c, and d closed and the remainder of the valves left open, the system was evacuated by means of a high vacuum rotary pump.

(2) Valves b and e were closed and the system opened to a nitrogen atmosphere by opening a.

(3) The empty vial B was replaced with one containing ca.10 cm^3 of water (or deuterium oxide). Valve a was closed and the water was frozen by immersion of the vial in liquid nitrogen. Valves b and e were then opened and the system was evacuated. Valve e was closed and the water was allowed to thaw *in vacuo*. The process of freezing and thawing *in vacuo* was repeated several times to degas the liquid reagent.

(4) A thermostatted bath ($\pm$ 0.1^{o}C) kept at ca.9^{o} below ambient temperature was placed around B. (At 16^{o}C, the vapour pressure of water is 13.6 Torr.[74])

Stability of the pressure within the inlet system was aided by the incorporation of an expansion volume of 1 litre (C) and a section of glass tubing formed into a spiral (not shown) in the system. The maximum pressure produced in the ion-source was ca.0.1

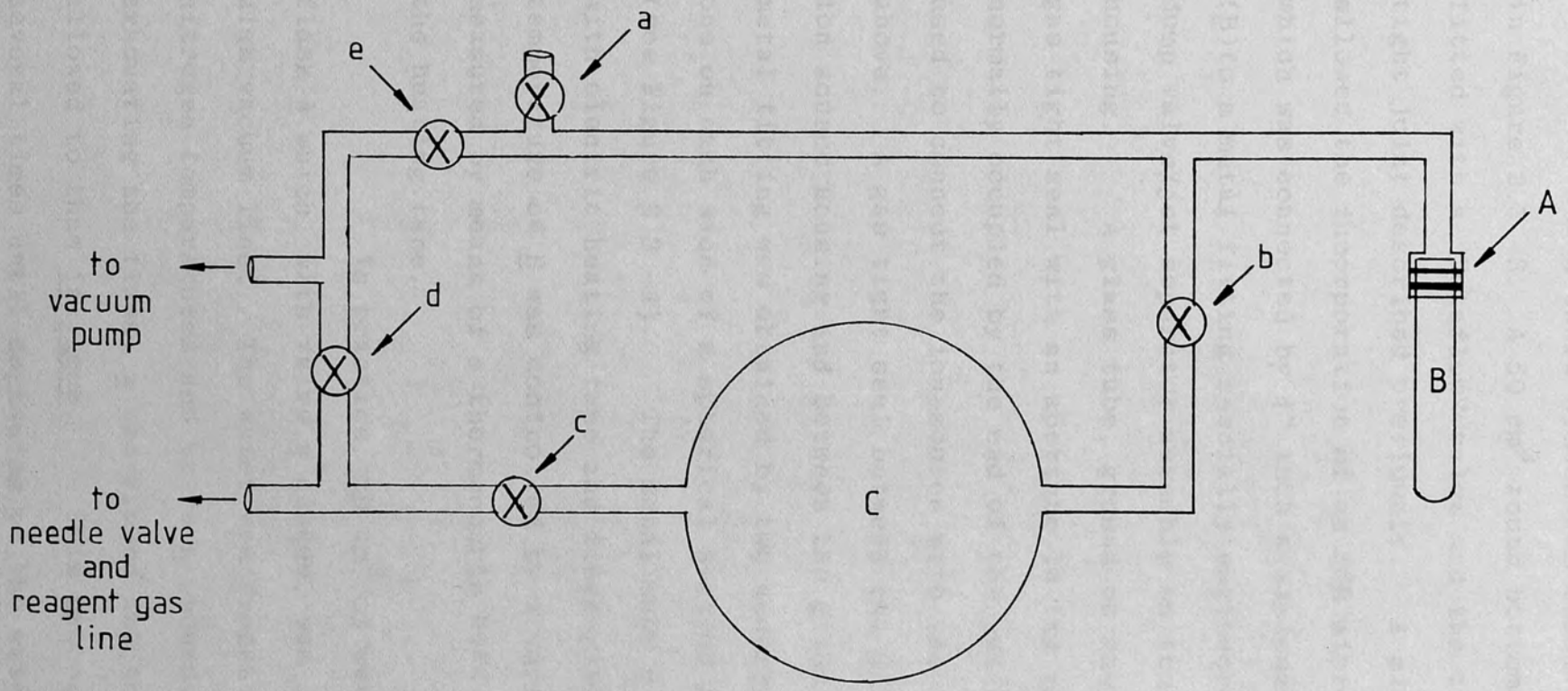

Figure 2.3-2: Schematic diagram of gas-handling system used for water, deuterium oxide and ammonia-d_3.

Torr (the higher limit in the pressure range of interest).

A third system was constructed, as shown in Figure 2.3 -3. A 50 cm^3 round bottomed flask was fitted with a "Rotaflow" valve and the type of gas tight joint described previously. A glass to metal seal allowed the incorporation of an SGE micro-needle valve, b, which was connected by ¼" inch stainless steel tubing (B)to a metal fitting specially engineered to replace the dump valve/jet separator assembly on the ion source housing. A glass tube, ground on one end to form a gas tight seal with an aperture in the ion-source normally occupied by the end of the jet separator, was used to connect the ion-source with the fitting described above. A gas tight seal between the glass tube and the ion source housing and between the glass tube and the metal fitting was obtained by two neoprene "O" rings, one on each side of a spherical section in the glass tube (see Figure 2.3 -4). The metal tube B was wrapped with electric heating tape and fibre-glass tape. The temperature of B was controlled by a variac and measured by means of a thermocouple held next to B by the heating tape.

In practice, 10 cm^3 of water was placed in flask A which, with valve a closed, was connected to a high vacuum line. The water was frozen at liquid nitrogen temperatures and valve a opened. After evacuating the flask, a was closed and the water was allowed to thaw *in vacuo*. This process was repeated several times until degassing of the water was complete.

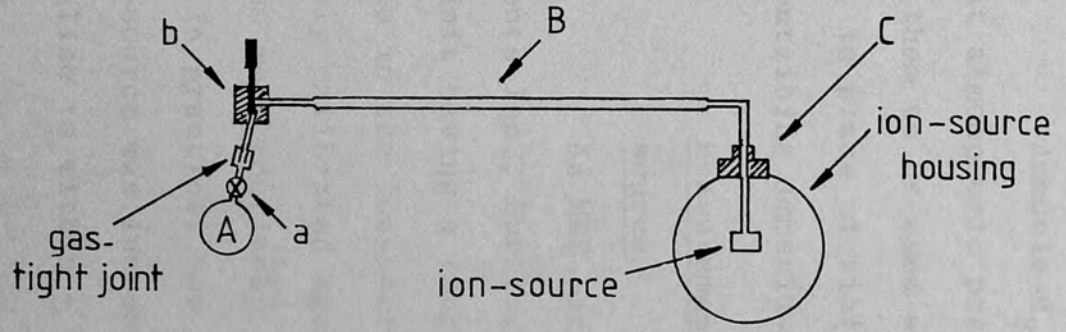

Figure 2.3-3: Schematic diagram of system used to generate pressures of up to 0.4 Torr of water and deuterium oxide vapour in the ion-source.

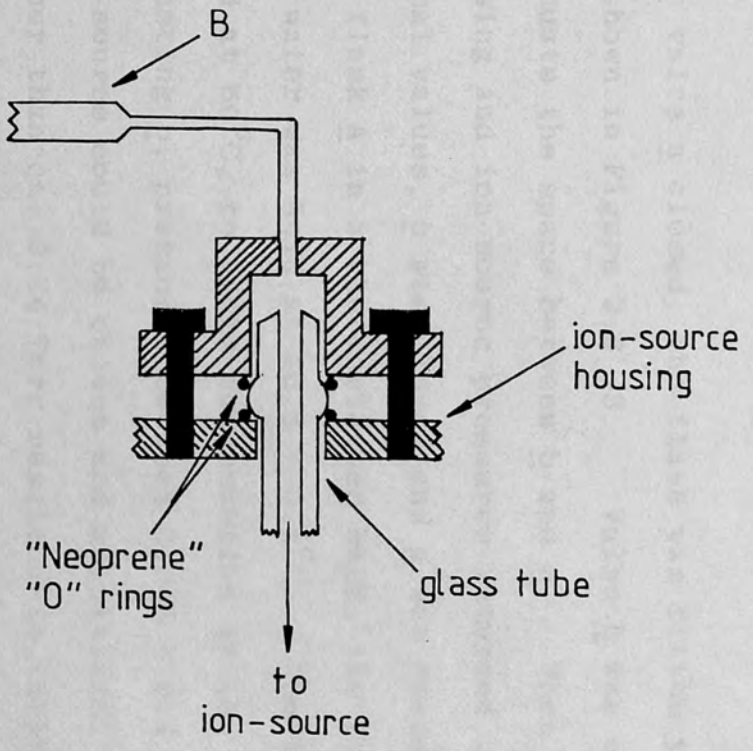

Figure 2.3-4: Schematic cross-section of assembly "C" (see Figure 2.3-3).

With valve a closed, the flask was fitted to the system as shown in Figure 2.3 -3. Valve b was opened to evacuate the space between b and a. When the source housing and ion-source pressures returned to their normal values, b was closed and a was opened. By placing the flask A in a thermostatted bath, the temperature of the water was held at 25.5 ± 0.1°C. The line B was held at 60°C, to avoid condensation in the line. By adjusting b, pressures between 0.005 - 0.4 Torr in the ion-source could be chosen and maintained. Pressures higher than ca. 0.34 Torr resulted in failure of the filament. Deuterium oxide was introduced in the same manner.

Ammonia-d_3 was supplied in 1 litre flasks at atmospheric pressure. The joints on the flasks allowed them to be used with the system shown in Figure 2.3 - 2, in place of vial B. The temperature of the flask containing ammonia-d_3 was not thermostatted.

2.4. Measurement of gas pressures in the ion-source

An MKS Baratron pressure gauge (MKS Instruments Inc., Burlington, Massachusetts) fitted with a head unit having a range of 1 Torr was used to monitor pressures in the ion-source. This gauge had been previously calibrated against a Bourdon-tube gauge. Pressures were routinely recorded to a precision of 10^{-4} Torr. In practice, the pressure of the reagent gas in the ion-source was increased incrementally and allowed to stabilise to within ± 0.5 m Torr before spectra were recorded.

2.5. Measurement of the variation of ion-abundances with pressure.

2.5.1 Experimental conditions.

2.5.1.1 Methylamine, dimethylamine and trimethylamine.

For each of these gases, the source temperature was maintained at 177 ± 1°C, the emission current was 20μA, the electron beam energy was 50 eV and the accelerating voltage was 4 KV. (Unless specified otherwise, these instrumental parameters were the same in every experiment).

The pressure was increased by 5 m Torr increments between 5 and 80 m Torr. At each pressure, spectra were recorded at several repeller voltages ranging from ca. 0.5 to 6 volts.

For each amine, another experiment was performed in which the pressure was increased from 5-400 m Torr in 10 m Torr increments.

Here, spectra were obtained with the repeller voltages of 0.5, 1.5, 2.5, 3.5 and 4.5 volts.

2.5.1.2 Ammonia-d_3.

Two 1 litre flasks of ammonia-d_3 at atmospheric pressure were obtained from a commercial source. One of these was connected to the system shown in Figure 2.3 -2, as described in section 2.3. The inlet system, reagent gas-line and ion-source were slowly flushed with the deuterated ammonia. When the mass spectrum indicated that hydrogen-deuterium exchange

was no longer occurring in the system, the 1-litre flask was replaced with the second flask. The pressure was varied from 5 - 280 m Torr in 10 m Torr increments. The ion-source pressure would not stabilise sufficiently above 280 m Torr and the experiment was terminated at this point. At each stage, spectra were obtained with repeller voltages equal to ca.0.5, 1.5, 2.5, 3.5 and 4.5 volts.

2.5.1.3 Water.

Using the inlet system shown in Figure 2.3 -2, water vapour was introduced into the ion-source and spectra obtained at 5 m Torr intervals from ca.5-60 m Torr. At each pressure, spectra were obtained with repeller voltages equal to 1,2,3,4 and 5 volts.

A further study in the pressure range 10 - 340 m Torr was performed, using the inlet system illustrated in Figure 2.3 -3. The accelerating voltage was reduced to 2KV owing to the tendency for arcing to occur in the glass tube at higher voltages. The other instrumental parameters were the same as described in Section 2.5.1. Spectra were obtained at 10 m Torr intervals and with repeller voltages of ca. 0.5, 1.5, 2.5, 3.5 and 4.5 volts.

2.5.1.4 Deuterium oxide.

Two investigations of deuterium oxide were undertaken. In the first study, using the system shown in Figure 2.3 -2, the pressure of deuterium oxide in the ion-source was varied from 5 - 90 m Torr in 5 m Torr stages and spectra were recorded with repeller voltages of 1,2,3,4 and 5 volts at each setting.

In the second experiment, the pressure was varied in the range 10 - 400 m Torr in ca. 10 m Torr intervals.

The same procedure as that described in Section 2.5.1.3 for the investigation of water vapour in this pressure region was followed. At every pressure interval spectra were obtained with the repeller voltage set at 1,2,3,4 and 5 volts.

2.5.2 Calculation of relative ion-abundances.

The heights of the peaks in the spectra were measured as described in Section 2.2 and corrected by means of equations (2.2 -1) and (2.2 -2). The relative abundance (normalised intensity) of an ion having $m/z = n$ is determined by dividing the height of the corresponding peak (I_n) by the sum of the heights of all the peaks in the spectrum (ΣI). Plots of the normalised intensities ($I_n/\Sigma I$) of reactant ions versus pressure were used to establish the kinetics of the corresponding reactions. (See Sections 3.2.1 - 3.2.6).

3. RESULTS

3.1 Determination of ion-molecule reaction rate coefficients by a continuous ion-extraction method.

Since the number of ions in the ion-source is necessarily very low in comparison to the number of neutral molecules present, reactions between ions and neutral molecules are far more probable than reactions between ions and neutral fragments, formed by the fragmentation of primary or secondary ions. In addition, the decrease in the neutral molecule concentration, resulting from ion molecule reactions is negligible. Thus, the ion-molecule reactions occurring in the ion-source are expected to follow pseudo first order kinetics.

The disappearance of R^+ in the ion-molecule reaction

$$R^+ + M \xrightarrow{k_n} \text{products}$$

can be described by the rate equation

$$-\frac{d\{R^+\}}{dt} = k_n\{R+\}\{M\} \qquad (3.1\text{ -}1)$$

Integration of (3.1 -1) gives

$$\ln(\{R^+\}/\{R^+\}_o) = -k_n\{M\}\,\tau \qquad (3.1\text{ -}2)$$

where $\{R^+\}$ is the abundance of R^+, $\{R^+\}_o$ is the abundance of R^+ in the absence of reaction, $\{M\}$ the number density (molec cm^{-3}) of M, τ the residence time (seconds) of R^+ in the ion-source and k_n the experimental rate coefficient. Assuming that normalised intensities truly reflect the

abundances of the corresponding ion in the ion source, equation (3.1 -2) may be written,

$$\ln (I_n/\Sigma I) = -k_n\{M\}\tau + \ln (I_n^o/\Sigma I^o) \qquad (3.1\text{ -}3)$$

($m/z = n$ for R^+).

The number density of M may be calculated from the equation of state for an ideal gas:

$$\{M\} = P_M/k_BT = P_MN \qquad (3.1\text{ -}4)$$

where P_M is the pressure of M (Nm^{-2}). k_B is Boltzman's constant (1.3806×10^{-23} JK^{-1}) and T is the absolute temperature. When P_M is measured in units of Torr, N contains the needed conversion factors and at the ion-source temperature employed for the experiments described herein (e.g. 450^oK) is equal to 2.146×10^{16}. Equation (3.1 -3) becomes

$$\ln (I_n/\Sigma I) = -k_nNP_M\tau + \ln(I_n^o/\Sigma I^o) \qquad (3.1\text{ -}5)$$

Thus, by plotting $\ln (I_n/\Sigma I)$ versus P_M, a straight line of slope $-k_nN\tau$ is obtained and if the residence time of R^+, τ, is known or can be calculated, then a value for the experimental rate coefficient k_n may be determined.

The ion-molecule reactions of the primary ions in the mass spectra of the six gases investigated were studied at low pressures with P_M <0.1 Torr. At such pressures it may be assumed that an ion experiences only a few collisions with the neutral molecule before leaving the ion-source and that these collisions do not significantly change the velocity of the ion. Under such

conditions the residence time of an ion in the ion-source may be calculated from the free-fall formula:[75]

$$\tau = (2\ md/zE)^{\frac{1}{2}} \qquad (3.1\ -6)$$

where d is the mean distance travelled by the ion (m), m is the mass (kg) of the ion, z is the charge (C) of the ion and E is the electric field strength, (Vm^{-1}). Assuming that the ion-plasma occupies the volume between the repeller plate and the ion-exit slit, the maximum distance the ions would have to travel is equal to the distance from the repeller plate to the ion exit slit (ℓ). Thus the mean distance travelled by the ions is 0.5 ℓ and, in this work, d was taken to be 0.2 cm. Since the ion-source used for this study has the electron-beam entrance port placed halfway between the repeller plate and the plate in which the ion exit slit is cut, the assumption of d = 0.2 cm is equally valid if a model is postulated in which the ions travel from an infinitely narrow ionising beam to the ion exit slit.

The clustering reactions observed occur at higher pressures at which the effects of collisions or the ion-velocities become significant and thus ion-mobilities have to be considered. Equation (3.1 -7) describes the drift velocity v of an ion having an ion-mobility K in an electric field of strength E.

$$v = KE \qquad (3.1\ -7)$$

If an experimental value of K is not available a calculated

value may be determined by means of equation (3.1 -8) from the reduced mobility K_o, the pressure P (Torr) and the absolute temperature T.

$$K = K_o\ (760/P)\ (T/273) \qquad (3.1\text{ -}8)$$

In turn, the reduced mobility may be calculated from equation (3.1 -9), where α is the angle averaged polarisability ($\mathring{A}^3$) of the neutral and μ is the reduced mass (atomic mass units).[76]

$$K_o = 13.876\ (\alpha\mu)^{\frac{1}{2}} \qquad (3.1\text{ -}9)$$

Since $\tau = d/v$, it can be seen that

$$\tau = 273(\alpha\mu)^{\frac{1}{2}} dP_M/(10546ET) \qquad (3.1\text{ -}10)$$

where d is taken to be 0.2 cm.

Thus, when the effects of collisions are important, the residence time is directly proportional to the pressure. If β is defined as τ/P_M, equation (3.1 -5) becomes

$$\ln\ (I_n/\Sigma I) = -k_n N\beta P_M^{\,2} + \ln\ (I_n^{\,o}/\Sigma I^o) \qquad (3.1\text{ -}11)$$

Experimental rate constants, k_n, for ions reacting at higher ion-source pressures can be obtained from the slopes of plots of $\ln(I_n/\Sigma I)$ against $P_M^{\,2}$.

3.2 Kinetic studies of ion-molecule reactions occurring in pure gases.

3.2.1 Methylamine

3.2.1.1 Evaluation of the disappearance rate coefficients of primary ions in methylamine -

The molecular ion $M^{+\cdot}$ and $(M - H)^+$ ion are the major primary ions in the mass spectrum of methylamine. These ions readily undergo proton transfer reactions with methylamine to give the $(M + H)^+$ ion [57,77,78], as shown in Schemes 3.2.1.1 -1 and 3.2.1.2 -2.

$$\underset{\text{m/z 31}}{CH_3NH_2^{+\cdot}} + CH_3NH_2 \longrightarrow \underset{\text{m/z 32}}{CH_3NH_3^+} + CH_2NH_2\cdot$$

Scheme 3.2.1.1 -1

$$\underset{\text{m/z 30}}{CH_2NH_2^+} + CH_3NH_2 \longrightarrow \underset{\text{m/z 32}}{CH_3NH_3^+} + CH_2NH$$

Scheme 3.2.1.1 -2

(Small peaks corresponding to m/z 45, m/z 46, m/z 59 and m/z 60 were present and, together account for ca.3% of the total ion current at 0.11 torr. These ions arise from trace impurities of dimethylamine and trimethylamine.) A plot of the normalised intensities of m/z 29, m/z 30, and m/z 31 versus pressure is given in Figure 3.2.1.1 -1. In agreement with earlier reports[57,77] the formation of the protonated molecular ion, m/z 32, was the only product ion observed, arising from the reaction of the primary ions.

Plots of the Naperian logarithms of the

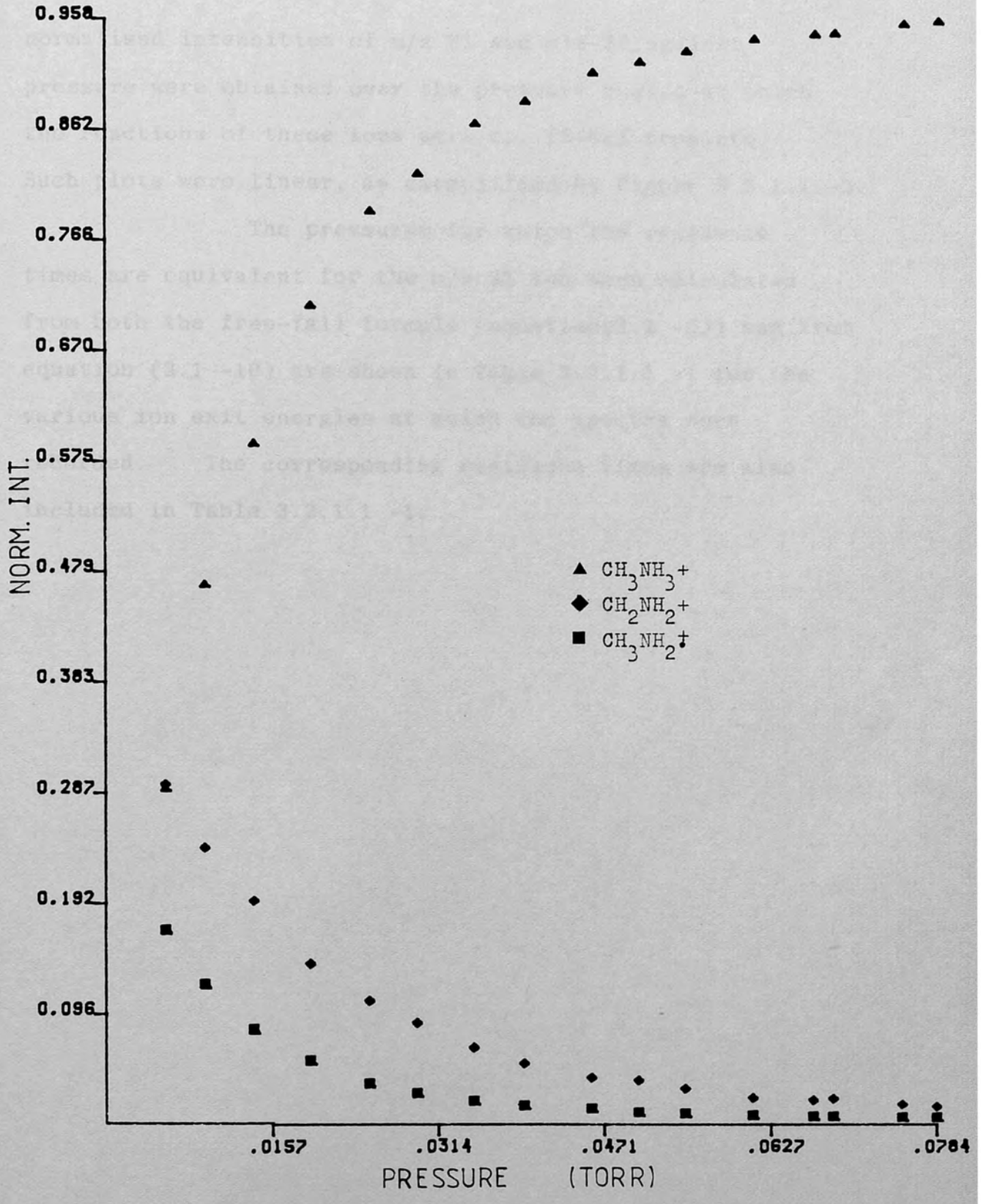

Figure 3.2.1.1-1 : Variation of normalised intensities of ions in methylamine with pressure (ion exit energy: 0.52 eV).

normalised intensities of m/z 31 and m/z 30 against pressure were obtained over the pressure region at which the reactions of these ions were ca. 75-85% complete. Such plots were linear, as exemplified by Figure 3.2.1.1 -2.

The pressures for which the residence times are equivalent for the m/z 31 ion when calculated from both the free-fall formula (equation(3.1 -6)) and from equation (3.1 -10) are shown in Table 3.2.1.1 -1 for the various ion exit energies at which the spectra were recorded. The corresponding residence times are also included in Table 3.2.1.1 -1.

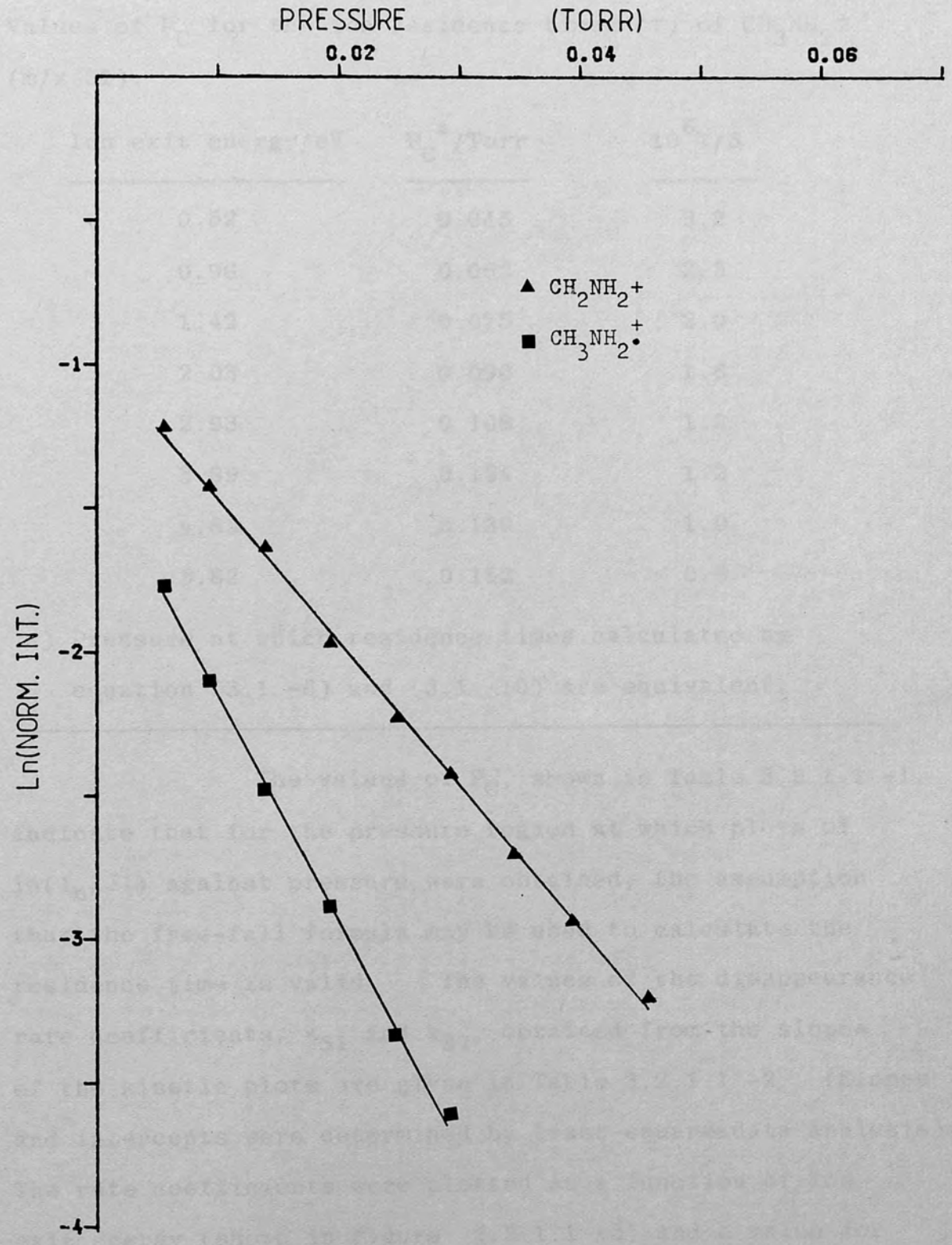

Figure 3.2.1.1-2: Kinetic plots for the reactions of methylamine primary ions with methylamine (ion exit energy: 0.52 eV).

TABLE 3.2.1.1 -1

Values of P_C for the ion residence times (τ) of $CH_3NH_2^+$ (m/z 31).

Ion exit energy/eV	P_C[a]/Torr	$10^6\tau$/S
0.52	0.045	3.2
0.96	0.062	2.3
1.42	0.075	2.0
2.03	0.090	1.6
2.93	0.108	1.3
3.89	0.124	1.2
4.85	0.139	1.0
5.82	0.152	0.9

a) Pressure at which residence times calculated by equation (3.1 -6) and (3.1 -10) are equivalent.

The values of P_C, shown in Table 3.2.1.1 -1, indicate that for the pressure region at which plots of $\ln(I_n/\Sigma I)$ against pressure were obtained, the assumption that the free-fall formula may be used to calculate the residence time is valid. The values of the disappearance rate coefficients, k_{31} and k_{30}, obtained from the slopes of the kinetic plots are given in Table 3.2.1.1 -2. (Slopes and intercepts were determined by least-squaresdata analysis). The rate coefficients were plotted as a function of ion exit energy (shown in Figure 3.2.1.1 -3) and a value for k_n^o corresponding to an ion exit energy of zero eV was determined by graphic extrapolation. (These extrapolated

values are indicated in Table 3.2.1.1 -2). As indicated by the curves in Figure 3.2.1.1 -3, a dependence of k_{30} and k_{31} upon ion exit energy was observed.

TABLE 3.2.1.1 -2

Disappearance rate coefficients[a] determined for the reactions of primary ions in methylamine at 450°K

Ion exit energy/eV	$10^{10}k_{30}$	$10^{10}k_{31}$
0	5.8[b]	10.0[b]
0.52	7.46 ± 0.22	11.5 ± 0.5
0.96	8.56 ± 0.23	12.8 ± 0.6
1.42	10.1 ± 0.3	14.1 ± 0.7
2.03	11.8 ± 0.4	15.6 ± 0.4
2.93	12.7 ± 0.4	16.0 ± 0.4
3.89	13.4 ± 0.4	17.9 ± 0.5
4.85	13.5 ± 0.8	17.8 ± 0.6
5.82	13.3 ± 0.4	17.7 ± 0.9

a) Units of $cm^3 molec^{-1} sec^{-1}$. Errors are with 95% confidence limits.

b) Extrapolated values from Figure 3.2.1.1 -3.

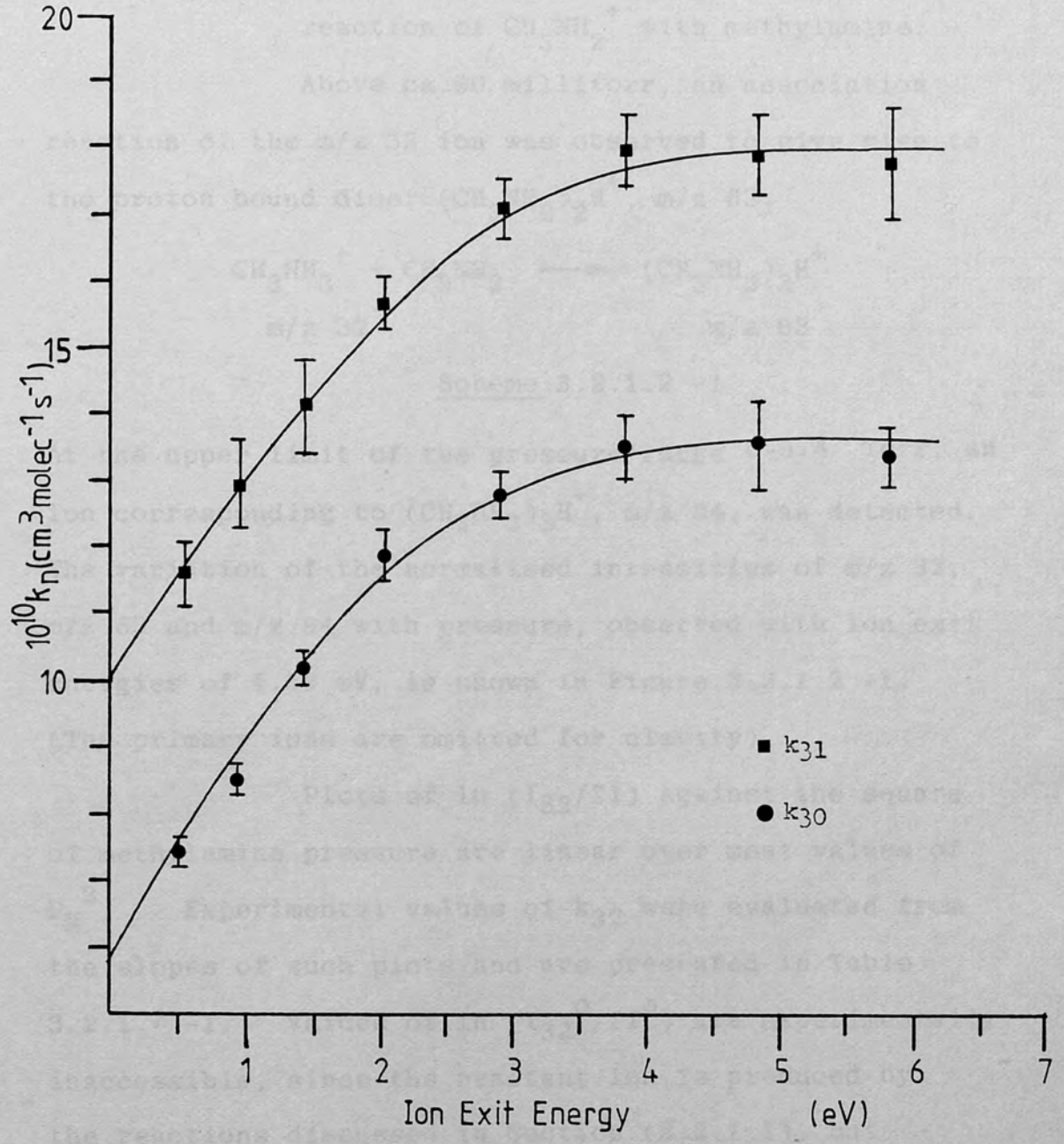

Figure 3.2.1.1-3 : Plots of disappearance rate coefficients of primary ions in methylamine against ion exit energy.

3.2.1.2 Kinetic studies of the association reaction of $CH_3NH_2^+$ with methylamine. - Above ca.80 millitorr, an association reaction of the m/z 32 ion was observed to give rise to the proton bound dimer $(CH_3NH_2)_2H^+$, m/z 63.

$$\underset{\text{m/z 32}}{CH_3NH_3^+} + CH_3NH_2 \longrightarrow \underset{\text{m/z 63}}{(CH_3NH_2)_2H^+}$$

Scheme 3.2.1.2 -1

At the upper limit of the pressure range 0-0.4 Torr, an ion corresponding to $(CH_3NH_2)_3H^+$, m/z 94, was detected. The variation of the normalised intensities of m/z 32, m/z 63 and m/z 94 with pressure, observed with ion exit energies of 4.59 eV, is shown in Figure 3.2.1.2 -1. (The primary ions are omitted for clarity).

Plots of ln $(I_{32}/\Sigma I)$ against the square of methylamine pressure are linear over most values of P_M^2. Experimental values of k_{32} were evaluated from the slopes of such plots and are presented in Table 3.2.1.2 -1. Values of ln $(I_{32}^o/\Sigma I^o)$ are experimentally inaccessible, since the reactant ion is produced by the reactions discussed in Section (3.2.1.1), but calculated values are obtained from the intercepts of kinetic plots. Such intercept values are also given in Table 3.2.1.2 -1. (A typical kinetic plot is shown in Figure 3.2.1.2 -2).

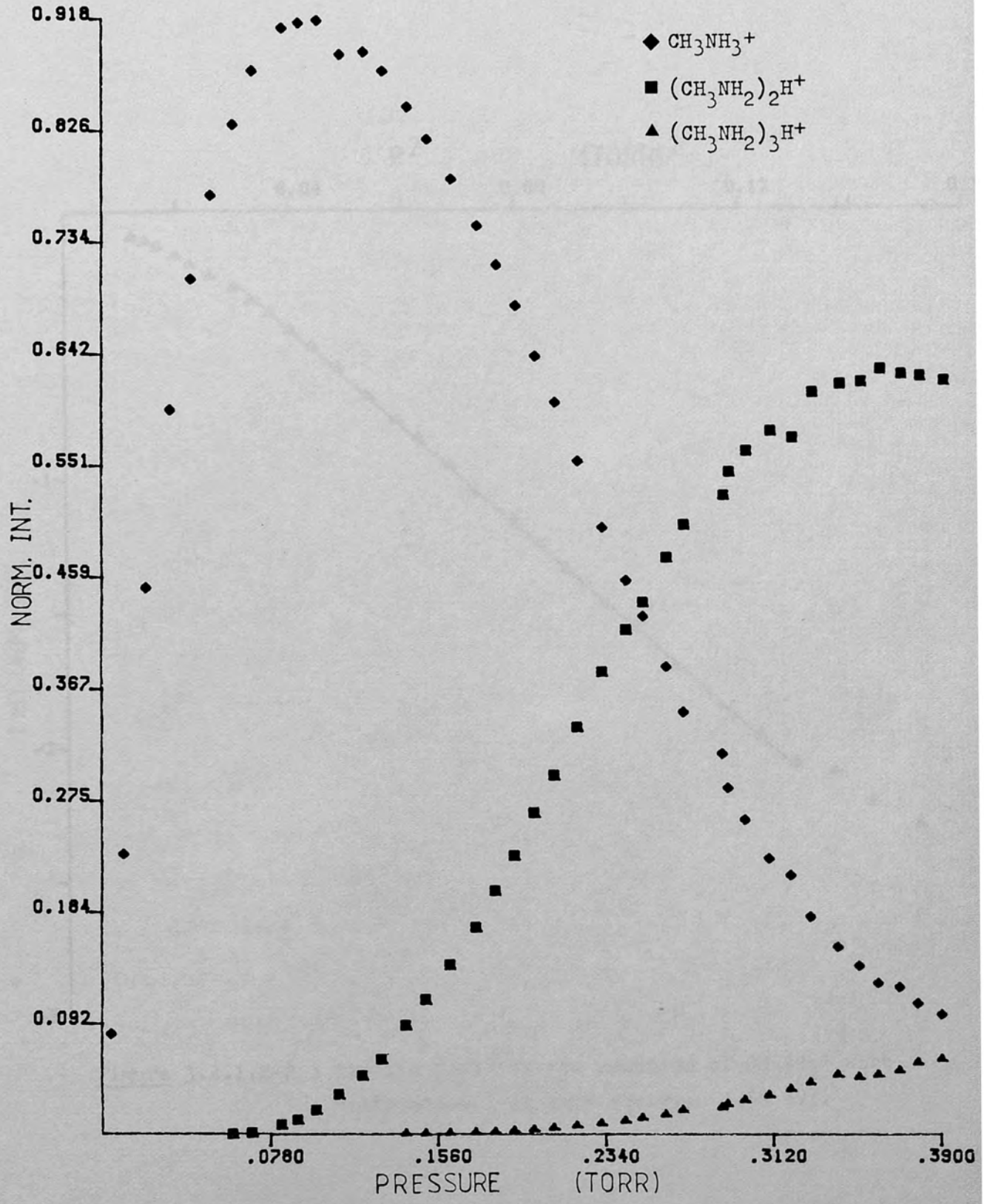

Figure 3.2.1.2-1 : Variation of normalised intensities of $CH_3NH_3^+$, $(CH_3NH_2)_2H^+$ and $(CH_3NH_2)_3H^+$ with methylamine pressure (ion exit energy: 4.59 eV).

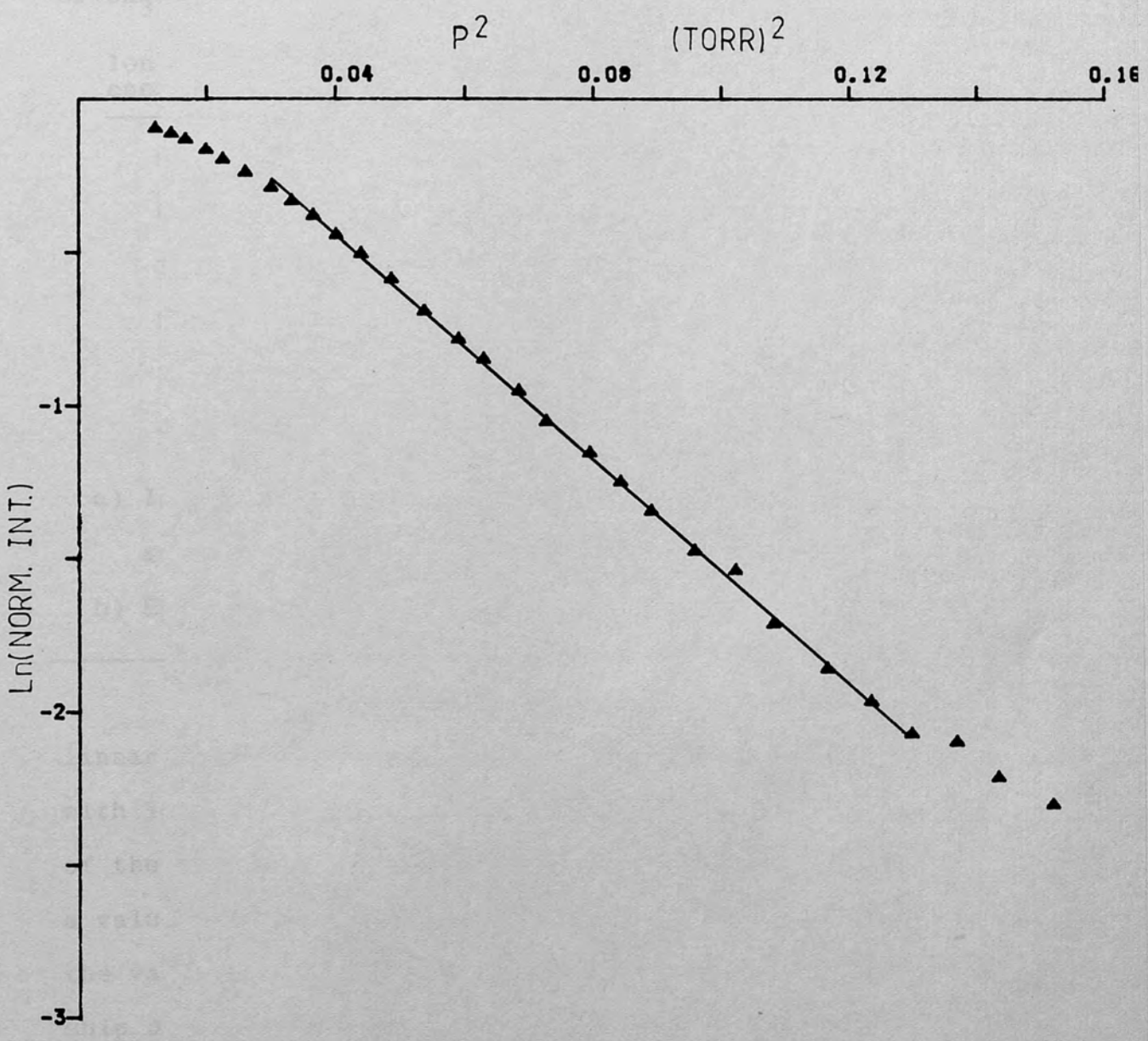

Figure 3.2.1.2-2 : Kinetic plot for the reaction of $CH_3NH_3^+$ with methylamine (ion exit energy: 4.59 eV).

TABLE 3.2.1.2 -1

Experimental values[b] of k_{32} for the clustering reaction of $CH_3NH_3^+$ with methylamine.

Ion exit energy/eV	$10^{11}k_{32}/cm^3molec^{-1}s^{-1}$	$\ln(I^o_{32}/\Sigma I_o)$
0	0.60 ± 0.02[a]	-
0.52	1.77 ± 0.04	0.07
1.53	3.92 ± 0.08	0.06
2.58	6.8 ± 0.1	0.15
3.58	9.0 ± 0.2	0.23
4.59	10.8 ± 0.1	0.30

a) Intercept value calculated by a weighted least squares fit for k_{32} versus ion exit energy.

b) Errors are with 95% confidence limits.

As evidenced by Figure 3.2.1.2 -3, a linear relationship was observed for the variation of k^o_{32} with ion exit energy. A weighted least squares analysis of the variation of k_{32} with ion exit energy resulted in a value of 0.60 ± 0.02 x 10^{-11} $cm^3molec^{-1}s^{-1}$ for k^o_{32}, the value of k_{32} at zero ion exit energy. The relationship observed between k_{32} and ion exit energy leads to the equation

$$k_{32} = (2.25V + 0.60) \times 10^{-11} \qquad (3.2.1.1\text{ -}1)$$

where V is the repeller voltage.

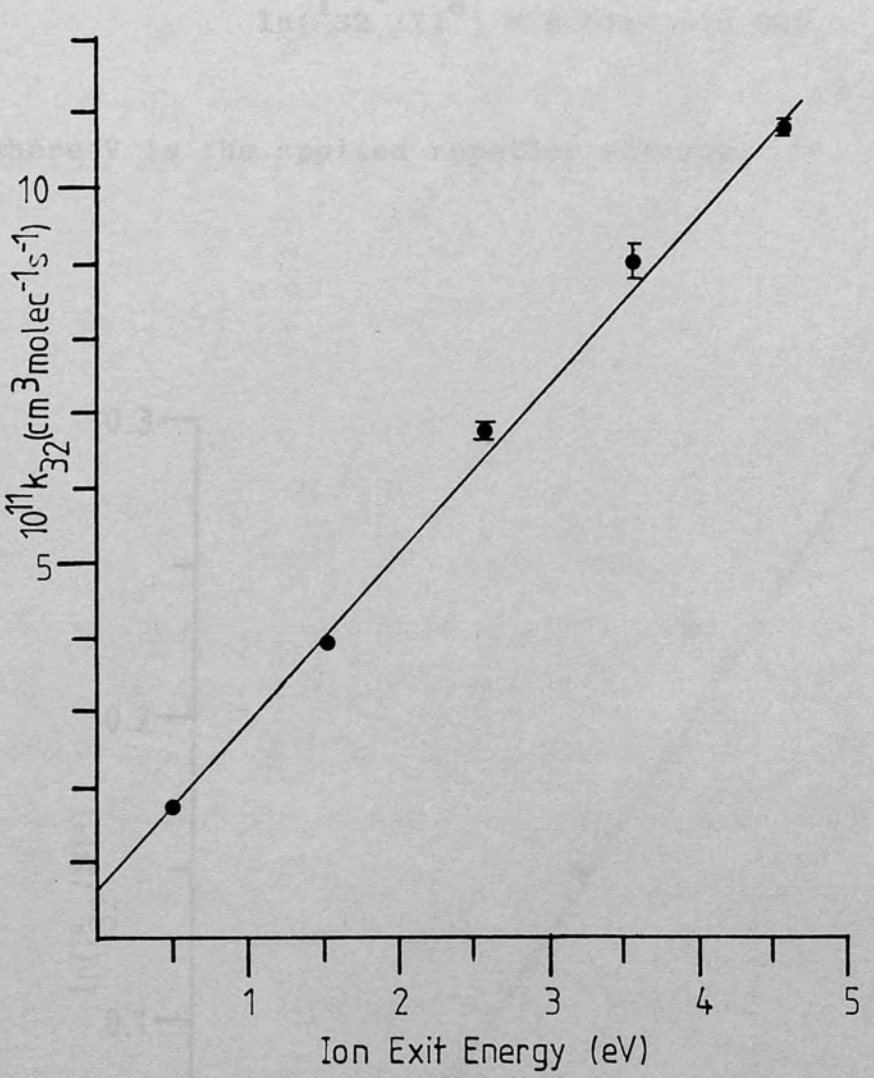

Figure 3.2.1.2-3 : Plot of k_{32} against ion exit energy for the association reaction of $CH_3NH_3^+$ with methylamine.

The value of $\ln ({}^{I}32^{o}/\Sigma I^{o})$ was found to vary linearly with ion exit energies greater than 1 eV (see Figure 3.2.1.2 -4) and is described by the equation:

$$\ln({}^{I}32^{o}/\Sigma I^{o}) = 0.078V - 0.056 \qquad (3.2.1.2\text{ -}2)$$

where V is the applied repeller voltage.

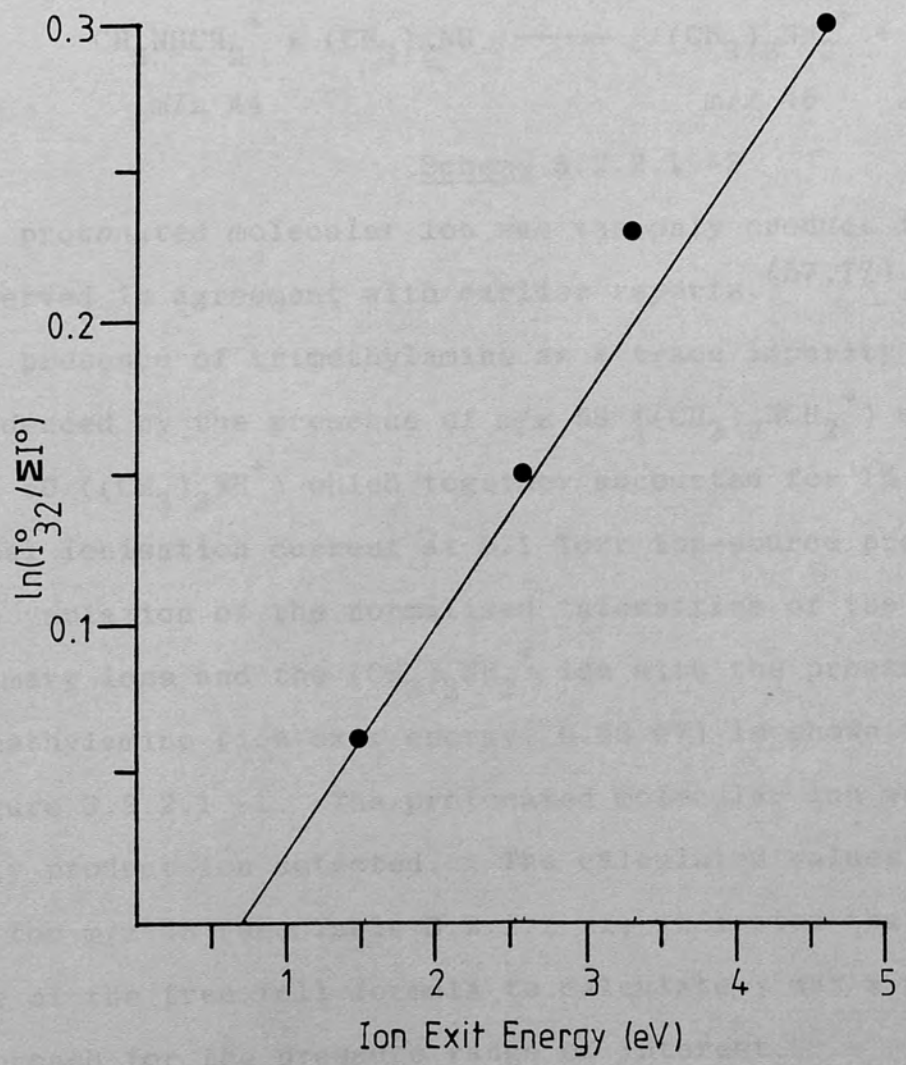

Figure 3.2.1.2-4 : Variation of $\ln(I^{o}_{32}/\Sigma I^{o})$ with ion exit energy.

3.2.2 Dimethylamine

3.2.2.1 Determination of the disappearance rate coefficients of primary ions in dimethylamine. -

The major primary ions in the mass spectrum of dimethylamine are m/z 45 and m/z 44, which undergo the following proton transfer reactions with dimethylamine:

$$\underset{\text{m/z 45}}{(CH_3)_2NH^{+\cdot}} + (CH_3)_2NH \longrightarrow \underset{\text{m/z 46}}{(CH_3)_2NH_2^{+}} + CH_3NHCH_2^{\cdot}$$

Scheme 3.2.2.1 -1

$$\underset{\text{m/z 44}}{CH_3NHCH_2^{+}} + (CH_3)_2NH \longrightarrow \underset{\text{m/z 46}}{(CH_3)_2NH_2^{+}} + CH_3NCH_2$$

Scheme 3.2.2.1 -2

The protonated molecular ion was the only product ion observed in agreement with earlier reports.[57,77] The presence of trimethylamine as a trace impurity was evidenced by the presence of m/z 58 ($(CH_3)_2NCH_2^{+}$) and m/z 60 ($(CH_3)_3NH^{+}$) which together accounted for 1% of the total ionisation current at 0.1 Torr ion-source pressure. The variation of the normalised intensities of the major primary ions and the $(CH_3)_2NH_2^{+}$ ion with the pressure of dimethylamine (ion exit energy: 0.52 eV) is shown in Figure 3.2.2.1 -1. The protonated molecular ion was the only product ion detected. The calculated values of P_C for m/z 45 (see Table 3.2.2.1 -1) indicated that the use of the free fall formula to calculate τ was a valid approach for the pressure range of interest.

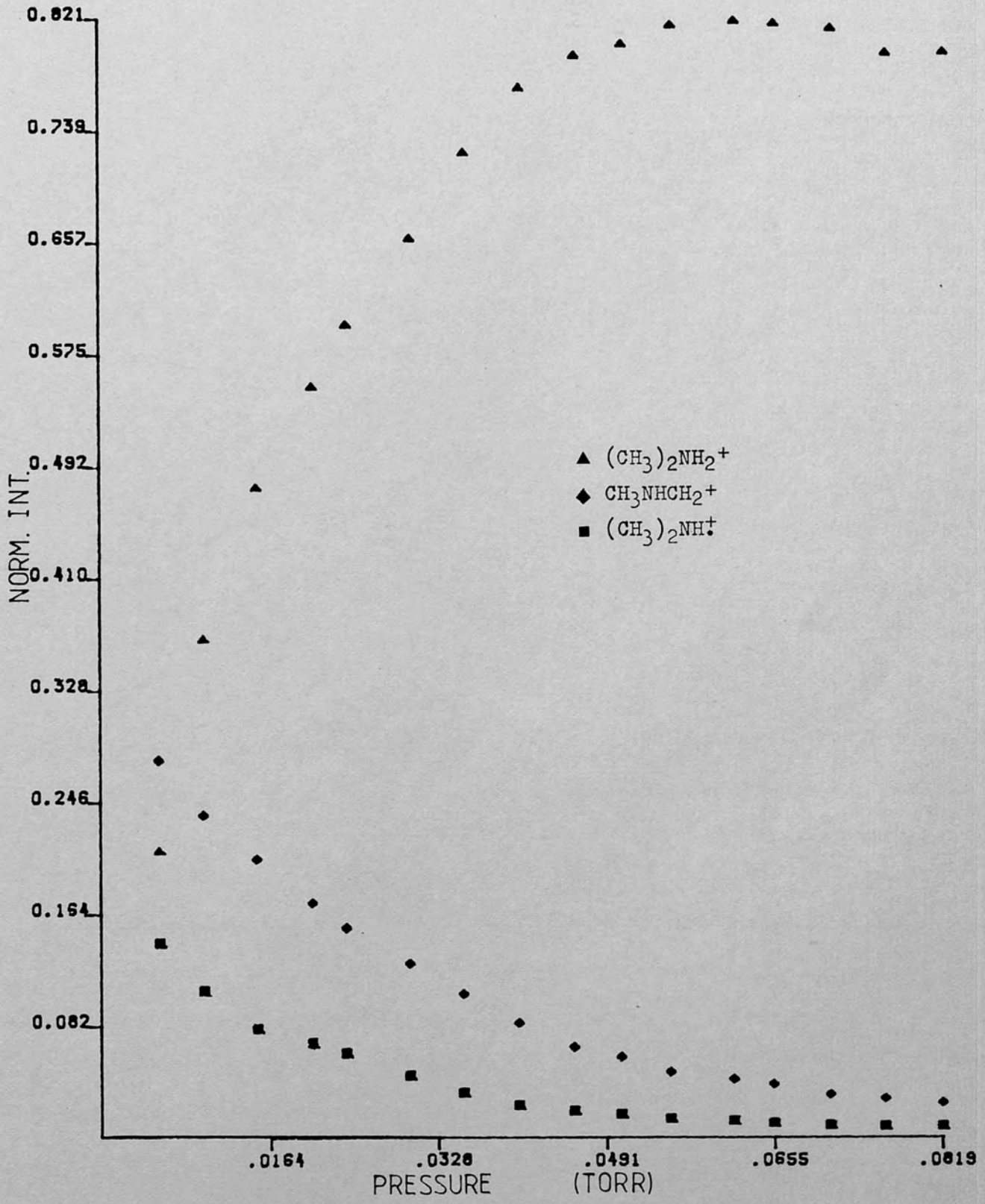

Figure 3.2.2.1-1 : Variation of normalised intensities of ions in dimethylamine with pressure (ion exit energy : 0.52 eV).

TABLE 3.2.2.1 -1

Values of P_C for the ion residence times (τ) of $(CH_3)_2NH^+$ (m/z 45)

Ion exit energy/eV	P_C^a/Torr	$10^6\tau$/s
0.52	0.038	3.8
0.96	0.051	2.8
1.42	0.063	2.3
2.03	0.075	1.9
2.44	0.081	1.8
3.41	0.096	1.5
3.89	0.103	1.4
4.40	0.110	1.3
5.33	0.121	1.2
6.31	0.131	1.1

a) Defined in Section 3.2.1.1

Figure 3.2.2.1 -2 shows the kinetic plot of the normalised intensities of $(CH_3)_2NH^+$ and $CH_3NHCH_2^+$, over the pressure range for which the greater portion of the ions react, at 0.52 eV ion exit energy. The disappearance rate coefficients for these ions, obtained for ion exit energies of 0.52 - 6.31 eV, are collected in Table 3.2.2.1 -2 and are plotted versus ion-exit energy in Figure 3.2.2.1 -3.

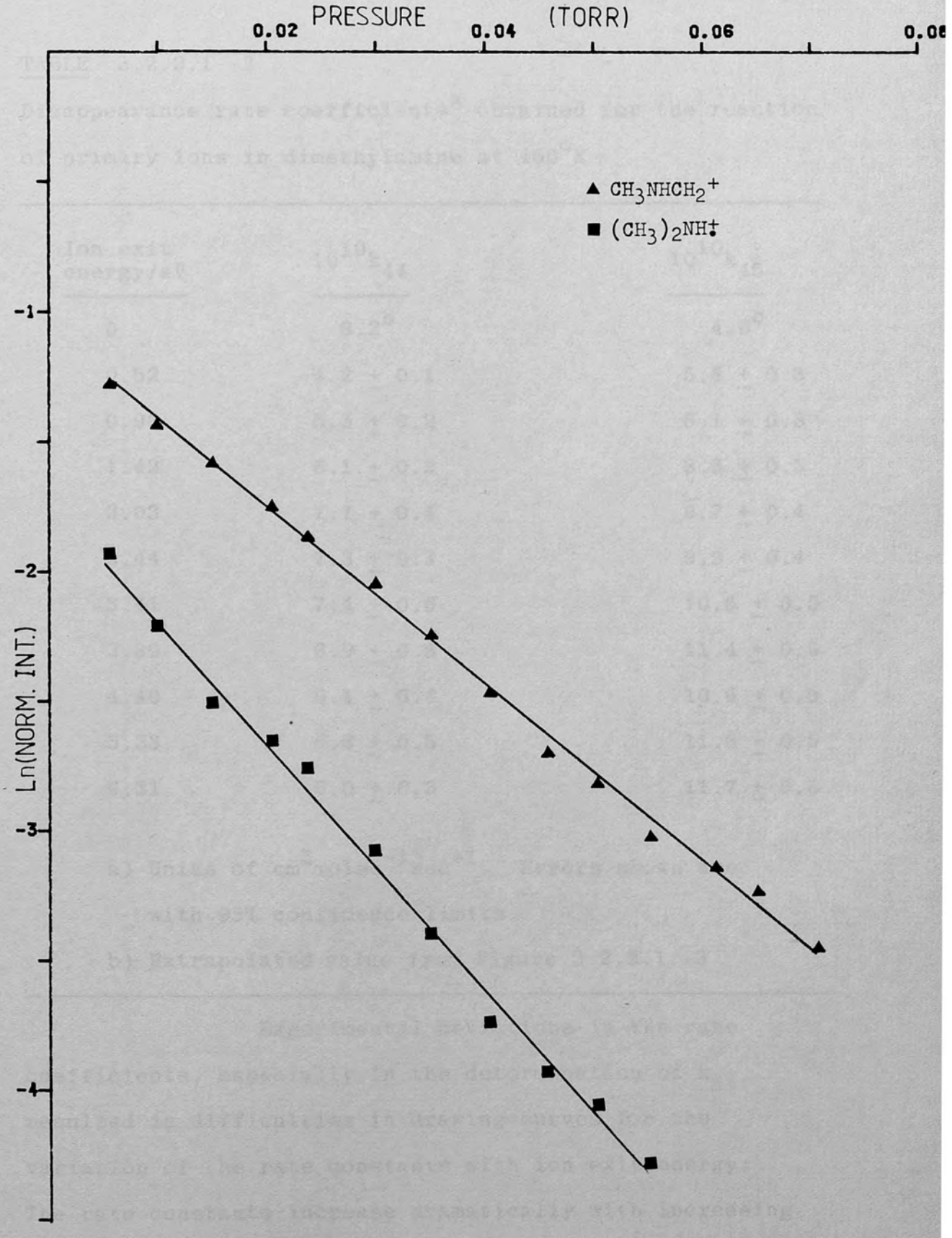

Figure 3.2.2.1-2 : Kinetic plots for the reaction of dimethylamine primary ions with dimethylamine (ion exit energy : 0.52 eV).

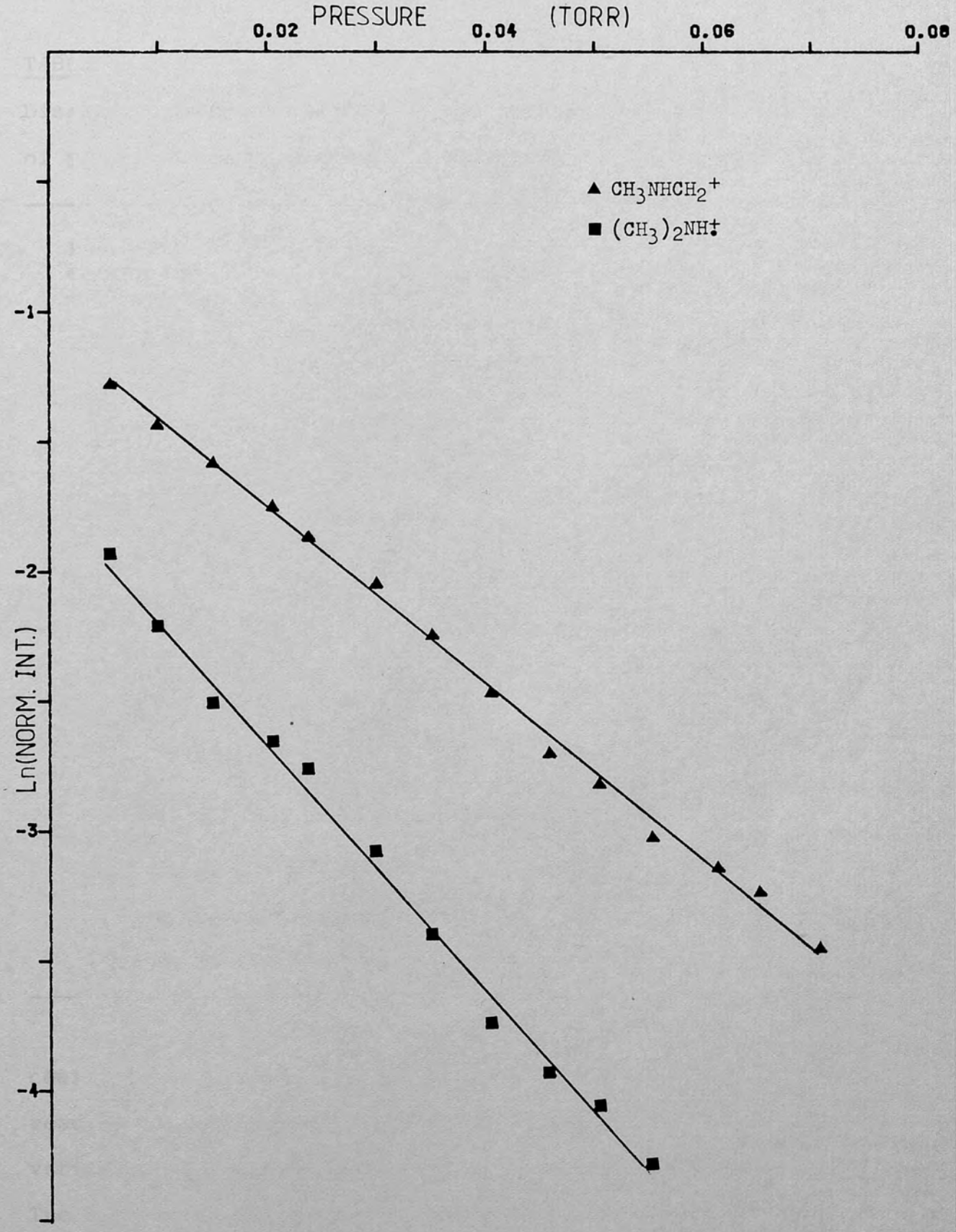

Figure 3.2.2.1-2 : Kinetic plots for the reaction of dimethylamine primary ions with dimethylamine (ion exit energy : 0.52 eV).

TABLE 3.2.2.1 -2

Disappearance rate coefficients[a] obtained for the reaction of primary ions in dimethylamine at 450°K

Ion exit energy/eV	$10^{10}k_{44}$	$10^{10}k_{45}$
0	3.2[b]	4.6[b]
0.52	4.2 ± 0.1	5.8 ± 0.3
0.96	5.5 ± 0.2	8.1 ± 0.3
1.42	6.1 ± 0.2	8.3 ± 0.3
2.03	7.7 ± 0.4	9.7 ± 0.4
2.44	7.3 ± 0.3	9.9 ± 0.4
3.41	7.4 ± 0.6	10.6 ± 0.5
3.89	6.9 ± 0.5	11.4 ± 0.5
4.40	6.1 ± 0.4	10.6 ± 0.5
5.33	6.6 ± 0.5	11.6 ± 0.5
6.31	6.0 ± 0.3	11.7 ± 0.5

a) Units of $cm^3 molec^{-1} sec^{-1}$. Errors shown are with 95% confidence limits.

b) Extrapolated value from Figure 3.2.2.1 -3

Experimental deviations in the rate coefficients, especially in the determination of k_{44}, resulted in difficulties in drawing curves for the variation of the rate constants with ion exit energy. The rate constants increase dramatically with increasing ion exit energies up to ca.3 eV and then appear to level off, similar to the trends observed for the primary ions

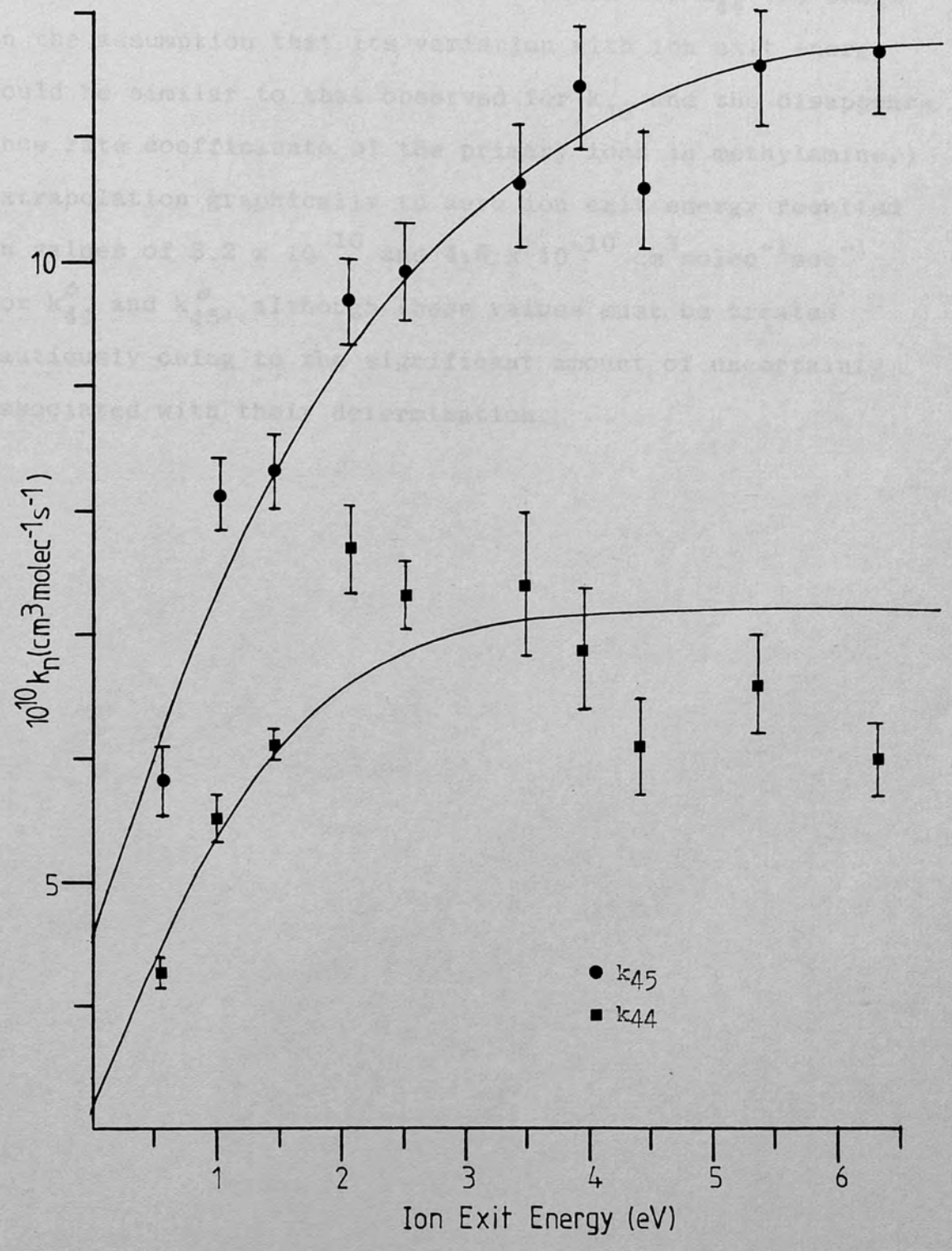

Figure 3.2.2.1-3 : Variation of the disappearance rate coefficients of primary ions in dimethylamine with ion energy.

in methylamine. (Indeed, the curve shown for k_{44} was based on the assumption that its variation with ion exit energy would be similar to that observed for k_{45} and the disappearance rate coefficients of the primary ions in methylamine.) Extrapolation graphically to zero ion exit energy resulted in values of 3.2×10^{-10} and 4.6×10^{-10} $cm^3 molec^{-1} sec^{-1}$ for k_{44}^o and k_{45}^o, although these values must be treated cautiously owing to the significant amount of uncertainty associated with their determination.

3.2.2.2 Kinetic studies of the formation of the cluster ion $((CH_3)_2NH)_2H^+$ in dimethylamine . -

At ion-source pressures greater than ca. 0.08 Torr, ions having m/z 91 and corresponding to the proton bound dimer $((CH_3)_2NH)_2H^+$ become prominent in the mass spectrum of dimethylamine (see Figure 3.2.2.2 -1). Above 0.14 Torr, plots of ln $(I_{46}/\Sigma I)$ versus the square of pressure becomes linear (a typical plot is shown in Figure 3.2.2.2 -2).

Experimental values of k_{46} for the reaction

$$\underset{\text{m/z 46}}{(CH_3)_2NH_2^+} + (CH_3)_2NH \longrightarrow \underset{\text{m/z 91}}{((CH_3)_2NH)_2H^+}$$

were obtained from the slopes of the linear portion of the kinetic plots and are given in Table 3.2.2.2 -1.

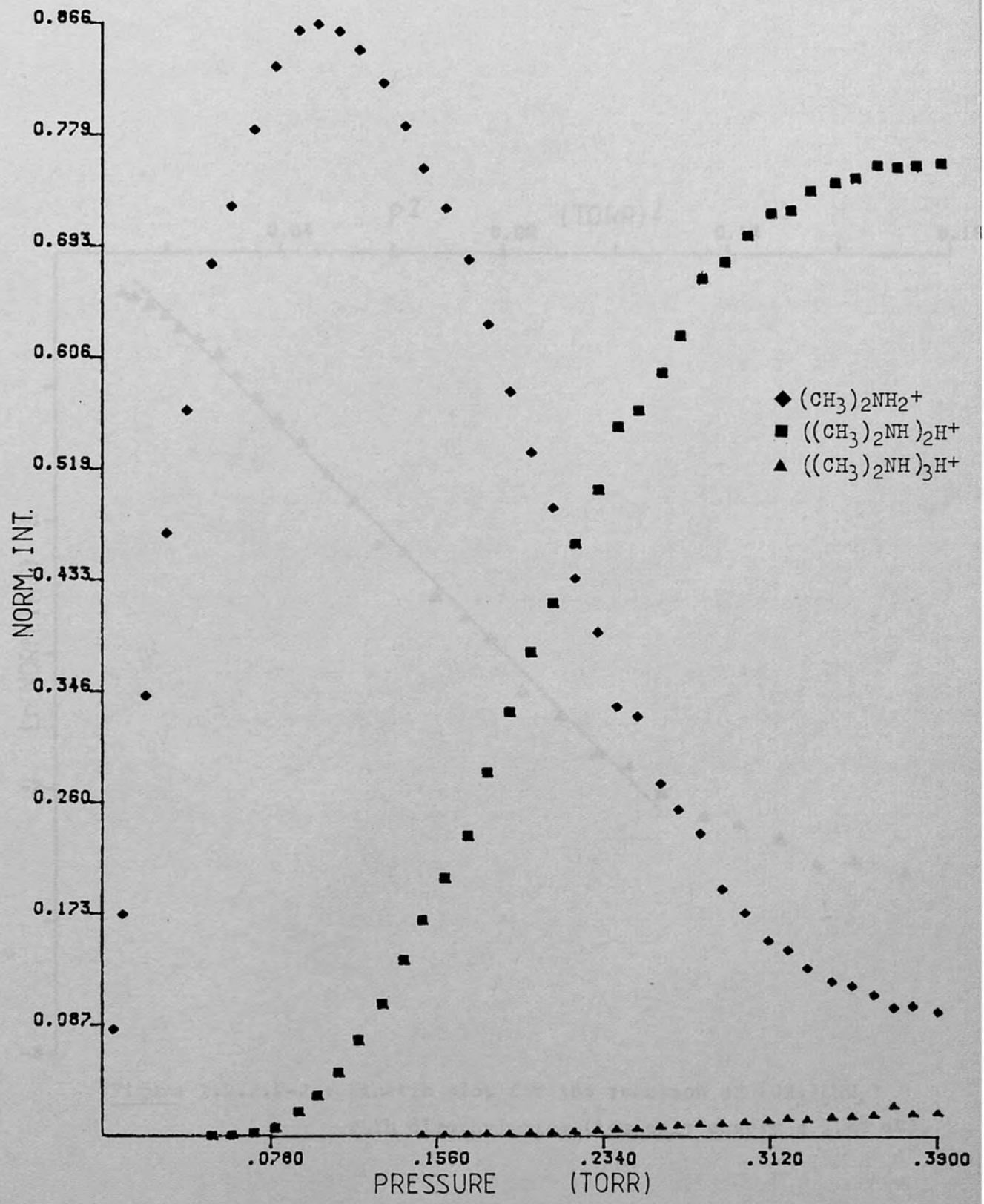

Figure 3.2.2.2-1 : Variation of normalised intensities of $(CH_3)_2NH_2^+$, $((CH_3)_2NH)_2H^+$ and $((CH_3)_2NH)_3H^+$ with dimethylamine pressure (ion exit energy : 3.58 eV).

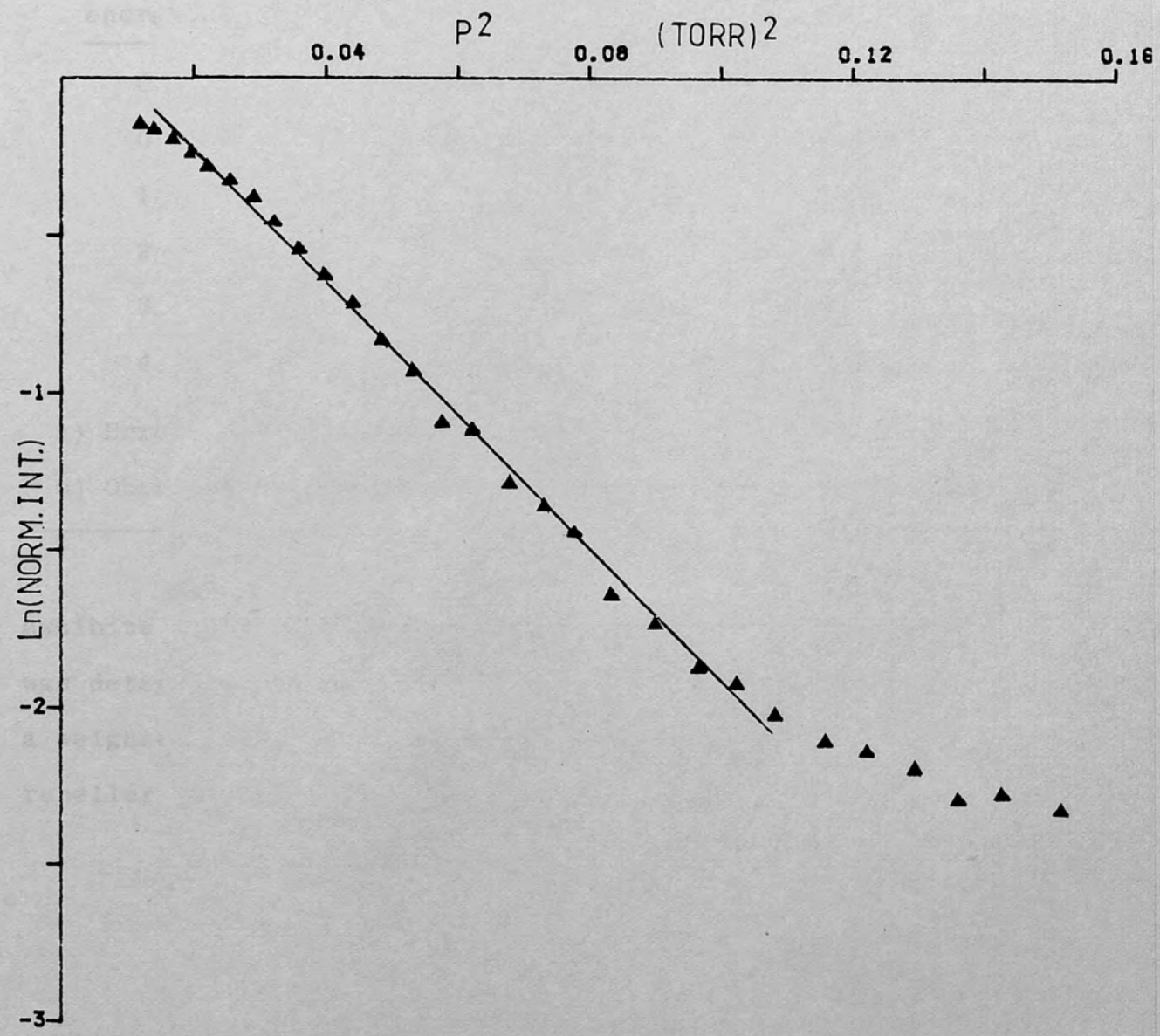

Figure 3.2.2.2-2 : Kinetic plot for the reaction of $(CH_3)_2NH_2^+$ with dimethylamine (ion exit energy : 3.58 eV).

TABLE 3.2.2.2-1

Experimental values[a] of k_{46} for the association reaction of $(CH_3)_2NH_2^+$ with dimethylamine.

Ion exit energy/eV	$10^{11}k_{46}/cm^3molec^{-1}s^{-1}$	$\ln(I_{46}^o/\Sigma I^o)$
0	0.216 ± 0.012[b]	-
0.52	1.18 ± 0.02	0.04
1.53	3.18 ± 0.06	0.1
2.58	5.3 ± 0.1	0.3
3.58	6.7 ± 0.2	0.4
4.59	8.6 ± 0.2	0.6

a) Errors are with 95% confidence limits.

b) Obtained by a weighted least squares line fit to data.

A plot of k_{46} versus ion exit energy exhibits linearity, as shown in Figure 3.2.2.2 -3, and k_{46}^o was determined to be $0.22 \pm 0.01 \times 10^{-11} cm^3 molec^{-1} s^{-1}$ by a weighted least squares method. Thus k_{46} is related to repeller voltage (V) by the equation

$$k_{46} = (1.89V + 0.216) \times 10^{-11} \qquad (3.2.2.2\text{ -}1)$$

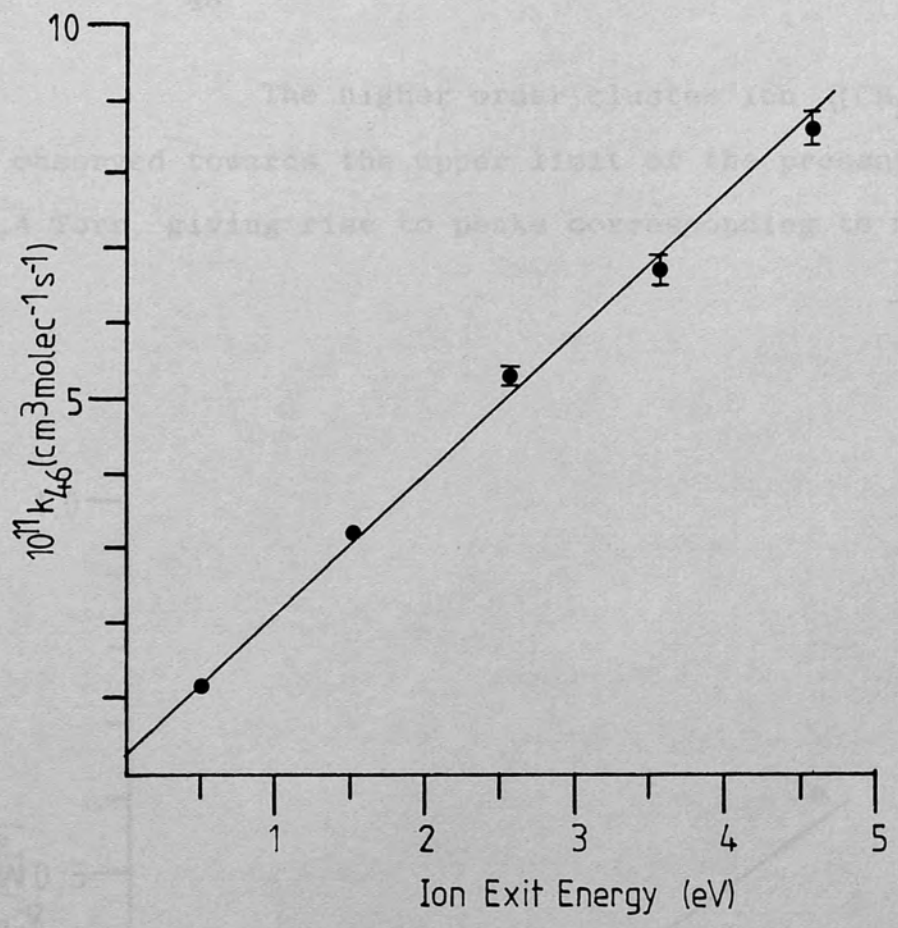

Figure 3.2.2.2-3 : Variation of k_{46} with ion exit energy for the reaction of $(CH_3)_2NH_2^+$ with dimethylamine.

A linear plot of ln ($I_{46}^{o}/\Sigma I_{o}$) against ion exit energy was obtained (shown in Figure 3.2.2.2 -4). Values of ln (I^{o}_{46}/ I_{o}) can be calculated by means of equation 3.2.2.2 -2), where V is the repeller voltage

$$\ln (I^{o}_{46}/\Sigma I^{o}) = 0.14V - 0.096 \qquad (3.2.2.2\ -2)$$

The higher order cluster ion $((CH_3)_2NH_2)_3H^+$ was observed towards the upper limit of the pressure region 0-0.4 Torr, giving rise to peaks corresponding to m/z 136.

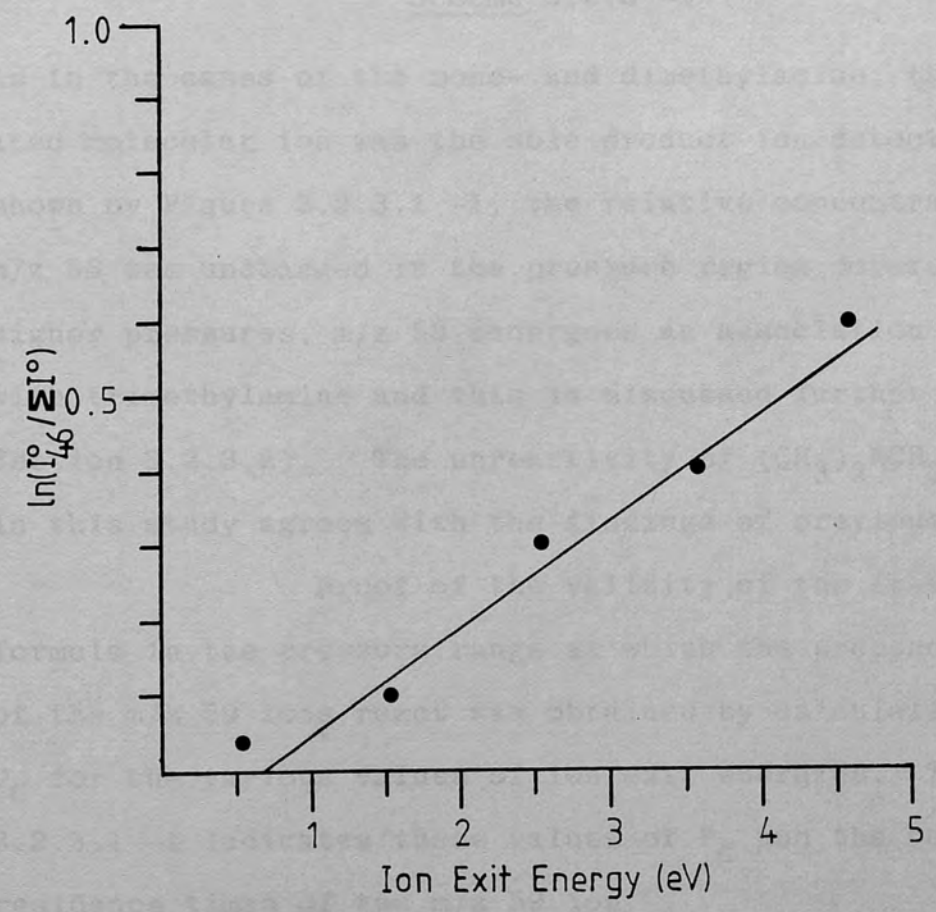

Figure 3.2.2.2-4 : Plot of $\ln(I^{o}_{46} / \Sigma I^{o})$ versus ion exit energy.

3.2.3 Trimethylamine

3.2.3.1 Determination of the disappearance rate coefficient of the $(CH_3)_2NCH_2^+$ ion in trimethylamine. -

The results of this study of the primary ions in the mass spectrum of trimethylamine in the pressure range 0-0.08 Torr and at ion exit energies of 0.52, 1.42, 2.44, 3.41 and 4.40 eV, indicate that of the two major primary ions (m/z 58 and m/z 59), only the m/z 59 ion undergoes a proton transfer reaction with trimethylamine.

$$\underset{\text{m/z 59}}{(CH_3)_3N^{+}\cdot} + (CH_3)_3N \longrightarrow \underset{\text{m/z 60}}{(CH_3)_3NH^{+}} + (CH_3)_2NCH_2\cdot$$

Scheme 3.2.3 -1

As in the cases of the mono- and dimethylamine, the protonated molecular ion was the sole product ion detected. As shown by Figure 3.2.3.1 -1, the relative concentration of m/z 58 was unchanged in the pressure region covered. (At higher pressures, m/z 58 undergoes an association reaction with trimethylamine and this is discussed further in Section 3.2.3.2). The unreactivity of $(CH_3)_2NCH_2^+$ observed in this study agrees with the findings of previous workers.[57,77]

Proof of the validity of the free fall formula in the pressure range at which the preponderance of the m/z 59 ions react was obtained by calculations of P_C for the various values of ion exit energies. Table 3.2.3.1 -1 indicates these values of P_C and the corresponding residence times of the m/z 59 ion.

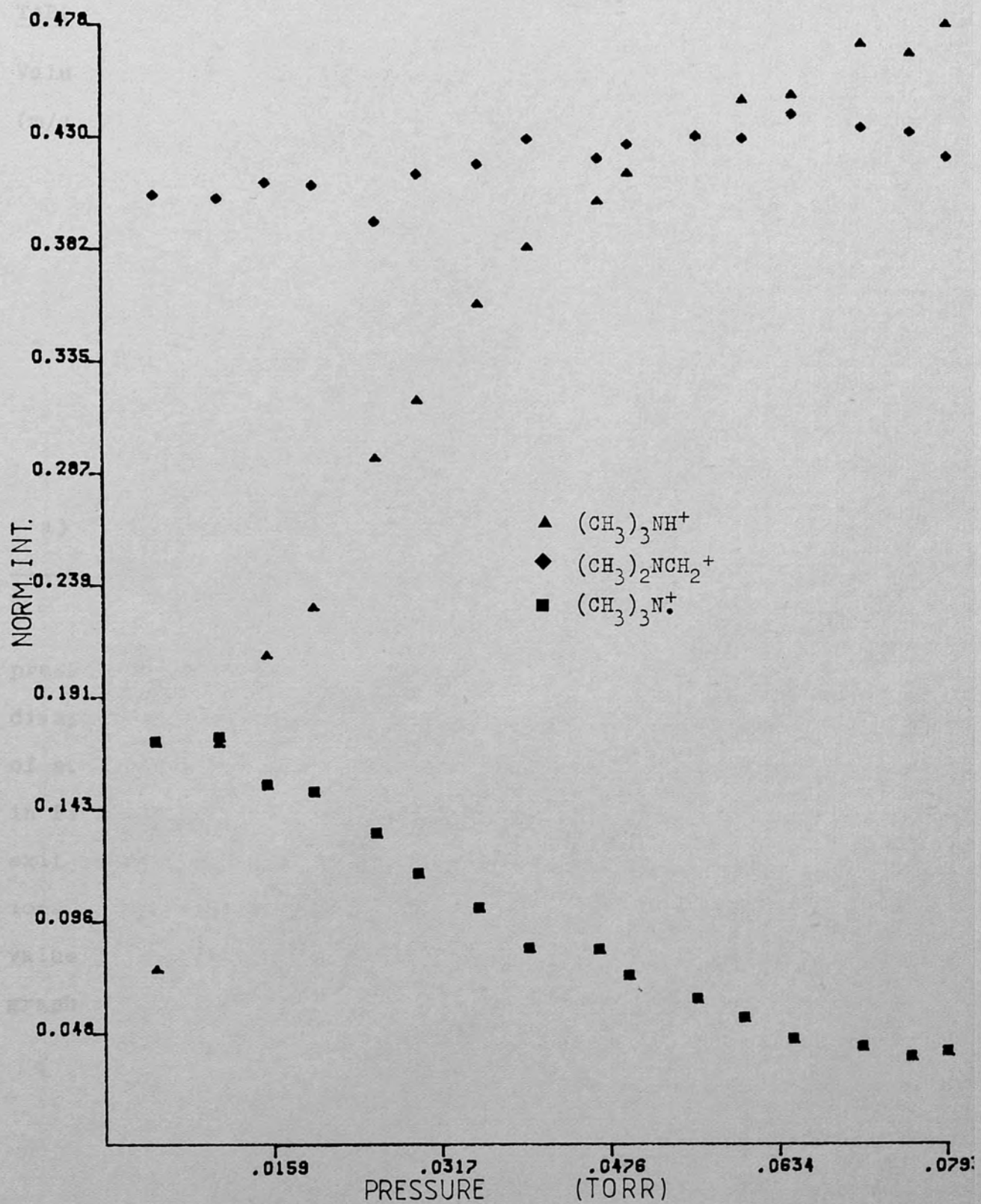

Figure 3.2.3.1-1 : Variation of normalised intensities of ions in trimethylamine with pressure (ion exit energy: 0.52 eV).

TABLE 3.2.3.1 -1

Values of P_C for the ion residence time (τ) of $(CH_3)_3N^{+\cdot}$ (m/z 59)

Ion exit energy/eV	P_C[a]/Torr	$10^6\tau$/s
0.52	0.033	4.4
1.42	0.054	2.6
2.44	0.071	2.0
3.41	0.084	1.7
4.40	0.095	1.5

a) Defined as in Table 3.2.1.1 -1

The plots obtained of $\ln(I_{59}/\Sigma I)$ against pressure were linear (see Figure 3.2.3.1 -2) and the disappearance rate coefficients obtained from the slope of such plots are given in Table 3.2.3.1 -2. As shown in Figure 3.2.3.1 -3, k_{59} displays a dependence upon ion exit energy, similar to that observed for the primary ions of methylamine and dimethylamine. An extrapolated value of $2 \times 10^{-10} cm^3 molec^{-1} s^{-1}$ for k_{59}^o was obtained graphically.

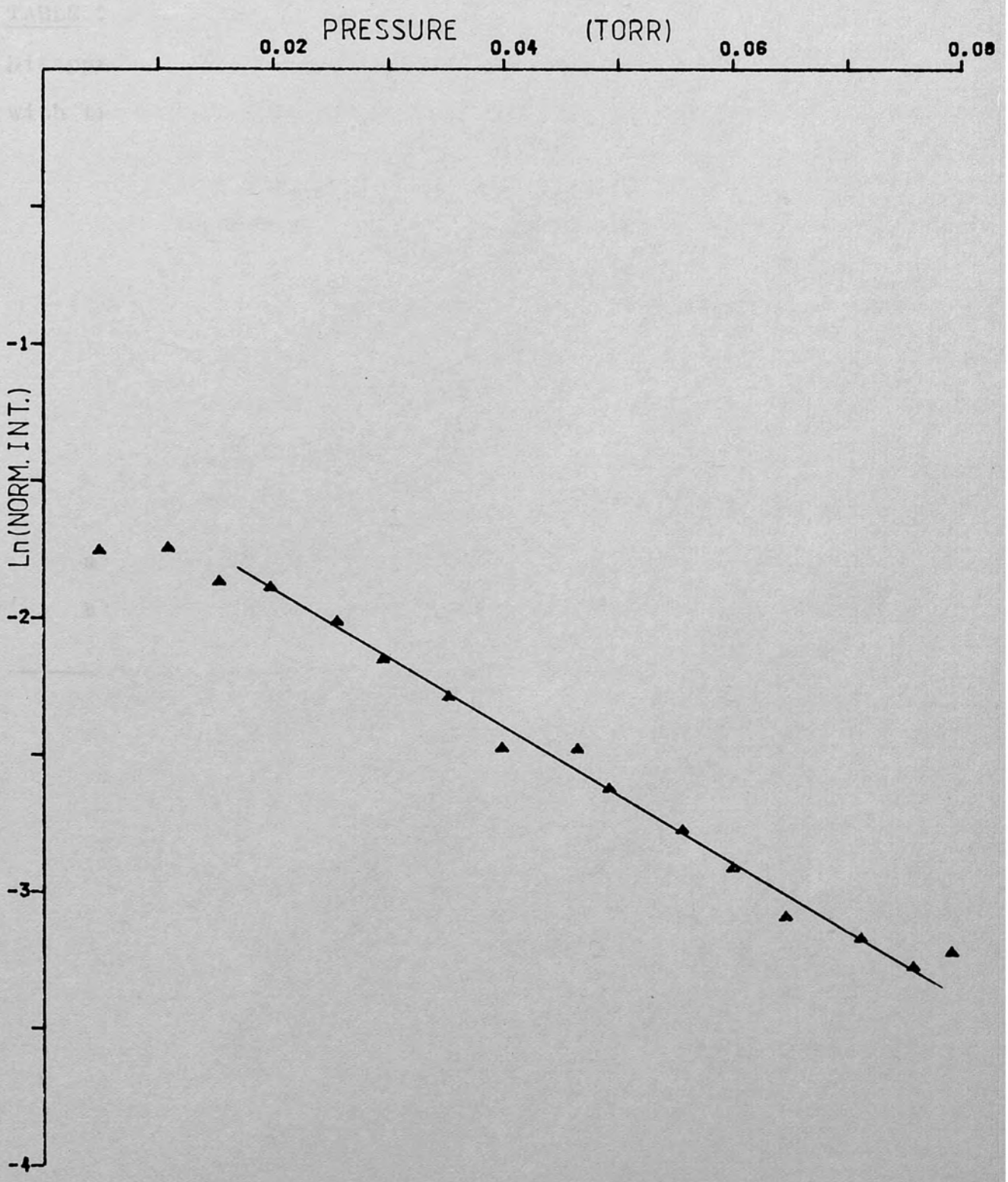

Figure 3.2.3.1-2 : Kinetic plot for the reaction of $(CH_3)_3N^{\dagger}$ with trimethylamine (ion exit energy: 0.52 eV).

TABLE 3.2.3.1 -2

Disappearance rate coefficients[a] for the reaction of $(CH_3)_3N^{+\cdot}$ with trimethylamine at 450°K

Ion exit energy/eV	$10^{10}k_{59}/cm^3molec^{-1}s^{-1}$
0	2.0[b]
0.52	2.7 ± 0.2
1.42	3.8 ± 0.1
2.44	4.6 ± 0.3
3.41	4.8 ± 0.4
4.40	4.7 ± 0.5

a) Errors shown are with 95% confidence.

b) Extrapolated value from Figure 3.2.3.1 -3

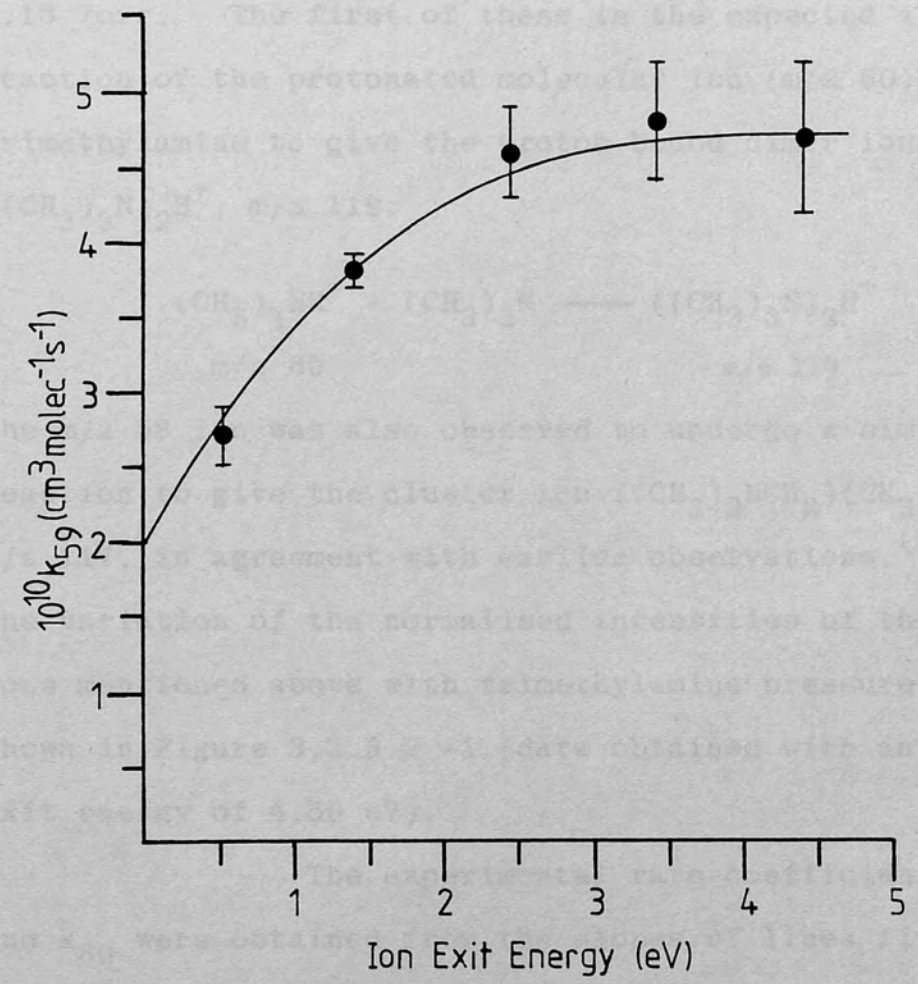

Figure 3.2.3.1-3 : Variation of k_{59} with ion exit energy for the reaction of $(CH_3)_3N^{\dagger}$ with trimethylamine.

3.2.3.2 Kinetic studies of association reactions in trimethylamine -

Two association reactions were observed in trimethylamine, occurring at pressures greater than 0.15 Torr. The first of these is the expected association reaction of the protonated molecular ion (m/z 60) with trimethylamine to give the proton bound dimer ion $((CH_3)_3N)_2H^+$, m/z 119:

$$\underset{m/z\ 60}{(CH_3)_3NH^+} + (CH_3)_3N \longrightarrow \underset{m/z\ 119}{((CH_3)_3N)_2H^+}$$

The m/z 58 ion was also observed to undergo a similar reaction to give the cluster ion $((CH_3)_2NCH_2)(CH_3)_3N^+$, m/z 117, in agreement with earlier observations.[57] The variation of the normalised intensities of the four ions mentioned above with trimethylamine pressure is shown in Figure 3.2.3.2 -1 (data obtained with an ion exit energy of 4.59 eV).

The experimental rate coefficients k_{58} and k_{60} were obtained from the slopes of lines fitted to the kinetic plots, which displayed linearity for values of P_M^2 greater than 0.04 $Torr^2$ (see Figures 3.2.3.2 -2). The values of k_{58}, k_{60} and ln $(I_{60}^{o}/\Sigma I^{o})$ thus obtained are presented in Table 3.2.3.2 -1.

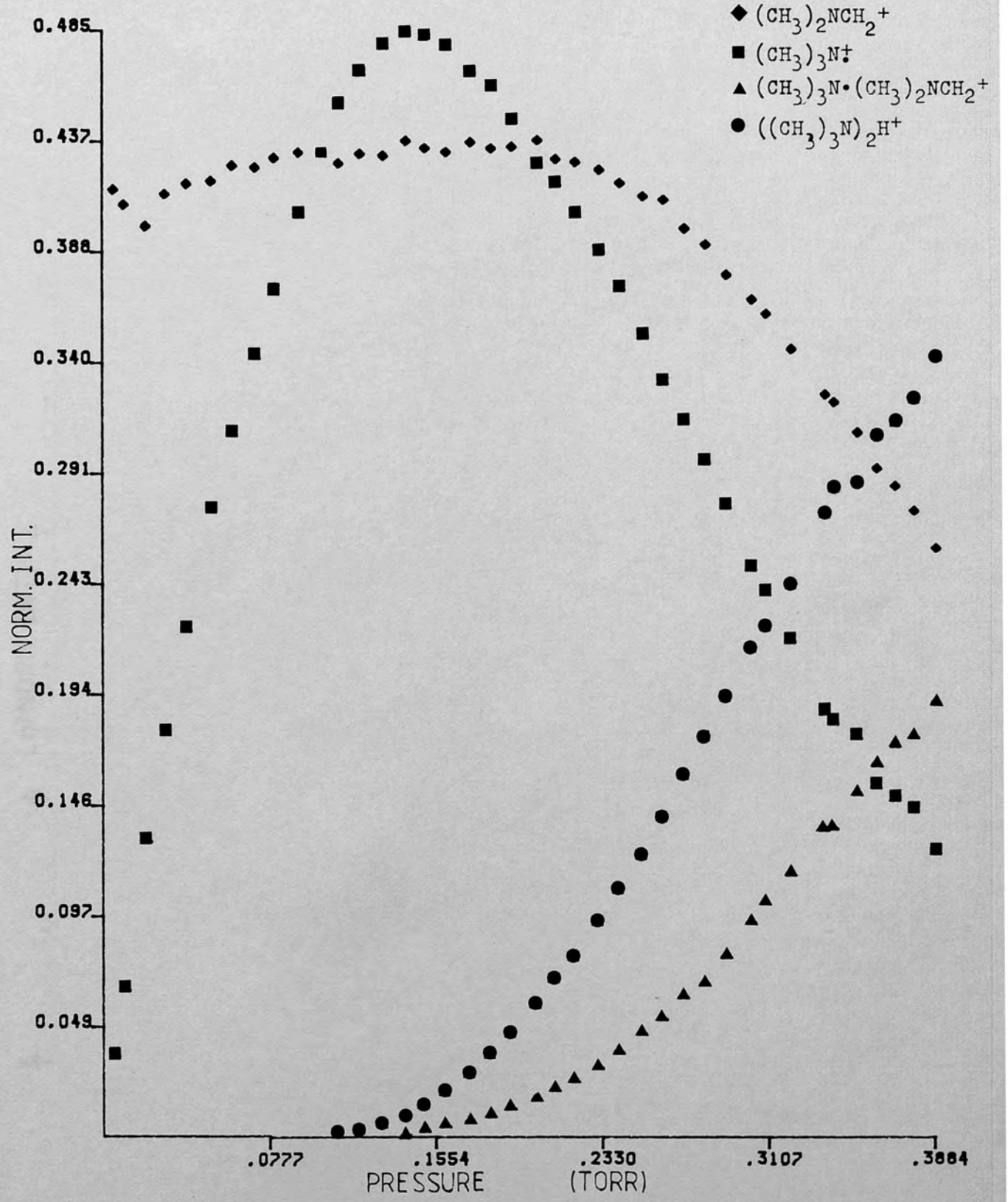

Figure 3.2.3.2-1 : Variation of normalised intensities of ions in trimethylamine with pressure (ion exit energy: 4.59 eV).

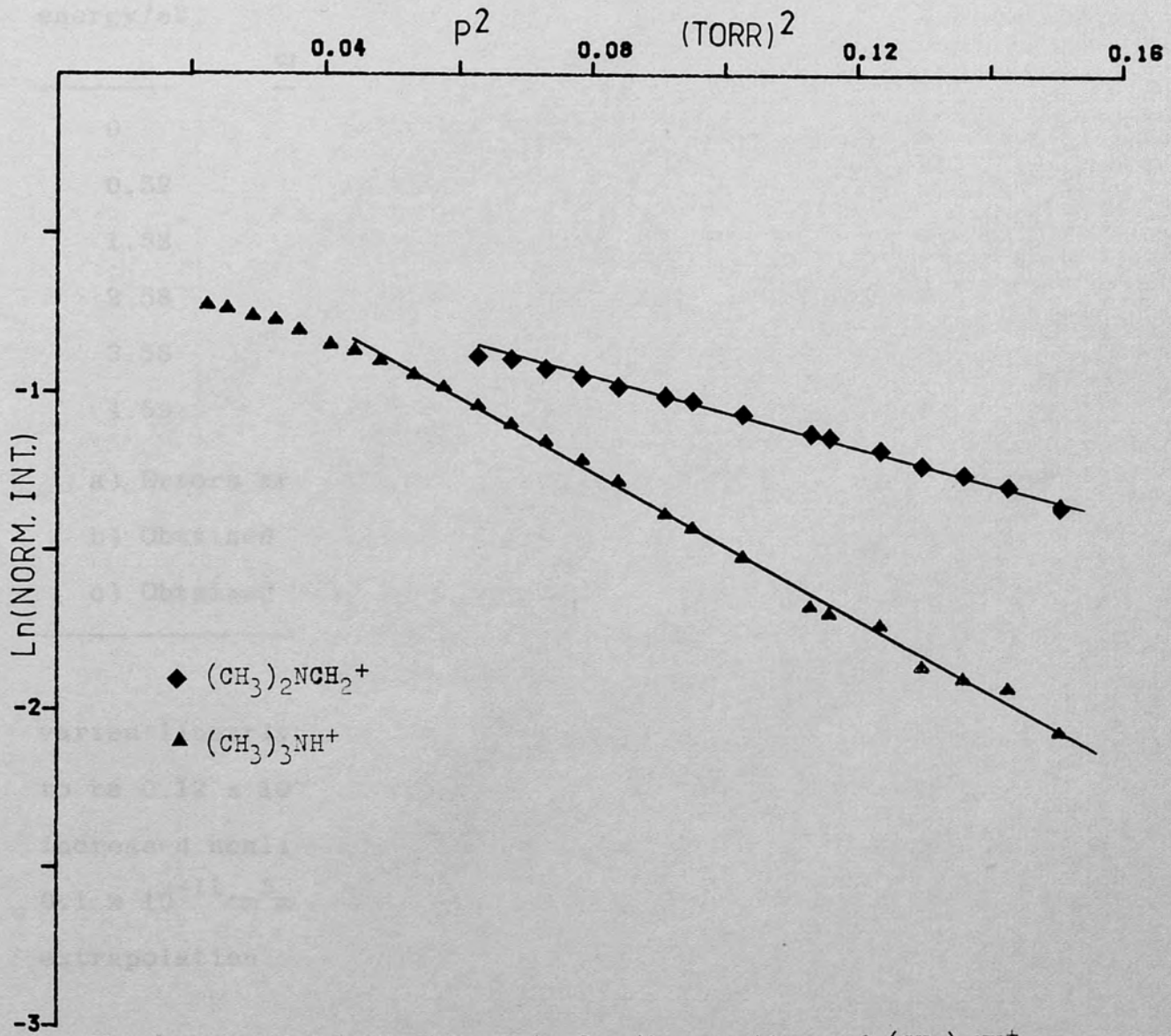

Figure 3.2.3.2-2 : Kinetic plots for the reactions of $(CH_3)_3NH^+$ and $(CH_3)_2NCH_2^+$ with trimethylamine (ion exit energy: 4.59 eV).

TABLE 3.2.3.2 -1

Experimental rate coefficients[a] for the association reactions of $(CH_3)_3NH^+$ and $(CH_3)_2NCH_2^+$ with trimethylamine.

Ion exit energy/eV	$10^{11}k_{58}$/ $cm^3molec^{-1}s^{-1}$	$10^{11}k_{60}$/ $cm^3molec^{-1}s^{-1}$	$\ln(I_{60}^o/\Sigma I^o)$
0	0.1[b]	0.12 ± 0.01[c]	-
0.52	0.34 ± 0.01	0.54 ± 0.01	-1.02
1.53	0.98 ± 0.03	1.48 ± 0.04	-0.90
2.58	1.31 ± 0.03	2.37 ± 0.06	-0.79
3.58	1.57 ± 0.08	3.01 ± 0.07	-0.71
4.59	1.70 ± 0.06	3.57 ± 0.1	-0.62

a) Errors are with 95% confidence limits.

b) Obtained by extrapolation.

c) Obtained from weighted least squares line fit.

As illustrated by Figure 3.2.3 -3, k_{60} varies linearly with ion exit energy and k_{60}^o was determined to be $0.12 \times 10^{-11} cm^3 molec^{-1} s^{-1}$. Values obtained for k_{58} increased nonlinearly with ion exit energy and a value of $0.1 \times 10^{-11} cm^3 mole^{-1} s^{-1}$ was obtained for k_{58}^o by graphic extrapolation.

Since the variation of k_{60} with ion exit energy is linear, it can be related to repeller voltage by the following equation

$$k_{60} = (0.834V + 0.12) \times 10^{-11} \qquad (3.2.3.2\ -1)$$

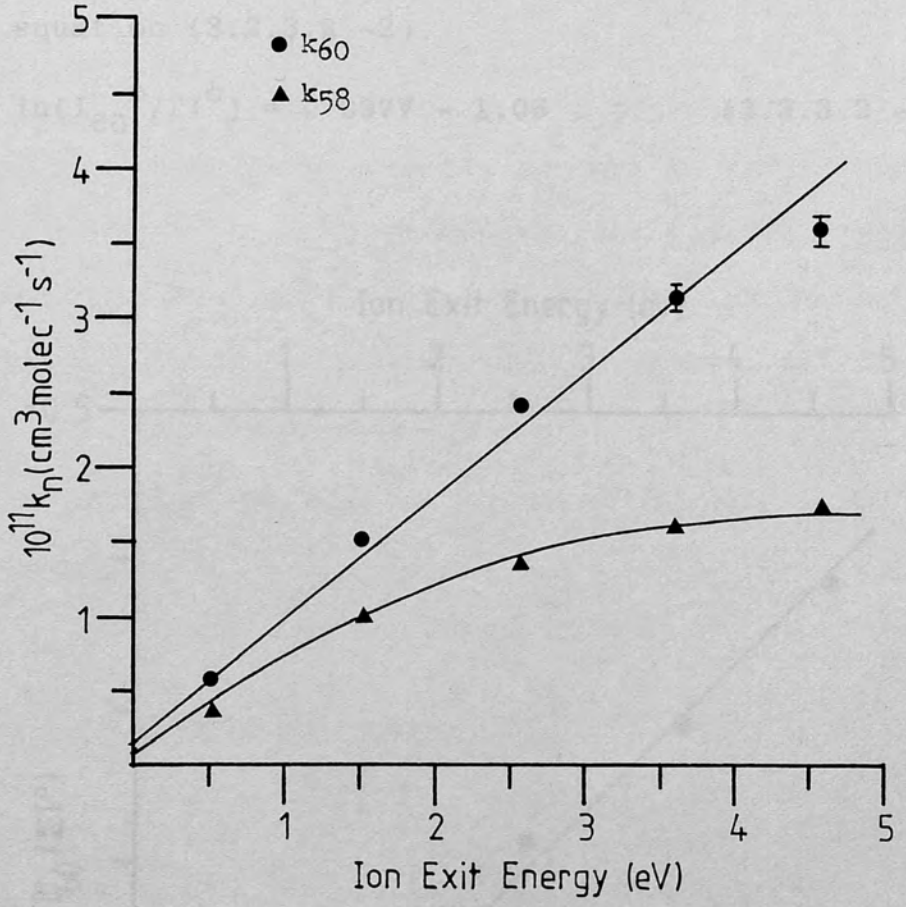

Figure 3.2.3.2-3 : Variation of k_{58} and k_{60} with ion exit energy.

The plot of values of ln ($I_{60}^{o}/\Sigma I^{o}$) against ion exit energy is also linear, as shown in Figure 3.2.3.2 -4, and ln ($I_{60}^{o}/\Sigma I^{o}$) can be related to repeller voltage by means of equation (3.2.3.2 -2).

$$\ln(I_{60}^{o}/\Sigma I^{o}) = 0.097V - 1.06 \qquad (3.2.3.2\ -2)$$

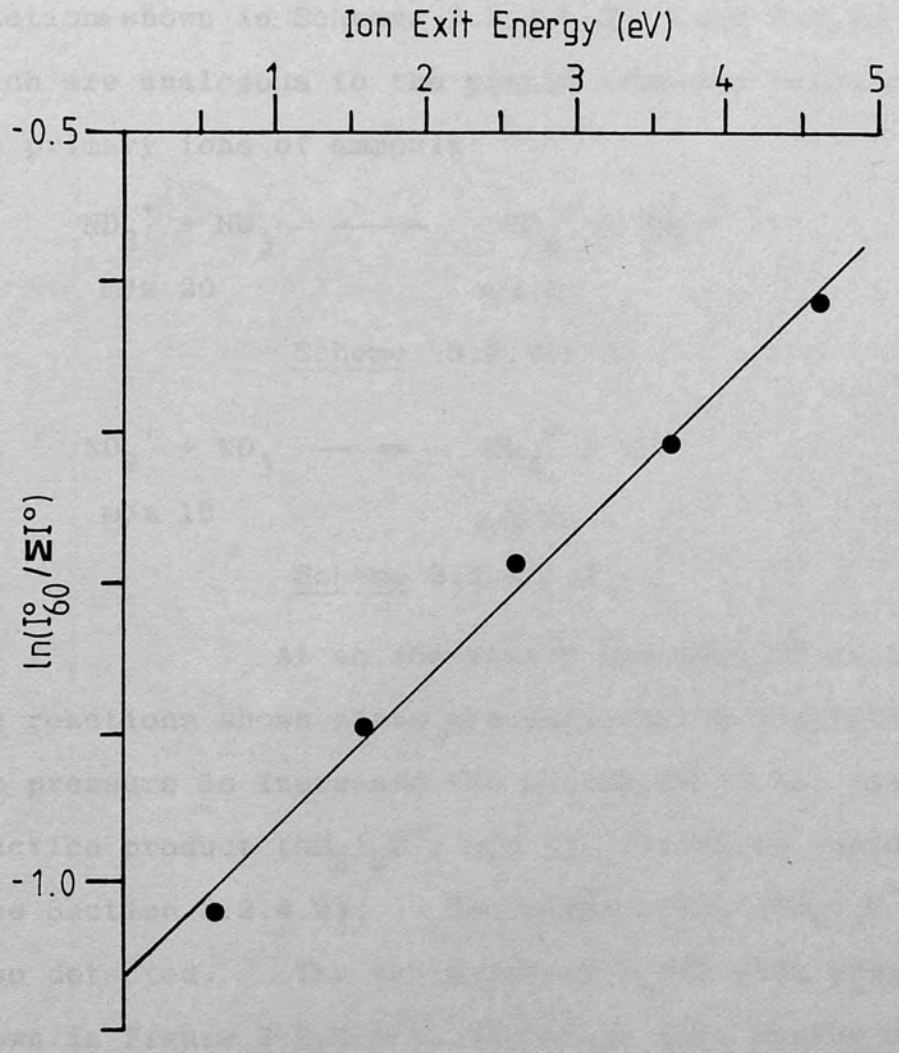

Figure 3.2.3.2-4 : Variation of $\ln(I_{60}^{o}/\Sigma I^{o})$ with ion exit energy.

3.2.4 Ammonia-d_3

3.2.4.1 Determination of the disappearance rate coefficients of the primary ions of ammonia-d_3. -

The primary ions arising from the electron impact ionisation of ammonia-d_3, m/z 20 ($ND_3^{+\cdot}$) and m/z 18 (ND_2^+), were observed to undergo the deuteron transfer reactions shown in Schemes 3.2.4.1 -1 and 3.2.4.1 -2, which are analogous to the proton transfer reactions of the primary ions of ammonia

$$\underset{\text{m/z 20}}{ND_3^{+\cdot}} + ND_3 \longrightarrow \underset{\text{m/z 22}}{ND_4^+} + ND_2\cdot$$

Scheme 3.2.4.1 -1

$$\underset{\text{m/z 18}}{ND_2^+} + ND_3 \longrightarrow \underset{\text{m/z 22}}{ND_4^+} + ND$$

Scheme 3.2.4.1 -2

At an ion-source pressure of ca.0.06 Torr, the reactions shown above are essentially complete and as the pressure is increased the abundance of the association reaction product $(ND_3)_2D^+$, m/z 42, increases rapidly. (See Section 3.2.4.2). The cluster ion $(ND_3)_3D^+$ was also detected. The variation of $I_n/\Sigma I$ with pressure is shown in Figure 3.2.4.1 -1 for these ions having an ion exit energy of 0.52 eV. Values of P_C are shown for the m/z 20 ion in Table 3.2.4.1 -1 along with the corresponding residence times. From these values of P_C it can be seen

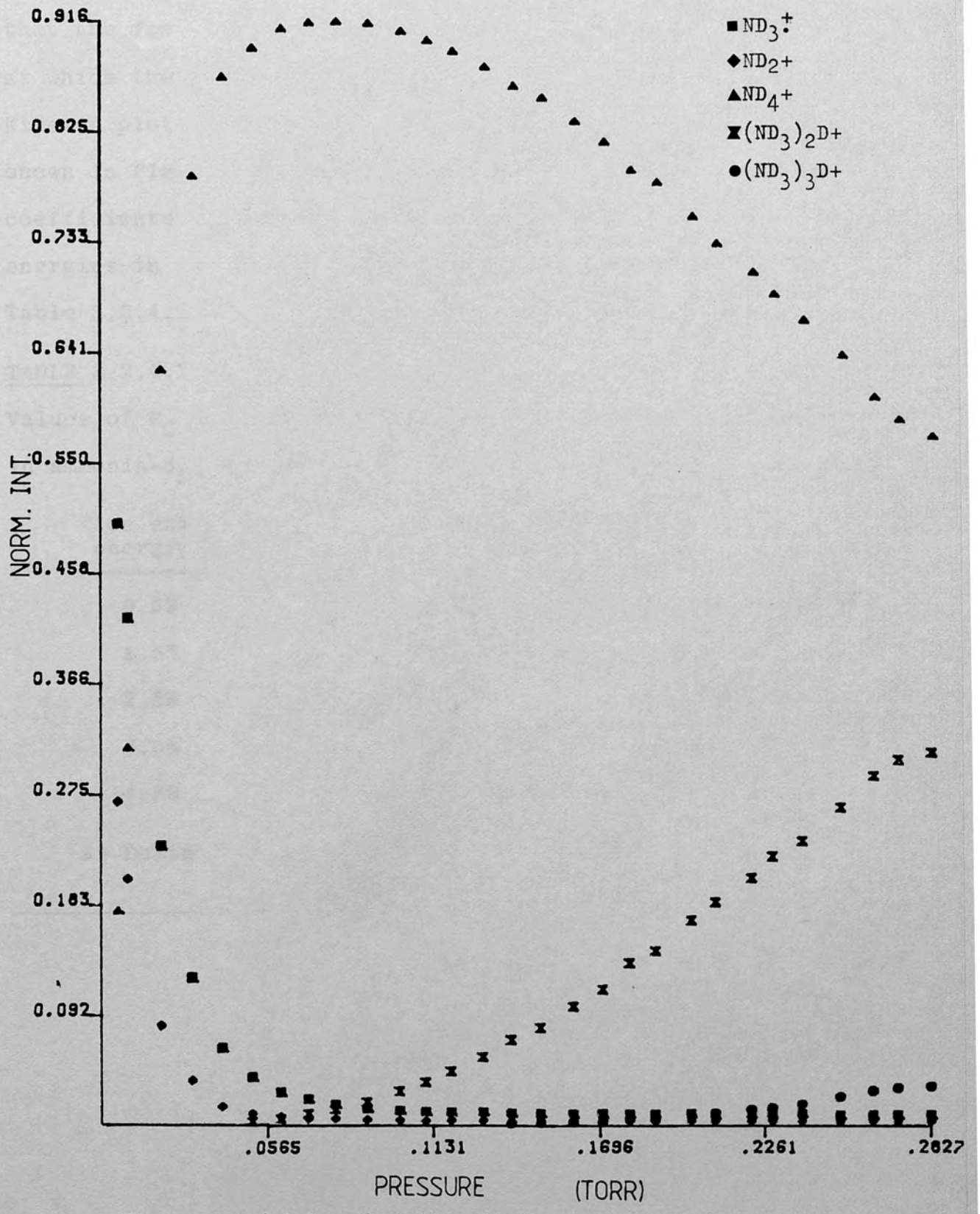

Figure 3.2.4.1-1 : Variation in the normalised intensities of ions in ammonia-d_3 with pressure (ion exit energy: 0.52 eV).

that the free-fall formula is valid in the pressure range at which the deuteron transfer reactions were observed. Kinetic plots for the reactions of m/z 18 and m/z 20 are shown in Figure 3.2.3.4 -2 and the disappearance rate coefficients k_{18} and k_{20}, determined with ion exit energies in the range 0.52 - 4.59 eV are collected in Table 3.2.4.1 -2.

TABLE 3.2.4.1 -1

Values of P_C and ion residence times (τ) for the $ND_3^{+\cdot}$ ion in ammonia-d_3.

Ion exit energy/eV	P_C[a]/Torr	$10^6\tau$/s
0.52	0.060	1.7
1.53	0.104	1.5
2.58	0.135	1.1
3.58	0.159	1.0
4.59	0.180	0.85

a) Defined in Table 3.2.1.1 -1

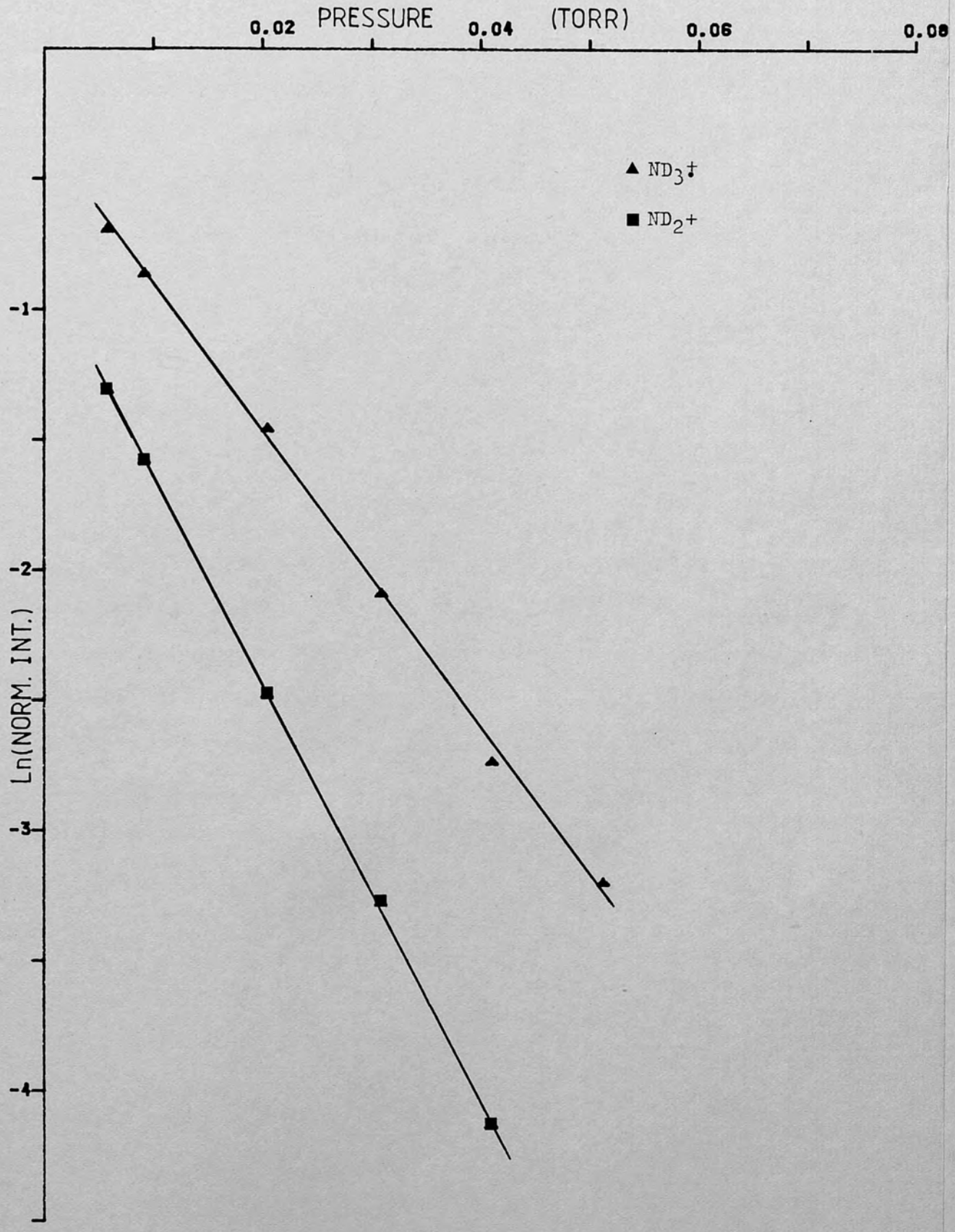

Figure 3.2.4.1-2 : Kinetic plots for the reactions of ND_3^+ and ND_2^+ with ammonia-d_3 (ion exit energy: 0.52 eV).

TABLE 3.2.4.1 -2

Disappearance rate coefficients[a] for the reactions of $ND_3^{+\cdot}$ and ND_2^+ with ammonia-d_3

Ion exit energy/eV	$10^9 k_{18}/cm^3 molec^{-1} s^{-1}$	$10^9 k_{20}/cm^3 molec^{-1} s^{-1}$
0	1.2[b]	0.8[b]
0.52	1.53 ± 0.02	1.04 ± 0.04
1.53	2.07 ± 0.07	1.50 ± 0.04
2.58	2.45 ± 0.03	1.62 ± 0.04
3.58	2.46 ± 0.07	1.78 ± 0.03
4.59	2.57 ± 0.05	1.77 ± 0.05

a) Errors shown are with 95% confidence limits.

b) Extrapolated value from Figure 3.2.4.1 -3

Both k_{18} and k_{20} increase non-linearly with increasing ion exit energy up to ca.2.6 eV. Little difference is then observed between the values obtained at 3.58 and 4.59 eV ion exit energy (see Figure 3.2.4.1 -3).

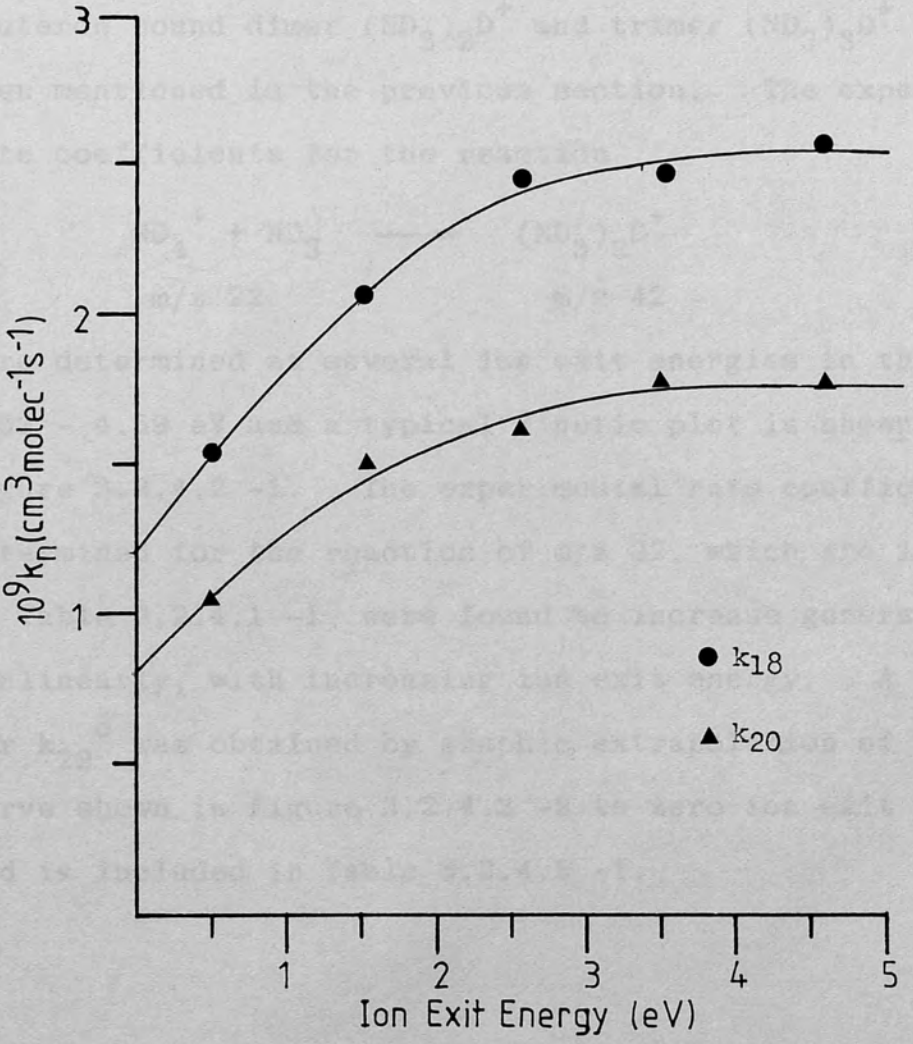

Figure 3.2.4.1-3 : Variation of k_{18} and k_{20} with ion exit energy.

3.2.4.2 Kinetic studies of the association reaction of ND_4^+ with ammonia-d_3

The observation of the formation of the deuteron bound dimer $(ND_3)_2D^+$ and trimer $(ND_3)_3D^+$ has been mentioned in the previous section. The experimental rate coefficients for the reaction

$$\underset{\text{m/z 22}}{ND_4^+} + ND_3 \longrightarrow \underset{\text{m/z 42}}{(ND_3)_2D^+}$$

were determined at several ion exit energies in the range 0.52 - 4.59 eV and a typical kinetic plot is shown in Figure 3.2.4.2 -1. The experimental rate coefficients determined for the reaction of m/z 22, which are indicated in Table 3.2.4.1 -1, were found to increase generally, but nonlinearly, with increasing ion exit energy. A value for k_{22}° was obtained by graphic extrapolation of the curve shown in Figure 3.2.4.2 -2 to zero ion exit energy, and is included in Table 3.2.4.2 -1.

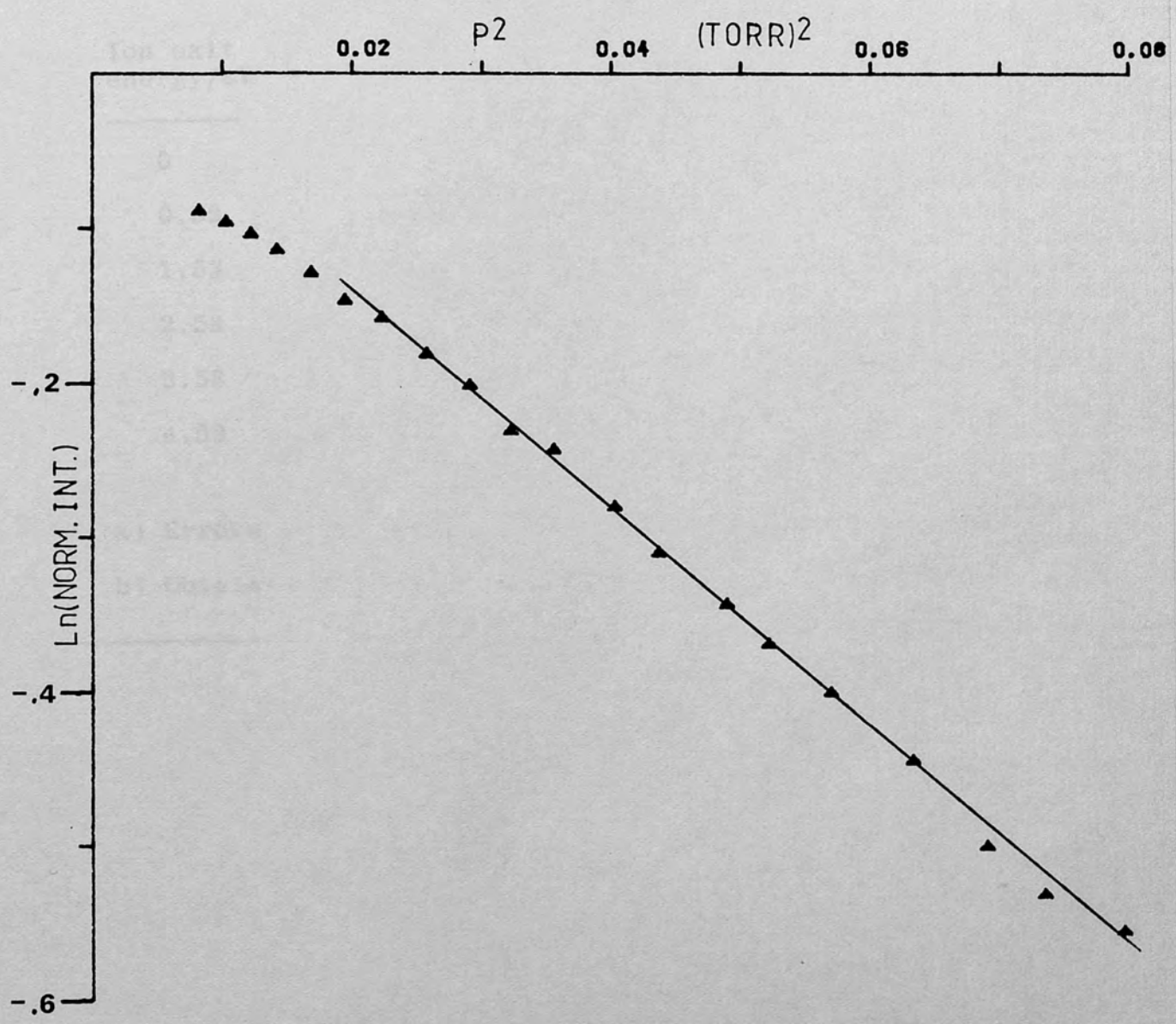

Figure 3.2.4.2-1 : Kinetic plot for the reaction of ND_4^+ with ammonia-d_3 (ion exit energy: 0.52 eV).

TABLE 3.2.4.2 -1

Experimental values of k_{22}[a] for the association reaction of ND_4^+ with ND_3.

Ion exit energy/eV	$10^{11}k_{22}/cm^3molec^{-1}s^{-1}$	$\ln(I_{22}^o/\ I^o)$
0	0.1[b]	-
0.52	0.77 ± 0.02	0.0028
1.53	2.1 ± 0.1	0.072
2.58	3.00 ± 0.09	0.094
3.58	3.4 ± 0.1	0.066
4.59	3.8 ± 0.1	0.066

a) Errors shown are with 95% confidence limits.

b) Obtained by extrapolation to zero ion exit energy.

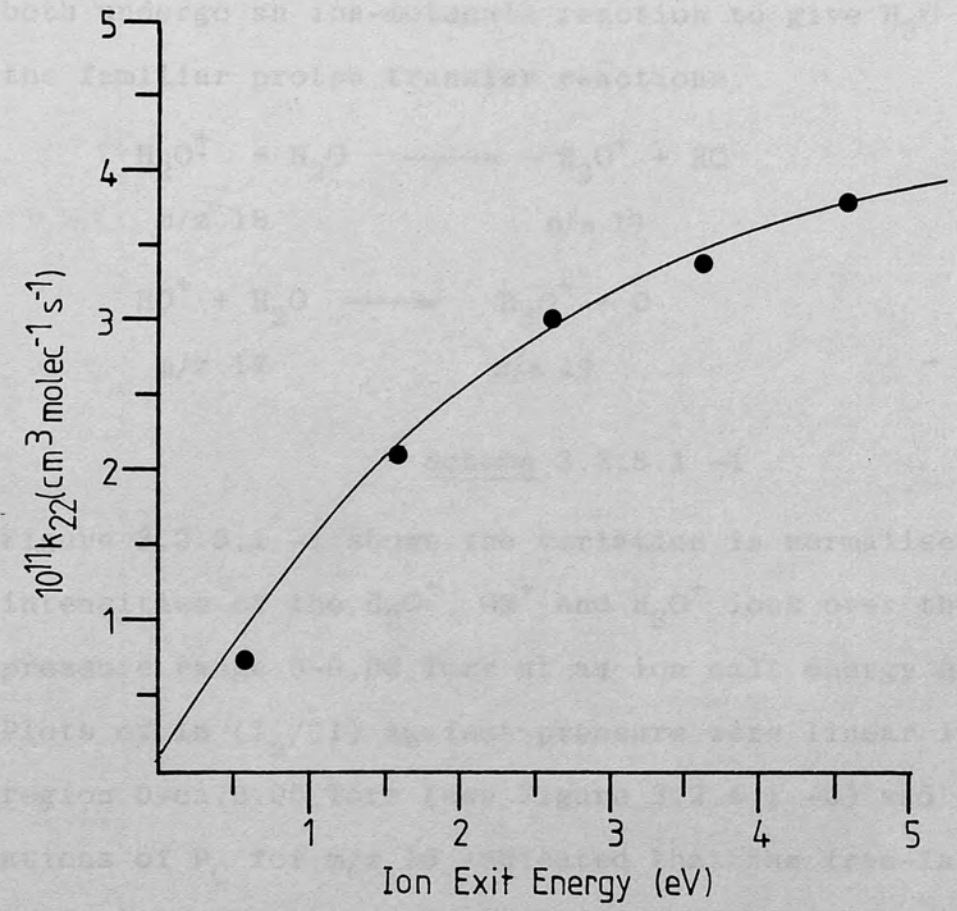

Figure 3.2.4.2-2 : Variation of k_{22} with ion exit energy.

3.2.5 Water

3.2.5.1 Determination of disappearance rate coefficients of primary ions in H_2O

The molecular ion and HO^+ ion of water both undergo an ion-molecule reaction to give H_3O^+ via the familiar proton transfer reactions:

$$H_2O^{+\cdot} + H_2O \longrightarrow H_3O^+ + HO\cdot$$
m/z 18 m/z 19

$$HO^+ + H_2O \longrightarrow H_3O^+ + O$$
m/z 17 m/z 19

Scheme 3.2.5.1 -1

Figure 3.2.5.1 -1 shows the variation in normalised intensities of the $H_2O^{+\cdot}$, OH^+ and H_3O^+ ions over the pressure range 0-0.06 Torr at an ion exit energy of 1eV. Plots of ln $(I_n/\Sigma I)$ against pressure were linear in the region 0-ca.0.05 Torr (see Figure 3.2.4.1 -2) and calculations of P_C for m/z 18 indicated that the free-fall assumption for the evaluation of residence times was valid for this pressure region (see Table 3.2.5.1 -1).

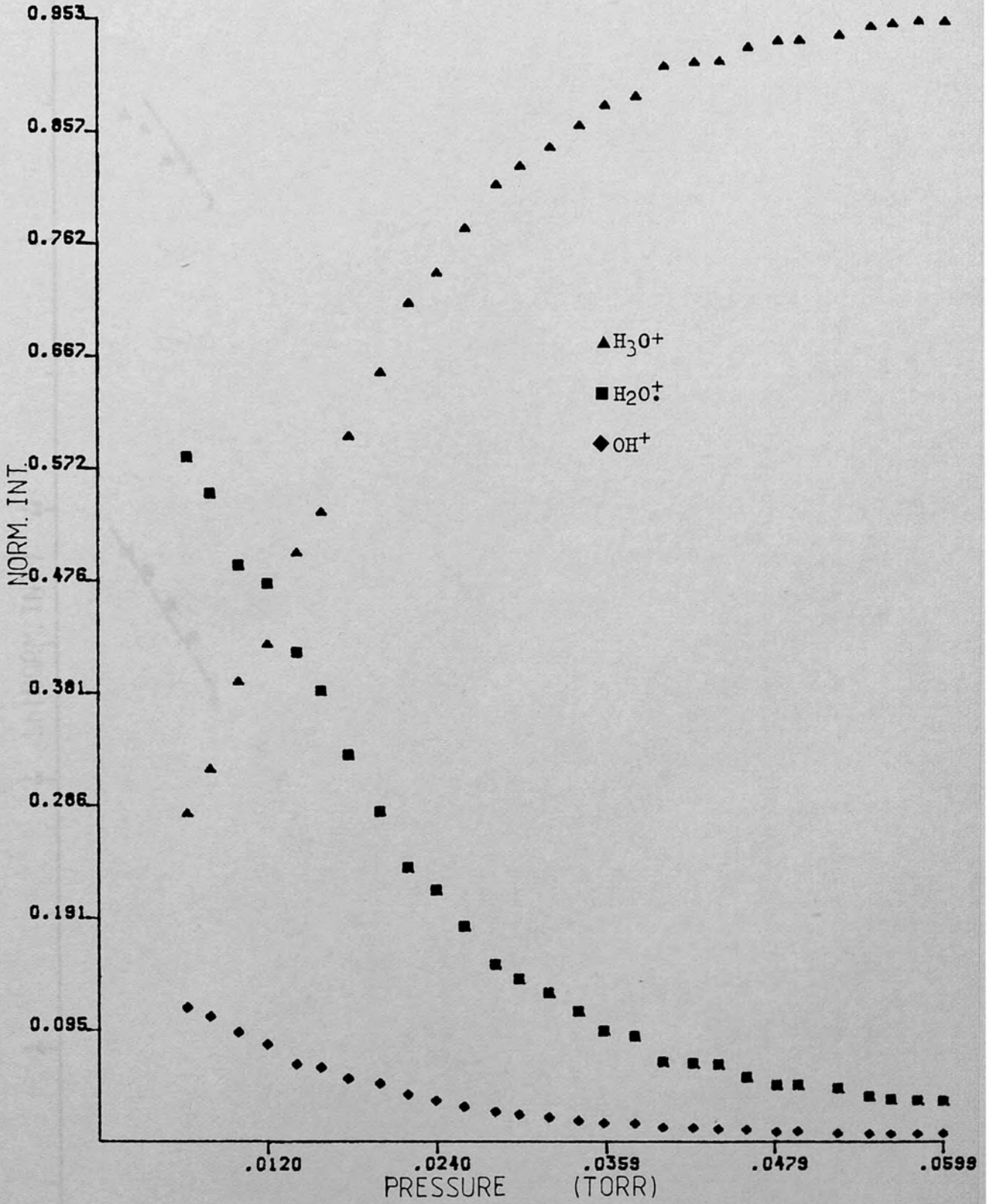

Figure 3.2.5.1-1 : Variation of normalised intensities of ions in water vapour with pressure (ion exit energy: 1 eV).

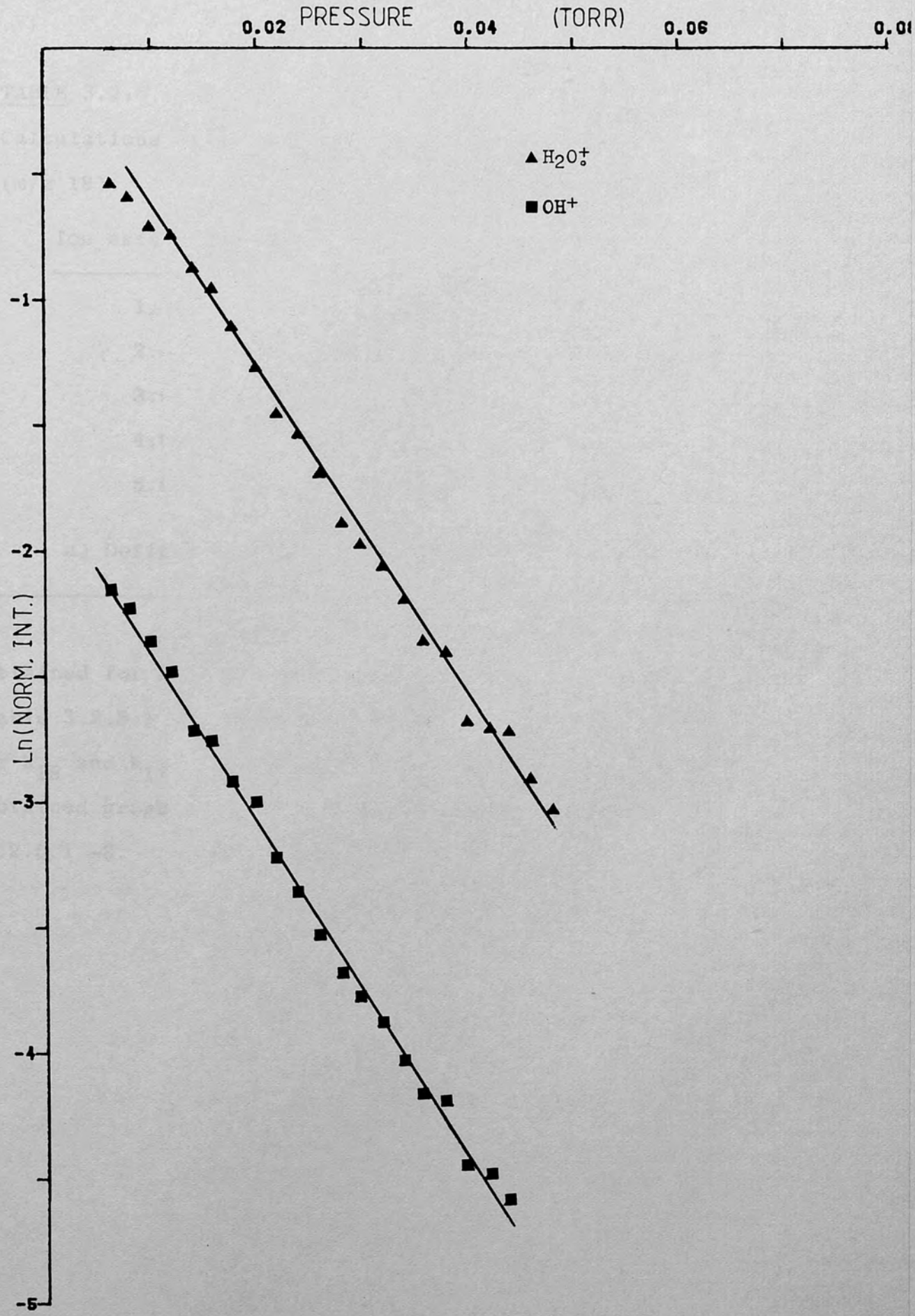

Figure 3.2.5.1-2 : Kinetic plots for the reactions of H_2O^+ and OH^+ with water (ion exit energy: 1 eV).

TABLE 3.2.5.1 -1

Calculations of P_C^a and residence times (τ) for $H_2O^{\cdot+}$ (m/z 18).

Ion exit energy/eV	P_C^a/Torr	$10^6 \tau$/s
1.00	0.105	1.73
2.08	0.151	1.20
3.08	0.184	0.99
4.09	0.212	0.86
5.09	0.236	0.75

a) Defined in Table 3.2.1.1 -1

The disappearance rate coefficients obtained for $H_2O^{\cdot+}$ and OH^+ in this study are given in Table 3.2.5.1 -2, which also shows the extrapolated values of k_{18} and k_{17} at zero ion exit energy (k_{18}^o and k_{17}^o) obtained graphically from the plots shown in Figure 3.2.5.1 -3.

TABLE 3.2.5.1 -2

Disappearance rate coefficients[a] for the reactions of H_2O^+ and OH^+ with water

Ion exit energy/eV	$10^9 k_{17}/cm^3 molec^{-1} s^{-1}$	$10^9 k_{18}/cm^3 molec^{-1} s^{-1}$
0	1.5[b]	1.4[b]
1.00	1.9 ± 0.06	1.8 ± 0.2
2.08	2.22 ± 0.05	1.96 ± 0.05
3.08	2.44 ± 0.05	2.12 ± 0.06
4.09	2.46 ± 0.08	2.14 ± 0.06
5.09	2.58 ± 0.06	2.19 ± 0.07

a) Errors shown are with 95% confidence limits.

b) Extrapolated from plots of k_n against ion exit energy.

The rate coefficients evaluated for ion exit energies of 4eV appear to be anomalously low. Owing to the magnitude the error band for the determination of k_{18} at 1 eV ion exit energy, the extrapolated value of k_{18}^{o} must be regarded with caution, since at best, the error in k_{18}^{o} cannot be less than ca. ± 0.4 x 10^{-9} $cm^3 molec^{-1} s^{-1}$.

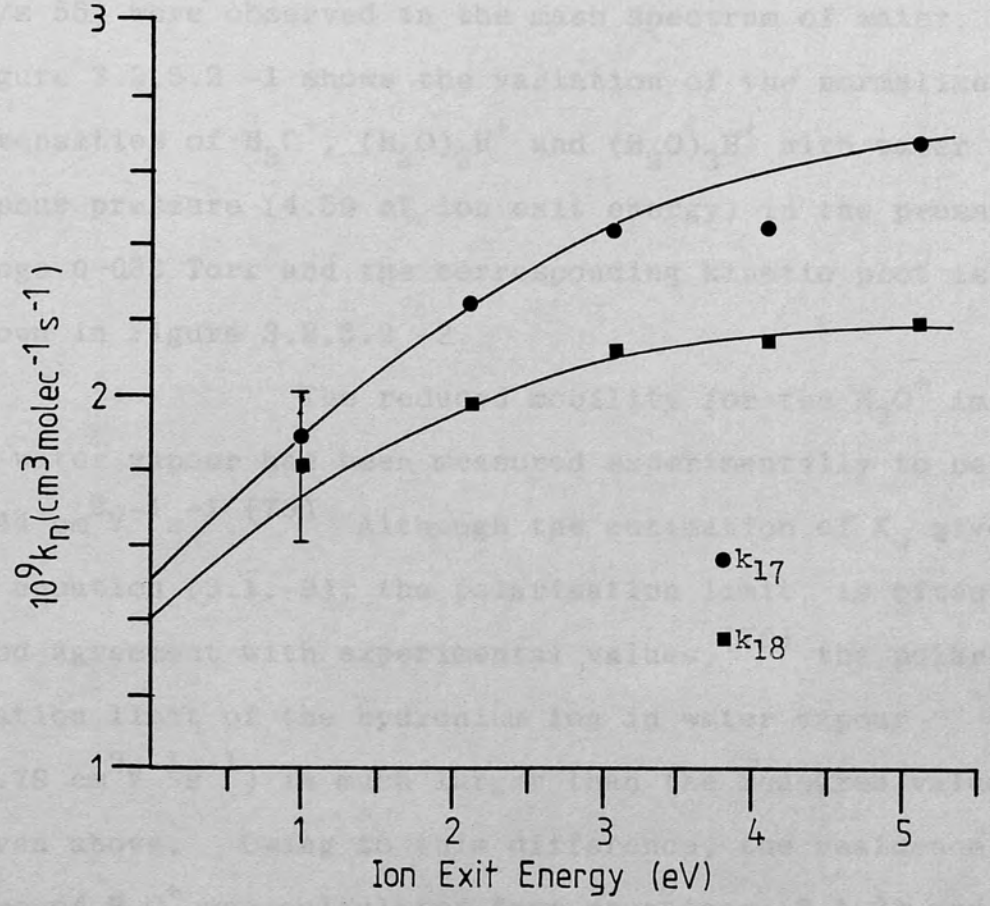

Figure 3.2.5.1-3 : Variation in k_{18} and k_{17} with ion exit energy.

3.2.5.2 Evaluation of rate coefficients for the association reaction of H_3O^+ with water.

At ion-source pressures greater than 0.06 Torr, peaks corresponding to $(H_2O)_2H^+$ (m/z 37) and $(H_2O)_3H^+$ (m/z 55) were observed in the mass spectrum of water. Figure 3.2.5.2 -1 shows the variation of the normalised intensities of H_3O^+, $(H_2O)_2H^+$ and $(H_2O)_3H^+$ with water vapour pressure (4.59 eV ion exit energy) in the pressure range 0-0.33 Torr and the corresponding kinetic plot is shown in Figure 3.2.5.2 -2.

The reduced mobility for the H_3O^+ ion in water vapour has been measured experimentally to be 1.44 $cm^2V^{-1}s^{-1}$.(79) Although the estimation of K_o given by equation (3.1.-9), the polarisation limit, is often in good agreement with experimental values,(79) the polarisation limit of the hydronium ion in water vapour (3.79 $cm^2V^{-1}s^{-1}$) is much larger than the measured value given above. Owing to this difference, the residence time of H_3O^+ was calculated from equations (3.1.8) and (3.1.7) such that

$$\tau = d/v = d/KE = 273\ d\ell P_M/760\ K_o TV \qquad (3.2.5.2\text{ -}1)$$

with the variables defined as in Section 3.1. The rate constants obtained by assuming K_o= 1.44 $cm^2V^{-1}s^{-1}$ are given in Table 3.2.5.2 -1 with those obtained by assuming a reduced mobility equal to the polarisation limit (K_o = 3.79 $cm^2V^{-1}s^{-1}$).

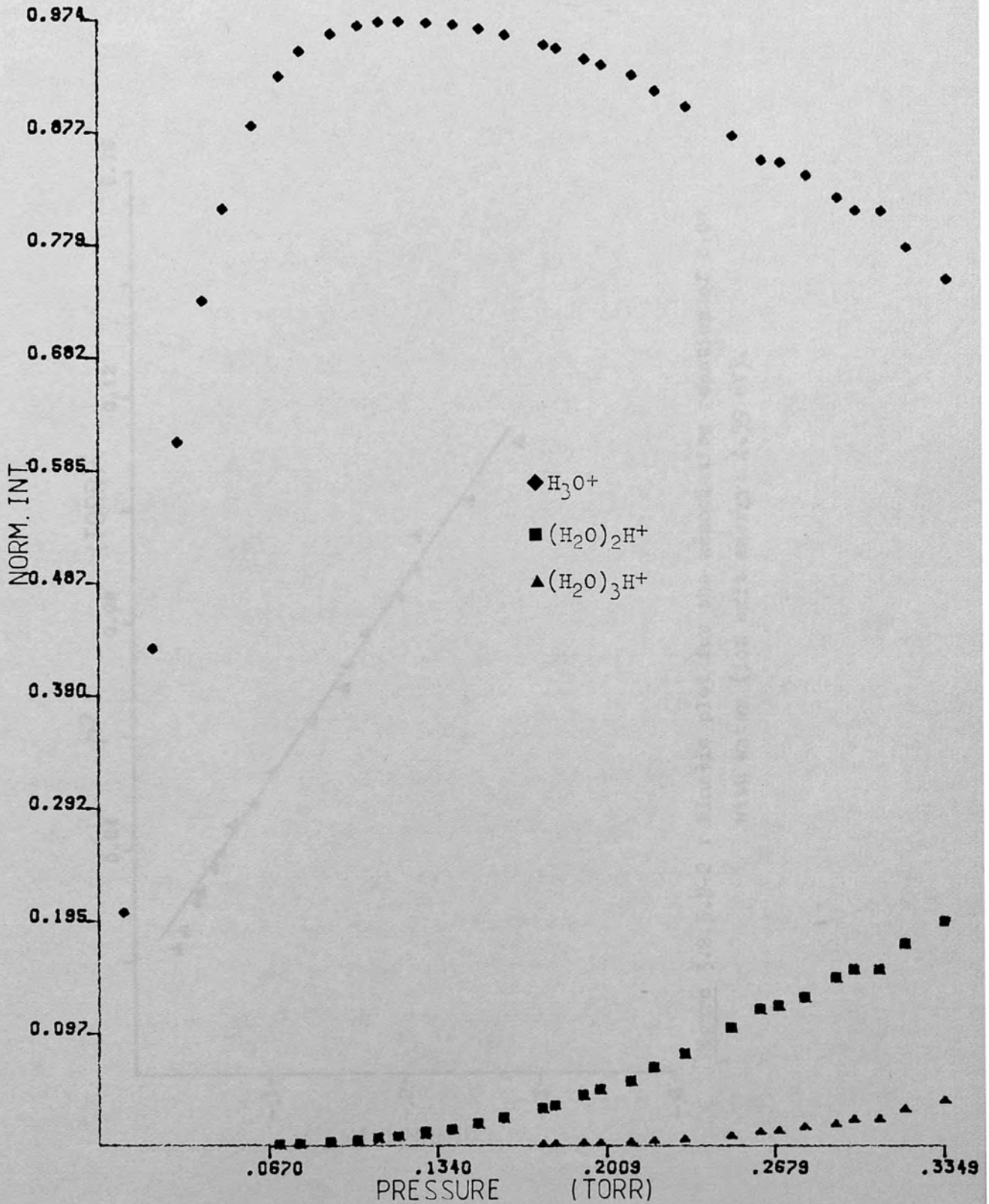

Figure 3.2.5.2-1 : Variation in the normalised intensities of ions in water vapour with pressure (ion exit energy: 4.59 eV).

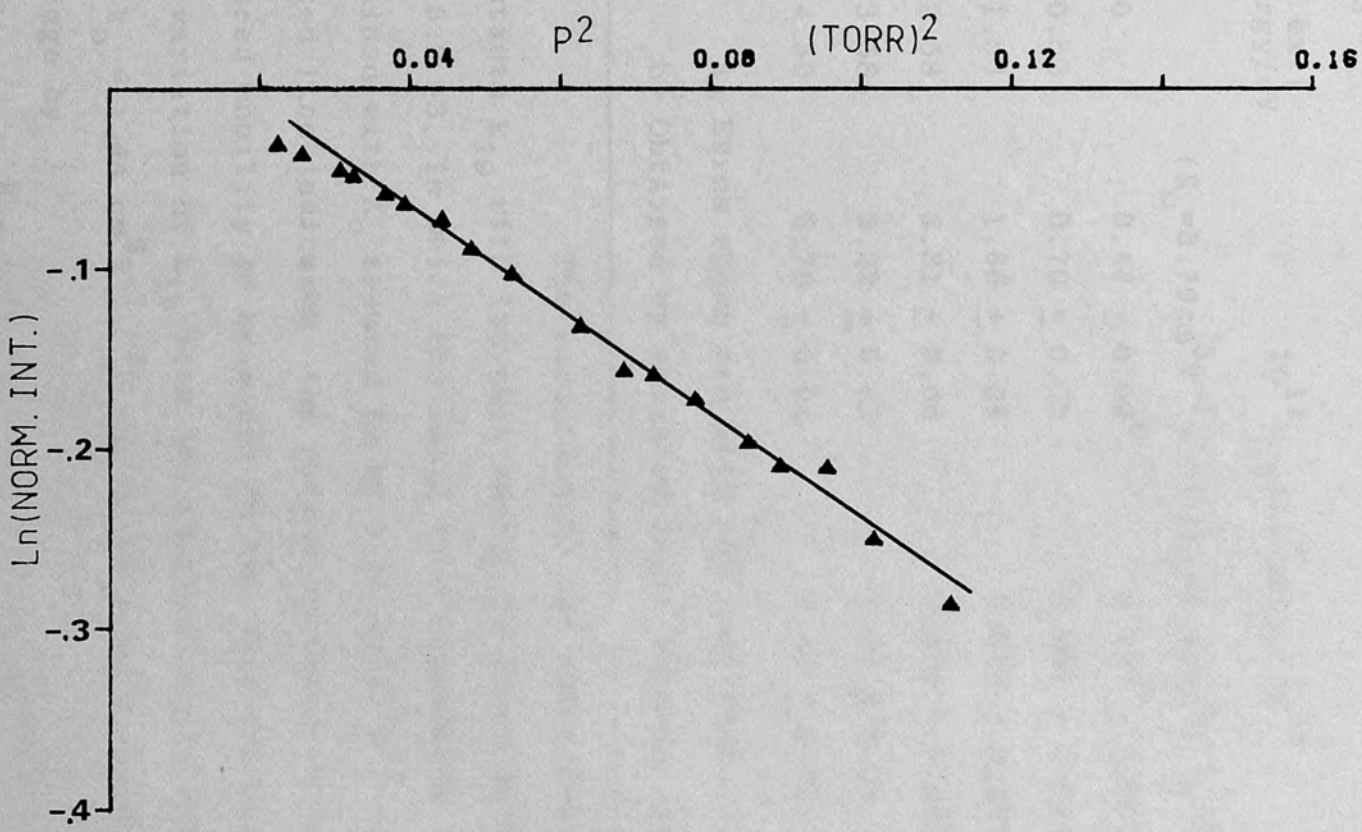

Figure 3.2.5.2-2 : Kinetic plot for the association reaction of H_3O^+ with water (ion exit energy: 4.59 eV).

TABLE 3.2.5.2 -1

Experimental values [a] of k_{19} for the association reaction of H_3O^+ with water.

Ion exit energy/eV	$10^{11}k_{19}/cm^3molec^{-1}s^{-1}$		
	(K_o=3.79$cm^3V^{-1}s^{-1}$)	(K_o=1.44$cm^2V^{-1}s^{-1}$)	$\ln(I_{19}^o/\Sigma I^o)$
0	0.44 ± 0.09[b]	0.117 ± 0.003[b]	-
0.52	0.70 ± 0.01	0.267 ± 0.006	-0.002
1.53	1.66 ± 0.04	0.630 ± 0.001	0.03
2.58	2.31 ± 0.05	0.875 ± 0.002	0.034
3.58	3.02 ± 0.09	1.14 ± 0.04	0.071
4.59	3.70 ± 0.02	1.40 ± 0.07	0.10

a) Erros shown are with 95% confidence limits.

b) Obtained by weighted least squares data fit.

The variation of the experimental rate constants k_{19} with ion exit energy is shown in Figure 3.2.5.2 -3, in which the solid line represents the data obtained with K_o assumed to be 1.44 $cm^2V^{-1}s^{-1}$ and the dotted line indicates the points obtained by assuming the reduced mobility to be equal to the polarisation limit. The variation of k_{19} with ion exit energy is linear and, for k_o = 1.44 $cm^2V^{-1}s^{-1}$, can be related to repeller voltage by

$$k_{19} = (0.301V + 0.117) \times 10^{-11} \qquad (3.2.5.2\text{ -}2)$$

where 0.117 x $10^{-11}cm^3molec^{-1}s^{-1}$ is the intercept value, corresponding to k_{19}^o. The variation of $\ln(I_{19}^o/\Sigma I^o)$ with

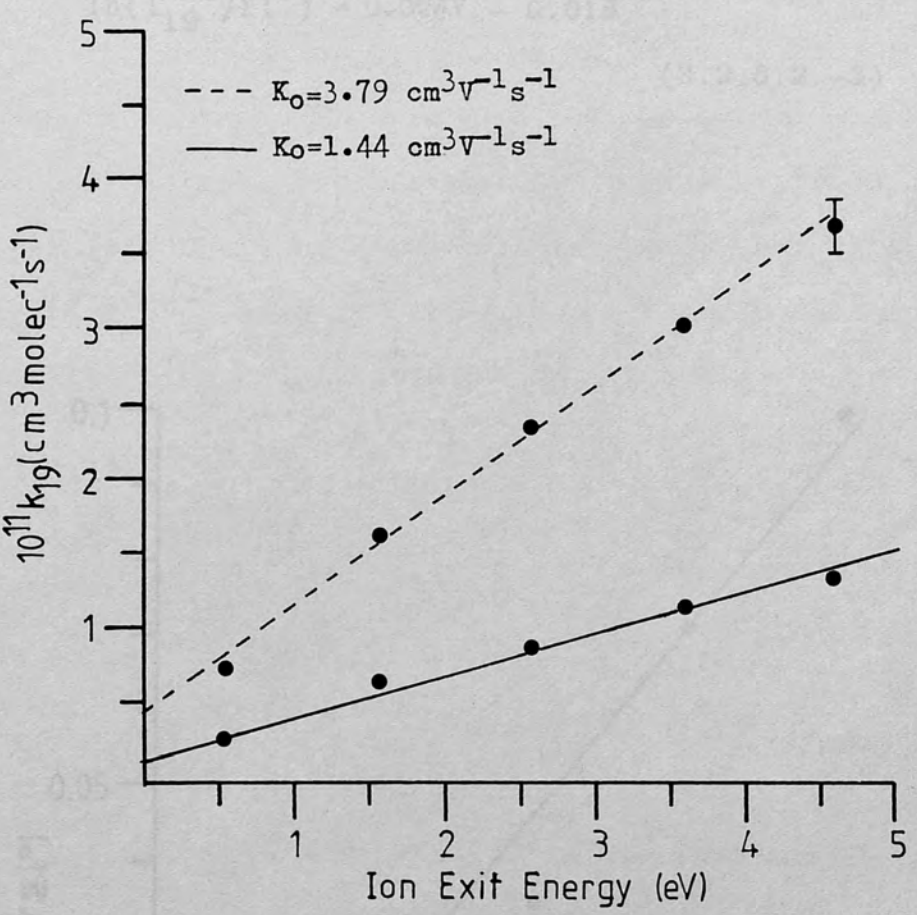

Figure 3.2.5.2-3 : Variation of k_{19} with ion exit energy.

ion exit energy is also linear (see Figure 3.2.5.2 -4) and can also be related to repeller voltage, e.g.

$$\ln(I_{19}^{o}/\Sigma I^{o}) = 0.024V - 0.015 \qquad (3.2.5.2\text{ -}3)$$

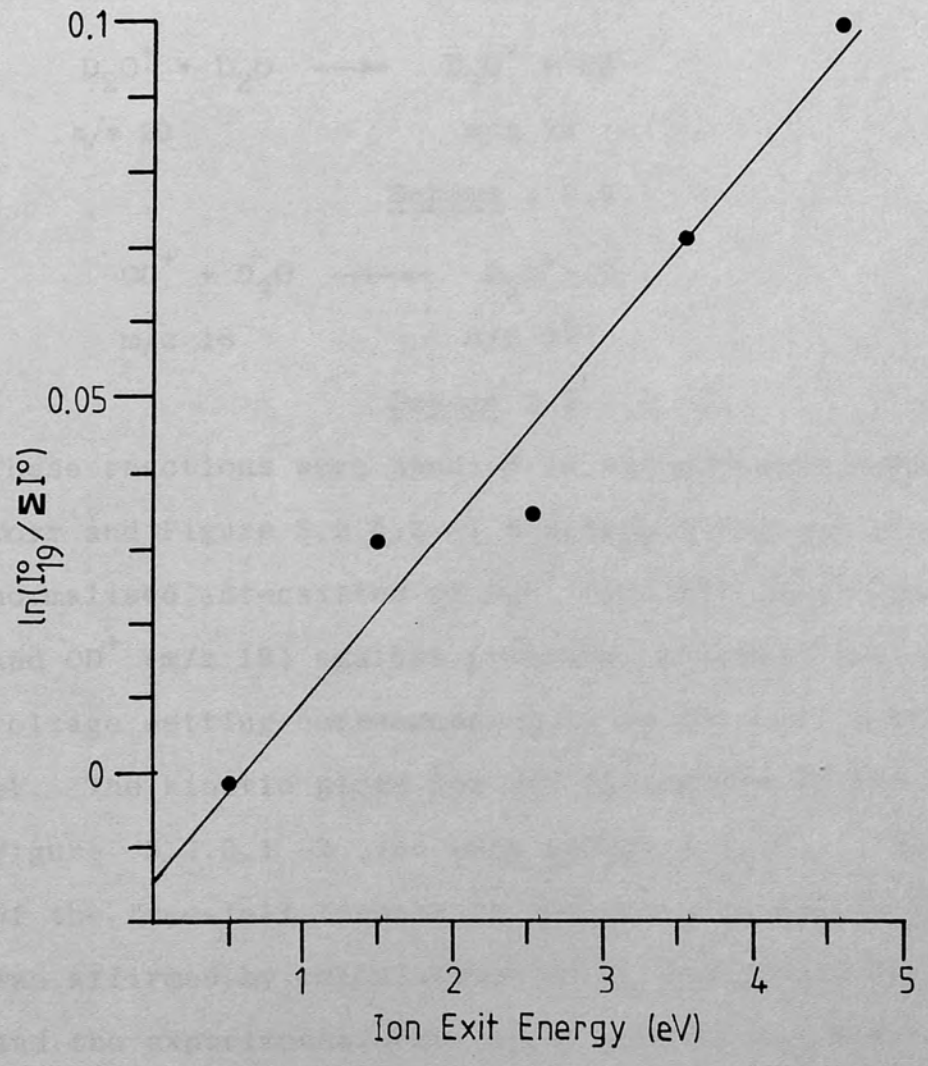

Figure 3.2.5.2-4 : Variation of $\ln(I_{19}^{o}/\Sigma I^{o})$ with ion exit energy.

3.2.6 Deuterium oxide.

3.2.6.1 Evaluation of the disappearance rate coefficients of the primary ions in deuterium oxide.

The primary ions in the mass spectrum of deuterium oxide were observed to undergo the deuteron transfer reactions shown in Schemes 3.2.6.1 -1 and 3.2.6.1 -2, which are analogous to the proton transfer reactions described in Section 3.2.5.1.

$$\underset{\text{m/z 20}}{D_2O^{+\cdot}} + D_2O \longrightarrow \underset{\text{m/z 22}}{D_3O^+} + OD\cdot$$

Scheme 3.2.6.1 -1

$$\underset{\text{m/z 18}}{OD^+} + D_2O \longrightarrow \underset{\text{m/z 22}}{D_3O^+} + O$$

Scheme 3.2.6.1 -2

These reactions were studied in the pressure range 0-0.09 Torr and Figure 3.2.6.1 -1 displays a typical plot of the normalised intensities of D_3O^+ (m/z 22), $D_2O^{+\cdot}$ (m/z 20) and OD^+ (m/z 18) against pressure, observed with a repeller voltage setting corresponding to an ion exit energy of 4.0 eV. The kinetic plots for m/z 18 and m/z 20 are shown in Figure 3.2.6.1 -2 (ion exit energy: 4.0 eV). The validity of the free-fall formula in the pressure region of interest was affirmed by calculations of P_C (see Table 3.2.6.1 -1) and the experimental rate coefficients, k_{20} and k_{22} obtained from the slopes of the kinetic plots, are given in Table 3.2.6.1 -2. These rate coefficients were found to

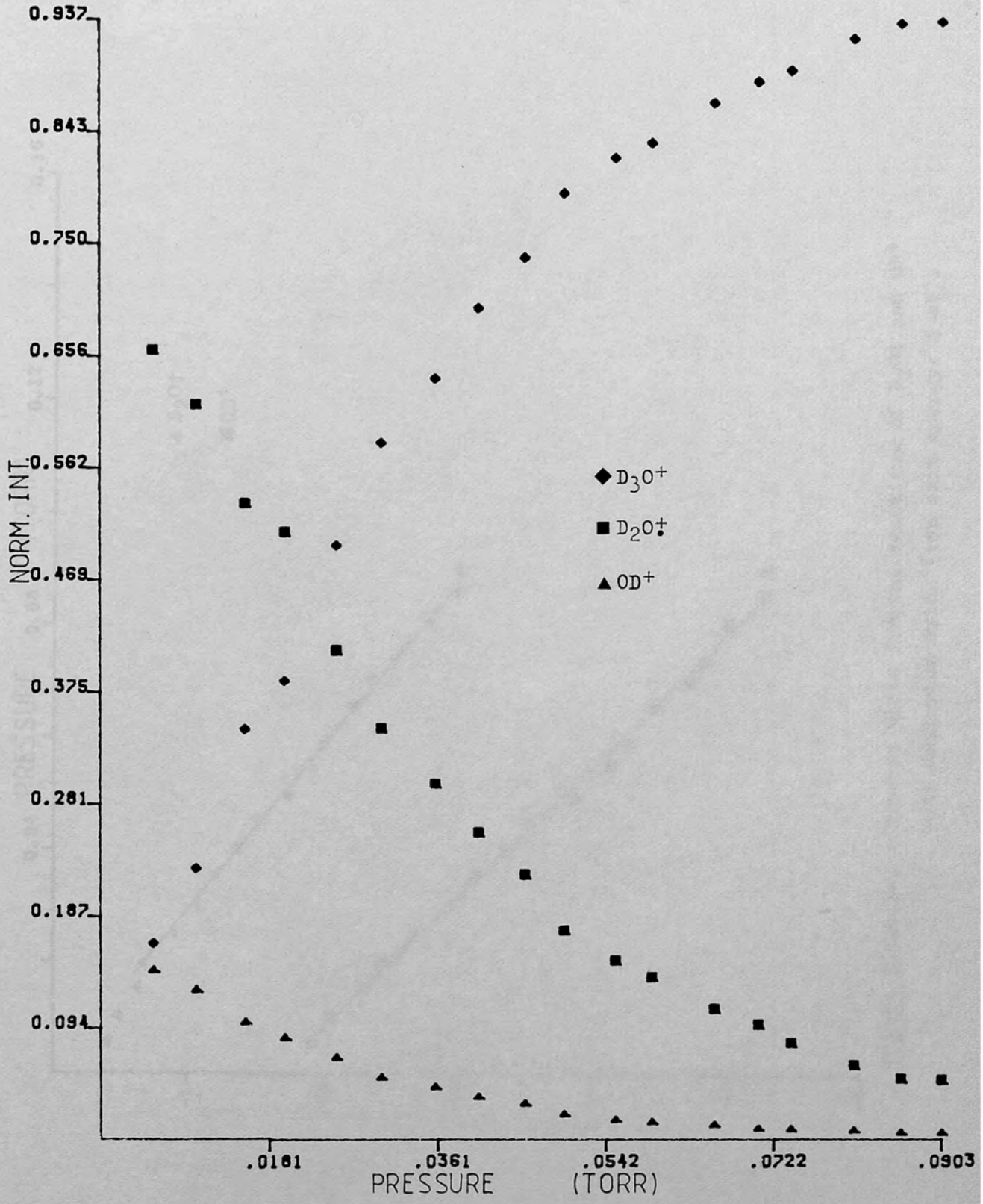

Figure 3.2.6.1-1 : Variation in the normalised intensities of ions in deuterium oxide with pressure (ion exit energy: 4 eV).

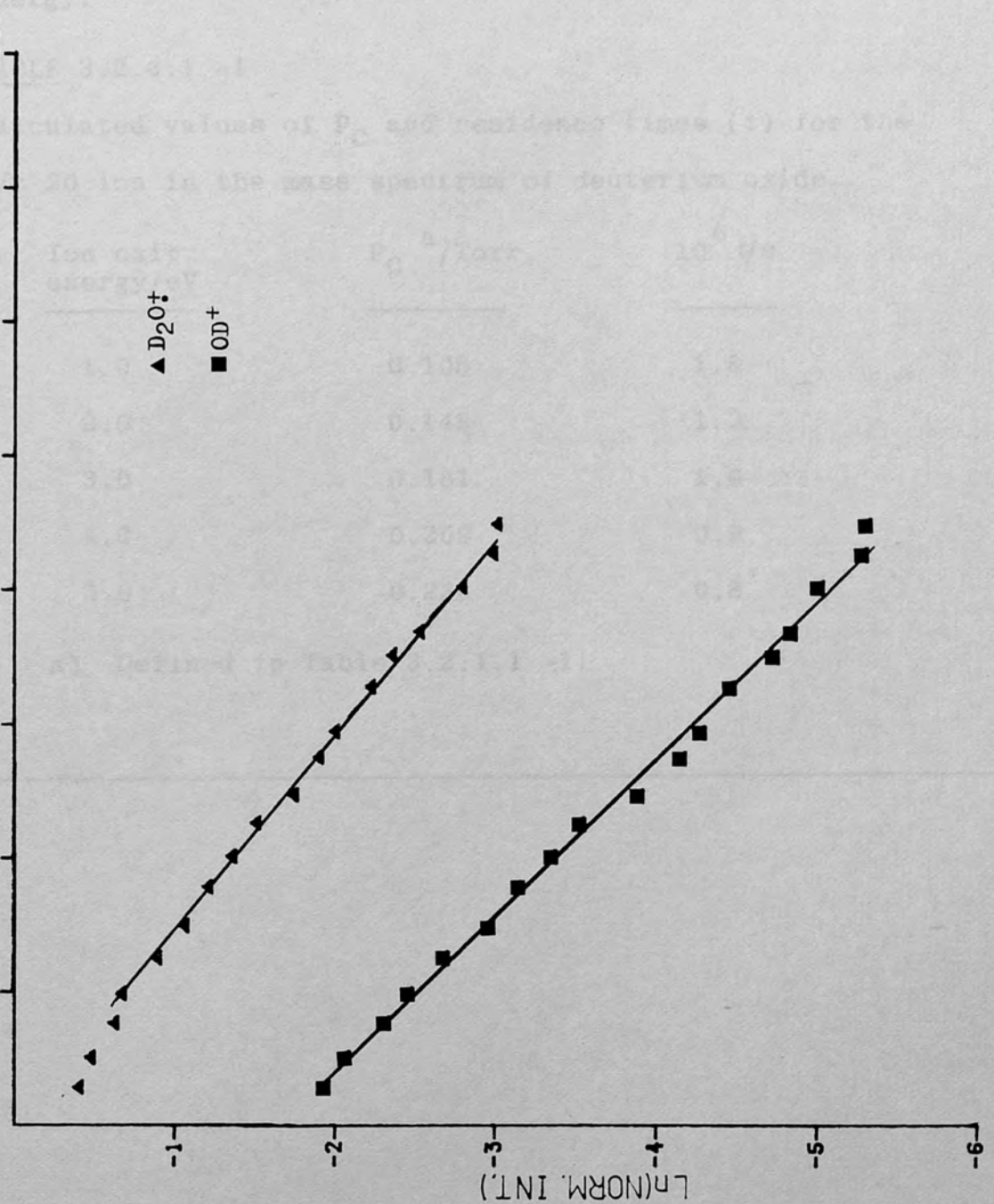

Figure 3.2.6.1-2 : Kinetic plots for the reactions of D_2O^+ and OD^+ with deuterium oxide (ion exit energy: 4 eV).

increase nonlinearly with increasing ion exit energy, as shown by Figure 3.2.6.1 -3. Estimation of k_{18}^{o} and k_{20}^{o} were obtained by graphic extrapolation to zero ion exit energy.

TABLE 3.2.6.1 -1

Calculated values of P_C and residence times (τ) for the m/z 20 ion in the mass spectrum of deuterium oxide.

Ion exit energy/eV	P_C [a]/Torr	$10^6 \tau$/s
1.0	0.105	1.8
2.0	0.148	1.3
3.0	0.181	1.0
4.0	0.209	0.9
5.0	0.234	0.8

a) Defined in Table 3.2.1.1 -1.

TABLE 3.2.6.1 -2

Disappearance rate coefficients[a] for the reactions of $D_2O^{+\cdot}$ and OD^+ in D_2O

Ion exit energy/eV	$10^9 k_{18}/cm^3 molec^{-1} s^{-1}$	$10^9 k_{20}/cm^3 molec^{-1} s^{-1}$
0	0.36[b]	0.52[b]
1.0	0.98 ± 0.06	0.09 ± 0.1
2.0	1.5 ± 0.1	1.27 ± 0.07
3.0	2.09 ± 0.09	1.56 ± 0.04
4.0	2.29 ± 0.08	1.73 ± 0.05
5.0	2.64 ± 0.09	1.82 ± 0.06

a) Errors shown are with 95% confidence.

b) Extrapolated value from Figure 3.2.6.1 -3.

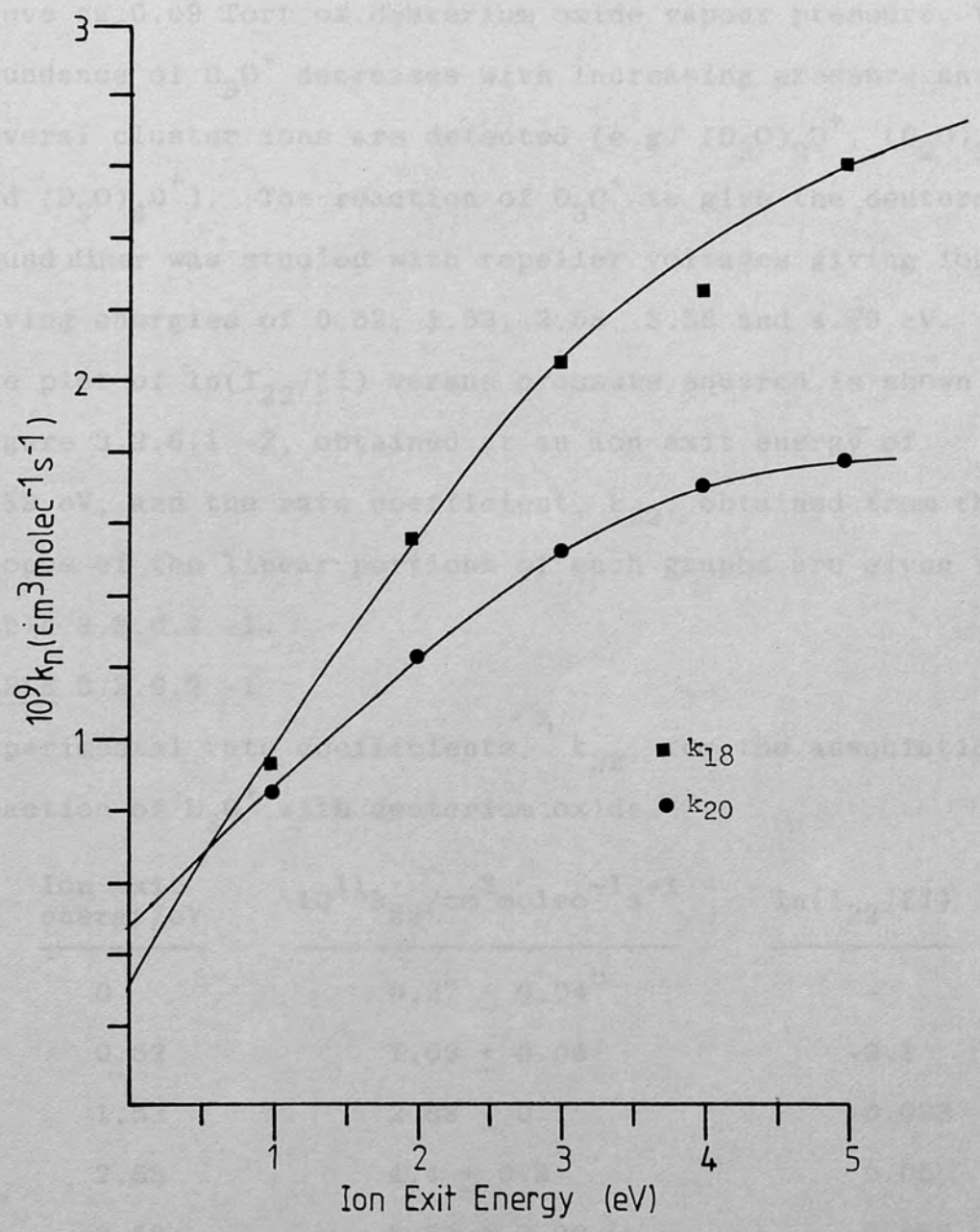

Figure 3.2.6.1-3 : Variation of disappearance rate coefficients of primary ions in deuterium oxide with ion exit energy.

3.2.6.2 Investigations of the association reaction of D_3O^+ with deuterium oxide.

As indicated previously in Figure 3.2.6.2 -1, above ca.0.09 Torr of deuterium oxide vapour pressure, the abundance of D_3O^+ decreases with increasing pressure and several cluster ions are detected (e.g. $(D_2O)_2D^+$, $(D_2O)_3D^+$, and $(D_2O)_4D^+$). The reaction of D_3O^+ to give the deuteron bound dimer was studied with repeller voltages giving ions having energies of 0.52, 1.53, 2.58, 3.58 and 4.59 eV. The plot of $\ln(I_{22}/\Sigma I)$ versus pressure squared is shown in Figure 3.2.6.1 -2, obtained at an ion exit energy of 4.59 eV, and the rate coefficient, k_{22}, obtained from the slopes of the linear portions of such graphs are given in Table 3.2.6.2 -1.

TABLE 3.2.6.2 -1

Experimental rate coefficients,[a] k_{22}, for the association reaction of D_3O^+ with deuterium oxide.

Ion exit energy/eV	$10^{11}k_{22}/cm^3molec^{-1}s^{-1}$	$\ln(I_{22}/\Sigma I)$
0	0.67 ± 0.04[b]	-
0.52	1.09 ± 0.06	-0.1
1.53	2.88 ± 0.1	-0.029
2.58	4.4 ± 0.2	0.05
3.58	5.34 ± 0.09	0.086
4.59	6.6 ± 0.1	0.1

a) Errors shown are with 95% confidence.

b) Determined from weighted least squares data fit.

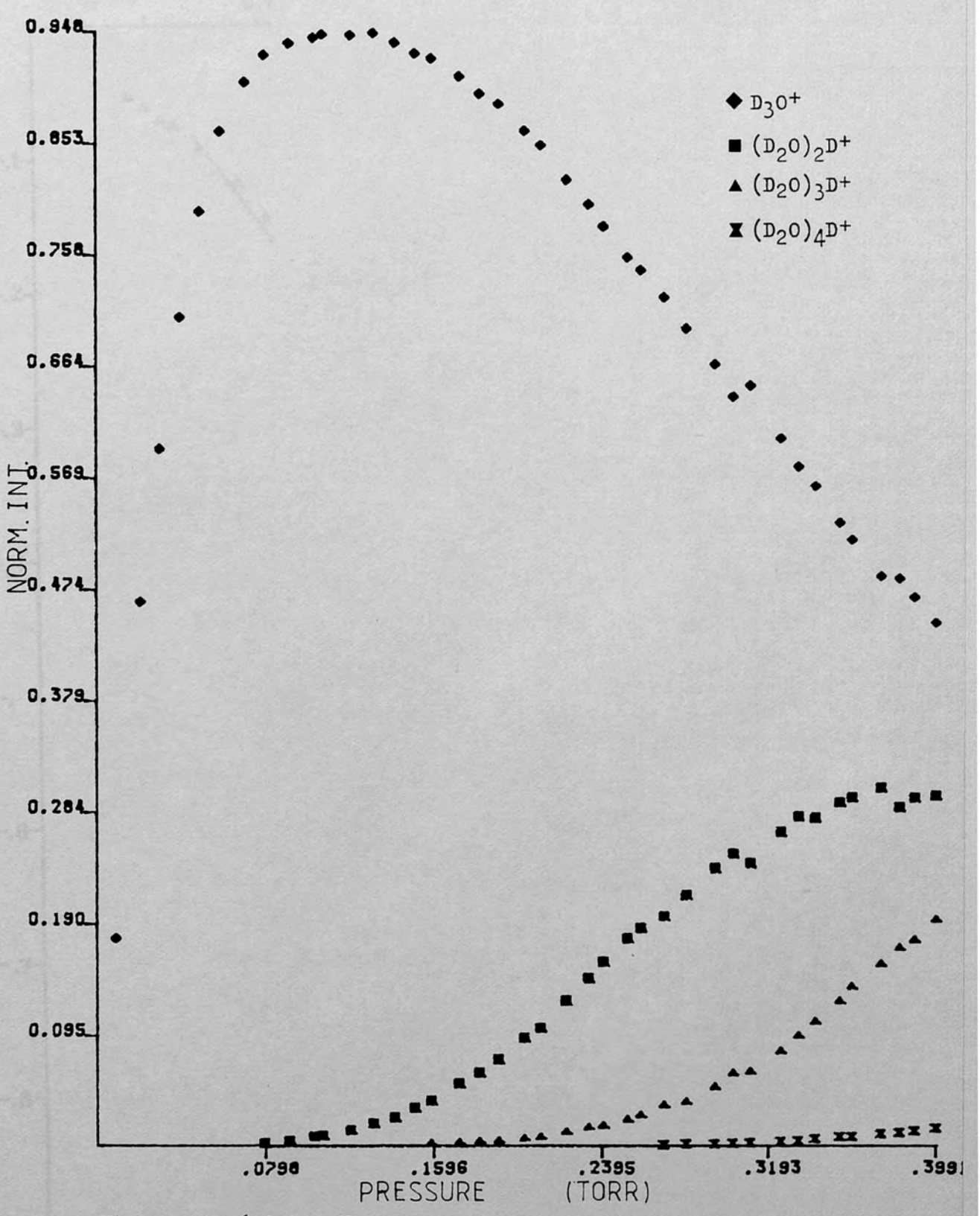

Figure 3.2.6.2-1 : Variation of the normalised intensities of ions in deuterium oxide with pressure (ion exit energy: 4.59 eV).

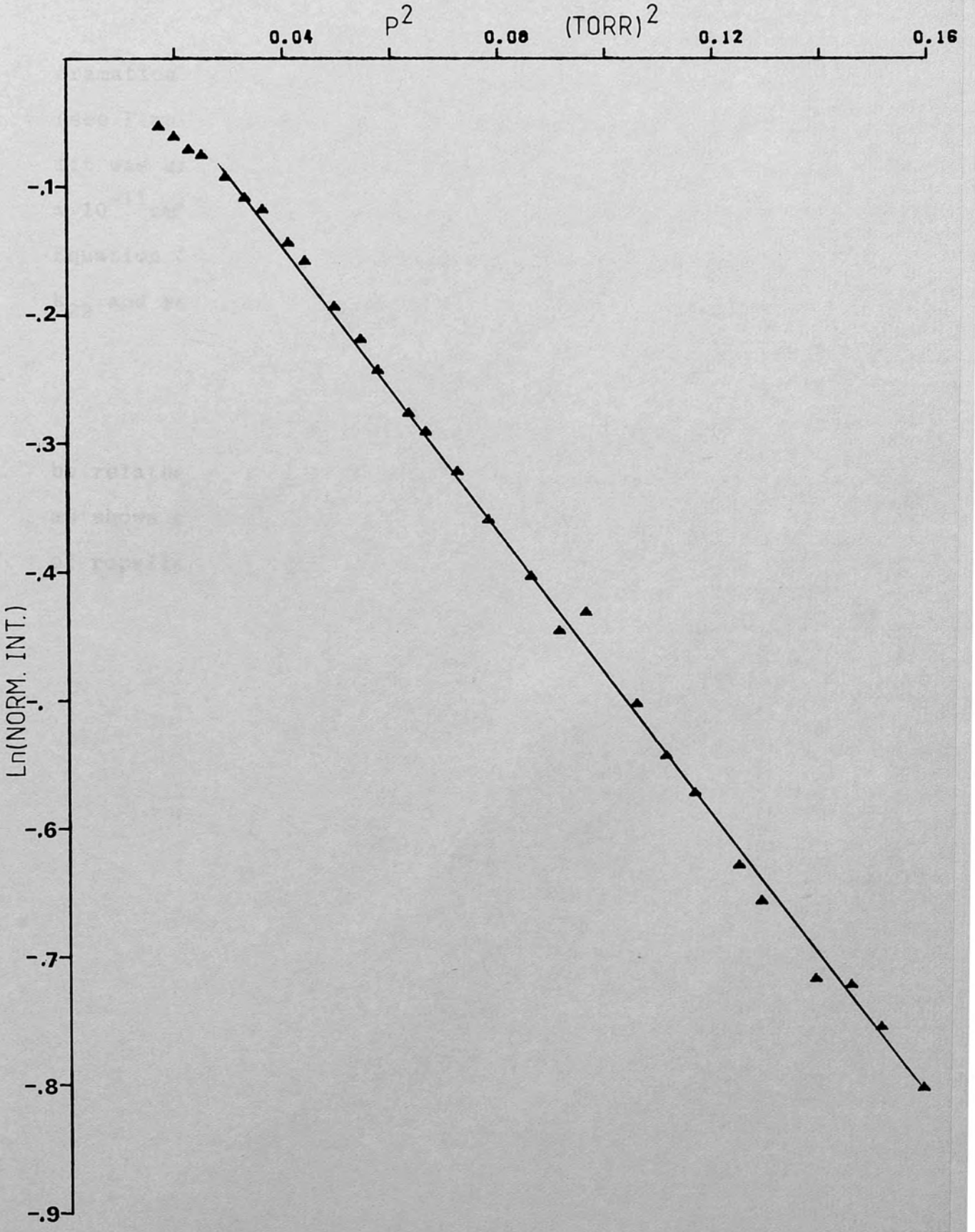

Figure 3.2.6.2-2 : Kinetic plot for the association reaction of D_3O^+ with deuterium oxide (ion exit energy: 4.59 eV).

The magnitude of k_{22} was found to increase dramatically and linearly with increasing ion exit energy (see Figure 3.2.6.2 -3). A weighted least squares line fit was used to obtained a value of k_{22}^{o} ($0.67 \pm 0.04 \times 10^{-11} cm^3 molec^{-1} s^{-1}$) from the calculated intercept. Equation 3.2.6.2 -1 describes the relationship between k_{22} and repeller voltage.

$$k_{22} = (1.30V + 0.67) \times 10^{-11} \qquad (3.2.6.2\text{ -}1)$$

The variation of $\ln(I_{22}^{o}/\Sigma I^{o})$ may also be related to ion exit energy by the equation of a line, as shown by Figure 3.2.6.2 -4, and expressed in terms of repeller voltage:

$$\ln(I_{22}^{o}/\Sigma I^{o}) = 0.051V - 0.108 \qquad (3.2.6.2\text{ -}2).$$

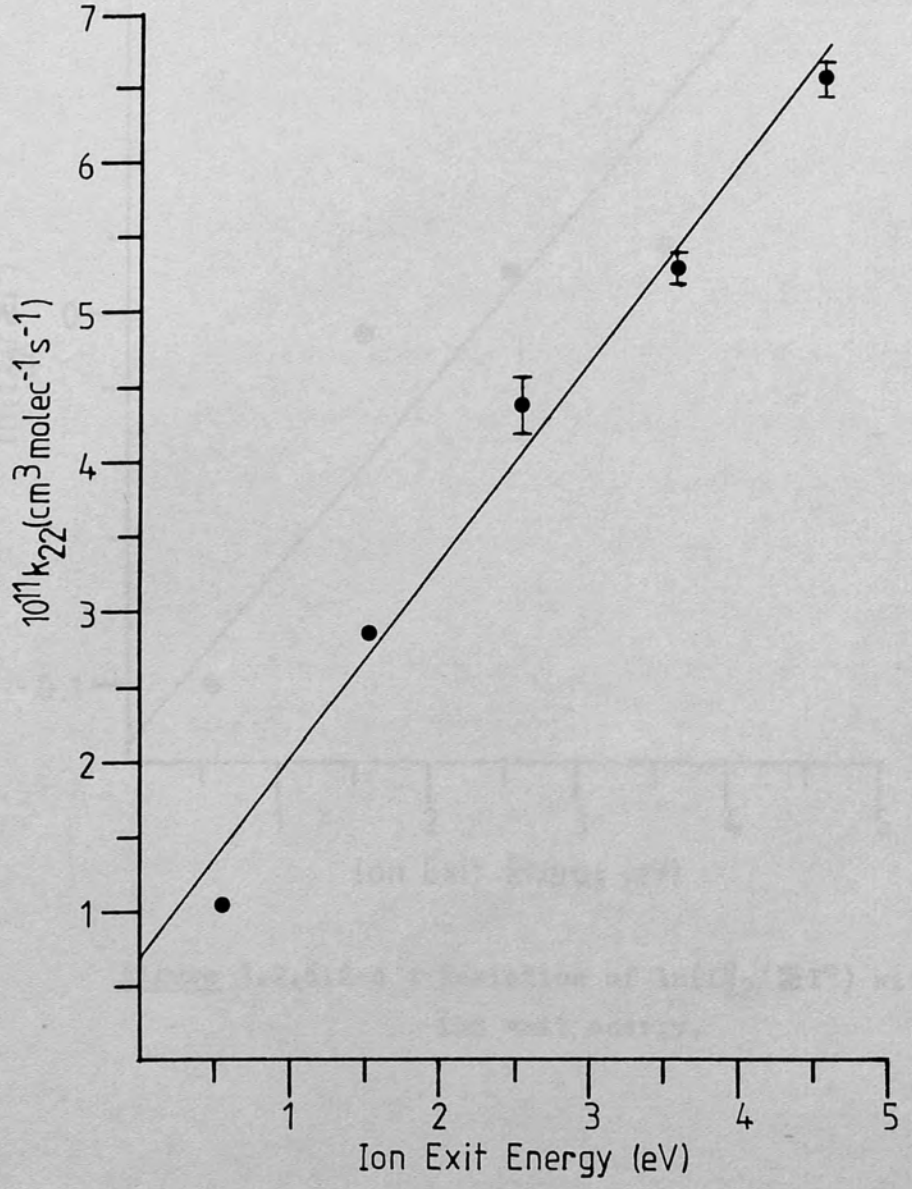

Figure 3.2.6.2-3 : Variation of k_{22} with ion exit energy.

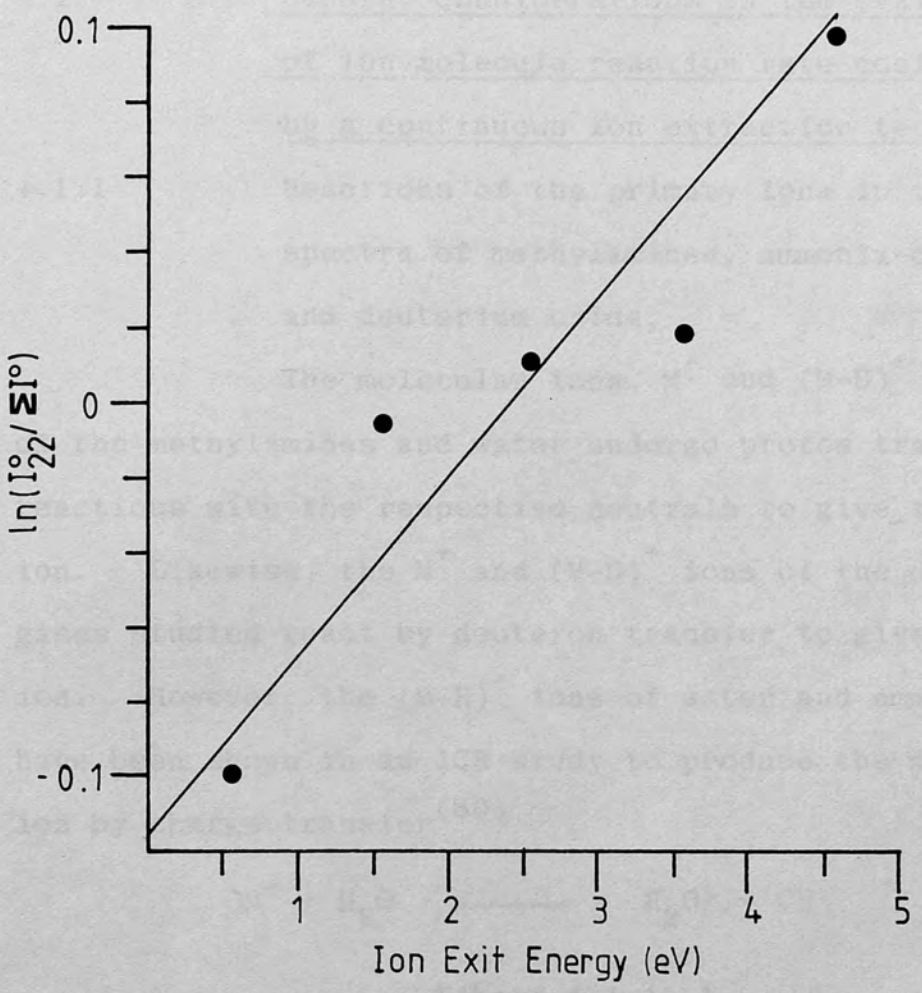

Figure 3.2.6.2-4 : Variation of $\ln(I^{\circ}_{22}/\Sigma I^{\circ})$ with ion exit energy.

4. DISCUSSION

4.1 General considerations in the evaluation of ion-molecule reaction rate coefficients by a continuous ion extraction technique.

4.1.1 Reactions of the primary ions in the mass spectra of methylamines, ammonia-d_3, water and deuterium oxide.

The molecular ions, $M^{+\cdot}$ and $(M-H)^+$ ions of the methylamines and water undergo proton transfer reactions with the respective neutrals to give the MH^+ ion. Likewise, the $M^{+\cdot}$ and $(M-D)^+$ ions of the deuterated gases studied react by deuteron transfer to give the MD^+ ion. However, the $(M-H)^+$ ions of water and ammonia have been shown in an ICR study to produce the molecular ion by charge transfer[80]:

$$OH^+ + H_2O \longrightarrow H_2O^{+\cdot} + OH\cdot$$

Scheme 4.1.1 -1

$$NH_2^+ + NH_3 \longrightarrow NH_3^{+\cdot} + NH_2\cdot$$

Scheme 4.1.1 - 2

Since such charge transfer reactions are not detectable under the experimental conditions described here the experimental rate coefficients obtained for the primary ions of the title gases are disappearance rate coefficients and not absolute rate coefficients for the proton or deuteron transfer reactions. The MH^+ (or MD^+) ions were the only product ions observed from the reaction of primary ions in the title gases.

The dependences upon ion exit energy exhibited by the disappearance rate coefficients of the primary ions were found to be similar, i.e. a nonlinear increase with increasing ion exit energy which becomes less pronounced at the higher ion exit energies in the range 0-5 eV. The theoretical expression derived by Gupta, Jones, Harrison and Myher[39] for the rate constants of ions accelerated by an electric field is

$$k_\varepsilon = 2\pi q(\alpha/\mu)^{\frac{1}{2}} + \frac{2\pi q\mu_D}{\mu}\left[\frac{m}{2\varepsilon}\right]^{\frac{1}{2}} x \ln\left[1 + 2\,(\mu\varepsilon/\pi k_B mT)^{\frac{1}{2}}\right] \qquad (4.1.1\text{-}1)$$

where ε is the ion exit energy, m is the mass of the ion and the other variables defined as before. (See the Appendix for the dipole moments and polarisabilities of neutrals used in this study). Because of the presence of $\varepsilon^{\frac{1}{2}}$ in the denominator of the second term, this expression leads to values of k_ε which increase rapidly as ε approaches zero. Thus, the observed dependences contradict that predicted by theory and can arise from an inadequacy in the use of the free fall formula to estimate ion residence times.

The magnitude of the disappearance rate coefficients of the primary ions are on the order of 10^{-9} cm^3 $molec^{-1}$ s^{-1} and thus correspond to "fast" ion-molecule reactions (i.e. reactions whose rate coefficients are of the same order as theoretical capture collision rate coefficients). The significance of this will

be made apparent in the following section.

4.1.2 Association reactions in methylamines, ammonia-d_3, water and deuterium oxide.

The association reactions of the MH^+ ions of methylamines and water and the MD^+ ions of ammonia-d_3 and D_2O are assumed to occur via an energy transfer mechanism, as shown for MH^+ in Scheme 4.1.2 -1.

$$MH^+ + M \underset{k_b}{\overset{k_f}{\rightleftharpoons}} MHM^{+*}$$

$$MHM^{+*} + M \xrightarrow{k_s} MHM^+ + M^*$$

Scheme 4.1.2 -1

If the lifetime of the excited collision complex MHM^{+*} is assumed to be short and the steady state approximation is applied, the disappearance of MH^+ is given by

$$d\{MH^+\}/dt = - \frac{k_f k_s \{MH^+\}\{M\}^2}{k_b + k_s\{M\}} \qquad (4.1.2\text{ -}1)$$

Integration of (4.1.2 -1) gives

$$\ln (\{MH^+\}/\{MH^+\}_o) = - \frac{k_f k_s \tau \{M\}^2}{k_b + k_s\{M\}} \qquad (4.1.2\text{ -}2)$$

Equation (4.1.2 -2) may be rewritten, for MH^+ of m/z=n, as

$$\ln (I_n/\Sigma I) = - \frac{k_f k_s \tau P_M{}^2 N^2}{k_b + k_s P_M N} + \ln(I_n{}^o/\Sigma I^o) \qquad (4.1.2\text{ -}3)$$

By defining $\beta=\tau/P_M$ and substituting into (4.1.2 -3), equation (4.1.2 -4) is obtained.

$$\ln(I_n/\Sigma I) = -\frac{k_f k_s \beta P_M{}^3 N^2}{k_b + k_s P_M N} + \ln (I_n^o/\Sigma I^o)$$

(4.1.2 -4)

At lower pressures, when $k_b >> k_s P_M N$, equation (4.1.2 -4) becomes

$$\ln(I_n/\Sigma I) = -\frac{k_f k_s \beta P_M{}^3 N^2}{k_b} + \ln (I_n{}^o/\Sigma I^o)$$

(4.1.2 -5)

and, the overall forward constant is expressed by:

$$k = k_f k_s P_M N/k_b = k_f k_s \{M\}/k_b.$$

Thus, the association reactions display third order kinetics at lower pressures. Such behaviour results in the deviation from linearity observed in the plots of $\ln(I_n/\Sigma I)$ against $P_M{}^2$ (vide infra) at lower values of $P_M{}^2$. At higher pressures, when the probability of collisional stabilisation of the activated complex, prior to dissociation, is high (i.e. $k_s P_M N >> k_b$) equation (4.1.2 -4) reduces to equation (4.1.2 -6) and $k = k_f$, with second order kinetics observed.

$$\ln (I_n/\Sigma I) = -k_f \beta N P_M{}^2 + \ln(I_n{}^o/\Sigma I^o)$$

(4.1.2 -6)

In the current study of clustering reactions in pure gases, the graphing of the Naperian logarithms of the normalised intensities of the reactant ions against pressure squared yielded plots which, although curved for the lower values of $P_M{}^2$, became linear as $P_M{}^2$ increased in magnitude. The above observation is consistent with a change from third to second order

kinetics as predicted by the energy transfer mechanism.

The slopes of the linear portions of the plots are equal to $k_f \beta N$ and thus the experimental rate coefficients obtained can be equated with k_f. The values of $\ln(I_n^o/\Sigma I^o)$ obtained from the intercepts of the kinetic plots have no real physical significance, since these correspond to hypothetical initial abundances of the reactant ion MH^+ (or MD^+) which is formed by the reaction of the primary ions in each gas. Indeed, positive intercepts were often obtained, which are clearly meaningless in terms of the initial abundance of the reactant ion.

The rate coefficients determined for the formation of the collision complex are on the order of $10^{-11} cm^3 molec^{-1} s^{-1}$ and are ca.two orders of magnitude smaller than those for the reactions of the primary ions. In order that the rate of disappearance of MH^+ (or MD^+) are not affected by the rate of its formation, the disappearance rate coefficients, should be at least an order of magnitude slower and this condition was valid for the association reactions studied.

A dependence of the experimental rate coefficients on ion exit energy was observed in which the rate coefficients increased rapidly with increasing ion exit energy and, for the most part, this dependence was linear. Again, this is contrary to theory and may result from the estimated values of the ion residue times being increasingly too small as ion exit energy is increased.

4.2 Determination of ion source pressures of methylamine, dimethylamine, trimethylamine, ammonia-d_3, water and deuterium oxide.

By rearranging equation (4.1.2 -6) and combining constants, an expression is derived by which the pressures of the title gases in the ion-source at 450°K may be estimated:

$$P_M = (9 \times 10^{-7})(\alpha\mu)^{-1/4} \left((-\ln I'_n + L)V/k_n d\ell\right)^{\frac{1}{2}} \qquad (4.2.\ -1)$$

In equation (4.2 -1), I_n' is the normalised intensity of the MH^+ (or MD^+) ion, L equals $\ln(I_n^o/\Sigma I^o)$, V is the repeller voltage, α is the angle averaged polarisability ($\mathring{A}^3$) and μ is the reduced mass. The application of this equation requires knowledge of the distance, ℓ, from the repeller plate to the ion exit slit (measured in centimetres) and d, the mean distance travelled by the ions, which may be assumed to be 0.5ℓ. Pressures in the range at which cluster ions are observed can thus be determined from the normalised intensities of the MH^+ ions in methylamine, dimethylamine, trimethylamine and water, and from the MD^+ ions of ammonia-d_3 and deuterium oxide. The use of equation (4.2 -1) will be discussed further in the following sections.

4.3 Rate coefficients determined for the reactions of ions in methylamine, dimethylamine and trimethylamine.

4.3.1 Methylamine

4.3.1.1 Evaluation of disappearance rate coefficients determined for primary ions in methylamine.

The structure of the $(M - H)^+$ ion in the mass spectrum of methylamine is assumed to be $CH_2{:}NH_2^+$ rather than CH_3NH^+. The observation that the loss of a deuterium atom from $CH_3CD_2NH_2^+$ is 12 times more probable than the loss of a hydrogen atom[81] lends support to this assumption.

Since it is desirable to determine the rate coefficient of ion-molecule reactions in the absence of electric and/or magnetic fields, an estimation of such rate coefficients, k_n^o, can be estimated by extrapolation of the k_n against ion exit energy plots to zero ion exit energy. Since such plots are curved, the values obtained for k_{30}^o and k_{31}^o via graphic extrapolation must be viewed with caution because a significant, but unknown degree of error is inherent in these k_n^o values. This uncertainty is present in all of the k_n^o values obtained for the primary ions in the six gases studied and the reservations expressed above hold throughout.

Values of $k_{30(ADO)}$ and $k_{31(ADO)}$ were determined from the parameterised average dipole orientation theory of Su and Bowers[42] and were found to be 16.8×10^{-10} and 16.6×10^{-10} $cm^3 molec^{-1} s^{-1}$, respectively.

Thus the extrapolated values of k_{30}^{o} and k_{31}^{o} are 34 and 60%, respectively, of the collision capture rate coefficients. For comparison, Table 4.3.1.1 -1 contains values reported in the literature for the disappearance rate coefficients of $CH_3NH_2^{+\cdot}$ and CH_3NH^{+}.

TABLE 4.3.1.1 -1

Disappearance rate coefficients of primary ions in methylamine

Rate coefficient	Experimental values ($cm^3 molec^{-1} sec^{-1}$ x 10^{10})	Method[a]	Reference
k_{30}	5.98	CIMS	82
	7 ± 1	CIMS[b]	77
	12	PIMS[c]	78
	11.0 ± 1	PhMS	57
	13.4 ± 0.4	CIMS	d
k_{31}	15.5	CIMS	82
	9 ± 1	CIMS[b]	77
	19	PIMS[c]	78
	12 ± 0.8	PhMS	57
	17.9 ± 0.5	CIMS	d

a) CIMS - chemical ionisation mass spectrometry,

PIMS - pulsed ion-source mass spectrometry,

PhMS - photoionisation mass spectrometry.

b) Ion exit energy : 2.5eV.

c) Ion exit energy : 3.4 eV, ion-source temperature: 373°K.

d) This work, 3.89 eV ion exit energy.

The agreement between the values of k_{30} obtained at 3.89 eV ion exit energy ((13.4 $\pm$ 0.4) x 10^{-10} $cm^3molec^{-1}s^{-1}$) and that reported by Jones and Harrison[78] for ions having an ion exit energy of 3.4 eV (12 x 10^{-10} $cm^3molec^{-1}s^{-1}$) is excellent. Likewise, their value for k_{31} at 3.4 eV ion exit energy (19 x $10^{-10}cm^3molec^{-1}s^{-1}$) and the value of (17.9 $\pm$ 0.5) x $10^{-10}cm^3molec^{-1}s^{-1}$ obtained at 3.89 eV ion exit energy are in close agreement. Indeed, such comparisons with rate coefficients obtained by similar techniques (see Table 4.3.1.1 -1) at similar ion exit energies are much more valid than the comparisons of k_n^o, obtained by graphic extrapolation, with the theoretical capture collision rate coefficients.

4.3.1.2 Evaluation of the rate coefficients obtained for the association reaction of $CH_3NH_3^+$ with methylamine.

The plots of normalised intensities of the $CH_3NH_3^+$ ion against pressure display a steady decrease towards the higher limit of the pressure range covered in this study, as the clustering reaction progresses. Such behaviour indicates that the reverse reaction (i.e. decomposition of the proton bound dimer) is not occurring to a significant extent, since a large contribution to the abundance of MH^+ from decomposition of the cluster ion would result in a large upward deflection in the normalised intensity plot. In the most extreme case, if there was achievement of equilibrium, the plot of the normalised intensities of MH^+ would behave

asymptotically at higher pressures. Clearly, the plots obtained represent conditions far removed from equilibrium. Moet-Ner and Field have determined the bimolecular rate coefficient for the back reaction in the equilibrium

$$CH_3NH_3^+ + CH_3NH_2 + M \rightleftharpoons (CH_3)NH_2)_2H^+ + M$$

to be 1.7×10^{-14} $cm^3molec^{-1}s^{-1}$ by pulsed, high pressure mass spectrometry.(83) This value is several orders of magnitude lower than the rate coefficients determined in the present study for the forward reaction. The observations mentioned above and the relative slowness of the back reaction as reported in the literature suggests that the assumption of negligible decomposition of the proton bound dimer under the conditions of the present study is valid.

The observed linear dependence of k_{32} with ion exit energy allows an estimation of k_{32}^o to be obtained easily, resulting in a value of $(0.60 \pm 0.02) \times 10^{-11} cm^3 molec^{-1} s^{-1}$. The observed rate coefficient k_{32} is equated with the rate coefficient, k_f, for the formation of the collision complex. Bowers and co-workers have determined k_f for methylamine in ion cyclotron resonance experiments employing pure methylamine.(56) By inverting equation (1.1.4.1 -1), they derived an expression for the apparent second order rate coefficient, k, such that

$$k^{-1} = (k'\{M\})^{-1} + k_f^{-1} \qquad (4.3.1.2\ -1)$$

where k' is the third order rate constant. By measuring k and plotting k^{-1} against $\{M\}^{-1}$, a straight line of

slope $1/k'$ and intercept $1/k_f$ is obtained. The uncertainty in the determination of k_f from the intercepts of such plots is given as $\pm$ 40%.(56)

The value of $(0.60 \pm 0.02) \times 10^{-11} cm^3 molec^{-1} s^{-1}$ obtained in this study for k^o_{32} is lower than that reported for k_f by Bowers(56) viz. $2.1 \times 10^{-11} cm^3 molec^{-1} s^{-1}$. However, this previously reported value for k_f was determined at a temperature of 302°K, which is 148° lower than the ion-source temperature employed in the current study. The rate coefficients of many association reactions display a negative temperature dependence(33) which can be expressed as

$$k = CT^n \qquad (4.3.1.2\text{ -}2)$$

where C is a constant related to the system of interest. The value of n for the temperature dependence of k_f for the formation of the collision complex $(CH_3NH_2)_2H^{+*}$ has been determined to be -2 ± 2 from the ion cyclotron resonance experiments mentioned above.(56) By using equation (4.3.1.2 -2) and assuming n = 2 (C was calculated to be 1.92×10^{-6} from the reported value of k_f at 302°K), the calculated value of k_f at 450°K was found to be 0.9×10^{-11} $cm^3 molec^{-1} s^{-1}$, which is in good agreement with k^o_{32} Thus, for the association reaction of $CH_3NH_3^+$ with methylamine, the assumption that the intercept of the plot of k_{32} against ion exit energy provides an estimation of the thermal rate constant appears to be valid.

The pressure of methylamine, P_{MA}, in the

ion-source can be estimated in the region of ca.80-400 millitorr at 450°K by means of equation (4.3.1.2 -3).

$$P_{MA} = (3.20 \times 10^{-7}) [(-\ln I'_{32} + L)V/k_{32}d\ell\ ]^{\frac{1}{2}} \qquad (4.3.1.2\text{ -3})$$

where I'_{32} is the normalised intensity of m/z 32 and V is the repeller voltage. The quantity L is equal to $\ln(I_{32}{}^{o}/\Sigma I^{o})$ and can be calculated for $V \geq 1$, by means of equation (3.2.1.2 -2). The value of k_{32} may be determined by equation (3.2.1.2 -1) and the other variables are defined as in Section 4.2.

4.3.2 Dimethylamine

4.3.2.1 Evaluation of disappearance rate coefficients determined for primary ions in dimethylamine.

In analogy with methylamine, the formation of the $(M-H)^+$ (m/z 44) ion of dimethylamine was assumed to occur via loss of a hydrogen from one of the methyl groups rather than cleavage of the N-H bond. The disappearance rate coefficients of the m/z 44 ion and the molecular ion show a dependence upon ion exit energy which is similar to that displayed by the primary ions of methylamine, discussed in the previous section, and the same comments apply here. Because of the curvature in the plots and the experimental scatter of the rate coefficients, especially in the plot of k_{44}, the values of k_{44}^o and k_{45}^o contain a high degree of uncertainty. The capture collision rate coefficients, $k_{44(ADO)}$ and $k_{45(ADO)}$, are 14.3×10^{-10} and 12.1×10^{-10} $cm^3 molec^{-1} s^{-1}$. These values are much higher than those obtained for k_{44}^o (3.2×10^{-10} $cm^3 molec^{-1} s^{-1}$) and k_{45}^o (4.6×10^{-10} $cm^7 molec^{-1} s^{-1}$). However, close agreement was observed between the disappearance rate coefficients obtained at an ion exit energy of 3.41 eV ($k_{44} = (7.4 \pm 0.6) \times 10^{-10} cm^3 molec^{-1} s^{-1}$ and $k_{45} = (10.6 \pm 0.5) \times 10^{-10} cm^3 molec^{-1} s^{-1}$) and those reported by Jones and Harrison[78] for the same ions at 3.4 eV viz. $k_{44} = 8 \times 10^{-10}$ $cm^3 molec^{-1} s^{-1}$ and $k_{45} = 12 \times 10^{-10}$ $cm^3 molec^{-1} s^{-1}$. For comparison Table 4.3.2.1 -1 contains these and other values reported in the literature for k_{44} and k_{45}.

TABLE 4.3.2.1 -1

Disappearance rate coefficients of primary ions in dimethylamine

Rate coefficient	Experimental values ($cm^3 molec^{-1} sec^{-1}$ x 10^{10})	Method[a]	Reference
k_{44}	4 ± 1	CIMS[b]	77
	8	PIMS[c]	78
	10 ± 1.3	PhMS	57
	7.4 ± 0.6	CIMS	d
k_{45}	6 ± 1	CIMS[b]	77
	12	PIMS[c]	28
	10.2 ± 0.8	PhMS	57
	10.6 ± 0.5	CIMS	d

a) Defined previously in Table 4.3.1.1 -1.

b) Ion exit energy : 2.5 eV.

c) Ion exit energy : 3.4 eV, ion source temperature: $373^{o}K$.

d) This work, ion exit energy : 3.41 eV.

4.3.2.2 Evaluation of the rate coefficients obtained for the association reaction of $(CH_3)_2NH_2^+$ with dimethylamine.

In the plot of the variation of the normalised intensity of the $(CH_3)_2NH_2^+$ ion with dimethylamine pressure, the abundance of $(CH_3)_2NH_2^+$ is shown to decrease less rapidly in the region above 0.31 Torr and a deviation from linearity is observed in the kinetic plot over the corresponding values of P_M. Moet-Ner and Field have determined the bimolecular rate coefficient for the decomposition of the proton bound dimer $((CH_3)_2NH)_2H^+$ to be 1.1×10^{-11} $cm^3molec^{-1}s^{-1}$ (83), which is of the same order of magnitude as the rate coefficients of the forward reaction determined in this study. The observed deviation from linearity in the kinetic plots for $P_M > 0.31$ can thus arise from the decomposition of the proton bound dimer being no longer negligible towards the high pressure limit of the current study. The kinetic plot is linear over the major part of the pressure range covered, however, which suggests that the reverse reaction is indeed negligible for $0.1 < P_M < 0.31$ and that the magnitude of the decomposition reaction rate coefficient reported by Moet-Ner and Field is possibly too large.

The rate coefficient, k_{46}, may be equated with the rate coefficient for the formation of the collision complex, k_f. The variation of k_{46} with ion exit energy is linear and the value of k_{46}^o obtained from the intercept of the plot of k_{46} versus ion exit energy

is $(0.216 \pm 0.012) \times 10^{-11}$ $cm^3 molec^{-1} s^{-1}$. Bowers and co-workers have also determined k_f for the formation of the proton bound dimer in pure dimethylamine in the ion cyclotron resonance study mentioned previously[56] and a value of 5.5×10^{-11} $cm^3 molec^{-1} s^{-1}$ ($\pm$ 40%) was obtained at 302°K. In the same study, a value of $n = 3 \pm 1$ was reported for the temperature dependence of k_f[56]. By using equation (4.3.1.2 -2) a calculated value of 1.7×10^{-11} $cm^3 molec^{-1} s^{-1}$ is obtained for k_f at 450°K, assuming $n = -3$. This value is much higher than that obtained for k_{46}^o in this study and further comment will be made in Section 4.3.4.2.

By employing repeller voltages in the range 0.5-5V, $\ln(I_{46}^o / \Sigma I_{46}^o)$ can be estimated by the linear relationship expressed by equation (3.2.2.2 -2) and substituted for the quantity L in equation (4.3.2.2 -1) below. The relationship between k_{46} and repeller voltage has been given by equation (3.2.2.2 -1) and by substituting the appropriate value into equation (4.3.2.2 -1), the pressure of dimethylamine, P_{DMA}, in the ion-source at 450°K can be estimated from, I'_{46}, the normalised intensity of m/z 46.

$$P_{DMA} = 2.66 \times 10^{-7} \left[(-\ln I'_{46} + L) V / k_{46} d\ell \right]^{\frac{1}{2}} \qquad (4.3.2.2\text{ -1})$$

The derivation of equation (4.3.2.2 -1) is the same as that given for equation (4.2-1) and the variables are defined as before.

4.3.3 Trimethylamine

4.3.3.1 Evaluation of disappearance rate coefficients determined for primary ions in trimethylamine.

Within the pressure range at which the primary ions of trimethylamine were studied, 5-80 millitorr, the normalised intensity of the $\{M-H\}^+$ ion is invariant within experimental error. This lack of reactivity has been noted previously by earlier workers.[57,77] Under the experimental conditions described for the current study, the hydride transfer reaction

$$(CH_3)_2NCH_2^+ + (CH_3)N \longrightarrow (CH_3)_3N + (CH_3)_2NCH_2^+ \quad ,$$

although possible, is not expected to be detectable.

The disappearance rate coefficients for the molecular ion of trimethylamine displayed a nonlinear dependence upon ion exit energy similar to those described previously for the disappearance rate constants of methylamine and dimethylamine. Extrapolation of the values of k_{59} to zero ion exit energy by a graphical method was used to estimate k_{59}^o and resulted in a value of $2 \times 10^{-10} cm^3 molec^{-1} s^{-1}$ which is 17% of $k_{59(ADO)}$. It should be noted that k_{59}, determined by photoionisation mass spectrometry, was reported by Hellner and Sieck[57] to be $(4.9 \pm 0.3) \times 10^{-10} cm^3 molec^{-1} s^{-1}$, which is only 41% of $k_{59(ADO)}$.

A more valid comparison can be made with the rate coefficient reported by Munson,[77] obtained at 2.5 eV ion exit energy. At 2.44 eV, in the current

study, k_{59} was found to be $(4.6 \pm 0.3) \times 10^{-10} cm^3 molec^{-1} s^{-1}$ and is in good agreement with Munson's value of 3.3×10^{-10} $cm^3 molec^{-1} s^{-1}$, determined by high pressure mass spectrometry.

4.3.3.2 Evaluation of the rate coefficients obtained for the association reactions of $(CH_3)_3NH^+$ and $(CH_3)_2NCH_2^+$ with trimethylamine.

Over the pressure region at which the clustering of $(CH_3)_3NH^+$ and $(CH_3)_2NCH_2^+$ with trimethylamine was observed in this study, the steady decrease in the abundances of these ions and the resulting linearity of the kinetic plots towards the high pressure limit are consistent with the absence of a significant amount of reverse reactions. As discussed in Section 4.3.1.2 for the association reaction of $CH_3NH_3^+$ with methylamine, such behaviour corresponds to conditions greatly removed from equilibrium.

The magnitude of k_f for the formation of the collision complex $((CH_3)_3N)_2H^{+*}$ has been determined to be $3.3 \times 10^{-11} cm^3 molec^{-1} s^{-1}$ ($\pm$ 40%) in trimethylamine at 302°K by Bowers and colleagues from an ion cyclotron resonance study.(56) In addition, they estimated k_f to have a temperature dependence of

$$k_f = CT^{-5\pm1} \qquad (4.3.3.2\text{-}1)$$

By determining C from k_f at 302°K, a value of 0.45×10^{-11} $cm^3 molec^{-1} s^{-1}$ for k_f at 450° is obtained.

In the current study, a least squares fit to the linear plot of k_{60} against ion exit energy

yielded an intercept of $(0.12 \pm 0.01) \times 10^{-11} cm^3 molec^{-1} s^{-1}$, which is equal to k_{60}^o. Although k_{60}^o is of the same order of magnitude as the calculated value of k_f at 450°, given above, the agreement is not particularly close. However, the error of ± 40% stated by Bowers should be kept in mind when comparing the two results.

The rate coefficients determined for the clustering reaction of $(CH_3)_2NCH_2^+$ were found to increase nonlinearly with increasing ion exit energy and k_{58}^o was estimated to be $0.1 \times 10^{-11} cm^3 molec^{-1} s^{-1}$ by extrapolation to zero ion exit energy. The rate coefficient for the association reaction of $(CH_3)_2NCH_2^+$ (m/z 58) with trimethylamine would not be expected to differ greatly from that for the reaction of $(CH_3)_3NH^+$ (m/z 60) with trimethylamine. Although the dependences of k_{60} and k_{58} with ion exit energy differ widely, the fact that k_{60}^o and k_{58}^o are identical within experimental error is supportive of the assumption that such intercepts, obtained by extrapolation of rate coefficient versus ion exit energy plots, are meaningful. Unfortunately, k_{58} has not been reported previously and no comparisons with data obtained by other methods can be made.

Since the variations of both k_{60} and $\ln(I_{60}^o/\Sigma I_{60}^o)$ with ion exit energy were found to be linear, these quantities may be easily calculated for repeller voltages of 0.52 - 5V by means of equations (3.2.3.2 -1) and (3.2.3.2 -2) respectively. The pressure of trimethylamine, P_{TMA}, in a chemical ionisation

ion-source at 450°K can thus be estimated by equation (4.2 -1), i.e.

$$P_{TMA} = 2.31 \times 10^{-7} [(-\ln I'_{60} + L)V/k_{60} d\ell\ ]^{\frac{1}{2}}$$

where I'_{60} is the normalised intensity of m/z 60, $L = \ln(I^{o}_{60}/\Sigma I^{o})$, V is the repeller voltage, d is the mean distance travelled by the ion (taken to be 0.5ℓ) and ℓ is the distance from the repeller plate to the ion exit slit.

4.3.4 Comparison of reaction rate coefficients obtained for ions in methylamine, dimethylamine and trimethylamine.

4.3.4.1 Disappearance rate coefficients of primary ions.

The trend of reactivities observed for the proton transfer reactions of the molecular ions of the title compounds ($CH_3NH_2^{+\cdot} > (CH_3)_2NH^{+\cdot} > (CH_3)_3N^{+\cdot}$) is the same as that observed in earlier studies.[57,77] This order is the reverse of that which would be predicted on the assumption that the neutrals of highest proton affinity would be more reactive, since the order of gas phase basicities for these amines is trimethylamine > dimethylamine > methylamine.[84] Hellner and Sieck have suggested that the observed order of reactivities may reflect the energy of activation required to abstract a proton from a methyl group.[57] Since increased methyl substitution results in greater stability of the ion, the above postulation is reasonable.

The order of reactivities of the $\{M-H\}^+$ ions follow the same trend. Assuming the $\{M-H\}^+$ ions of methylamine, dimethylamine and trimethylamine to have the structures 1,2, and 3, respectively, it becomes apparent that the loss of a proton from 3 to give a neutral molecule is not possible, whereas proton transfer from 1 and 2 yields the imines 4 and 5 as the neutral products.

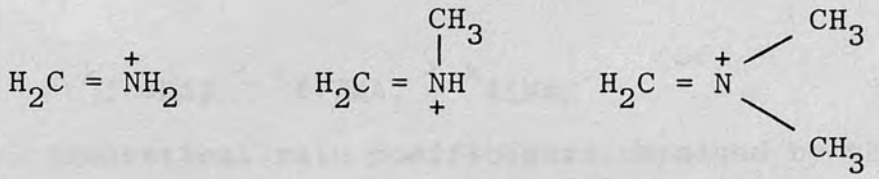

1 2 3

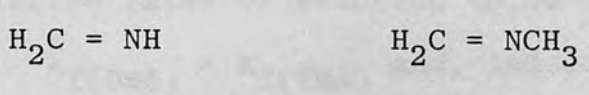

4 5

The unreactivity of the $\{M-H\}^+$ ion of trimethylamine is thus consistent with its existence as the immonium ion 3.

One would expect 5 to have a greater proton affinity than 4 and thus, removal of a proton from 2 should be more difficult than from 1. The order of reactivity observed suggests that the relative ease with which a proton is removed from 1 and 2 is the rate determining factor, rather than the proton affinity of the neutral reactant.

4.3.4.2 Rate coefficients determined for the formation of the excited collision complex M_2H^{+*} in the methylamines.

The values of k_f (the rate coefficient associated with the formation of M_2H^{+*}) reported by Bowers for the methylamines[56] and those determined in this study agree in the order of magnitude (10^{-11} $cm^3molec^{-1}s^{-1}$) but differ on the relative order of reactivities. The trend observed for the rate coefficients determined in the ion cyclotron resonance study by Bowers and co-workers is

$$k_{f(DMA)} > k_{f(TMA)} > k_{f(MA)}. \quad (56)$$

However, theoretical rate coefficients obtained by the parameterised average dipole orientation theory predict the relative rates of reaction to be in the order $k_{f(MA)} > k_{f(DMA)} > k_{f(TMA)}$ and, indeed, this is the same order which is observed in the present study. This trend is also consistent with steric considerations, since steric hindrance in the excited collision complex would be expected to increase with increased substitution on the nitrogen atom.

The order of magnitude of the values of k_f determined by Bowers[56] and by this study are substantially lower than the capture collision rate coefficients ($k_{f(ADO)}$) for the association reactions of the MH^+ ions of methylamine, dimethylamine and trimethylamine (1.6, 1.4 and 1.2 x 10^{-9} $cm^3 molec^{-1} s^{-1}$, respectively). Moet-Ner has proposed the mechanism shown in Scheme 4.3.4.2 -1 to account for such apparent discrepancies between experimentally determined values of the rate coefficients for the formation of the excited collision complexes in association reactions and those predicted by theory.[33]

$$A^+ + M \underset{k_b}{\overset{k_f}{\rightleftharpoons}} AM_L^{+*} \underset{k'_b}{\overset{k'_f}{\rightleftharpoons}} AM_T^{+*} \xrightarrow{k_s} AM^+$$

Scheme 4.3.4.2 -1

In Scheme 4.3.4.2 -1, a "loose" collision complex, AM_L^{+*}, is formed initially in which

A^+ and M undergo multiple collisions while experiencing changes in orientation. If a collision occurs with A^+ and M in the required orientation, a "tight" collision complex, AM_T^{+*}, is formed in which specific bonding exists. (In the case of the association reactions discussed herein, AM_T^{+*} is held together by hydrogen bonding). A steady state approximation towards AM_T^{*+} and AM_L^{*+} results in the following expression for the overall rate coefficient:

$$k_f = \frac{k_s k_f' k_f\{M\}}{k_s\{M\}(k_f' + k_b) + k_b' k_b} \qquad (4.3.4.2\text{ -}1)$$

At low pressure,

$$k_f = k_s k_f' k_f\{M\}/k_b' k_b \qquad (4.3.4.2\text{ -}2)$$

and thus, k_f is proportional to $\{M\}$, with the reaction exhibiting third order behaviour. At high pressures,

$$k = k_f k_f'/(k_f' + k_b) \qquad (4.3.4.2\text{ -}3)$$

and the reaction displays second order kinetics. If k_b is greater than or comparable to k_f' the observed overall rate coefficient at the high pressure limit can be significantly smaller than the capture collision rate constant, k_f. Assuming Moet-Ner's postulate of the formation of a loose collision complex,[33] as in Scheme 4.3.4.2 -1, k_f' depends only on the frequency of collisions within AM_L^{+*} and in steric factors. A lower value for the overall rate coefficient will be observed in the presence of steric hindrance. Scheme

4.3.4.2 -1 can thus be used to rationalise both the observed trend in reactivities and the lower values obtained experimentally for the formation of the collision complex.

4.4 Rate coefficients determined for the reactions of ions in ammonia-d_3

4.4.1 Evaluation of the disappearance rate coefficients of primary ions in ammonia-d_3.

The disappearance rate coefficients of the $M^{+\cdot}$, m/z 20, and $(M-D)^+$, m/z 18 ions of ammonia-d_3 vary nonlinearly with ion exit energy, as shown by Figure 3.2.4.1 -3. In the range 0-5eV, they increase rapidly to 1.62 and 2.45 x $10^{-9}cm^3molec^{-1}s^{-1}$, respectively, at 2.58 eV ion exit energy and then increase only slightly. An estimation of k^o_{18} and k^o_{20} was obtained by graphic extrapolation of the data points and intercepts of 1.2 and 0.8 x $10^{-9}cm^3molec^{-1}s^{-1}$, respectively, were obtained. These values for k^o_{18} and k^o_{20} are 63% and 42% of $k_{n(ADO)}$ respectively, which, in view of the uncertainties in k^o_n imposed by a graphic determination, represent a reasonable agreement.

Unfortunately, literature values for k_{18} and k_{20} are not available for comparison. The disappearance rate coefficients for the molecular and $(M-H)^+$ ions of ammonia have been determined by previous workers using the same instrument, procedure and experimental conditions as described in this Part and values of 1.42 x $10^{-9}cm^3molec^{-1}s^{-1}$ for k^o_{17} and 2.18 x 10^{-9} $cm^3molec^{-1}s^{-1}$ for k^o_{16} were obtained.[85,86] Thus, the primary ions of ammonia-d_3 react at rates which are ca.30% slower than those of the analogous ions in

ammonia. This observation will be discussed further in Section 4.4.3.

4.4.2 Evaluation of rate coefficients obtained for the association reaction of ND_4^+ with ammonia-d_3.

A pulsed, high pressure mass spectral study of the formation of the proton bound dimer $(NH_3)_2H^+$, using methane as the major gas, has been reported by Moet-Ner and Field, from which a value of 3.1×10^{-15} $cm^3 molec^{-1} s^{-1}$ was obtained for the bimolecular rate coefficient for the reverse reaction.(83) The corresponding rate coefficient for the decomposition $(ND_3)_2D^+$ would not be expected to differ greatly. Since the magnitude of the reverse reaction rate coefficient mentioned above is four orders of magnitude smaller than that for the forward reaction, the amount of reverse reaction can be assumed to be negligible. This assumption is supported by the steady decrease in the abundance of ND_4^+ over the pressure range at which the association reaction was observed and is also consistent with the linearity of the kinetic plots (vide infra).

Within the pressure range 0.08 - 0.28 Torr, the plot of $\ln(I_{22}/\Sigma I)$ against the square of pressure displays only a little curvature, becoming linear for values of P_{ND_3} greater than 0.014 Torr. Such behaviour (see Figure 3.2.4.2 -1) is consistent with the energy transfer mechanism discussed in Section 4.1.2. The variation of k_{22} increases nonlinearly with increasing ion exit energy as shown in Figure 3.2.4.2 -2. This

nonlinear dependence results in an estimation of k_{22}^{o} having to be made from a graphic extrapolation of the data points to zero in exit energy and k_{22}^{o} was thus determined to be $0.1 \times 10^{-11} cm^3 molec^{-1} s^{-1}$. Although no literature values are available for comparison, the analogous reaction of NH_4^+ with ammonia has been investigated by the same method by previous researchers[85] and k_{18} was determined to be $0.24 \times 10^{-11} cm^3 molec^{-1} s^{-1}$ at 1 eV ion exit energy. Comparison of this value with the corresponding value of k_{22} on the plot shown in Figure 3.2.4.2 -2 indicates that the formation of $(ND_3)_2D^+$ in ND_3 proceeds ca.6 times faster than the formation of $(NH_3)_2H^+$ in ammonia. This observation will be discussed further in Section 4.4.3.

By means of the data given in Table 3.2.4.2 -1, the pressure of ammonia-d_3 may be estimated for chemical ionisation applications from equation (4.2.1). Combining constants give

$$P_{ND_3} = (4.09 \times 10^{-7}) \left[(-\ln I'_{22} + L)V/k_{22} d\ell\right]^{\frac{1}{2}} \qquad (4.4.2\text{ -}1)$$

Thus, by choosing a repeller voltage (V) corresponding to one of the ion exit energies shown in the aforementioned table, the correct value of $\ln(I_{22}^{o}/\Sigma I^{o})$ may be substituted for L and k_{22} is read directly from the table (the other variables defined as in 4.2). A simple measurement of the normalised intensity of m/z 22 (I'_{22}) then allows the ion-source pressure to be determined.

4.4.3 Comparison of the rate coefficients determined for the reaction of ions in ND_3 with those for the analogous ions in NH_3.

4.4.3.1 Primary ions.

As mentioned previously in Section 4.4.1, the reactions of $ND_3^{+\cdot}$ and ND_2^+ with ND_3 are slower than the analogous reactions of $NH_3^{+\cdot}$ and NH_2^+ with ammonia. This is consistent with a primary isotope effect and suggests that the difference in rates is due to the difference in the energy requirement for the abstraction of a deutron versus the abstraction of a proton from analogous ions. This difference can be illustrated by the energy diagrams shown in Figure 4.4.3.1 -1. Here it is assumed that proton or deuteron transfer is the main exit channel for the primary ions. The collision complex (RHM^{+*} or $R'DM'^{+*}$) is formed with excess energy and can proceed to form products or decompose to reactants. Since the energy barrier for the forward reaction of the collision complex is higher for the deuterated system, as compared with the ammonia system, the reaction proceeds more slowly in the case of the former.

4.4.3.2 Comparison of rate coefficients for the formation of proton and deutron bound dimers in ammonia and ammonia-d_3, respectively.

The rate coefficients determined in this study for the reaction of ND_4^+ with ND_3 can be equated

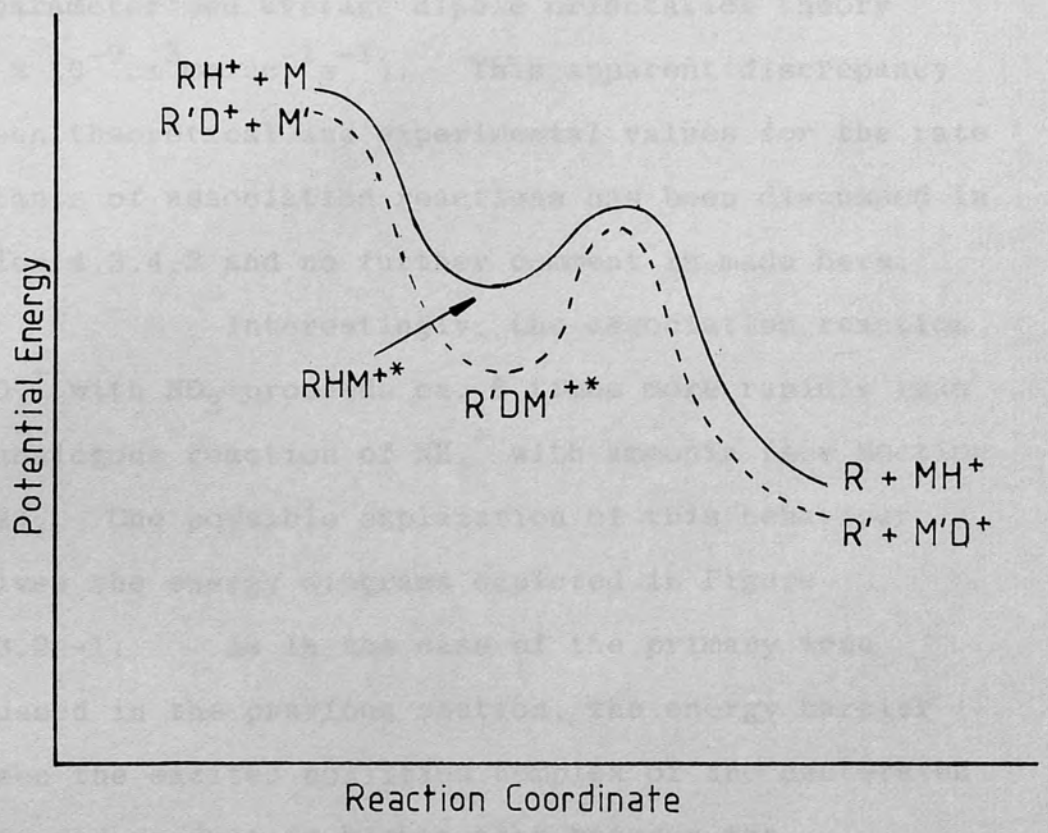

Figure 4.4.3.1-1 : Notional energy diagrams for the reaction of primary ions in ammonia and ammonia-d_3.

with the rate coefficient for the formation of the excited collision complex, $(ND_3)_2D^{+*}$, as discussed in Section 4.1.2. Again, these rate coefficients are ca.2-3 orders of magnitude lower than that predicted by the parameterised average dipole orientation theory ($1.9 \times 10^{-9} cm^3 molec^{-1} s^{-1}$). This apparent discrepancy between theoretical and experimental values for the rate constants of association reactions has been discussed in Section 4.3.4.2 and no further comment is made here.

Interestingly, the association reaction of ND_4^+ with ND_3 proceeds ca. 6 times more rapidly than the analogous reaction of NH_4^+ with ammonia (see Section 4.4.2). One possible explanation of this behaviour involves the energy diagrams depicted in Figure 4.4.3.2 -1. As in the case of the primary ions discussed in the previous section, the energy barrier between the excited collision complex of the deuterated system and product is higher than between the corresponding states in the ammonia system. However, the rate coefficients obtained for the association reactions studied in this work are identified with the formation of the excited collision complex. Thus, such rate coefficients would be expected to be insensitive to the differences in the relative heights of the energy barriers between the collision complexes and products. The observed larger rate for the association reaction of ND_4^+ may be rationalised in terms of the greater stability of the deuterated system and the greater probability of

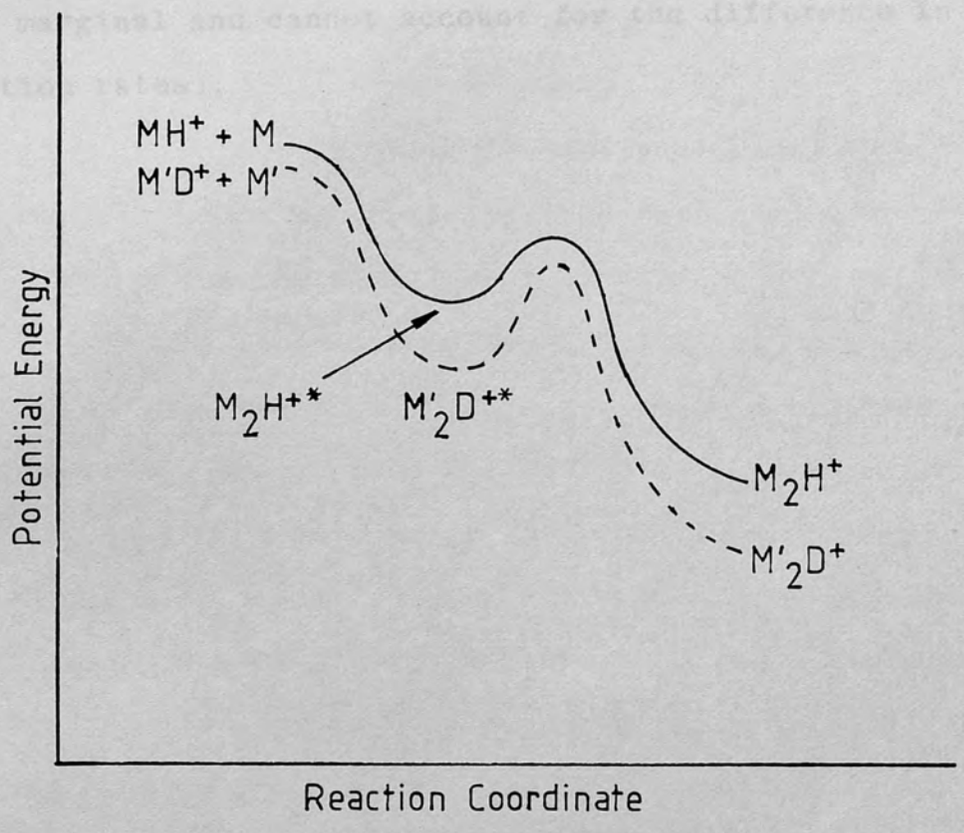

Figure 4.4.3.2-1 : Notional energy diagrams for the association reactions of NH_4^+ and ND_4^+.

decomposition of the excited collision complex $(NH_3)_2H^{+*}$. (Although ND_3 might be expected to show an increase in third body efficiency for the removal of excess energy from the collision complex, this increase is probably only marginal and cannot account for the difference in reaction rates).

4.5 Rate coefficients obtained for the reactions of ions in water and deuterium oxide vapour.

4.5.1 Evaluation of disappearance rate coefficients determined for primary ions in water vapour.

The parameterised average dipole orientation theory predicts that the thermal rate coefficients for the reaction of OH^+ (m/z 17) and $H_2O^{+\cdot}$ (m/z 18) should be on the order of 2.1 x $10^{-9}cm^3molec^{-1}s^{-1}$ and the estimations of k^o_{17} and k^o_{18}, obtained by graphical extrapolation, are 71% and 67% of the $k_{n(ADO)}$ rates. Although this is a reasonable agreement, the nonlinear dependence of k_{17} and k_{18} upon ion exit energy induces a certain degree of uncertainty into k^o_{17} and k^o_{18}. Harrison and co-workers have reported the rate coefficients for the disappearance of OH^+ and $H_2O^{+\cdot}$ to be 1.92 x 10^{-9} and 1.96 x 10^{-9} $cm^3molec^{-1}s^{-1}$, respectively, employing a pulsed electron beam ion-source operating with a repeller voltage corresponding to 3.4 eV ion exit energy.(39) The agreement between these values and those obtained in this study at 3.08 eV ion exit energy is quite close (k_{17} = (2.44 $\pm$ 0.05) x $10^{-9}cm^3molec^{-1}s^{-1}$, k_{18}= (2.12 $\pm$ 0.06) x $10^{-9}cm^3molec^{-1}s^{-1}$). For comparison, literature values for k_{18} and k_{17}, including those by Harrison and colleagues are given in Table 4.5.1.1 -1, together with those determined in this study. The current results are consistent with the data of earlier workers.

TABLE 4.5.1.1 -1

Disappearance rate coefficients of primary ions in water vapour.

Rate coefficient	Experimental Values ($cm^3 molec^{-1} s^{-1} \times 10^9$)	Method[a]	Reference
k_{17}	1.92	PIMS[b]	39
	3.7 ± 0.3	PIMS(α)[c]	88
	2.0 ± 0.5	PIMS	89
	2.89 ± 0.27	ICR[d]	80
	2.44 ± 0.05	CIMS	e
k_{18}	1.96	PIMS[b]	39
	2.19	PIMS	87
	2.5 ± 0.2	PIMS(α)[c]	88
	2.62 ± 0.3	PIMS	89
	2.05 ± 0.1	ICR[d]	80
	2.12 ± 0.06	CIMS	e

a) PIMS - Pulsed ion-source mass spectrometry;
ICR - Ion cyclotron resonance
CIMS - Chemical ionisation mass spectrometry.

b) Ion exit energy - 3.4 eV.

c) Alpha - particle bombardment source.

d) Rate constants determined by this method are absolute rate coefficients for the proton transfer reactions of the primary ions in water.

e) This work, ion exit energy: 3.08 eV.

4.5.2 Evaluation of disappearance rate coefficients for primary ions in deuterium oxide vapour.

The experimental rate coefficients determined for the reactions of OD^+ and $D_2O^{+\cdot}$ with D_2O display a dependence upon ion exit energy which is similar to that observed for the reactions of the primary ions of the other reagent gases studied, i.e. a generally increasing but nonlinear reliance.

An unusual aspect of the curves observed for the relationship of k_{18} and k_{20} upon ion exit energy is their intersection at a point corresponding to ca. 0.6 eV ion exit energy. The calculated capture collision rate coefficients ($k_{18(ADO)} = 1.98 \times 10^{-9} cm^3 molec^{-1} s^{-1}$ and $k_{20(ADO)} = 1.95 \times 10^{-9} cm^3 molec^{-1} s^{-1}$) indicate that the OD^+ ion should react faster, albeit only slightly. The intersection of the two plots shown in Figure 3.2.6.1 -3 is probably an artifact owing to experimental error in the determination of k_{18} (and/or k_{20}) at 1 eV ion exit energy. Because of the unrealistic weighting placed on the rate coefficient determined at the lowest ion exit energy and the graphical method employed to extrapolate to zero ion exit energy, only a small error in that rate coefficient results in a large difference in the intercept obtained. For this reason, such intercepts are highly unreliable.

Harrison and co-workers have studied the reactions of OD^+ and $D_2O^{+\cdot}$ at 3.4 eV ion exit energy.[39] At an ion-source temperature of 373°K, these authors

obtained values of 0.86×10^{-9} $cm^3 molec^{-1} s^{-1}$ and 1.15×10^{-9} $cm^3 molec^{-1} s^{-1}$ for k_{18} and k_{20} respectively.(39) Reasonable agreement is thus present between the value of k_{20} determined in this work at 3.0 eV ion exit energy ($(1.56 \times 0.04) \times 10^{-9}$ $cm^3 molec^{-1} s^{-1}$) and the value quoted above. In comparison with the current results, their value for k_{18} (3.4 eV ion exit energy) appears to be very low, even when the higher ion-source temperature employed in the current study (450^{o}) is taken into consideration.

Comparison of the rate coefficients obtained for the reactions of the primary ions in water vapour and deuterium oxide vapour indicates that the deuteron transfer reactions are slower. The deuteron affinity of deuterium oxide has been experimentally determined to be ca.0.1 eV greater than the proton affinity of water(53) and thus the proton/deuteron affinity of the neutral reactant is not a rate determining factor. The lower reactivity of the primary ions in deuterium oxide vapour can result from a primary isotope effect such as that described previously for the ions in ammonia-d_3 (see Section 4.4.3.1) and the energy diagrams shown in Figure 4.4.3.1 -1 can also be applied to the water and deuterium oxide systems. The results of Harrison and co-workers also display a comparatively higher reactivity for the primary ions in water vapour versus the analogous reactions in the deuterated system.(39)

4.5.3 Comparison of rate coefficients for the association reactions of H_3O^+ and D_3O^+

The plots of the normalised intensities of H_3O^+ and D_3O^+ against pressure display a steady decrease in the abundance of these ions over the pressure range at which the association reactions predominate. The bimolecular rate coefficient for the decomposition of the proton bound dimer $(H_2O)_2H^+$ has been determined by Moet-Ner and Field to be 8.2×10^{-23} $cm^3 molec^{-1} s^{-1}$ (83) which is 12 orders of magnitude smaller than the forward reaction rate coefficients obtained in the current study. Such a large difference suggests that the degree of reverse reaction may be assumed to be negligible. The linearity of the kinetic plots for H_3O^+ and D_3O^+ is supportive of such an assumption.

The rate coefficients for the reactions of H_3O^+ and D_3O^+ displayed a strong linear dependence on ion exit energy. The use of a weighted least squares data fit to a line allows k_{19}^o and k_{22}^o, the respective reaction rate coefficients for H_3O^+ and D_3O^+ in the absence of a repeller field, to be estimated. A value of $(0.117 \pm 0.003) \times 10^{-11} cm^3 molec^{-1} s^{-1}$ was obtained for k_{19}^o and k_{22}^o was determined to be $(0.67 \pm 0.04) \times 10^{-11}$ $cm^3 molec^{-1} s^{-1}$. An experimental value for the reduced mobility of D_3O^+ in D_2O was not available and the polarisability limit was used instead. In view of the large difference between the polarisation limit of water

and the measured value for its reduced mobility, the experimental rate coefficients for the reaction of D_3O^+ are probably ca.60% larger than those which would have been obtained if an experimental reduced mobility for D_3O^+ in deuterium oxide had been used to calculate ion residence times.

Literature values for the formation of the collision complexes $(H_2O)_2H^{+*}$ and $(D_2O)_2D^{+*}$ are not available for comparison, but the order of magnitude in this work (10^{-11}) is consistent with those discussed previously for the methylamines and ammonia-d_3. The values of k_{19}, the rate coefficient for the association reaction of H_3O^+, and k_{22}, the rate coefficient for the reaction of D_3O^+, are smaller than those predicted by the parameterised average dipole orientation theory (ca.10^{-9} $cm^3 molec^{-1} s^{-1}$) and mechanisms involving inter-conversion of a tight and loose collision complex, as discussed in Section 4.3.4.2, may be operative.

In comparing the rate coefficients obtained by use of the polarisation limit to calculate residence times, it becomes apparent that formation of $(D_2O)_2D^+$ is more rapid than the analogous formation of $(H_2O)_2H^+$. This effect of deuteration upon the observed rate coefficient was also observed in the ammonia system and the same rationale applies here. The reader is thus directed to the discussion in Section 4.4.3.2.

4.5.4 Estimation of the ion-source pressures of water and deuterium oxide.

By dividing equation (3.2.5.2 -1) by P, substituting the right hand side for β in equation (4.1.2 -6) and solving for P, the following expression is obtained:

$$P_{H_2O} = 2.90 \times 10^{-7} \left[(-\ln I'_{19} + L)V/k_{19}d\ell\right]^{\frac{1}{2}} \qquad (4.5.4. -1)$$

where $I'_{19} = (I_{19}/\Sigma I)$ and $L = \ln(I^{o}_{19}/\Sigma I^{o})$.
Since both k_{19} and L vary linearly with ion exit energy, equations (3.2.5.2 -2) and (3.2.5.2 -3) may be used to obtain these values for repeller voltages (V) in the range 0-5V. As before, d is taken to be one-half of the distance from the repeller plate to the ion-exit slit. Equation (4.5.4 -1) can thus be used to estimate ion source pressures from the normalised intensity of m/z 19 when water is used as a reagent gas.

Similarly, equation 4.2 -1 may be used to estimate the pressure of deuterium oxide in the ion-source, P_{D_2O}, and takes the form

$$P_{D_2O} = 4.56 \times 10^{-7} \left[(-\ln I'_{22} + L)V/k_{22}d\ell)\right]^{\frac{1}{2}} \qquad (4.5.4 -2)$$

Equation (4.5.4 -2) requires a measurement of the normalised intensity of m/z 22 (I'_{22}) and calculated values of k_{22} and L ($\ln(I^{o}_{22}/\Sigma I)$) from equations (3.2.6.2 -1) and (3.2.6.2 -2), respectively. Pressures of deuterium oxide with $0 < V \leq 5$ may thus be estimated.

4.6 Summary and Conclusions.

The molecular ions and the $(M-H)^+$ or $(M-D)^+$ ions of methylamine, dimethylamine, trimethylamine, ammonia-d_3, water and deuterium oxide undergo ion-molecule reactions to give the protonated or deuteronated molecular ion, which was the only product ion detected. The rates of these reactions are pressure dependent and plots of the logarithm of the normalised intensities of the reactant ions against pressure were linear over the pressure range at which the bulk of the ions react. Since the reactions were essentially complete at pressures of less than 0.1 Torr, the free fall equation of the residence time of an ion drifting under the influence of an applied electric field was used to determine ion residence times in the ion-source. Rate coefficients obtained from the slopes of the kinetic plots showed a strong, but nonlinear, dependence on ion-exit energy, which resulted in extrapolated values of k_n^o (the rate coefficient which should be observed in the absence of a repeller field) having large and unknown uncertainties. The nonlinear increase of the rate coefficients with increasing ion exit energy is contrary to theory[39] and possibly arises from inadequacies in the free-fall formula as a model for ion residence times in a chemical ionisation ion source.

The $(M-H)^+$ ions of ammonia and water have been shown previously, by ion cyclotron resonance, to undergo charge transfer reactions to give the molecular ion.[80] Since such reactions are undetectable in the

current study, the rate coefficients obtained are disappearance rate coefficients and not absolute rate coefficients for the specific proton or deuteron reactions. The disappearance rate coefficients are on the order of $10^{-9}cm^3molec^{-1}s^{-1}$ and thus correspond to fast ion-molecule reactions. The values of k_n^o, obtained from the graphically determined intercepts of the plots of k_n against ion exit energy, agreed only moderately well with theoretical capture collision rate coefficients as calculated by average dipole orientation theory.(42) Good agreement was found with literature values of rate coefficients determined for ions accelerated by a constant electric field, with the exception of ammonia $-d_3$, for which no literature values were available.

The molecular ions of the methylamine display relative reactivities in the trend MA > DMA > TMA, in agreement with earlier studies.(57,77) This ordering is the reverse of the proton affinities of these three bases and the observed order of reactivities may reflect the relative ease with which a proton is removed from a methyl group.(57) The $(M-H)^+$ ions of the three methylamines probably exist as immonium ions and the inability of the $(M-H)^+$ ion of trimethylamine to lose a proton from the amino functionality to give an imine can account for its absence of reactivity towards proton transfer to trimethylamine. However, at higher pressures the $(M-H)^+$ ion of trimethylamine

undergoes an association reaction.

The primary ions of the deuterated compounds studied were found to react more slowly than their non-deuterated counterparts. This observation is consistent with a primary isotope effect.

The MH^+ or MD^+ ions of the methylamines, ammonia-d_3, water and deuterium oxide undergo clustering reactions to form the proton or deuteron bound dimers, at pressures greater than ca.0.1 Torr. Plots of $\ln(I_n/\Sigma I)$ versus pressure squared were curved towards the lower limit, but were linear towards the higher pressure limit. This behaviour is predicted by the energy transfer mechanism[33]:

$$MH^+ + M \underset{k_b}{\overset{k_f}{\rightleftharpoons}} MHM^{+*} \xrightarrow{k_s} MHM^+$$

Thus the rate coefficients obtained from the linear portion of the kinetic plots correspond to the high pressure limit, second order rate coefficients with $k_n = k_f$. Bowers and colleagues have reported values of k_f for the methylamines, obtained by ion cyclotron resonance experiments,[56] and obtained rate coefficients which were ca.two orders of magnitude slower (10^{-11} cm^3 $molec^{-1}$ s^{-1}) than those predicted by the parameterised average dipole orientation theory. In the current study, the variation of k_n with ion exit energy was linear, with the exception of k_{22} for ammonia-d_3, and values of k_n^o were obtained from the intercepts of weighted least squares fitted lines to the data (except

for ammonia -d_3 for which a graphical method was employed). The rate coefficients obtained in this study are of the same order of magnitude as those reported by Bowers,[56] suggesting that the reactions of the MH^+ ions with the respective neutrals do indeed react at rates much slower than those predicted by theory. A possible explanation has been advanced by Moet-Ner[33] to account for the differences observed in experimental determinations of k_f and those predicted by theory, and invokes the interconversion of the excited collision complex between loose and tight states. Substantiation of such a mechanism is not possible with the current data.

The order of reactivities observed for the MH^+ ions in the methylamines is

$$CH_3NH_3^+ > (CH_3)_2NH_2^+ > (CH_3)_3NH^+ \quad ,$$

as shown by respective values of $k_n^o \times 10^{11} cm^3 molec^{-1} s^{-1}$ (0.6, 0.216, 0.12). This order agrees with that predicted by the average dipole orientation theory. The observed trend is also consistent with steric considerations, since steric hindrance in the excited collision complex would be expected to increase with increasing substitution, resulting in a slowing of the rate of reaction.

The association reactions of the MD^+ ions of ammonia -d_3 and deuterium oxide were found to be faster in comparison with the association reactions

of their analogous ions in ammonia and water. This effect can arise from the greater stability of the excited collision complexes of the deuterated systems.

The observed large, positive dependences of the association reaction rate coefficients upon ion exit energy is, again, contrary to theory. This effect can arise from the ion residence times, calculated here from ion mobilities, being increasingly underestimated as ion exit energy is increased.

Kinetic methods of determining the pressures of methylamine, dimethylamine, trimethylamine ammonia -d_3, water and deuterium oxide in a chemical ionisation ion-source were developed and described in the current study. By observation of the normalised intensity of the MH^+ or MD^+ ion, the reagent gas pressure in the ion-source is easily determined. As exemplified by the reactions investigated in this study, ion-molecule reactions occurring in a chemical ionisation ion-source are pressure dependent and since the method of chemical ionisation itself is based on ion-molecule reactions, it is vital for the reagent gas pressure to be known for the sake of reproducibility. Thus, it is hoped that the methods of measuring reagent gas pressures described in this Part will be of value to the practising analytical chemist.

APPENDIX:

Dipole moments and polarisabilities.

Table A-1 contains the dipole moments and polarisabilities of the six reagent gases employed in the present study. The majority of the gas phase dipole moments and polarisabilities were obtained from tabulated values in the references quoted in Table A-1. The direct determination of the dipole moment and polarisability differences between ammonia and ammonia $-d_3$ has been recently reported.[90] Values of $\mu_p(ND_3) - \mu_p(NH_3) = 0.0135 \pm 0.001D$ and $\alpha(ND_3) - \alpha(NH_3) = -(2.2 \pm 1.7) \times 10^{-26} cm^3$ were obtained.[90] Thus the dipole moment and polarisability of ammonia $-d_3$ were estimated from $\mu_p(NH_3)$ and $\alpha(NH_3)$, respectively, by adding the appropriate correction factor. The polarisability of deuterium oxide was assumed to be the same as that for water and, in view of the small difference observed between ammonia and ammonia $-d_3$ (vide supra), the error introduced by such an assumption is probably negligible.

TABLE I -1

Dipole moments[a] and angle averaged polarisabilities[b] of various compounds

Compound	Dipole moment (D)	Polarisability ($\AA^3$)
H_2O	1.85	1.45
D_2O	1.86[c]	d
NH_3	1.47	2.26
ND_3	1.48[e]	2.24[e]
CH_3NH_2	1.31	3.96
$(CH_3)_2NH$	1.03	5.79
$(CH_3)_3N$	0.612	7.69

a) Obtained from tables for dipole moments of molecules in the gas phase.(91)

b) Obtained from tables(92) unless specified otherwise.

c) Experimental value, gas phase.(93)

d) Assumed to be the same as for water.

e) Calculated from the values for ammonia.(90)

REFERENCES

1. M. Henchman, in "Ion-Molecule Reactions", Vol.1, edited by J.L.Franklin, Plenum Press, New York (1972), p.101.

2. V. L. Talroze and E.L.Frankevich, Russian J.Phys. Chem., 34: 1275 (1960).

3. E.W.McDaniel, D.W.Martin and W.S.Barnes, Rev.Sci. Instr., 33: 2 (1962)

4. E.W.McDaniel, J.Chem.Phys., 52 : 3931 (1970).

5. J.Heimerl, R.Johnson and M.Biondi, J.Chem.Phys., 51 : 5041 (1969).

6. E.E.Ferguson, F.C.Fehsenfield and A.L.Schmeltkopf, Adv.At.Mol.Phys., 5 : 1 (1969).

7. A.L.Farragher, Trans.Faraday Soc., 66 : 1411 (1970)

8. R.C.Bolden, R.S.Hensworth, M.J.Shaw and N.D.Twiddy, J.Phys., B3 : 45 (1970).

9. N.G.Adams and D.Smith, Int.J.Mass Spectrom.Ion Phys., 21 : 349 (1976).

10. D.Smith and N.G.Adams, in "Gas Phase Ion Chemistry", Vol.1, edited by M.T.Bowers, Academic Press, New York (1979).

11. L.R.Anders, J.T.Beauchamp,R.C.Dunbar and J.D. Balderschwieler, J.Chem.Phys., 45 : 1062 (1966)

12. A.J.Dempster, Phil.Mag., 31 : 438 (1916).

13. H.D.Smith, Phys.Rev., 25 : 452 (1925).

14. T.R.Hogness and E.G.Lunn, Phys.Rev., 26 : 44 (1925).

15. T.R.Hogness and R.W.Harkness, Phys.Rev., 32 : 784 (1928).

16. H.Eyring, J.O.Hirschfielder and H.S.Taylor, J.Chem.Phys., 4 : 479 (1936).

17. B. G. Reuben and L. Friedman, J. Chem. Phys., 37: 1636 (1962).

18. V.L.Talroze and A.K.Lyubrimova, Dokl.Akad.Nauk SSSR, 86 : 909 (1952).

19. D.P.Stevenson and D.O.Schissler, J.Chem.Phys., 23 : 1353 (1955).

20. F.H.Field, J.L.Franklin and F.W.Lampe, J.Am.Chem.Soc., 79 : 2419 (1957).

21. F.H.Field, J.Am.Chem.Soc., 83 : 1523 (1961).

22. M.S.B.Munson and F.H.Field, J.Am.Chem.Soc., 88 : 2621 (1966).

23. F.H.Field and F.W.Lampe, J.Am.Chem.Soc., 80 : 5587 (1958).

24. R.D.Doepker and P.Ausloos, J.Chem.Phys., 44 : 1951 (1966).

25. P.Kebarle in "Interaction Between Ions and Molecules" edited by P.Ausloos, Plenum Press, New York (1975). p.459.

26. P.Kebarle in "Ion-Molecule Reactions", edited by J.L.Franklin, Plenum Press, New York (1972), p.315.

27. A Good, Chem.Rev., 75 : 561 (1975).

28. E.Rabinowitz, Trans.Faraday Soc., 33 : 283 (1937).

29. D.K.Bohme, D.B.Dunkin, F.C.Fehsenfeld and E.E. Ferguson, J.Chem.Phys., 49 : 5201(1968).

30. V.G.Anicich and M.T.Bowers, J.Am.Chem.Soc., 96: 1279 (1974).

31. R.F.Porter in "Interactions Between Ions and Molecules", edited by P.Ausloos, Plenum Press, New York (1975) p.231.

32. M.Moet-Ner and F.H.Field, J.Am.Chem.Soc., 97 : 5339 (1975).

33. M.Moet-Ner in "Gas Phase Ion Chemistry", Vol.1, edited by M.T. Bowers, Academic Press, New York (1979), p.197.

34. P.Langevin, Ann.Chim.Phys., 5 : 245 (1905).

35. G.Gioumousis and D.P.Stevenson, J.Chem.Phys., 29 : 294 (1958).

36. T.Su and M.T.Bowers in "Gas Phase Ion Chemistry", Vol.1, edited by M.T.Bowers, Academic Press, New York (1979), p.83.

37. L.P.Theard and W.H.Hamill, J.Am.Chem.Soc., 84 : 1134 (1962).

38. T.F.Moran and W.H.Hamill, J.Chem.Phys., 39 : 1413 (1963).

39. S.K.Gupta, E.G.Jones, A.G.Harrison and J.J.Myher, Can.J.Chem., 45 : 3107 (1967).

40. M.T.Bowers and J.B.Laudenslager, J.Chem.Phys., 56 : 4711 (1972).

41. T.Su and M.T.Bowers, J.Chem.Phys., 58 : 3027 (1973).

42. T.Su and M.T.Bowers, Int.J.Mass Spectrom.Ion Phys., 12 : 347 (1973).

43. J.A.Burt, Ph.D.thesis, York University, Toronto, 1968.

44. A.Good, D.A.Durden and P.Kebarle, J.Chem.Phys., 52 : 222 (1970).

45. C.E.Young and W.E.Falconer, J.Chem.Phys., 57 : 918 (1972).

46. A.Good, D.A.Durden and P.Kebarle, J.Chem.Phys., 50 : 212 (1970)

47. D.P.Beggs and F.H.Field, J.Am.Chem.Soc., 93 : 1567 (1971).

48. A.J.Cunningham, J.D.Payzant and P.Kebarle, J.Am.Chem. Soc., 94 : 7627 (1972).

49. Y.K.Lau, S.Ikuta and P.Kebarle, J.Am.Chem.Soc., 104 : 1462 (1982).

50. D.P.Beggs and F.H.Field, J.Am.Chem.Soc., 93 : 1576 (1971).

51. C.V.Howard, V.M.Bierbaum, H.W.Rundle and F.Kaufman, J.Chem.Phys., 57 : 3491 (1972).

52. C.E.Young, D.Edelson and W.E.Falconer, J.Chem.Phys., 53 : 4295 (1970).

53. M.DePaz, J.J.Levanthal and L.Friedman, J.Chem.Phys., 51 : 3748 (1969).

54. D.K.Bohme and F.C.Fehsenfeld, Can.J.Chem., 47 : 2715 (1969).

55. M.Moet-Ner and F.H.Field, J.Am.Chem.Soc., 97 : 5339 (1975).

56. P.V.Neilson, M.T.Bowers, M.Chau, W.R.Davidson and D.H.Aue, J.Am.Chem.Soc., 100 : 3649 (1978).

57. L.Hellner and L.W.Sieck, Int.J.Chem.Kin., 5 : 177 (1973).

58. M.S.B.Munson and F.H.Field, J.Am.Chem.Soc., 88 : 2621 (1966).

59. P.Vouroos and L.A.Carpino, J.Org.Chem., 39 : 3777 (1974).

60. A.K.Bose, H.Fujiward, N.Praminik, N.Birenda, E.Lazaro and C.R.Spilliert, Anal.Biochem., 89 : 284 (1978).

61. F.H.Field in "Ion-Molecule Reactions", Vol.1, edited by J.L.Franklin, Plenum Press, New York (1972), p.261.

62. D.F.Hunt, Adv.Mass Spectrom., 6 : 517 (1974).

63. J.M.Wilson, in "Mass Spectrometry", Vol.3, edited by R.W.A.Johnstone, Specialist Periodical Reports, The Chemical Society, London (1975), p.96.

64. J.M.Wilson in "Mass Spectrometry", Vol.4, edited by R.W.A.Johnstone, Specialist Periodical Reports, The Chemical Society, London (1977), p.111.

65. B.Munson, in "Interactions Between Ions and Molecules", edited by P.Ausloos, Plenum Press, New York (1975), p.505.

66. R.A.Hancock, R.Walder and H.Weigel, Org.Mass. Spectrom., 14 : 507 (1979).

67. I.Dzidic, J.Am.Chem.Soc., 94 : 8333 (1972).

68. H.Budzikiewicz and E.Busker, Tetrahedron, 36 : 255 (1980).

69. D.F.Hunt, C.N.McEwan and R.A.Upham, Tet.Lett., p.4539 (1971).

70. M.V.Buchanan, Anal.Chem., 54 : 570 (1982).

71. D.F.Hunt, C.N.McEwan and R.A.Upham, Anal.Chem., 44 : 1292 (1972).

72. C.La Lau, in "Topics in Organic Mass Spectrometry", edited by A.L.Burlingame, Wiley-Interscience, New York (1970), p.93.

73. R.Walder, Ph.D.thesis, University of London (1979).

74. "Handbook of Chemistry and Physics", edited by R.C.Wedat, CRC Press Inc., Boca Ruton, Florida (1979), p.D-196.

75. R.W.Kiser, "Introduction to Mass Spectrometry", Prentice-Hall Inc., Englewood Cliffs, New Jersey (1965), p.134.

76. D.P.Ridge and J.L.Beauchamp, J.Chem.Phys., 64 : 2735 (1976).

77. M.S.B.Munson, J.Phys.Chem., 70 : 2034 (1966).

78. E.G.Jones and A.G.Harrison, Can.J.Chem., 45 : 3119 (1967).

79. C.W.Polley, A.J.Illies and G.G.Meisels, Anal.Chem., 52 : 1797 (1980).

80. W.T.Huntress and R.F.Pinizotto, J.Chem.Phys., 59 : 4742 (1973).

81. J.Collin, in "Advances in Mass Spectrometry", edited by J.Waldron, Pergamon Press, New York (1959), p.384.

82. M.Henchman, Disc.Faraday Soc., 39 : 63 (1965).

83. M.Moet-Ner and F.Field, J.Am.Chem.Soc., 99 : 998 (1977).

84. R.Walder and J.L.Franklin, Int.J.Mass Spectrom.Ion Phys., 36 : 85 (1980).

85. R.A.Hancock and M.G.Hodges, Int.J.Mass Spectrom.Ion Phys., 46 : 329 (1983).

86. M.G.Hodges and R.A.Hancock, unpublished results.

87. K.R.Ryan and J.H.Futrell, J.Chem.Phys., 42 : 824 (1965).

88. R.A.Fluegge, J.Chem.Phys., 50 : 4373 (1969).

89. K.R.Ryan, J.Chem.Phys., 52 : 6009 (1970).

90. C.Scher, B.Ravid and E.A.Halevi, J.Phys.Chem., 86 : 654 (1982).

91. R.D.Nelson, D.R.Lide and A.A.Maryott, "Selected Values of Electric Dipole Moments for Molecules in the Gas Phase", National Standard Reference Data Series - National Bureau of Standards 10,(1967).

92. H.H.Landolt and R.Börnstein, "Zahlenwerte und Functionen", Vol.1, Part 3, Springer-Verlag, Berlin (1951), p.509.

93. S.A.Clough, Y.Beers, G.P.Klein and S,L.Rothman, J.Chem.Phys., 59 : 2254 (1977).